

VOLUME XLVI

GEMS & GEMOLOGY

SUMMER 2010



*The Wittelsbach-Graff and Hope Diamonds . . . Opals from Ethiopia—and Madagascar
Composite Turquoise . . . Microtomography of Pearls . . . A New Gem, Hibonite*

THE QUARTERLY JOURNAL OF THE GEMOLOGICAL INSTITUTE OF AMERICA

EXPERTISE THAT SPREADS CONFIDENCE. AROUND THE WORLD AND AROUND THE CLOCK.



ISRAEL 5:00 PM
Cutter checks parameters online with GIA Facetware® Cut Estimator.

NEW YORK 10:00 AM
GIA Master Color Comparison Diamonds confirm color quality of a fancy yellow.

CARLSBAD 7:00 AM
Laboratory technicians calibrate measurement devices before the day's production begins.

MUMBAI 7:30 PM
Staff gemologist submits new findings on coated diamonds to GIA global database.

HONG KONG 10:00 PM
Wholesaler views grading results and requests additional services online at My Laboratory.

JOHANNESBURG 5:00 PM
Diamond graders inscribe a diamond and issue a GIA Diamond Dossier®



All across the planet, GIA labs and gemological reports are creating a common language for accurate, unbiased gemstone evaluation. From convenient locations in major gem centers, to frontline detection of emerging treatments and synthetics, to online services that include ordering, tracking, and report previews – GIA is pioneering the technology, tools and talent that not only ensure expert service, but also advance the public trust in gems and jewelry worldwide.

WWW.GIA.EDU



GIA
GEMOLOGICAL INSTITUTE OF AMERICA®

CARLSBAD NEW YORK LONDON ANTWERP FLORENCE GABORONE JOHANNESBURG
DUBAI MOSCOW MUMBAI BANGKOK HONG KONG TAIPEI SEOUL OSAKA TOKYO

EDITORIAL

- 79 **GIA Symposium 2011: Advances in Gemological Research**
Alice S. Keller

FEATURE ARTICLES

- 80 **The Wittelsbach-Graff and Hope Diamonds: Not Cut from the Same Rough**
Eloïse Gaillou, Wuyi Wang, Jeffrey E. Post, John M. King, James E. Butler, Alan T. Collins, and Thomas M. Moses
Two famous diamonds are tested to see if they originated from the same crystal.
- 90 **Play-of-Color Opal from Wegel Tena, Wollo Province, Ethiopia**
Benjamin Rondeau, Emmanuel Fritsch, Francesco Mazzero, Jean-Pierre Gauthier, Bénédicte Cenki-Tok, Eyassu Bekele, and Eloïse Gaillou
Describes a major new source of high-quality opal with a mostly white bodycolor.

NOTES & NEW TECHNIQUES

- 106 **A New Type of Composite Turquoise**
Gagan Choudhary
- 114 **New Occurrence of Fire Opal from Bemia, Madagascar**
Martina Simoni, Franca Caucia, Ilaria Adamo, and Pietro Galinetto
- 122 **X-ray Computed Microtomography Applied to Pearls: Methodology, Advantages, and Limitations**
Stefanos Karamelas, Jürgen Michel, Mingling Zheng-Cui, Jens-Oliver Schwarz, Frieder Enzmann, Emmanuel Fritsch, Leon Leu, and Michael S. Krzemnicki
- 128 **X-ray Computed Microtomography: Distinguishing Natural Pearls from Beaded and Non-Beaded Cultured Pearls**
Michael S. Krzemnicki, Sebastian D. Friess, Pascal Chalus, Henry A. Hänni, and Stefanos Karamelas

RAPID COMMUNICATIONS

- 135 **Hibonite: A New Gem Mineral**
Thomas Hainschwang, Franck Notari, Laurent Massi, Thomas Armbruster, Benjamin Rondeau, Emmanuel Fritsch, and Mariko Nagashima

REGULAR FEATURES

- 139 **Thank You, Donors**
- 140 **Lab Notes**
Unusual polyphase inclusions in corundum • Black diamond with solid CO₂ micro-inclusions and phosphorescent zones • Fancy Vivid blue HPHT-treated diamond • Interesting display of the H3 defect in colorless diamond • CVD synthetic diamond over one carat • Synthetic diopside in manufactured glass • Green Be-diffused sapphire • Heat-treated spinel
- 147 **Gem News International**
Unusual facet arrangement produces scalloped appearance in diamond • Chrysocolla chalcedony from Peru • Recent finds of kunzite in Pala, California • Natural pearls of the Pectinidae family • More on ruby from Cabo Delgado, Mozambique • Update on ruby, sapphire, and spinel mining in Vietnam • Sphene from northern Pakistan • Spinel from Bawma, Myanmar • Green garnets reportedly from Afghanistan • Calcium niobium gallium garnet • Glass imitations of emerald • “Nanogems,” a new synthetic • Serpentine doublets, sold as pietersite • Composite coral bangle • Lead glass-filled ruby in antique jewelry • Gems set with colored adhesive
- S1 **Book Reviews**
- S4 **Gemological Abstracts**



pg. 81



pg. 91



pg. 159

EDITORIAL STAFF

Editor-in-Chief

Alice S. Keller
akeller@gia.edu

Managing Editor

Thomas W. Overton
tom.overton@gia.edu

Associate Editor

Stuart D. Overlin
soverlin@gia.edu

Consulting Editor

Carol M. Stockton

Contributing Editor

James E. Shigley

Editor

Brendan M. Laurs
Gemological Institute of America
The Robert Mouawad Campus
5345 Armada Drive
Carlsbad, CA 92008
(760) 603-4503
blaurs@gia.edu

Circulation Coordinator

Martha Rivera
(760) 603-4000, ext. 7142
martha.rivera@gia.edu

Editors, Lab Notes

Thomas M. Moses
Shane F. McClure

Editor, Gem News International

Brendan M. Laurs

Editors, Book Reviews

Susan B. Johnson
Jana E. Miyahira-Smith
Thomas W. Overton

Editors, Gemological Abstracts

Brendan M. Laurs
Thomas W. Overton

PRODUCTION STAFF

Art Director

Nanette Newbry, Studio 2055

Image Specialist

Kevin Schumacher

G@G Online:

gia.metapress.com

EDITORIAL REVIEW BOARD

Ahmadjan Abduriyim
Tokyo, Japan

Shigeru Akamatsu
Tokyo, Japan

Edward W. Boehm
Chattanooga, Tennessee

James E. Butler
Washington, DC

Alan T. Collins
London, UK

John L. Emmett
Brush Prairie, Washington

Emmanuel Fritsch
Nantes, France

Jaroslav Hyřl
Prague, Czech Republic

A. J. A. (Bram) Janse
Perth, Australia

E. Alan Jobbins
Caterham, UK

Mary L. Johnson
San Diego, California

Anthony R. Kampf
Los Angeles, California

Robert E. Kane
Helena, Montana

Lore Kiefert
Lucerne, Switzerland

Michael S. Krzemnicki
Basel, Switzerland

Thomas M. Moses
New York, New York

Mark Newton
Coventry, UK

George R. Rossman
Pasadena, California

Kenneth Scarratt
Bangkok, Thailand

James E. Shigley
Carlsbad, California

Christopher P. Smith
New York, New York

Wuyi Wang
New York, New York

Christopher M. Welbourn
Reading, UK

SUBSCRIPTIONS

Copies of the current issue may be purchased for \$35 in the U.S., \$50 elsewhere. Online subscriptions are \$74.95 for one year (4 issues), \$194.95 for three years (12 issues). Combination print/online subscriptions are \$139.95 in the U.S. and \$160 elsewhere for one year, and \$399.95 in the U.S. and \$465 elsewhere for three years. Canadian subscribers should add GST. Discounts are available for group subscriptions, renewals, GIA alumni, and current GIA students. Subscriptions include G@G's monthly gemological e-newsletter, the *G@G eBrief*.

To purchase subscriptions and single issues, visit store.gia.edu or contact the Circulation Coordinator.

Electronic (PDF) versions of individual articles and sections from Spring 1981 forward can be purchased at gia.metapress.com for \$12 each.

To obtain a Japanese translation of *Gems & Gemology*, contact GIA Japan at info@giajpn.gr.jp. Our Canadian goods and service registration number is 126142892RT.

Gems & Gemology's impact factor is 1.172 (ranking 12th out of the 26 journals in the Mineralogy category), according to the Thomson Reuters 2008 Journal Citation Reports (issued July 2009). *Gems & Gemology* is abstracted in Thomson Reuters products (*Current Contents: Physical, Chemical & Earth Sciences* and *Science Citation Index—Expanded*, including the Web of Knowledge) and other databases. For a complete list of sources abstracting G@G, see www.gia.edu/gandg.

Gems & Gemology welcomes the submission of articles on all aspects of the field. Please see the Guidelines for Authors on our Website, or contact the Managing Editor. Letters on articles published in *Gems & Gemology* are also welcome.

Abstracting is permitted with credit to the source. Libraries are permitted to photocopy beyond the limits of U.S. copyright law for private use of patrons. Instructors are permitted to photocopy isolated articles for noncommercial classroom use without fee. Copying of the photographs by any means other than traditional photocopying techniques (Xerox, etc.) is prohibited without the express permission of the photographer (where listed) or author of the article in which the photo appears (where no photographer is listed). For other copying, reprint, or republication permission, please contact the Managing Editor.

Gems & Gemology is published quarterly by the Gemological Institute of America, a nonprofit educational organization for the gem and jewelry industry.

Postmaster: Return undeliverable copies of *Gems & Gemology* to GIA, The Robert Mouawad Campus, 5345 Armada Drive, Carlsbad, CA 92008.

Any opinions expressed in signed articles are understood to be the opinions of the authors and not of the publisher.

DATABASE COVERAGE

MANUSCRIPT SUBMISSIONS

COPYRIGHT AND REPRINT PERMISSIONS

ABOUT THE COVER

Identification of pearls—natural, bead-cultured, beadless-cultured, and “keshi”—has become more challenging than ever. Two articles in this issue, by Stefanos Karamelas and Michael Krzemnicki and coauthors, review the use of X-ray computed microtomography in pearl analysis. The 31 natural pearls in this estate necklace range from 11.88 × 11.25 mm to 7.95 × 6.48 mm (courtesy of Mr. and Mrs. Mohammed Idris Jabir, Malaysia); the ring holds a 9.9 mm cultured pearl (courtesy of Kalati Co., Great Neck, New York). Photo by Robert Weldon.

Color separations for *Gems & Gemology* are by Pacific Plus, Carlsbad, California.

Printing is by Allen Press, Lawrence, Kansas.

© 2010 Gemological Institute of America All rights reserved. ISSN 0016-626X



GIA Symposium 2011: Advances in Gemological Research

The premier event in gemology is back! In celebration of its 80th anniversary, GIA is bringing its International Gemological Symposium home. Next **May 29 and 30**, immediately preceding the 2011 JCK Show, GIA will host a conference dedicated to the latest developments in gemological research and the gem and jewelry industry. Combining the best of Symposium, which has educated thousands over the last three decades, and the more recent Gemological Research Conference, **GIA Symposium 2011** will have two parallel tracks: **Advances in Gemological Research** and **Advancing the Gem Industry**. It will be held at GIA's world headquarters in Carlsbad, California. This event will marry technological advances with a search for solutions to the problems jewelers and gemologists face in the laboratory and in their businesses.



GIA will host Symposium 2011 at its ocean-view Carlsbad headquarters.

- **Advances in Gemological Research**, co-chaired by noted research scientist Dr. James Shigley and *G&G* editor Brendan Laurs, will focus on topics such as diamond and colored stone identification, new technologies and instrumentation, and gem localities and locality determination.
- **Advancing the Gem Industry**, which GIA's Kathryn Kimmel and I will co-chair, will explore topics in the broader gem and jewelry industry, such as appraisals, pearls, jewelry history, and challenges in the buying and selling of gems.

Each session will feature presentations by prominent scientists and industry experts from around the world. Symposium 2011 will also include a poster session, chaired by GIA Library director Dona Dirlam, where presenters will display innovative research projects on various aspects of gemology.

To take advantage of the proximity to San Diego's historic pegmatite district, we will offer field trips to working gem mines before the conference. Other optional activities include hands-on workshops and a visit to the spectacular "All That Glitters" gem

and jewelry exhibit at the San Diego Museum of Natural History.

If you're interested in participating in either track as a speaker or a poster presenter, please submit an abstract no later than January 10, 2011. Guidelines are available on the conference website at symposium2011.gia.edu. All abstracts will be reviewed by experts in the field, and abstracts of oral and poster presentations given at the conference will be published in *Gems & Gemology*. The nominal registration fee will include meals during the event, and discounts will be given for students and early registration.

We're pleased to report that travel grants will again be available to presenters who demonstrate appropriate need. For more information on travel grants, please see the conference website.

Since our last symposium and research conference in 2006, gemology has faced a number of new challenges and developments: 1+ ct CVD synthetic diamonds, composite rubies, sophisticated coatings on diamonds and other gem materials, and numerous new localities and gem minerals. Likewise, the business of gems has had to wrestle with economic woes, political embargoes, and heightened consumer awareness of issues such as fair trade and environmental protection. By bringing together the best and brightest from the many disciplines involved in the study of gems and jewelry, we can address these issues more effectively. You won't want to miss it.

For more information on **GIA Symposium 2011**, go to symposium2011.gia.edu.

May 29–30, 2011. Save the date!

A handwritten signature in black ink that reads "Alice S. Keller".

Alice S. Keller • Editor-in-Chief • akeller@gia.edu

THE WITTELSBACH-GRAFF AND HOPE DIAMONDS: NOT CUT FROM THE SAME ROUGH

Eloïse Gaillou, Wuyi Wang, Jeffrey E. Post, John M. King, James E. Butler,
Alan T. Collins, and Thomas M. Moses

Two historic blue diamonds, the Hope and the Wittelsbach-Graff, appeared together for the first time at the Smithsonian Institution in 2010. Both diamonds were apparently purchased in India in the 17th century and later belonged to European royalty. In addition to the parallels in their histories, their comparable color and bright, long-lasting orange-red phosphorescence have led to speculation that these two diamonds might have come from the same piece of rough. Although the diamonds are similar spectroscopically, their dislocation patterns observed with the DiamondView differ in scale and texture, and they do not show the same internal strain features. The results indicate that the two diamonds did not originate from the same crystal, though they likely experienced similar geologic histories.

The earliest records of the famous Hope and Wittelsbach-Graff diamonds (figure 1) show them in the possession of prominent European royal families in the mid-17th century. They were undoubtedly mined in India, the world's only commercial source of diamonds at that time.

The original ancestor of the Hope diamond was an approximately 115 ct stone (the Tavernier Blue) that Jean-Baptiste Tavernier sold to Louis XIV of France in 1668. Tavernier purchased the diamond in India, possibly at the Kollur mine, but its exact source is not known. Louis XIV had Tavernier's stone recut into the ~69 ct diamond called the *Diamant Bleu de la Couronne* (Blue Diamond of the Crown), later known as the French Blue. The diamond was set into the Golden Fleece of the Colored

Adornment (*Toison d'Or de la Parure de Couleur*) in 1749, but was stolen in 1792 during the French Revolution. Twenty years later, a 45.52 ct blue diamond appeared for sale in London and eventually became part of the collection of Henry Philip Hope. Recent computer modeling studies have established that the Hope diamond was cut from the French Blue, presumably to disguise its identity after the theft (Attaway, 2005; Farges et al., 2009; Sucher et al., 2010). For a thorough look at the history of the Hope diamond, see Patch (1976), Morel (1988), and Kurin (2006), along with the references cited above.

The first reliable record of the Wittelsbach Blue diamond dates to 1673 in Vienna, when it was listed as part of the estate of Empress Margarita Teresa of Austria. As with the Hope diamond, its exact source in India is unknown, though the Kollur mine has been mentioned (e.g., Balfour, 2009). The stone passed from the Hapsburg court to the Bavarian Wittelsbach family in 1722 as part of a dowry, and it remained in the Bavarian crown jewels until the

See end of article for About the Authors and Acknowledgments.
GEMS & GEMOLOGY, Vol. 46, No. 2, pp. 80–88.
© 2010 Gemological Institute of America



Figure 1. In late January 2010, the 31.06 ct Wittelsbach-Graff diamond (left) joined the 45.52 ct Hope diamond (right) for a seven-month display at the Smithsonian Institution's National Museum of Natural History. Photo by Chip Clark.

creation of the German republic after World War I. To support the former Bavarian royal family, the Wittelsbach diamond was put up for auction in 1931 with other royal jewels. When the bidding was too low, it went back to a government safe for the next 20 years until it was secretly sold. It briefly reappeared, anonymously, during the 1958 World Exhibition in Brussels.

In 1962, the Wittelsbach Blue was recognized by a Belgian diamond dealer who had been asked to recut it; he refused and bought the stone instead. The gem was then sold to a private owner and remained out of the public eye until a Christie's auction on December 10, 2008. London jeweler Laurence Graff purchased the 35.56 ct stone for just over \$24.3 million. Graff decided to have the diamond recut to remove numerous chips around the girdle, enhance its color grade (from Fancy Deep grayish blue to Fancy Deep blue), and reduce the size of its large culet, while attempting to preserve the original shape. The renamed Wittelsbach-Graff diamond now weighs 31.06 ct. The reader is referred to Dröschel et al. (2008) for a comprehensive review of the Wittelsbach's history.

The Wittelsbach-Graff diamond was placed on public display near the Hope diamond at the Smithsonian Institution's National Museum of Natural History from January 28 to September 1, 2010. This marked the first time the two great blue diamonds were brought together. Because of the rarity of large blue diamonds and the historical parallels between the Hope and the Wittelsbach Blue, there has been considerable speculation over the years as to whether they might have been cut from the same piece of rough or from stones that were

once part of the same parent crystal (e.g., Balfour, 2009). This speculation is supported by the fact that the Wittelsbach-Graff, like the Hope, exhibits a rare long-lasting orange-red phosphorescence. The exhibition of the two diamonds at the Smithsonian Institution provided an unprecedented opportunity to conduct a side-by-side study. In addition to addressing the question of a common pedigree, this was a rare occasion to gain additional insight into natural blue diamonds by studying two of the largest and finest examples known. All the experiments were conducted during a single night, just before the Wittelsbach-Graff was mounted into its bracket to go on exhibition and while the Hope was unmounted from its necklace.

MATERIALS AND METHODS

Both diamonds were graded by GIA prior to this study. The 31.06 ct Wittelsbach-Graff is a Fancy Deep blue, internally flawless, cushion modified brilliant cut. The 45.52 ct Hope is a Fancy Deep grayish blue, very slightly included (VS₁), antique cushion cut (Crowningshield, 1989). Both stones have relatively large culets (though the Wittelsbach-Graff's culet is significantly larger; again, see figure 1), which enabled us to perform spectroscopy through the parallel table and culet facets.

As our testing had to be conducted in a vault at the National Museum of Natural History for security reasons, portable equipment was necessary. Infrared (IR) spectra were acquired using a Thermo iS10 Fourier-transform infrared (FTIR) spectrometer (2 cm⁻¹ resolution). Mirrors were used as beam condensers (figure 2), enabling us to focus the beam through the table and culet of each stone. No purge

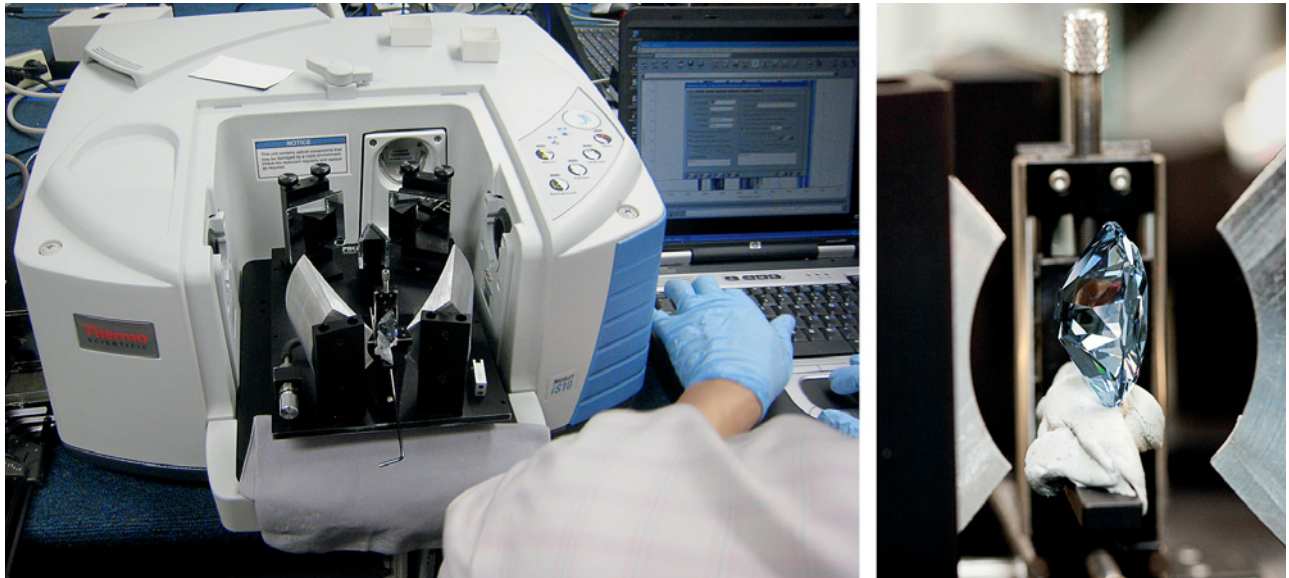


Figure 2. The portable FTIR equipment was mounted with a mirror beam condenser. The photo on the left shows the general apparatus, in which the Hope diamond is set. On the right, the mirrors focus the beam through the table and culet of the Wittelsbach-Graff. Photos by J. Post (left) and Chip Clark (right).

system was used during data collection.

UV fluorescence was tested with a Super Bright long- and short-wave UV lamp (365 and 254 nm, respectively).

Phosphorescence spectra were collected using the portable spectrometer described previously by Eaton-Magaña et al. (2008). The stones were excited with an Ocean Optics DH-2000 deuterium UV lamp (which emits in the 215–400 nm range), and the signal was acquired with an Ocean Optics charge-coupled device (CCD) spectrometer (USB 2000) through a fiber-optic bundle. In this bundle, the UV radiation was transferred through six optical fibers (600 μm diameter each); a seventh fiber in the core of the bundle collected the emitted light from the diamond and delivered it to the entrance aper-

ture of the CCD spectrometer. The tip of the fiber-optic bundle was placed in contact with the diamond's surface, which made it possible to illuminate and measure approximately equivalent volumes for each sample. The phosphorescence spectra were collected after 20 seconds of UV exposure. During decay, the spectra were integrated and recorded at intervals of 0.5, 1, and 2 seconds.

Luminescence imaging under ultra-short-wave UV radiation (~ 225 nm) was performed with a Diamond Trading Company DiamondView instrument (Welbourn et al., 1996). High-intensity short-wave UV close to the diamond absorption edge was used to excite the fluorescence and phosphorescence so that only the outermost layer of the diamond was excited, yielding sharp and clear fluorescence images. Birefringence resulting from internal strain was examined in transmitted light between crossed polarizers through a Nikon SMZ1500 microscope.

Attempts were made to acquire UV-visible spectra with a portable spectrometer, but the equipment was not configured for such large stones, so the measurements are not reported here.

RESULTS AND DISCUSSION

Results for both diamonds are summarized in table 1. Based on previous color grading of the two diamonds, we expected their appearances to be quite similar when observed side by side. Diamonds graded by GIA as Fancy Deep are medium to dark in

NEED TO KNOW

- The Wittelsbach-Graff and the Hope, two of the world's most famous blue diamonds, share similarities in history, color, and phosphorescence.
- Slight differences in phosphorescence and distinct differences in luminescence emission and internal strain patterns demonstrate that the diamonds did not originate from the same crystal.
- The two diamonds' overall resemblance and common origin (India) suggest that they formed in similar geologic settings.

TABLE 1. Summary of the main characteristics of the Hope and Wittelsbach-Graff diamonds.

Characteristic	Hope	Wittelsbach-Graff
GIA color grade	Fancy Deep grayish blue	Fancy Deep blue
Weight	45.52 ct	31.06 ct
Dimensions	25.60 × 21.78 × 12.00 mm	23.23 × 19.65 × 8.17 mm
FTIR spectroscopy		
Diamond type	IIb	IIb
Boron (uncompensated)	0.36 ± 0.06 ppm	0.19 ± 0.03 ppm
UV fluorescence	None	None
Phosphorescence		
Observed (from short-wave UV)	Intense orange-red, ~1 minute	Intense orange-red, ~1 minute
I_0 500 nm / I_0 660 nm ^a (avg.)	~0.104	~0.093
$\tau_{660\text{ nm}}$ ^a (avg.)	~9 seconds	~14 seconds
DiamondView imaging	Moderate-to-strong blue luminescence, mosaic patterns <100 μm	Moderate-to-strong blue luminescence, mosaic patterns >200 μm
Internal strain patterns	Coarse banded internal strain pattern, predominantly in a single direction, with blue, orange, and red interference colors.	"Tatami" pattern visible in all directions, with gray and blue interference colors.

^a Abbreviations: I_0 = initial intensity, τ = half-life.

tone (the lightness to darkness of the color) and moderate to strong in saturation (the strength or purity of the color; King et al., 1998). The Hope's grayish blue color, compared to the blue of the Wittelsbach-Graff, led us to expect a very slightly less saturated and more "steely" appearance, which we did observe. Many factors influence a diamond's color appearance, including size, shape, and proportions. Even

with the similar bodycolor, the different proportions and cutting styles of these two stones would lead us to expect different face-up color appearances. The difference was subtle under standard color grading conditions, but more pronounced in less-controlled lighting and viewing environments.

FTIR spectroscopy confirmed that both diamonds were type IIb (figure 3); that is, their substitutional

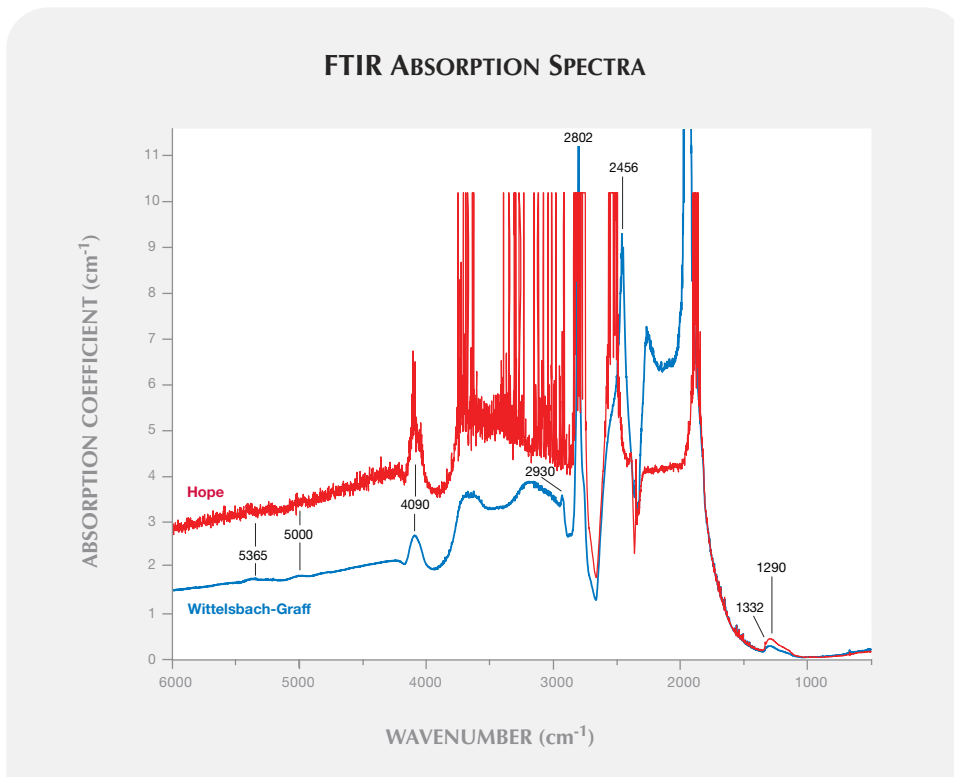


Figure 3. The FTIR spectra of the Hope and Wittelsbach-Graff diamonds confirmed that they were type IIb. Because the stones are thick (12.00 and 8.17 mm, respectively), they fully absorb in the two- and three-phonon regions (especially the Hope diamond, from 3700 to 1800 cm^{-1}). All but one of the labeled peaks correspond to boron; the 1332 cm^{-1} feature is the Raman line (activated by the boron impurities).

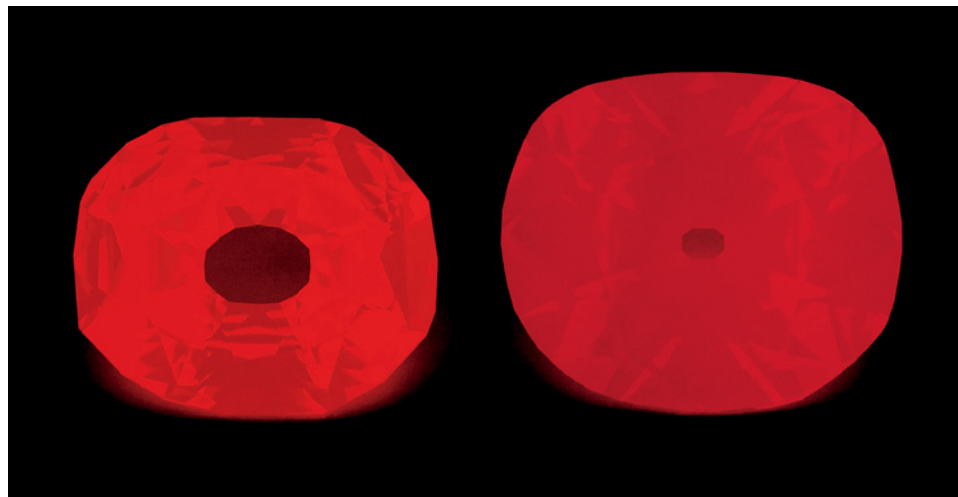


Figure 4. Both the Wittelsbach-Graff (left) and Hope (right) display bright, long-lasting, orange-red phosphorescence after exposure to short-wave UV radiation. Note, however, that the Wittelsbach-Graff is slightly brighter and more orange. This phosphorescence is actually better captured with the camera than with the unaided eye, and agrees with the spectra shown in figure 5. Photo by Chip Clark.

boron concentration exceeds the substitutional nitrogen concentration, if any (Breeding and Shigley, 2009). Due to the long path of the IR beam from the culet facet through the table (12.00 mm for the Hope and 8.17 mm for the Wittelsbach-Graff), both spectra showed complete absorption in the main boron region, which was more pronounced in the thicker Hope. The boron peaks were positioned at 5365, 5000, 4090, 2930, 2802, 2456, and 1290 cm^{-1} . The area of the peak at 2802 cm^{-1} is typically used to calculate the concentration of noncompensated boron (Collins and Williams, 1971; Fisher et al., 2009), but this peak was saturated for both diamonds. However, it was recently shown that it is also possible to estimate the uncompensated boron concentration from the absorption coefficient of the one-phonon peak at 1290 cm^{-1} (Collins, 2010). Using the procedure and the calibration given by Collins (2010) yielded boron concentrations of 0.36 ± 0.06 ppm (atomic) for the Hope and 0.19 ± 0.03 ppm for the Wittelsbach-Graff. For comparison, the uncompensated boron concentrations in natural blue diamonds studied by Collins and Williams (1971) ranged from 0.19 to 0.44 ppm. Thus, the boron concentrations in the Hope and Wittelsbach-Graff are characteristic of other natural type IIb diamonds, and most likely their intense blue color results primarily from their large size rather than an abnormally high boron concentration.

Both diamonds were inert to long- and short-wave UV radiation. As indicated above, after exposure to short-wave UV both diamonds exhibited intense orange-red phosphorescence, which was visible to the unaided eye in a dark room for approximately one minute (figure 4). The Wittelsbach-Graff's phosphorescence was a bit more intense,

lasted slightly longer, and was perhaps more orange. To better quantify these observations, phosphorescence spectra were acquired from several areas of the diamonds. Both diamonds showed the two bands previously observed by Eaton-Magaña et al. (2008) in natural type IIb blue diamonds (figure 5), centered at 500 nm (blue) and 660 nm (orange-red).

The study by Eaton-Magaña et al. (2008) of more than 70 natural blue diamonds revealed that their phosphorescence spectra typically display a relatively strong blue emission with a relatively weak red emission (figure 6). The Wittelsbach-Graff and the Hope, however, are among the minority of blue diamonds that have intense 660 nm and weak 500 nm emissions. In these stones, the 500 nm band decays in the first few seconds after UV excitation is stopped, whereas the red luminescence persists for a minute or more. Eaton-Magaña et al. (2008) showed that when the half-life of the 660 nm band is plotted against the ratio of the initial intensities of the 500 and 660 nm bands, each natural blue diamond has a specific combination of these parameters, which might be helpful in their identification. The Wittelsbach-Graff and Hope diamonds plot in the bottom to bottom-right portion of this graph (again, see figure 6) and have the longest-lasting red emissions of any natural blue diamonds measured to date.

At first glance, the phosphorescence spectra from the Hope and Wittelsbach-Graff diamonds (again, see figure 5) looked strikingly similar. The initial relative intensities of the 500 and 660 bands were nearly identical, and the relative decay times corresponded closely. In fact, no other blue diamond from the Eaton-Magaña et al. (2008) study exhibited phosphorescence behavior as similar to the Hope's

PHOSPHORESCENCE SPECTRA

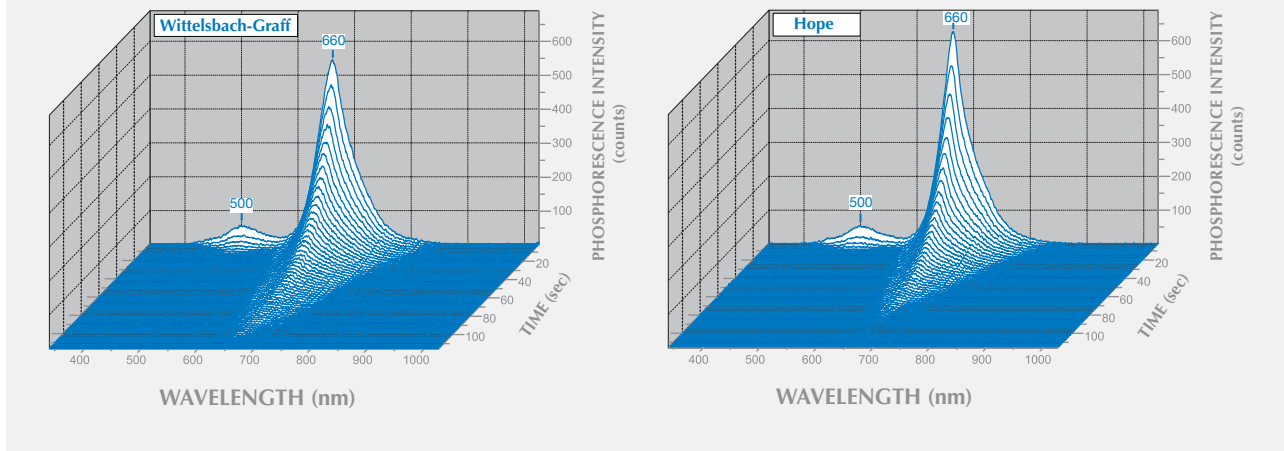


Figure 5. Some differences were seen in the phosphorescence spectra of the Wittelsbach-Graff and Hope diamonds. The Hope shows a greater initial intensity, at about 625 counts compared to 545, but its red (and even blue) phosphorescence fades sooner (85 seconds compared to 110). The abscissa spans just over the range of visible light. Each spectrum was acquired at two-second intervals, until the phosphorescence completely faded away.

as that of the Wittelsbach-Graff. On closer examination, however, the decay time of the Wittelsbach-Graff's 660 nm band was slightly but reproducibly longer than that of the Hope (again, see figure 5).

Both diamonds had a heterogeneous phosphorescence distribution, with initial intensity and half-life variations depending on the probed areas (table 2). This heterogeneity was not mentioned by Eaton-

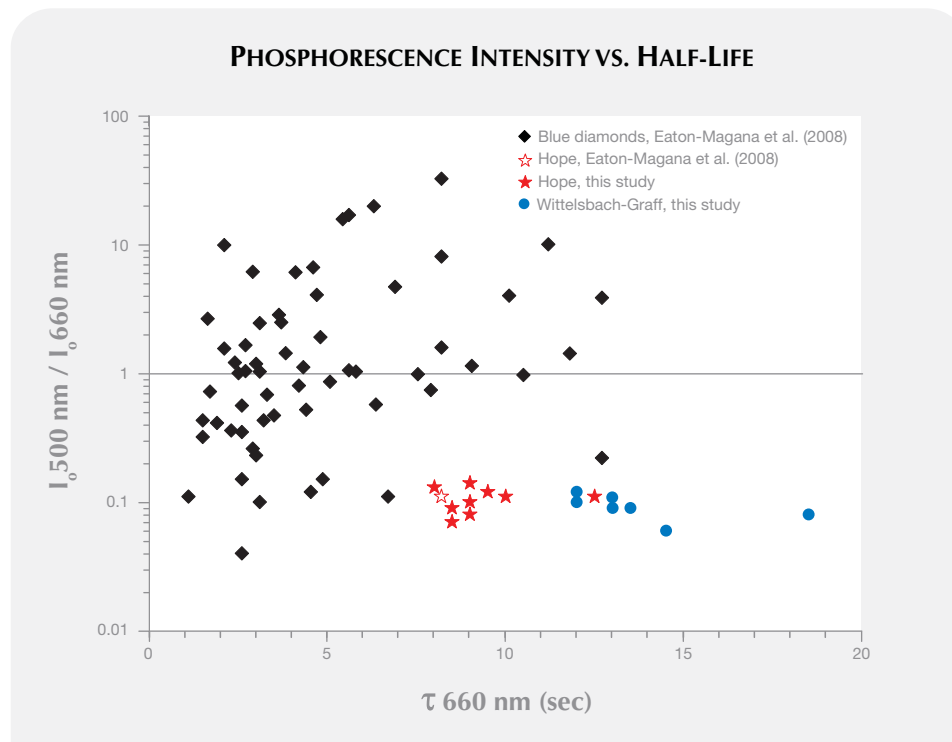


Figure 6. This graph of the phosphorescence data plots the ratios of initial intensities of the 500 and 660 nm bands against measured half-lives of the 660 nm emission for the Wittelsbach-Graff and Hope, compared to some natural type IIb diamonds (from Eaton-Magaña et al., 2008). For y-axis values greater than 1, the blue band dominates, whereas the red band dominates for values less than 1. The Hope and the Wittelsbach-Graff diamonds have extremely long-lasting red phosphorescence. " I_0 " represents initial intensity, and " τ " the half-life.

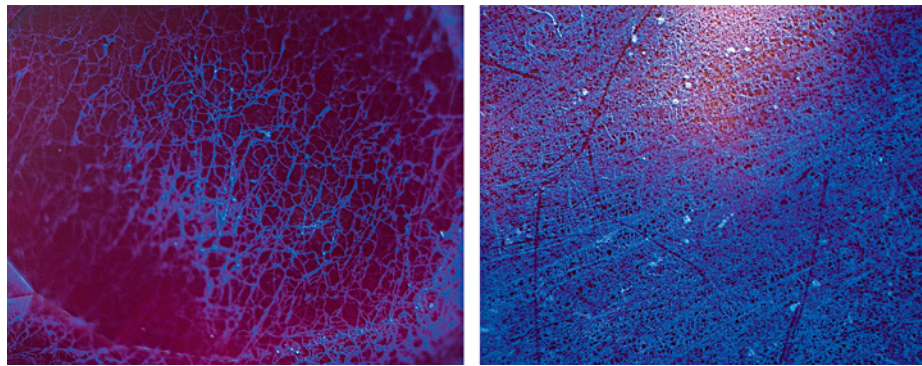


Figure 7. In these DiamondView images from the culet of the Wittelsbach-Graff (left) and table of the Hope (right), the texture of the mosaic patterns is much finer for the Hope (<100 μm vs. >200 μm). Fields of view 6.1mm (left), 6.4 mm (right); exposure time 2.8 seconds.

Magaña et al. (2008), who also examined the Hope diamond, possibly because the present study probed more areas on the diamonds.

In addition to the table and culet facets, spectra were collected from some of the crown facets, which produced the more extreme values. Curiously, phosphorescence intensity was stronger in the crown facets than in the culet and table for both diamonds, suggesting that the angle of illumination in large stones might affect their phosphorescence spectra. The average decay half-life of the 660 nm band for the Wittelsbach-Graff was ~14 seconds, compared to ~9 seconds for the Hope. (The 500 nm band decayed too quickly for a half-life measurement to be meaningful.) The cause of the 500 and 660 nm emissions is not fully understood, but it is

generally agreed that the phosphorescence is due to donor-acceptor pair recombination, and that the acceptor is boron. The fact that there are two emission bands with peaks at different energies suggests that two donor centers are involved, neither of which has been positively identified, although nitrogen may play a role (Watanabe et al., 1997; Eaton-Magaña et al., 2008).

In the ultra-short-wave UV excitation of the DiamondView, both diamonds exhibited a moderate-to-strong blue emission throughout the entire stone. The blue emission was not homogeneous, but formed a mosaic pattern (figure 7). This pattern has been observed previously in type II diamonds, and studies suggest that the cell walls of the mosaic network consist of dislocations (e.g., Hanley et al., 1977; Kanda et al., 2005). It is also known that the polygonization of these dislocations occurs during plastic deformation at high pressure and high temperature in the earth's lower crust/upper mantle (Kanda et al., 2005). Note that the scale and texture of the mosaic pattern was coarser in the Wittelsbach-Graff (mainly features >200 μm) than in the Hope (<100 μm). Doubling the imaging exposure time from 2.8 to 5.6 seconds revealed superimposed red phosphorescence for both diamonds, consistent with the phosphorescence results described above.

Last, when examined between crossed polarizers, the two diamonds exhibited dramatically different internal strain patterns (figure 8). The Wittelsbach-Graff displayed a typical "tatami" pattern (two directions of strain lamination), with gray and blue interference colors (figures 8A–8C) visible in all directions through the diamond. The Hope, on the other hand, showed a distinctly coarser banded internal strain pattern, predominantly in a single direction, with blue, orange, and red interference colors (figures 8D–8F). The components of the tatami patterns, oriented in the {111} planes, are due to strain caused by plastic deformation with little or

TABLE 2. Phosphorescence data acquired for the Hope and Wittelsbach-Graff diamonds.^a

Spectral interval (seconds)	Area probed	I_0 500 nm (arbitrary units)	I_0 660 nm (arbitrary units)	I_0 500 nm/ I_0 660 nm	τ 660 nm (seconds)
Hope					
0.5	Table-3	20.14	168.14	0.120	9.5
1	Table-1	18.71	277.86	0.067	8.5
1	Table-2	23.71	310.14	0.076	9
1	Table-5	28.71	295.57	0.097	9
1	Culet-1	38.43	283.86	0.135	9
1	Culet-2	29.71	234.71	0.127	8
1	Crown-1	43.14	375.29	0.115	10
1	Crown-2	30.29	268.43	0.113	12.5
2	Table-4	53.86	628.71	0.086	8.5
Wittelsbach-Graff					
0.5	Table-3	16.29	138.00	0.118	12
1	Table-1	25.57	245.57	0.104	12
1	Culet-1	8.29	145.14	0.057	14.5
1	Culet-2	15.86	169.14	0.094	13.5
1	Crown-1	30.71	328.57	0.093	13
1	Crown-2	21.43	253.86	0.084	18.5
2	Table-2	54.43	545.57	0.100	13

^a Abbreviations: I_0 = initial intensity, τ = half-life.

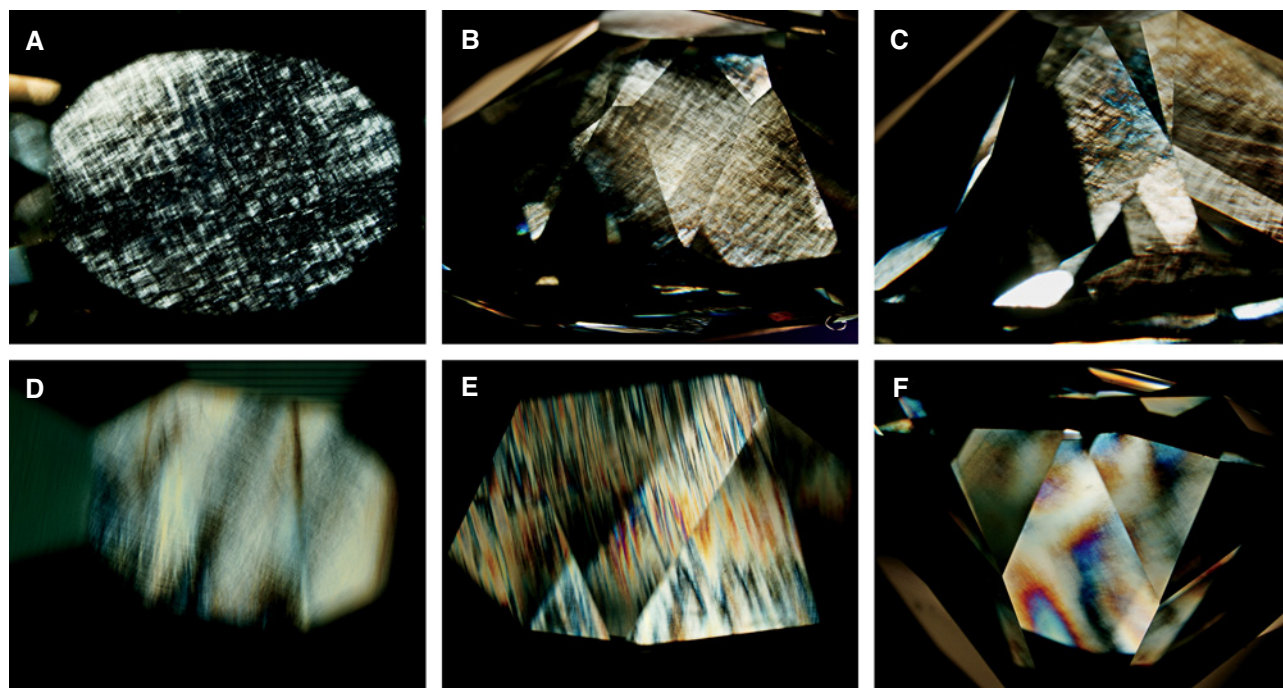


Figure 8. These images of the Wittelsbach-Graff (top row) and the Hope (bottom row) were taken in transmitted light with crossed polarizers. Both diamonds show internal strain, but with different patterns. The Wittelsbach-Graff displays the typical tatami pattern when viewed in all three directions: (A) through the culet, (B) through the longest side, and (C) through the shortest side. The Hope has strongly banded strain, shown here: (D) through the culet, (E) through the longest side, and (F) through the shortest side (which is perpendicular to the bands, so no strong direction of strain can be observed). A subtle tatami pattern can also be seen in the Hope. Fields of view: (A) 7.9 mm, (B) 11.8 mm, (C) 9.9 mm, (d) 3.8 mm, (E) 9.9 mm, (F) 14.8 mm. Photomicrographs by W. Wang.

no subsequent annealing (e.g., Hanley et al., 1977; Collins et al., 2000; Kanda et al., 2005).

CONCLUSION

Despite their uncanny similarities in history, color, and phosphorescence, our study clearly shows that the Wittelsbach-Graff and Hope diamonds did not originate from the same crystal. Small but signifi-

cant differences were observed in their red phosphorescence, as the Wittelsbach-Graff's is slightly longer and more intense. Major differences were noticed during the examination with crossed polarizers and in the luminescence patterns observed with the DiamondView. Nevertheless, their overall resemblance and common origin (India) suggest that both diamonds formed under similar geologic conditions.

ABOUT THE AUTHORS

Dr. Gaillou (asteriee@yahoo.fr) is a postdoctoral fellow at, and Dr. Post is the curator of, the National Gem and Mineral Collection at the Smithsonian Institution's National Museum of Natural History in Washington, DC. Dr. Wang is director of research and development, Mr. King is chief quality officer, and Mr. Moses is senior vice president, at the GIA Laboratory in New York. Dr. Butler is a consultant in Huntingtown, Maryland, retired from the Naval Research Laboratory in Washington, DC. Dr. Collins is emeritus professor of physics at King's College London.

ACKNOWLEDGMENTS

The authors are grateful to Dr. Sally Eaton-Magaña of the GIA Laboratory, who provided the original graph (figure 6) showing the phosphorescence of the Wittelsbach-Graff and the Hope. We also thank Drs. Christopher Welbourn and Ilene Reinitz for their reviews, which improved the quality of this article.


REFERENCES

- Attaway N. (2005) The French connection. *Lapidary Journal*, Vol. 59, No. 3, pp. 24–28.
- Balfour I. (2009) *Famous Diamonds*. Antique Collectors' Club, Woodbridge, Suffolk, UK, 335 pp.
- Collins A.T. (2010) Determination of the boron concentration in diamond using optical spectroscopy. Diamond Conference, University of Warwick, July 13–16 (unpublished abstract).
- Collins A.T., Williams A.W.S. (1971) The nature of the acceptor centre in semiconducting diamond. *Journal of Physics C: Solid State Physics*, Vol. 4, pp. 1789–1799.
- Collins A.T., Kanda H., Kitawaki H. (2000) Colour changes produced in natural brown diamonds by high-pressure, high-temperature treatment. *Diamond and Related Materials*, Vol. 9, pp. 113–122.
- Crowningshield R. (1989) Grading the Hope diamond. *G&G*, Vol. 25, No 2, pp. 91–94.
- Dröschel R., Evers J., Ottomeyer H. (2008) The Wittelsbach Blue. *G&G*, Vol. 44, No. 4, pp. 348–363.
- Eaton-Magaña S., Post J.E., Heaney P.J., Freitas J., Klein P., Walters P., Butler J.E. (2008) Using phosphorescence as a fingerprint for the Hope and other blue diamonds. *Geology*, Vol. 36, pp. 83–86.
- Farges F., Sucher S., Horovitz H., Fourcault J.-M. (2009) The French Blue and the Hope: New data from the discovery of a historical lead cast. *G&G*, Vol. 45, No. 1, pp. 4–19.
- Fisher D., Sibley S.J., Kelly C.J. (2009) Brown colour in natural diamond and interaction between the brown related and other colour-inducing defects. *Journal of Physics: Condensed Matter*, Vol. 21, article no. 364213 [10 pp.].
- Hanley P.L., Kiflawi I., Lang A.R. (1977) On topographically identifiable sources of cathodoluminescence in natural diamonds. *Philosophical Transactions of the Royal Society of London A*, Vol. 284, No. 1324, pp. 329–368.
- Kanda H., Abduriyim A., Kitawaki H. (2005) Change in cathodoluminescence spectra and images of type II high-pressure synthetic diamond produced with high pressure and temperature treatment. *Diamond and Related Materials*, Vol. 14, pp. 1928–1931.
- King J.M., Moses T.M., Shigley J.E., Welbourn C.M., Lawson S.C., Cooper M. (1998) Characterizing natural-color type IIb blue diamonds. *G&G*, Vol. 3, No. 4, pp. 246–268.
- Kurin R. (2006) *Hope Diamond: The Legendary History of a Cursed Gem*. Harper Collins, New York, 400 pp.
- Morel B. (1988) *The French Crown Jewels*. Fonds Mercator, Antwerp, 417 pp.
- Patch S.S. (1976) *Blue Mystery: The Story of the Hope Diamond*. Smithsonian Institution Press, Washington, DC.
- Sucher S.D., Attaway S.W., Attaway N.L., Post J.E. (2010) Possible “sister” stones of the Hope diamond. *G&G*, Vol. 46, No. 1, pp. 28–35.
- Watanabe K., Lawson S.C., Isoya J., Kanda H., Sato Y. (1997) Phosphorescence in high-pressure synthetic diamond. *Diamond and Related Materials*, Vol. 6, pp. 99–106.
- Welbourn C.M., Cooper M., Spear P.M. (1996) De Beers natural versus synthetic diamond verification instruments. *G&G*, Vol. 32, No. 3, pp. 156–169.

THANK YOU, REVIEWERS



GEMS & GEMOLOGY requires that all articles undergo a peer review process in which each manuscript is evaluated by at least three experts in the field. This process is vital to the accuracy and readability of the published article, but it is also time consuming for the reviewer. Because members of our Editorial Review Board cannot have expertise in every area, we sometimes call on other experts to share their intellect and insight. In addition to the members of our Editorial Review Board, we extend a heartfelt thanks to the following individuals who reviewed manuscripts for *G&G* in 2009.



Mr. Akiva Caspi
Dr. Robert Coenraads
Dr. François Farges
Dr. Eloïse Gaillou
Mr. Ron Geurts
Mr. Al Gilbertson
Dr. Lee Groat
Mr. Hertz Hasenfeld
Mr. John King
Mr. John Koivula
Ms. Maggie Pedersen
Dr. Federico Pezzotta
Dr. Ilene Reinitz
Dr. Andy Shen

What's *missing* from your collection?



Spring-Winter 2009

Spring 2006

"Paraíba"-type Tourmaline from Brazil, Nigeria, and Mozambique: Chemical Fingerprinting by LA-ICP-MS
 Identification and Durability of Lead Glass-Filled Rubies
 Characterization of Tortoise Shell and Its Imitations

Summer 2006

Applications of LA-ICP-MS to Gemology
 The Cullinan Diamond Centennial
 The Effects of Heat Treatment on Zircon Inclusions in Madagascar Sapphires
 Faceting Transparent Rhodonite from New South Wales, Australia

Fall 2006—Special Issue

Proceedings of the 4th International Gemological Symposium and GIA Gemological Research Conference

Winter 2006

The Impact of Internal Whitish and Reflective Graining on the Clarity Grading of D-to-Z Diamonds at the GIA Laboratory
 Identification of "Chocolate Pearls" Treated by Ballerina Pearl Co.
 Leopard Opal from Mexico
 The Cause of Iridescence in Rainbow Andradite from Japan

Spring 2007

Pink-to-Red Coral: Determining Origin of Color
 Serenity Coated Colored Diamonds
 Trapiche Tourmaline from Zambia

Summer 2007

Global Rough Diamond Production since 1870
 Durability Testing of Filled Diamonds
 Chinese Freshwater Pearl Culture
 Yellowish Green Diopside and Tremolite from Tanzania
 Polymer-Impregnated Turquoise

Fall 2007

The Transformation of the Cultured Pearl Industry
 Nail-head Spicule Inclusions in Natural Gemstones
 Copper-Bearing Tourmalines from New Deposits in Paraíba State, Brazil
 Type Ia Diamond with Green-Yellow Color Due to Ni

Winter 2007

Latest CVD Synthetic Diamonds from Apollo Diamond Inc.
 Yellow Mn-Rich Tourmaline from Zambia
 Fluorescence Spectra of Colored Diamonds
 An Examination of the Napoleon Diamond Necklace

Spring 2008

Copper-Bearing (Paraíba-type) Tourmaline from Mozambique
 A History of Diamond Treatments
 Natural-Color Purple Diamonds from Siberia

Summer 2008

Emeralds from Byrud (Eidsvoll), Norway
 Creating a Model of the Koh-i-Noor Diamond
 Coated Tanzanite
 Coloring of Topaz by Coating and Diffusion Processes

Fall 2008

Identification of Melee-Size Synthetic Yellow Diamonds
 Aquamarine, Maxixe-Type Beryl, and Hydrothermal Synthetic Blue Beryl
 A New Type of Synthetic Fire Opal: Mexifire
 The Color Durability of "Chocolate Pearls"

Winter 2008

Color Grading "D-to-Z" Diamonds at the GIA Laboratory
 Rubies and Sapphires from Winza, Tanzania
 The Wittelsbach Blue

Spring 2009

The French Blue and the Hope: New Data from the Discovery of a Historical Lead Cast Gray-Blue-Violet Hydrogen-Rich Diamonds from the Argyle Mine
 Hackmanite/Sodalite from Myanmar and Afghanistan
 Pink Color Surrounding Growth Tubes and Cracks in Cu Tourmalines from Mozambique
 Identification of the Endangered Pink-to-Red Stylaster Corals by Raman Spectroscopy

Summer 2009

Celebrating 75 Years of *Gems & Gemology*
 The "Type" Classification System of Diamonds
 Spectral Differentiation Between Copper and Iron Colorants in Gem Tourmalines
 Andalusite from Brazil
 Peridot from Sardinia, Italy

Fall 2009

Characterization of "Green Amber"
 Crystallographic Analysis of the Tavernier Blue "Fluorescence Cage": Visual Identification of HPHT-Treated Type I Diamonds
 Ammolite Update
 Polymer-Filled Aquamarine
 Yellow-Green Haiyue from Tanzania
 Aquamarine from Masino-Bregaglia Massif, Italy

Winter 2009

Ruby and Sapphire Production and Distribution: A Quarter Century of Change
 Cutting Diffraction Gratings to Improve Dispersion ("Fire") in Diamonds
 Chrysoprase and Prase Opal from Haneti, Central Tanzania
 Demantoid from Val Malenco, Italy

GEMS & GEMOLOGY[®]

The Quarterly Journal
 That Lasts A Lifetime

Now Available
 Online:

All Articles
 and Issues 1981–2009

Get PDF Articles at
gia.metapress.com

Electronic (PDF) versions of all articles from Spring 1981 forward are available as part of *Gems & Gemology* Online.

Order Print and PDF

Back Issues at store.gia.edu

or Call Toll Free 800-421-7250 ext. 7142

or 760-603-4000 ext. 7142

Fax 760-603-4070

E-Mail gandg@gia.edu

or write to

Gems & Gemology

PO Box 9022, Carlsbad, CA

92018-9022, USA

Complete volumes of 1992–2009 print back issues are available, as are limited issues from 1985–1991.

10% discount for GIA Alumni and active GIA students.

Order Your
BACK ISSUES
 CHARTS & BOOKS

Today!



PLAY-OF-COLOR OPAL FROM WEGEL TENA, WOLLO PROVINCE, ETHIOPIA

Benjamin Rondeau, Emmanuel Fritsch, Francesco Mazzero, Jean-Pierre Gauthier,
Bénédicté Cenki-Tok, Eyassu Bekele, and Eloïse Gaillou

A new opal deposit was discovered in 2008 near the village of Wegel Tena, in volcanic rocks of Ethiopia's Wollo Province. Unlike previous Ethiopian opals, the new material is mostly white, with some brown opal, fire opal, and colorless "crystal" opal. Some of it resembles Australian and Brazilian sedimentary opals, with play-of-color that is often very vivid. However, its properties are consistent with those of opal-CT and most volcanic opals. Inclusions consist of pyrite, barium-manganese oxides, and native carbon. Some samples show "digit patterns": interpenetrating play-of-color and common opal, resembling fingers. The opaque-to-translucent Wegel Tena opals become transparent when soaked in water, showing a remarkable hydrophane character. White opals from this deposit contain an elevated Ba content, which has not been reported so far in opal-CT. The fire and crystal opals are prone to breakage, while the white, opaque-to-translucent opals are remarkably durable. The proportion of gem-quality material in the Wegel Tena deposit seems unusually high, and 1,500 kg have already been extracted using rudimentary mining techniques. The deposit may extend over several kilometers and could become a major source of gem-quality opal.

In early 2008, a new source of play-of-color opal was discovered by farmers near Wegel Tena in northern Ethiopia (Fritsch and Rondeau, 2009; Mazzero et al., 2009; Rondeau et al., 2009). Since January 2009, the deposit has been worked by about 200 local miners. The opals are mostly white, which is uncommon for play-of-color volcanic opal, and may resemble material from Australia or Brazil (figure 1). Some fairly large pieces have been polished (figures 2 and 3). The Wegel Tena opals differ from those found at Mezezo, in Ethiopia's Shewa Province, or in neighboring Somalia, which are mostly orange to red to brown (e.g., Koivula et al.,

1994; Gauthier et al., 2004, and references therein).

Two of the authors (FM and EB) traveled to the locality on several occasions. They gathered representative gem material, as well as surrounding rocks, and discussed the opal and its extraction with the miners to develop a better understanding of this promising new deposit.

LOCATION AND ACCESS

The opal mining area lies in Wollo Province (also spelled Wolo or Welo), ~550 km north of Addis Ababa and ~200 km north of the Mezezo opal deposit (figure 4). The locality has also been referred to as "Delanta," which corresponds to a former subdivision (or "awraja") of Wollo Province. The region containing the deposit is called Tsehay Mewcha, a large area that encompasses scattered farms and a small village, about 17 km northeast of the village

See end of article for About the Authors and Acknowledgments.
GEMS & GEMOLOGY, Vol. 46, No. 2, pp. 90–105.
© 2010 Gemological Institute of America

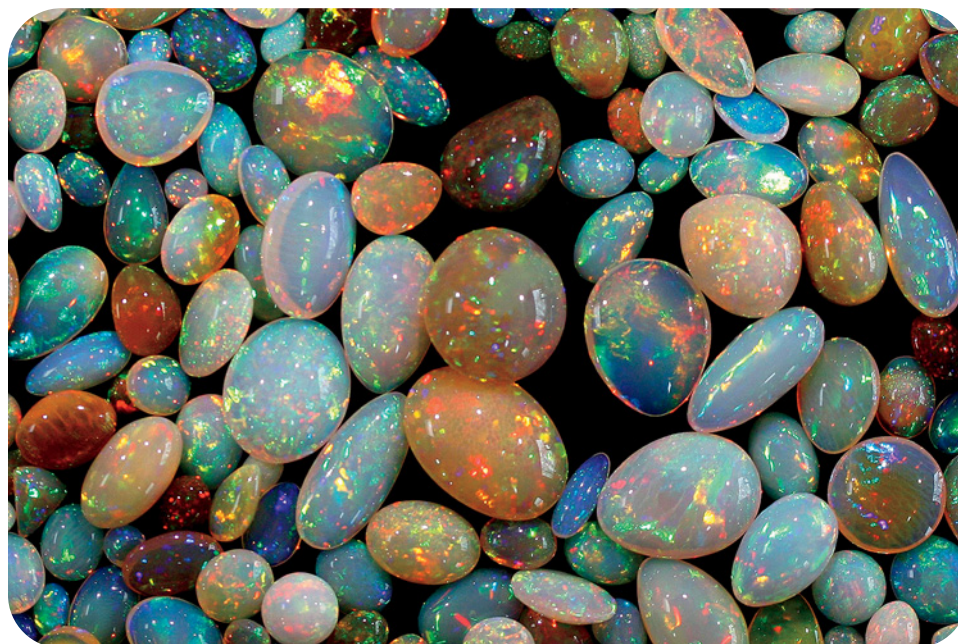


Figure 1. Volcanic play-of-color opals mined at Wegel Tena, Ethiopia, are mostly white, translucent to opaque, and show vivid play-of-color. The round orange cabochon in the center weighs 41.70 ct, and the white cabochon to its right is 31.30 ct. Photo by F. Mazzero.

of Wegel Tena (figure 4). Tsehay Mewcha is situated on a plateau at an altitude of about 3,200 m. The opal occurs in a horizontal layer that is exposed on a cliff above a canyon tributary of the Blue Nile River. This layer is ~350 m below the top of the plateau (figure 5). Tsehay Mewcha is accessible with a four-wheel-drive vehicle, and the various mine workings are reached by walking down the steep canyon for 30 minutes to more than one hour. Hazardous conditions are created by cliffs in the digging areas, as well as by falling rocks due to mining activities (see www.opalinda.com for more information on access conditions).

GEOLOGY

The entire region around Wegel Tena consists of a thick (>3,000 m) volcano-sedimentary sequence of alternating layers of basalt and rhyolitic ignimbrite. The layers of basalt or ignimbrite are a few meters to hundreds of meters thick. (Ignimbrite is a vol-

canic rock of andesitic-to-rhyolitic composition that forms sedimentary-like layers after the volcanic plume collapses and falls to the ground. The particles that form this rock are a heterogeneous mixture of volcanic glass, crystals, ash, and xenoliths.) This volcanic sequence was emplaced with the opening of the East African continental rift during the Oligocene epoch (Cenozoic age), about 30 million years ago (Ayalew and Yirgu, 2003; Ayalew and Gibson, 2009).

Over the entire volcanic series, only one very thin seam (<1 m thick), hosted by ignimbrite, is mineralized with opal (again, see figure 5). Common opal and play-of-color opal most often cement grains of volcanic debris (figures 6 and 7) or sometimes fill in fractures or cavities in the rock. As a result, the rough gem material often has an irregular shape. Microscopic examination of our samples revealed that, for the most part, the host rock consists of mixed altered material, including clays,



Figure 2. Some of the large, fine white opal specimens from Wegel Tena display vivid play-of-color, such as the 20.95 ct oval and 14.87 ct round cabochons shown here. Photos by F. Mazzero (left) and Robert Weldon (right).

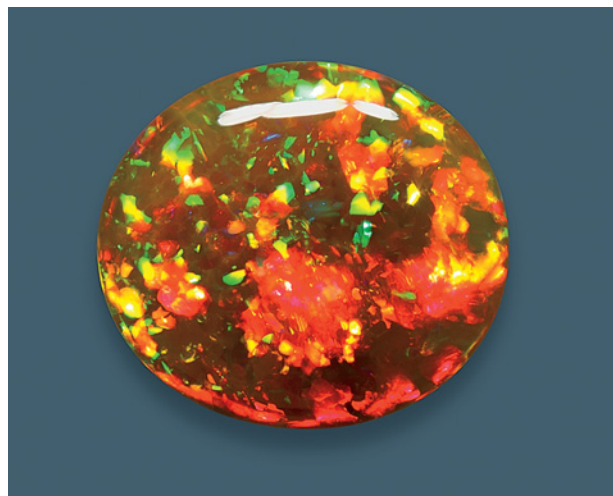


Figure 3. This 9.12 ct specimen, which measures 17 × 19 mm, is one of the few play-of-color fire opals that have been mined at Wegel Tena. Photo by F. Mazzero.

common opal, and some minor iron oxy-hydroxides. Some large crystals of alkali feldspar were unaltered, while others were transformed into clays. By comparison, the ignimbrite sampled only a few meters above the opal-bearing layer was unaltered and contained abundant quartz crystals.



Figure 4. The opal deposit is located in north-central Ethiopia, close to the village of Wegel Tena.



MINING AND PRODUCTION

The opal is extracted by artisanal miners using homemade tools (figures 8 and 9), as well as picks, hammers, and shovels provided by the Ethiopian government. The mineralized layer extends for hundreds of meters along the flank of the canyon (again, see figures 5 and 8), but the excavations only penetrate 1–2 m into the mountain. Because the diggings are not supported by timbers or other means, mining is very dangerous in some extensively worked places. Tragically, at least 20 miners have died from collapsing rock. The miners are organized in cooperatives that control the distribution of the rough opal sold to gem dealers and eventually cutters in Addis Ababa. Opal production has been significant, with over 1,500 kg of rough extracted to date.

MATERIALS AND METHODS

We examined hundreds of rough and polished samples to determine the typical characteristics for this locality. We selected 33 samples to document the gemological properties and note interesting inclusions and growth features, hydrophane character, matrix, and the like (table 1). Eight of these were fashioned as cabochons of various shapes and colors (4.43–18.85 ct). The other 25 samples consisted of rough pieces ranging from ~4 to 965 g (e.g., figure 7), and most contained significant portions of play-of-color opal. Some had considerable matrix material. Several of these were sliced or crushed for specific testing, as detailed below.

Selected samples were examined by standard gemological methods to determine their refractive index, hydrostatic specific gravity, and microscopic features (see table 1). Play-of-color was observed with the stone against a dark background (when necessary), and spot illumination placed above, behind (when appropriate), and then perpendicular to the viewing direction (the latter to observe any *contra luz* effect, i.e., play-of-color revealed by transmitted light). Luminescence was observed with long- and short-wave UV radiation using 6-watt lamps.

We tested the hydrophane character of 14 samples by observing the specific gravity, transparency, and play-of-color before and after immersing the samples in water for a few minutes to one hour. For the same 14 stones, the following optical tests were conducted: Polarization behavior was studied using a GIA Instruments polariscope, absorption spectra were observed with an OPL prism-type spectroscope, and the Chelsea filter reaction was determined with illu-

mination from a strong halogen lamp.

Fourier-transform Raman spectra were recorded on all samples using a Bruker RFS 100 spectrometer. Each spectrum included 1,000 scans to increase the signal-to-noise ratio, as opal is a poor Raman scatterer.

The microstructure of five samples (1071, 1073, 1074, 1076, and 1101) was investigated with a JEOL 7600 scanning electron microscope (SEM) equipped with a hot cathode/field-effect electron gun, and a Hitachi H9000-NAR transmission electron micro-

NEED TO KNOW

- Play-of-color opal has been mined from volcanic deposits near Wegel Tena (Wollo Province) since 2008.
- The bodycolor is typically white, with some brown, fire, and colorless “crystal” opal.
- As with other Ethiopian opal, some of the material shows “digit patterns” of interpenetrating play-of-color and common opal.
- The opaque-to-translucent opals from Wegel Tena become transparent when soaked in water (hydrophane), are resistant to crazing, and are remarkably durable.

scope (TEM) operated at 10 kV. TEM samples were obtained by crushing a small piece of each sample with a mortar and pestle. The chemical composition of eight representative samples (1071, 1073, 1074, 1076, 1078, 1100, 1111, and 1121), their inclusions, and accompanying minerals (in samples 1100, 1106, 1113, and 1122) was measured by energy-dispersive spectroscopy (EDS) with a Princeton Gamma Tech IMIX-PTS detector installed on a JEOL 5800LV SEM. We prepared two thin sections (30 μm thick) of the opal’s host rock for petrographic microscopy and analysis of the minerals by EDS.

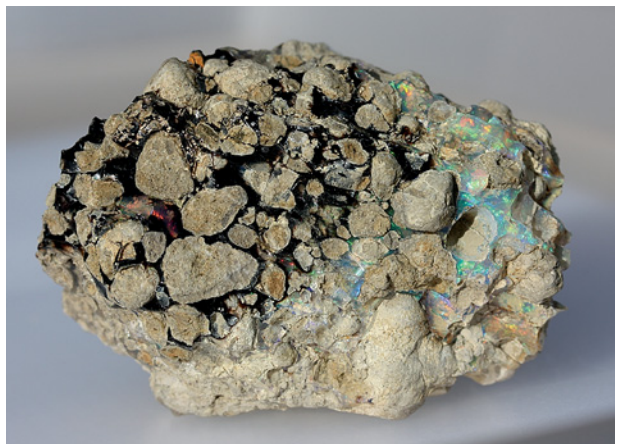
We conducted preliminary analyses of trace-element composition by laser ablation–inductively coupled plasma–mass spectrometry (LA-ICP-MS) at the Institute of Geological Sciences in Bern. We investigated two rough samples representative of the marketable opal: one white translucent and the other zoned white translucent and orange transparent, both with play-of-color. (These are not listed in table 1 because they were examined apart from the other samples and only with the LA-ICP-MS technique.) The LA-ICP-MS system consisted of a



Figure 5. The opal deposit consists of a thin horizontal layer (see arrow) in the cliffs above a canyon. It is located ~350 m below the top of the plateau. The cliffs consist of alternating layers of basalt and rhyolitic ignimbrite. Photo by F. Mazzero.

pulsed 193 nm ArF excimer laser with an energy-homogenized beam profile coupled with an Elan DRCE quadrupole mass spectrometer. Laser parameters were set to 16 J/cm² energy density on the sample, with a pulse duration of 15 ns and a repetition rate of 10 Hz. Pit sizes were 60 and 90 μm . The laser-ablation aerosol was carried to the ICP-MS by a mixed He-H₂-Ar carrier gas. Details on the LA-ICP-MS measurement conditions are available in

Figure 6. The opal typically fills spaces between pieces of volcanic rock debris, acting as a cement. The black areas in this sample also consist of opal, together with Ba-Mn oxides. This 105 g specimen measures 7 × 5 × 3 cm. Photo by F. Mazzero.



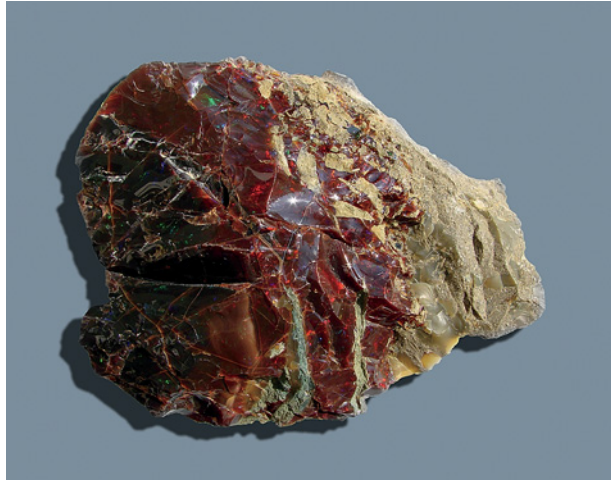


Figure 7. Some rare samples of Wegel Tena opal showed a dark “chocolate” brown bodycolor with play-of-color. This exceptional 965 g specimen, which also demonstrates how the opal occurs in matrix, is on permanent display at the Museum of Natural History in Nantes, France. Photo by F. Mazzero.

the *G&G* Data Depository (gia.edu/gandg).

Stability to crazing was assessed after cutting and preforming by one of us (FM) who has handled numerous Wegel Tena opals since their discovery. A few representative samples from various Wegel Tena parcels were kept at ambient temperature and humidity, and visually observed over time. As part of a proprietary fashioning process, about 50 high-quality play-of-color Wegel Tena opals were cycled between water and air (at room temperature) for one

Figure 8. Miners at Wegel Tena often use rudimentary tools, such as the hammer and chisel shown here, to extract the opal from the exposed seam along the flank of the canyon. Photo by Thomas Cenki.



hour and then longer periods (up to several days).

We tested for toughness by dropping five fashioned opals on a concrete surface from a height of ~1.5 m, to simulate dropping a stone by accident.

RESULTS

The standard gemological properties are summarized in tables 1 and 2 and presented below.

Visual Appearance and Optical Phenomena. From observing hundreds of rough and faceted samples, we determined that most opals from Wegel Tena have a white bodycolor, while some are pale yellow and a few are darker orange (fire opal) to brownish red (again, see figures 2 and 3). Rare samples have a dark “chocolate” brown bodycolor (again, see figure 7). Some zoned samples show several layers of contrasting bodycolor and play-of-color (figure 10).

The opals range from opaque to transparent, but most are translucent. Because the material is turbid, it scatters light efficiently, creating the white bodycolor typical of this deposit. Some of the highest-quality opals are translucent and display a blue scattering bodycolor (figure 11).

Among the 33 samples tested, we observed that all opaque-to-translucent samples became more transparent when immersed in water for a few minutes to one hour, depending on the thickness of the sample. This behavior is typical of hydrophane. There were several degrees of change, the most dramatic being a transformation from opaque white to transparent colorless (figure 12). During this process, play-of-color appeared to strengthen. This phenomenon was fully reversible in one to a few hours, depending on ambient humidity and the thickness of the gem.

The opals typically displayed a mosaic of pure spectral color patches against a translucent white bodycolor. Generally all spectral colors (from red to violet) were observed in the play-of-color samples, often with large patches of red and orange. The intensity of the play-of-color varied on the millimeter scale, from intense to none, even within the same sample. We did not notice any *contra luz* material (which is typically transparent).

Play-of-color was commonly distributed along parallel columns that resembled fingers. We refer to such features as *digit patterns* (figure 13). The play-of-color digits were embedded within common opal of slightly different color or transparency. Their cross-section was rounded, or sometimes quite polygonal when there was little interstitial common



Figure 9. Note the carved wooden pick used by some of these miners to extract the rough opal at Wegel Tena. Photo by F. Mazzero.

opal present. The digits' tips were often rounded. Some samples showed planar zoning of common and play-of-color opal that we interpreted as horizontal. When digit patterns were observed in such samples, they were always perpendicular to these planes (figures 10 and 14). Digit patterns were seen in nine of the 33 samples (nos. 1072, 1104, 1105, 1109, 1111, 1113, 1114, 1121, and 1122).

Figure 10. The strong zoning of this exceptional 18.68 ct cabochon represents most of the opal varieties found at Wegel Tena: brownish orange to white, transparent to opaque, with and without play-of-color. The zoning probably corresponds to successive deposition of horizontal opal layers in a cavity. The white layer with strong play-of-color shows parallel columns that we refer to as digit patterns. Note that they are perpendicular to the plane of zoning, which means they developed vertically. Photo by Robert Weldon.



Some much rarer play-of-color features also have been observed in Wegel Tena opals. The cabochon in figure 15 (sample 1075) showed diffraction concentrated in points (not patches) that moved together in a synchronized fashion and changed color when the stone was tilted, or the intense pinpoint light source moved around. This revealed a perfect organization of the silica spheres that was distributed throughout the entire cabochon (pseudo single crystal; Fritsch and Rondeau, 2009). This “perfect diffraction” of light is seen only very rarely in natural gem opals. For a video and more comments on this phenomenon, see

Figure 11. The highest-quality opals, such as this 20.62 ct cabochon, are translucent and display a blue body-color due to light scattering. Photo by Robert Weldon.



TABLE 1. Characteristics of the 33 Wegel Tena opal samples studied for this report.^a

Sample no.	Description	Size ^b	Bodycolor	POC	Hydrophane character	RI
1071	Round cabochon, then sawn; partly broken for SEM	5.07 ct	Translucent light yellow	Green to red	na	1.37, 1.38
1072	Truncated cone	8.19 ct	Nearly opaque white	All colors	Str	na
1073	Double cabochon, then sawn; partly broken for SEM	6.95 ct	Nearly opaque white	All colors	Mod	1.42, 1.44
1074	Formerly a cabochon; broken for SEM	~15 x 6.3 x 4.7 mm	Nearly opaque whitish yellow	All colors	na	na
1075	Elongated sphere	4.43 ct	Translucent white	Pinpoint diffraction	na	na
1076	Oval cabochon, then sawn; partly broken for SEM	~14 x 9 x 3.5 mm	Transparent light yellow	Violet to green	Wk	1.37
1077	Pyramidal cabochon	4.94 ct	Translucent whitish yellow	All colors	Wk	1.36, 1.40
1078	Large rough with matrix; thin section	~50 x 35 x 20 mm	Dark "chocolate" brown	All colors	None	na
1084	Rough nodule, cut in two halves	24.0 g	Transparent orange with a large white "egg" in the core	None	na	na
1099	Rough nodule	8.21 g	Translucent white rim + orange core	Violet in rim, none in core	na	na
1100	Rough, with long, tubular inclusions	3.82 g	Colorless	All colors	None	na
1101	Rough	4.44 g	Transparent orange	All colors	na	na
1103	Rough, broken because of instability	9.81 g	Transparent orange	None	na	na
1104	Rough, broken nodule with a little matrix	4.88 g	Translucent orange + opaque rim	All colors (none in rim)	na	na
1105	Rough, broken nodule with a little matrix	11.61 g	Opaque white rim + transparent orange core	All colors	na	na
1106	Rough, broken nodule with a little matrix, including black coating	4.69 g	Translucent white rim + translucent orange core	All colors	na	na
1107	Rough, broken nodule with a little matrix	16.9 g	Opaque white rim + colorless core	All colors in rim, none in core	na	na
1108	Matrix with few opal veins	28.17 g	Transparent to opaque, orange to colorless	Violet to green	na	na
1109	Rough nodule	23.83 g	Opaque white	All colors	na	na
1110	Rough, broken nodule with a little matrix	42.96 g	Transparent orange	Green to red	None	na
1111	Rough nodule with a little matrix; thin section	49.53 g	Layered, from opaque white to colorless and yellow	All colors	na	na
1112	Rough, broken nodule with a little matrix	81.33 g	Colorless	All colors	None	na
1113	Rough, broken nodule with a little matrix	34.42 g	Colorless with translucent white rim	All colors	na	na
1114	Oval cabochon	7.21 ct	Translucent yellow	All colors	na	na
1116	Rough nodule, sliced into 2 plates	19.68 g	Nearly opaque white	All colors	V str	na
1117	Rough nodule, sliced into 1 plate	16.07 g	Nearly transparent	Violet to green	Wk	na
1118	Rough nodule, sliced into 3 plates	28.67 g	Nearly opaque white	All colors	V str	1.37, 1.42, 1.52
1119	Rough nodule, sliced into 3 plates	40.0 g	Nearly opaque white	All colors	V str	na
1120	Rough nodule, sliced into 1 plate	6.71 g	Transparent	Violet to green	Wk	na
1121	Rough nodule with a little matrix; thin section	25.29 g	Layered translucent yellow to white	All colors	na	na
1122	Rough nodule with fractures filled with black material	12.65 g	Translucent yellow to orange	All colors	na	na
1123	Double cabochon with green inclusions	18.85 ct	Opaque white	All colors	na	na
1124	Rough, in matrix	~100 x 60 x 30 mm	Dark "chocolate" brown	All colors	None	na

^a Abbreviations: *Cont* = continuous, *inter* = interference, *Mod* = moderate, *na* = not analyzed, *POC* = play-of-color, *sec* = seconds, *Str* = strong, *V* = very, *Wk* = weak.

^b Weights were measured before soaking.

^c All dominantly white luminescence is turbid by definition.

UV fluorescence ^c		Phosphorescence ^c		Chelsea filter	Polariscope	Hand spectroscope
Long-wave	Short-wave	After long-wave	After short-wave			
Wk yellowish white	Turbid, wk-to-mod whitish yellow	Inert	Inert	Red, because of green diffraction	Cont change of inter colors; no extinction	Cutoff in violet and blue
Turbid, str whitish green	Turbid, str whitish green	Inert	Inert	Red, because of green diffraction	No reaction	Cutoff in violet and blue
Mod bluish white	Wk bluish white	Wk-to-mod green, few sec	Mod green, few sec	Red, because of green diffraction	Cont change of inter colors; no extinction	No absorption
Inert	Inert	Inert	Inert	Opaque	na	Cutoff in violet and blue
Mod bluish white	Mod yellowish white	Wk green, few sec	Wk green, few sec	Red to orangy red	Reflects the inter patterns	Cutoff in violet and blue
Wk bluish white	Wk bluish white	V wk green, few sec	Wk green, few sec	No reaction	Anomalous hues	Cutoff in violet and blue
Wk yellowish white	V wk to wk yellowish white	Wk yellowish green, 10 sec	V wk	Partly red	Cont change of inter colors; no extinction	Cutoff in violet and part of blue
Inert	Inert	Inert	Inert	na	na	na
Inert	Inert	Inert	Inert	na	na	na
Rim: wk white; core: inert	Rim: V wk white; core: inert	Inert	V wk, few sec	Red to orange	No reaction, diffusion of light	Cutoff in violet and blue
Wk blue	V wk whitish blue	Str whitish blue, ~18 sec	Mod white, ~6 sec	na	na	na
Inert	Inert	Inert	Inert	Deep red	No reaction	na
Turbid, mod green	V wk green	Inert	White, 10 sec	No reaction	No reaction	Cutoff in violet and blue
Rim: yellowish white; core: inert	Rim: yellowish white; core: inert	V wk	V wk, 3-4 sec	na	na	na
Rim: str white; core: inert	Homogeneous, str bluish white	V wk	Inert	Red	Cont change of inter colors; no extinction	Cutoff in violet and blue
Rim: wk yellowish green; core: inert	Core: inert; rim: wk yellowish green	Inert	Inert	Red (rim only)	No reaction	Partly absorbs violet
Rim: str white; core: mod white	Rim: mod white; core: str green	Mod white, 10 sec	Mod green, 8 sec	No reaction	No reaction	No absorption
Wk to V wk greenish white in colorless opal, inert in orange	Wk greenish white in colorless opal, inert in orange	Inert	Inert	na	na	na
Wk-to-mod bluish white	Wk-to-mod bluish white	Mod white, 10 sec	Mod greenish white, 12 sec	Deep red	Extinction every 90°	Cutoff in violet and blue, partly absorbs green
V wk	Inert	Inert	Inert	na	na	na
Homogeneous, wk bluish white	Homogeneous, wk bluish white	Mod white, 15 sec	Wk bluish white, 20 sec	na	na	na
Wk greenish white	Wk yellowish white	Inert	Wk white, 10 sec	na	na	na
Wk bluish white	Wk bluish white	Str white, 15 sec	Greenish white, 20 sec	Partly red	No reaction	Cutoff in violet, partly absorbs blue
Turbid, mod-to-str whitish yellow	Wk-to-mod greenish white	Few sec	Few sec	na	na	na
Mod-to-str blue-white	Mod blue-white	Mod-to-str blue-white, 10 sec	Wk-to-mod white, ~5 sec	na	na	na
Mod-to-str whitish blue	Mod whitish blue	Wk white, ~2 sec	Wk white, ~2 sec	na	na	na
Mod-to-str white	Mod white	Mod white, ~7 sec	Mod white, ~7 sec	na	na	na
Mod-to-str white	Mod-to-str white	Mod white, ~7 sec	Mod white, ~7 sec	na	na	na
Wk bluish white	Wk white	Wk bluish white, ~4 sec	Wk white, ~3 sec	na	na	na
Mod-to-str white	Wk white	Mod white, ~7 sec	Mod white, ~5 sec	na	na	na
Mod white in yellow opal, inert in orange	Wk white in yellow opal, inert in orange	Mod white, ~7 sec	Wk white, ~3 sec	na	na	na
Mod white	Wk-to-mod white	Wk white, ~3 sec	Wk white, ~2 sec	na	na	na
Inert	Inert	Inert	Inert	na	na	na

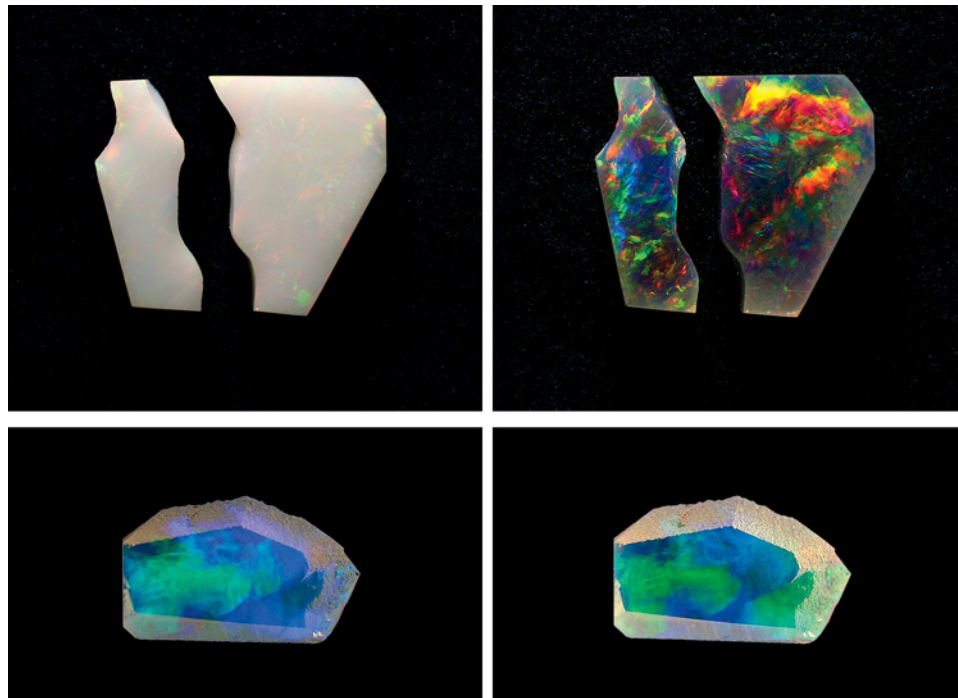


Figure 12. The opaque-to-translucent opal samples we examined became more transparent after immersion in water, as demonstrated by the top photos (samples 1118b and c; 3.96 and 4.68 ct). The sample in the bottom photos (no. 1120, 1.50 ct) showed little change, as it was already quite transparent before immersion. Photos by B. Rondeau.

www.gemnant.es.fr/research/opal/index.php#reciproque.

Another rare optical phenomenon seen in one opal that we were only able to keep for a short time was the presence of small, curved rainbows of diffraction (figure 16). Usually in play-of-color opals, each patch of diffraction is homogeneous in color. Here, the spectral colors within each patch were diffracted along a small area, ranging from 1 to

Figure 13. This spectacular 11.91 ct opal specimen provides a good example of digit patterns: columnar zones of transparent play-of-color opal within a network of common opal of similar bodycolor. Photo by Robert Weldon.



5 mm. For a video of this phenomenon, see www.gemnant.es.fr/research/opal/index.php#rainbow.

Specific Gravity. SG values (before being soaked in water) ranged from 1.74 to 1.89. After immersion in water for less than one hour, some samples weighed as much as 10.2% more, resulting in higher SG values of 1.90 to 2.00 (table 2). This effect, related to the samples' porosity, was fully reversible and repeatable.

Refractive Index. Because of the opals' porosity, we measured the refractive index of only five samples. In some instances, reaction with the contact liquid

Figure 14. This opal (no. 1121, 25.29 g) shows parallel zoning with the digits developed vertically, perpendicular to this layering. Photo by B. Rondeau.

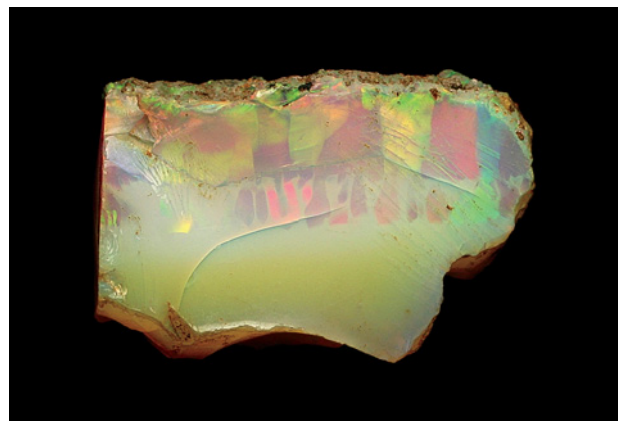


TABLE 2. Specific gravity of representative Wegel Tena opals.

Sample no.	Transparency before/after soaking	Weight (ct) before/after soaking	Weight increase (% of dry weight)	SG before/after soaking
1116a	Nearly opaque white/ transparent	2.54/2.69	5.6	1.87/1.95
1116b		0.53/0.56	5.3	1.89/2.00
1117	Nearly transparent/ transparent	5.07/5.63	9.9	1.77/1.91
1118a	Nearly opaque white/ transparent	1.95/2.17	10.1	1.74/1.90
1118b		3.96/4.38	9.6	1.80/1.91
1118c		4.68/5.17	9.5	1.79/1.91
1119a	Nearly opaque white/ transparent	8.01/8.60	6.7	1.82/1.94
1119b		5.01/5.40	7.2	1.82/1.94
1120	Transparent/transparent	1.50/1.67	10.2	1.76/1.92

caused white opaque spots to form on the opal, adversely affecting the gem's transparency and even its UV luminescence. RI values measured on sample 1073 were 1.42 and 1.44. However, we measured RIs as low as 1.36 to 1.38 on other samples (1071, 1076, and 1077). Some indices were easy to read, but most were difficult or simply impossible. Surprisingly, sample 1118a, a plate, showed an RI of 1.37 on one face and two indices on the other: 1.42 and a very sharp reading at 1.52.

Luminescence. UV luminescence was quite variable, ranging from bluish white to greenish white, yellow, and green. Luminescence intensity ranged from inert to strong. All brown samples or zones were inert. In long-wave UV, most non-brown samples had weak to very weak luminescence that was fairly turbid, and bluish to greenish white, with weak to very weak greenish white phosphorescence that lasted a few seconds. The typical short-wave UV reaction was slightly weaker, though the phosphorescence sometimes lasted longer. Some samples—particularly white opals with very good play-of-color—luminesced more strongly, with a moderate, mostly white fluorescence. One transparent, near-colorless, play-of-color opal had a strong, pure green luminescence.

Polariscope Reaction. Seven transparent light color stones, with and without play-of-color, showed no reaction viewed between crossed polarizing filters. Five translucent stones with play-of-color showed cyclic variations in diffraction colors as the stones were rotated a full 360°. Two opals (no. 1076 and 1109) showed anomalous double refraction (ADR).

Optical Absorption Spectrum. No spectrum was seen in the two lighter-color, transparent stones tested with the hand spectroscope. The remaining 12 milky or orange-to-brown stones showed absorption in the violet and blue regions, sometimes extending

into the green. This absorption increased with the amount of light scattered by the stone (from slightly milky to white), the darkness of the bodycolor (from yellow to brown), and the thickness of the sample.

Color Filter. Three transparent, light-colored gems showed no reaction when viewed through the Chelsea color filter. Eleven transparent brown or strongly diffusing (milky to white) opals appeared orange to bright red.

Inclusions. One sample (no. 1100) contained elongated, cylindrical inclusions measuring approximately 800 $\mu\text{m} \times 1 \text{ cm}$ (figure 17). Their surface was very irregular. EDS showed that these “tubes” were filled with silica, which may correspond to chalcedony. The outside surface of the inclusions also consisted of silica. They appeared more difficult to

Figure 15. This very unusual opal (no. 1075, 4.43 ct) displays a perfect diffraction pattern. Spectral colors formed small points that moved in a synchronized fashion and changed color when the light source was moved. Photo by B. Rondeau.

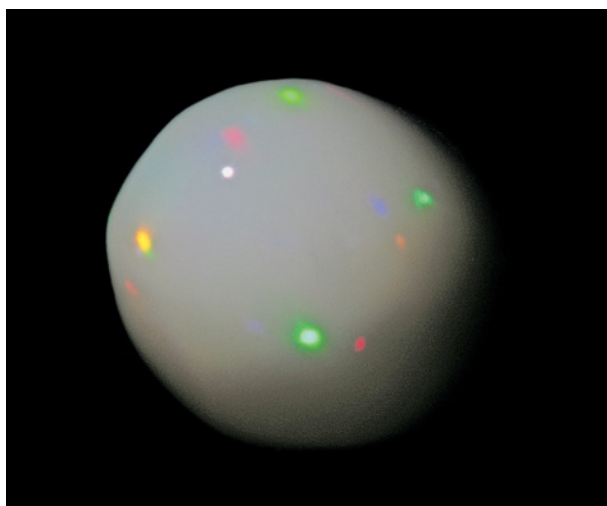




Figure 16. The diffraction of light by opal usually produces patches of pure spectral colors. On rare occasions, such as this 9.51 ct cabochon, we observed these colors diffracted from millimeter-size areas, forming small rainbows. Photo by F. Mazzero.

polish than the host opal.

Dispersed micro-inclusions of black, opaque crystals were abundant in some samples (in particular, no. 1113). EDS analyses revealed iron and sulfur, which suggests they were pyrite (pyrite usually appears black in such small dimensions).

Some of the rough opal samples were outlined by a thin layer (less than 0.1 mm thick) of black, opaque minerals. These were identified by EDS as barium-manganese oxides (probably hollandite) and native carbon (probably graphitic carbon). Also present in such layers were micrometer-sized crystals that were identified by EDS as titanium oxides (probably rutile). In rare instances, the black minerals were included in the body of the opal, filling fissures or forming dendrites.

Chemical Composition. We measured the chemical composition of several samples by EDS (both major and minor elements; see table 3) and LA-ICP-MS (trace elements; see table 4 and the *G&G* Data Depository). In addition to silica, we detected a significant proportion of Al (0.6–1.9 atomic %) and minor amounts of Ca (0.05–0.6 at. %), Na (up to 0.4 at. %), K (0.2–0.5 at. %), and Fe (up to 0.3 at. %). Iron

was not detected in the white samples. These compositions are typical for opal (Gaillou et al., 2008a). Among the trace elements, white opal contained abundant Ba (140–226 ppm [by weight]), Sr (127–162 ppm), and Rb (44–73 ppm). The orange fire opal portion of one sample showed Ba, Sr, and Rb contents consistent with those of opal-CT (Gaillou et al., 2008a). For the concentrations of other elements, see table 4 and the *G&G* Data Depository.

Raman Scattering. We obtained similar spectral features for all samples (e.g., figure 18). The apparent maximum of the strongest Raman band ranged from 360 to 335 cm^{-1} . Other, sharper Raman bands were present at ~ 3230 – 3200 , 2940, 1660, 1470, 1084, 974, and 785 cm^{-1} .

Microstructure. Observing the microstructure of an opal helps us characterize it and understand its growth conditions. Most often, as shown in Gaillou et al. (2008b), two main categories of structures can be observed: “smooth sphere” structure in opal-A (A for amorphous) or “lepisphere” structure in opal-CT (CT for cristobalite and tridymite; opal-A and opal-CT were originally defined on the basis of their X-ray diffraction patterns, and later on their Raman scattering patterns—see Jones and Segnit, 1971; Smallwood et al., 1997). To reveal the internal structure of an opal, one must first etch the sample in hydrofluoric acid (HF) and then observe the sur-

Figure 17. Elongated, cylindrical inclusions were present in one opal sample. This coated cylinder was made of silica, most likely chalcedony. Photomicrograph by B. Rondeau; magnified 40 \times .

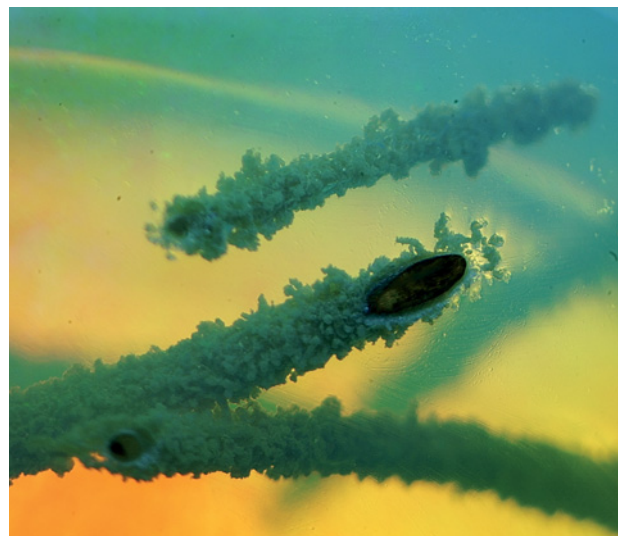


TABLE 3. Chemical composition of five opals from Wegel Tena, Ethiopia, measured by EDS.^a

Sample no.	Color	Si	Al	Ca	K	Na	Fe	O
1100	Colorless	31.5–31.7	1.4–1.5	0.5–0.6	0.2	nd	nd	66.1–66.1
1078	Brown	32.4–32.7	0.6	0.05–0.1	0.2–0.3	nd–0.1	nd	66.2–66.4
1106	White	31.1	1.7	0.4	0.4	0.4	nd	65.82
1111	Yellow	31.9	1.9	0.4	0.3	nd	0.3	65.9
1111	White	30.9	1.2	0.3	0.2	0.4	nd	66.2
1113	Colorless	31.6	1.5	0.3	0.5	nd	nd	66.1

^a Values are expressed in atomic percent. O is calculated for a sum of 100%. Samples 1078 and 1100 were analyzed in three spots; others are one spot. Abbreviation: nd = not detected.

face by SEM. Gaillou et al. (2008b) showed that etching in a 10% solution of HF for about 10 seconds can reveal the structure of opal. We encountered an unexpected reaction, however: Our samples were strongly affected by the acid, tending to flake away and develop networks of cracks. We modified both the concentration of HF (from 0.01% to 10%) and the duration of acid exposure (from 1 second to 3 minutes, with longer times using weaker acid), but we did not observe any organization of smooth spheres or lepispheres. Thus, we could not see any packing of spheres in opals from Wegel Tena using this technique.

We subsequently studied the structure of the opal using TEM, which revealed a regular network of spheres ~170 nm in diameter (figure 19). In another attempt to explore the structure, we studied the same sample using SEM with an unusually high voltage (15 kV) for a sample that was not coated to make it electrically conductive. Because the opal specimen was so thin, the electrons were able to pass through it to the backscattered electron detector. The similar image that was generated by this significantly different technique confirmed the TEM observations. Yet neither method helped us determine if the opal's structure is characterized by lepispheres (as are typical of opal-CT) or smooth spheres (typical of opal-A). Regardless, the regular network of these spheres is responsible for the diffraction of visible light that results in the play-of-color shown by the opals.

Stability and Toughness. Opals from certain localities (e.g., Querétaro, Jalisco, and Nayarit States in Mexico, and Shewa Province in Ethiopia, both opal-A and -CT) are known to destabilize, or “craze” with time. Cracks develop at the surface, and/or a white, opaque egg-like structure develops in the center of the stone (mostly in opal-CT; Aguilar-Reyes et al., 2005).

In the authors' experience, ~5% of Wegel Tena opals develop cracks after initial sawing and pre-forming. Until now, out of approximately 3,000

play-of-color opal cabochons from Wegel Tena released into the market during 2008–2010 by one of us (FM), only three samples were returned after

TABLE 4. Range of chemical composition of two opals from Wegel Tena, Ethiopia, measured by LA-ICP-MS.^a

Composition	1B	3B	
	White	White	Orange
No. analyses	8	7	2
Element (ppm)			
Li	0.061–0.205	<0.064–0.173	0.092–0.104
B	6.97–9.55	8.12–12.1	<0.179
Cu	0.267–0.555	0.159–0.640	0.069–0.091
Zn	11.6–18.9	1.19–16.2	<0.203–0.218
Pb	0.131–0.274	0.017–0.225	0.013–0.021
Sc	1.46–2.12	1.49–2.25	1.79–2.02
V	0.060–0.152	0.024–0.069	<0.007–0.011
Co	<0.009–0.046	0.001–0.031	<0.010
Ni	0.655–1.56	0.442–1.53	0.586–0.863
As	<0.090	<0.045–0.288	0.061–0.063
Rb	58.7–73.1	43.7–73.2	38.7–43.2
Sr	127–161	128–162	72.1–75.1
Y	0.093–0.314	0.087–0.241	0.067–0.103
Zr	51.1–245	34.3–201	29.2–31.2
Nb	0.944–2.81	0.321–0.408	0.477–0.588
Mo	<0.047	<0.030	<0.017
Cd	0.475–1.84	0.446–0.608	0.240–0.345
Ba	140–166	196–226	81.8–91.8
La	0.036–0.187	0.011–0.064	0.013–0.013
Ce	0.074–0.552	0.010–0.098	0.020–0.027
Pr	0.007–0.047	<0.001–0.013	<0.001–0.004
Nd	0.032–0.222	<0.010–0.069	0.012–0.019
Sm	<0.012–0.066	<0.009–0.013	<0.020
Eu	<0.003–0.014	<0.003–0.008	<0.004
Gd	<0.011–0.029	<0.022	<0.014
Tb	<0.002–0.012	<0.002–0.005	<0.002
Dy	0.010–0.031	<0.009–0.021	<0.005–0.007
Ho	<0.002–0.015	<0.001–0.008	<0.001–0.004
Er	<0.010–0.042	<0.007–0.029	<0.006
Tm	<0.001–0.007	<0.002–0.004	<0.001
Yb	<0.010–0.047	<0.008–0.037	<0.001
Lu	<0.002–0.003	<0.002–0.008	<0.002–0.004
Th	0.008–0.064	<0.003–0.006	0.141–0.196
U	0.197–0.361	0.103–0.135	<0.001

^a Values are expressed in ppm by weight. For detailed analyses, see the G&G Data Depository.

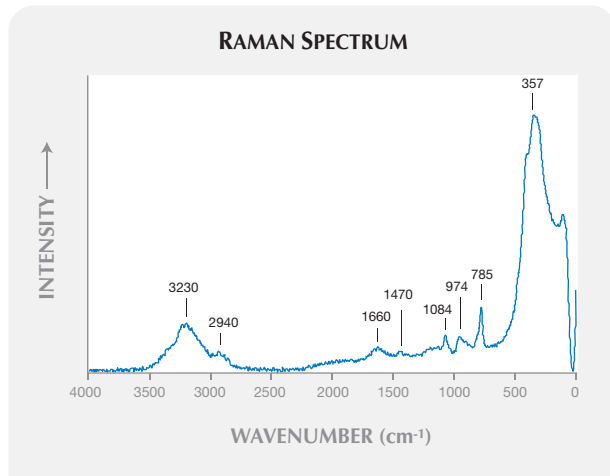


Figure 18. This Raman spectrum of sample no. 1072 is representative of opal from Wegel Tena. The main Raman bands at ~1470, 1084, 974, 785, and 357 cm^{-1} are typical for opal-CT. The bands at about 3230–3200, 2940, and 1660 cm^{-1} are attributed to water.

cracking. A parcel of seven opals (including sample 1072) thought to be from Mezezo was set aside in 2005 because of their unusual appearance; they are now known to be from Wegel Tena, and all the stones are still intact. Any crazing appears to be restricted to transparent material, in particular pale yellow to orange samples (fire opal) and near-colorless “crystal” opals. A few samples showed spectacular “egg” development (figure 20), as seen in some Mexican fire opal. In general, opaque white-to-yellow-to-brown opals from Wegel Tena appear very stable. There is no noticeable difference in crazing behavior between common and play-of-color opal.

There was no change in appearance (color, diaphaneity, crazing, or play-of-color) in the samples that were submitted to alternating periods of immersion in water. One customer who wears her opal constantly complained that it became more transparent when she took a shower, swam, or otherwise put her hands in water. She recognized, however, that the opal always returned to its original appearance after some time (depending on the duration of immersion)—which is due to its hydrophane character.

We noticed by accident that Wegel Tena opals could sustain a fall from 1.5 m onto a concrete floor with no visible damage, even under the microscope. Repetition of this test on five oval cabochons did not produce any sign of damage. The same experiment with five oval cabochons from the Mezezo deposit and three oval cabochons of white opal from Australia (including one boulder opal) led to breakage of all samples.

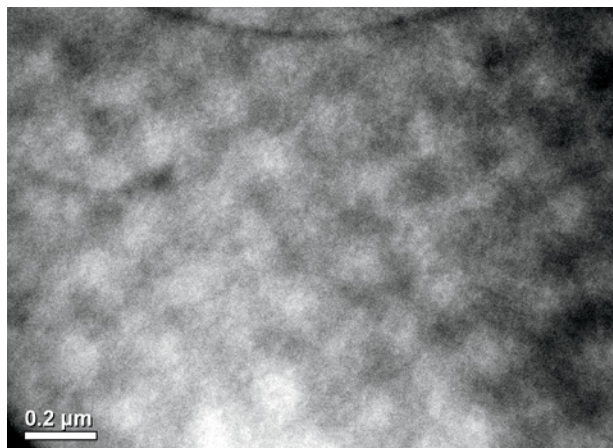
DISCUSSION

Gemological Properties. SG was in the reported range for opal (Webster, 1975). However, some samples showed large weight gains during immersion in water, up to 10.2%. This is probably related to the high porosity of these samples, detectable simply by touching a sample with the tongue to test its “stickiness.” RI ranged from as low as 1.36 to 1.43, with one “secondary” reading of 1.52. Values as low as 1.36 have been previously measured in hydrophane from Slovakia (Reusch, 1865) and in opals from Mexico (Spencer et al., 1992). The RI sometimes varied strongly even within a single sample, depending on the orientation. Similar effects were seen in Shewa opals (Johnson et al., 1996). They are probably due to local physical or chemical heterogeneities, as commonly observed in opals.

The large patches of red and orange seen in some of the play-of-color Wegel Tena opals are not common in Brazilian and Australian opals. We found the digit patterns to be very common in Wegel Tena opals, though in some cases they were only visible with a microscope. Digit patterns were described previously only in opals from Mezezo (see figure 14 in Johnson et al., 1996; Gauthier et al., 2004). We know of only one non-Ethiopian opal with digit patterns; it was seen in Australia by one of the authors (EF). Also, Choudhary (2008) described another such opal from an unspecified source. In contrast, the planar zoning of common and play-of-color opal is often observed in opals from other deposits, volcanic or otherwise.

As expected, the spectroscopy spectrum and

Figure 19. Transmission electron microscopy of sample 1071 reveals a microstructure consisting of spheres ~170 nm in diameter.



color filter reaction were not useful for identification. The red color filter reaction, as well as the absorption of the violet and blue regions in most stones, stems from two possible factors that may combine in a given stone. Intense light scattering (the corresponding stones were milky or white) attenuates violet and blue wavelengths, as they are scattered preferentially at an angle. Also, the yellow-to-brown bodycolor is due to a continuum of absorption, increasing from the red toward the violet region. Hence it will also contribute to blocking the violet-to-blue (and even some green) wavelengths. The resulting color in rectilinearly transmitted light in both cases is orange or red, as seen with the spectroscope or the Chelsea filter. Note that this is a good example of a bright red Chelsea filter reaction that has nothing to do with the presence of chromium in the stone.

The UV luminescence properties were typical for opal. The fluorescence is a mix of intrinsic silica surface-related violetish blue emissions and extrinsic uranium-related green emission. The latter is often more visible with short-wave UV (Fritsch et al., 2001; Gaillou, 2006; Gaillou et al., 2008a).

The observed hydrophane behavior is already known for some rare opals (Webster, 1975), particularly from Opal Butte, Oregon (Smith, 1988). In the samples studied here, there was no relationship between the capacity of opal to absorb water and the change in its visual appearance (compare figure 11 and table 2).

Raman Scattering. The main Raman peaks at ~ 1084 , 974 , 785 , and 357 cm^{-1} are typical for opal-CT and distinctly differ from those of opal-A, for which the Raman spectrum displays a main band around 420 cm^{-1} (Smallwood et al., 1997; Fritsch et al., 1999; Ostrooumov et al., 1999). The bands at ~ 3230 and 1660 cm^{-1} are attributed to the presence of water (Ostrooumov et al., 1999; Zarubin, 2001), and the band at 2940 cm^{-1} to cristobalitic water (Gaillou et al., 2004; Aguilar-Reyes et al., 2005).

Geology. The occurrence of digit patterns remains something of a mystery, but they seem to have been vertical at the time of their formation. To date, digit patterns have been observed almost exclusively in material from the two Ethiopian deposits, Wegel Tena and Mezezo. It follows, then, that the geologic conditions under which opals formed at these areas share common characteristics. However, the dispo-

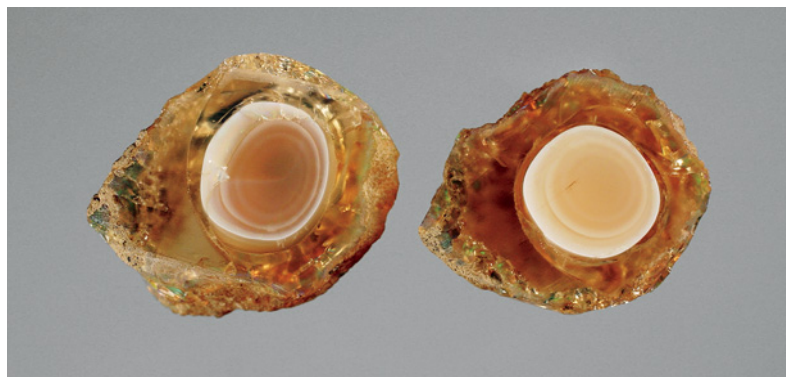


Figure 20. This orange opal (24 g total weight) from Wegel Tena was sliced to show the internal 15-mm-diameter egg-shaped zone of destabilization. Photo by B. Rondeau.

sition of opal in its host rock differs between the two localities. At Wegel Tena, opal most often cements volcanic grains, while at Mezezo it usually forms nodules filling the cavities in volcanic rock. The latter is the case for most volcanic opal localities, such as Mexico and Oregon. Also, the inclusion scenes observed in opals from Wegel Tena are different from those observed in opal from any other deposit (e.g., Gübelin and Koivula, 1986).

At Wegel Tena, the opal-mineralized layer is concordant with volcano-sedimentary deposits that extend for hundreds of kilometers. No systematic prospecting for opal has been conducted, but a local miner reported to one of us (EB) that opal samples have been found in the same geologic unit and at a similar depth on the flank of the Great Rift Valley, 40 km from the present workings (Yapatsu Purpikole, pers. comm., 2009). We believe, then, that the extent of the opal-bearing layer is probably much greater than what is known today.

Chemical Composition. From our preliminary measurements of two samples, trace-element composition was comparable to opals from Mezezo (Gaillou et al., 2008a), with the following notable exceptions: Y (0.07–0.3 ppm), Nb (0.3–2.8 ppm), and Th (<0.2 ppm) were lower in the Wegel Tena opals, whereas Sc (1.5–2.3 ppm), Rb (39–73 ppm), Sr (72–162 ppm), and Ba (82–226 ppm) were higher. The enriched Ba concentration in opals from Wegel Tena is surprising. Looking at opals from elsewhere (Gaillou et al., 2008a), we see that those that formed in a volcanic environment always have low Ba (<100 ppm), whereas those from a sedimentary environment contain 100–300 ppm Ba. However, we note that the relatively high Ba contents in some Wegel Tena opals are consistent with the geologic environment that



Figure 21. Opal from Wegel Tena is being incorporated into innovative jewelry designs. The Meduse Lune Clip features two opals (16.72 and 16.77 ct) that are set with diamonds and natural pearls. Courtesy of Van Cleef & Arpels, Paris.

also resulted in the presence of Ba-Mn oxides in fissures mentioned above.

Areas of different composition within single samples raise the question of their petrogenesis. The orange opal is richer in Fe and presents a typical opal-CT trace-element composition (compare with Gaillou et al., 2008a), whereas the white opal has unusually high contents of Ba, Sr, and Br compared to volcanic opals.

Identification. Digit patterns are typical of Ethiopian opal, from either Mezezo or Wegel Tena, regardless of the bodycolor. The digit patterns somewhat resemble the columnar structure observed in synthetic opals (such as Gilson), but they also have significant differences. Digit patterns are made of two materials: one transparent with play-of-color and the other more turbid, often without play-of-color. They form rounded columns, whereas the columns in synthetics are far more regular and polygonal. Hence,

careful observation is sufficient to distinguish the natural from synthetic opal.

To our knowledge, white opals from Wegel Tena represent the only example of opal-CT with a Ba content greater than 100 ppm. Therefore, the combination of a satisfactory Raman spectrum with trace-element analysis makes it possible to identify white opals from this locality. The fire opals displayed a chemical composition comparable to that of opal-CT from other localities.

Stability. Translucent opals from Wegel Tena resist hydration/dehydration cycles much better than opals from Mezezo, which crack and break more easily during such tests. A stabilization process has been developed to prevent crazing of Ethiopian opal (Filin and Puzynin, 2009), but in our experience this appears unnecessary for translucent opals from Wegel Tena.

CONCLUSION

Wegel Tena, Ethiopia, is a source of significant quantities of high-quality play-of-color opal (e.g., figure 21), with a mostly white bodycolor that is more market-friendly than the mostly brown material from Mezezo, ~200 km to the south. The opals are found in a specific layer of a thick volcanic sequence of alternating basalt and ignimbrite of Oligocene age. Systematic prospecting is needed to assess the extent of the opal-containing layer and the production potential, which appears quite significant.

Many of these new opals showed what we describe as “digit patterns,” a common feature in Ethiopian opals. The Wegel Tena samples typically showed the Raman spectrum of opal-CT, as do most opals that formed in a volcanic environment. Among the inclusions, we noted cylinders of silica (probably chalcedony), black microcrystals (probably pyrite), and coatings/fissures filled with barium-manganese oxides and graphite-like carbon. The combination of an enriched Ba content in the white opals (>100 ppm), a Raman spectrum typical of opal-CT, and the presence of digit patterns characterizes opals from Wegel Tena. Further trace-element analyses are necessary to strengthen the chemical criterion for Ba. The opaque-to-translucent opals from Wegel Tena are much more stable than those from Mezezo, which have a tendency to craze. Also, physically they are surprisingly tough. The Wegel Tena area has the potential to become a leading supplier of high-quality white play-of-color opal.

ABOUT THE AUTHORS

Dr. Rondeau (benjamin.rondeau@univ-nantes.fr) is assistant professor at the Laboratoire de Planétologie et Géodynamique, University of Nantes, France, and belongs to the Centre National de la Recherche Scientifique (CNRS), Team 6112. Dr. Fritsch is professor of physics at the University of Nantes, Institut des Matériaux Jean Rouxel (IMN)-CNRS, Team 6205. Mr. Mazzero and Mr. Bekele are principals of Opalinda in Paris and Eyaopal in Addis Ababa, Ethiopia. Dr. Gauthier is a former professor of crystallography at the University of Lyon, France. Dr. Cenki-Tok is a teaching and research assistant at the Institute of Geological Sciences, University of Bern, Switzerland. Dr. Gaillou is postdoctoral fellow at the National Museum of Natural History, Smithsonian Institution, in Washington, DC.

ACKNOWLEDGMENTS

The authors thank Nicolas Stephant, Stéphane Grolleau, Eric Gautron, and Luc Lajaunie of the Centre de Micro-Caractérisation (IMN, University of Nantes) for their help with electron microscopy. T. Pettke is thanked for assistance with LA-ICP-MS analysis. Messrs. Mazzero and Bekele are grateful to the Ethiopian Ministry of Mines and Energy for their help with their visit to the mining area. In particular, they thank Mrs. Hadas Sherif, gemologist at the Mines Works Department, for her assistance in collecting field data and research samples, together with Thomas Cenki.

REFERENCES

- Aguilar-Reyes B.O., Ostrooumov M., Fritsch E. (2005) Estudio mineralógico de la desestabilización de ópalos Mexicanos [Mineralogical study of the destabilization of Mexican opals]. *Revista Mexicana de Ciencias Geológicas*, Vol. 22, No. 3, pp. 391–400.
- Ayalew D., Yirgu G. (2003) Crustal contribution to the genesis of Ethiopian plateau rhyolitic ignimbrites: Basalt and rhyolite geochemical provinciality. *Journal of the Geological Society of London*, Vol. 160, pp. 47–56.
- Ayalew D., Gibson S.A. (2009) Head-to-tail transition of the Afar mantle plume: Geochemical evidence from a Miocene bimodal basalt-rhyolite succession in the Ethiopian Large Igneous Province. *Lithos*, Vol. 112, pp. 461–476.
- Choudhary G. (2008) Gem News International: An interesting opal. *G&G*, Vol. 44, No. 2, pp. 172–174.
- Filin S.V., Puzynin A.I. (2009) Prevention of cracking in Ethiopian opal. *Australian Gemmologist*, Vol. 23, No. 12, pp. 579–582.
- Fritsch E., Rondeau B. (2009) Gem News International: Rare optical phenomenon in play-of-color opal. *G&G*, Vol. 45, No. 2, pp. 147–148.
- Fritsch E., Rondeau B., Ostrooumov M., Lasnier B., Marie A.-M., Barreau A., Wery J., Connoué J., Lefrant S. (1999) Découvertes récentes sur l'opale [Recent discoveries about opal]. *Revue de Gemmologie a.f.g.*, No. 138/139, pp. 34–40.
- Fritsch E., Mihut L., Baibarac M., Baltog I., Ostrooumov M., Lefrant S., Wery J. (2001) Luminescence of oxidized porous silicon: Surface-induced emissions from disordered silica micro- to nano-structures. *Journal of Applied Physics*, Vol. 90, No. 9, pp. 4777–4782.
- Gaillou E. (2006) Relation entre Nanostructure, Propriétés Physiques et Mode de Formation des Opales A et CT [Relationship between Nanostructure, Physical Properties and Mode of Formation of Opal-A and Opal-CT]. PhD thesis, University of Nantes, 278 pp.
- Gaillou E., Mocquet B., Fritsch E. (2004) Gem News International: A new gem material from Madagascar. *G&G*, Vol. 40, No. 4, pp. 339–340.
- Gaillou E., Delaunay A., Rondeau B., Bouhnik-le Coz M., Fritsch E., Cornen G., Monnier C. (2008a) The geochemistry of opals as evidence of their origin. *Ore Geology Reviews*, Vol. 34, pp. 113–126.
- Gaillou E., Fritsch E., Rondeau B., Aguilar-Reyes B., Barreau A., Ostrooumov M., Post J. (2008b) Common gem opal: An investigation of micro- to nano-structure. *American Mineralogist*, Vol. 93, pp. 1865–1873.
- Gauthier J.-P., Mazzero F., Mandaba Y., Fritsch E. (2004) L'opale d'Ethiopie: Gemmologie ordinaire et caractéristiques exceptionnelles [Opal from Ethiopia: Usual gemology and unusual characteristics]. *Revue de Gemmologie a.f.g.*, No. 149, pp. 15–23.
- Gübelin E.J., Koivula J.I. (1986) *Photoatlas of Inclusions in Gemstones*, ABC Edition, Zürich, 532 pp.
- Johnson M.L., Kammerling R.C., DeGhionno D.G., Koivula J.I. (1996) Opal from Shewa Province, Ethiopia. *G&G*, Vol. 32, No. 2, pp. 112–120.
- Koivula J.I., Kammerling R.C., Fritsch E., Eds. (1994) Gem News: Opal from Ethiopia. *G&G*, Vol. 30, No. 1, pp. 52–53.
- Mazzero F., Gauthier J.-P., Rondeau B., Fritsch E., Bekele E. (2009) Nouveau gisement d'opales d'Ethiopie dans la Province du Welo: Premières informations [New deposit of Ethiopian opals in Welo Province: Early information]. *Revue de Gemmologie a.f.g.*, No. 167, pp. 4–5.
- Ostrooumov M., Fritsch E., Lefrant S. (1999) Spectres Raman des opales: aspect diagnostic et aide à la classification [Raman spectra of opals: Identification aspects and help for classification]. *European Journal of Mineralogy*, Vol. 11, No. 5, pp. 899–908.
- Reusch E. (1865) Ueber einen Hydrophan von Czerwenitz [On a hydrophane from Czerwenitz]. *Annalen der Physik*, Vol. 200, No. 3, pp. 431–448.
- Rondeau B., Mazzero F., Bekele E., Gauthier J.-P., Fritsch E. (2009) Gem News International: New play-of-color opal from Welo, Ethiopia. *G&G*, Vol. 45, No. 1, pp. 59–60.
- Smallwood A., Thomas P.S., Ray A.S. (1997) Characterisation of sedimentary opals by Fourier transform Raman spectroscopy. *Spectrochimica Acta Part A*, Vol. 53, No. 13, pp. 2341–2345.
- Smith K.L. (1988) Opals from Opal Butte, Oregon. *G&G*, Vol. 24, No. 4, pp. 229–236.
- Spencer R.J., Levinson A.A., Koivula J.I. (1992) Opal from Querétaro, Mexico: Fluid inclusions study. *G&G*, Vol. 28, No. 1, pp. 28–34.
- Webster R. (1975) *Gems: Their Sources, Descriptions and Identification*, 3rd ed. Butterworth & Co., 938 pp.
- Zarubin D.P. (2001) The two-component bands at about 4500 and 800 cm⁻¹ in infrared spectra of hydroxyl-containing silicas. Interpretation in terms of Fermi resonance. *Journal of Non-Crystalline Solids*, Vol. 286, No. 1–2, pp. 80–88.

A NEW TYPE OF COMPOSITE TURQUOISE

Gagan Choudhary

Several conspicuously colored specimens marketed as dyed and/or stabilized turquoise were recently examined. They were purple to purple-pink, yellow-green, and blue, in veined and unveined varieties. Testing revealed that all the specimens were composites of turquoise pieces bonded together; the purple to purple-pink and yellow-green samples were bonded with a colored polymer, and the blue ones had a colorless polymer. This article presents the gemological properties and EDXRF and FTIR analyses of this material, along with its reaction to the solvents acetone and methylene chloride.

Turquoise, best known for its splendid blue color, has been used for adornment since antiquity. Chemically a hydrous copper aluminium phosphate, it has a cryptocrystalline structure composed of fine, randomly oriented groups of triclinic crystals (Webster, 1994). This cryptocrystalline structure gives rise to the gem's porosity, making it susceptible to body oils, ordinary solvents, or even dirt, which can alter its color. For decades, turquoise has been impregnated with wax, plastics, or polymers—a process known as stabilization, which enhances not only the material's durability but also its color and surface luster (Nassau, 1994). Another established treatment is the dyeing of pale-colored turquoise to give it a rich blue color (see, e.g., Kammerling, 1994). In recent years, a few other proprietary treatments have been developed for turquoise. The most prominent is Zachery treatment, which decreases the porosity of the original material, so it takes a better polish; the blue color may

also be enhanced through an additional step in the process (Fritsch et al., 1999). Yet another form of treatment seen on the market, developed by Eljen Stones, involves polymer impregnation (Owens and Eaton-Magaña, 2009).

Recently, this author had the opportunity to study a group of distinctively colored purple and yellow-green turquoise samples, as well as blue turquoise (figure 1). When first seen at the Jaipur Jewellery Show in December 2008, their market availability was limited. Since the beginning of 2010, however, the Gem Testing Laboratory of Jaipur has received an increasing number of these treated turquoises for identification. While previous studies have reported on dyed and impregnated blue turquoise (Kammerling, 1994) and green turquoise produced by immersion in mineral oil (Koivula et al., 1992), these specimens were quite different. Upon inquiry, the supplier said they were pieces of natural turquoise that had been dyed and bonded together, though he knew little about the process involved. He did divulge that this material is being manufactured in the United States. We subsequently received a variety of rough and cut samples for study, and this article reports on the properties of these samples, some of which appear similar to those seen by McClure and Owens (2010) in the GIA Laboratory.

MATERIALS AND METHODS

The 21 samples were purple to purple-pink, yellow-green, and blue. Fifteen were fashioned as cabochons weighing 8.10–21.83 ct (again, see figure 1), and the other six were rough pieces with a total weight of 47.90 g (figure 2). The samples were divided into seven groups of three each on the basis of bodycolor, the presence/absence of veining, and whether they were rough or fashioned. The groups were: unveined purple to purple-pink rough, unveined yellow-green rough, unveined and veined purple to purple-pink cabochons (two groups), unveined and veined yellow-green cabochons (two groups), and veined blue cabochons.

Standard gemological tests were performed on all the cabochons to determine their RI, hydrostatic SG, and UV fluorescence. Absorption spectra were observed with a desk-model GIA Prism 1000 spectroscope. A binocular gemological microscope with fiber-optic lighting in addi-

See end of article for About the Author and Acknowledgments.
GEMS & GEMOLOGY, Vol. 46, No. 2, pp. 106–113.
© 2010 Gemological Institute of America



Figure 1. The 15 treated turquoise cabochons examined for this study are divided here into veined and unveined (or minimally veined) varieties that are purple to purple-pink (11.82–21.83 ct), yellow-green (8.10–18.12 ct), and blue (9.78–20.10 ct). Photo by G. Choudhary.

tion to the overhead white light was used to examine the structure and surface features. A needle was used to probe various parts of both the rough and cut samples.

We also noted the reaction of two samples to solvents such as acetone and methylene chloride. Acetone is commonly used to check for the presence of dye in gem materials, and methylene chloride is an excellent solvent for polymers. We brushed an acetone-dipped cotton swab on an unveined yellow-green cabochon and soaked a piece from the same sample in acetone for 48 hours to observe the changes; the rest of this sample was retained for comparison. We also soaked one veined yellow-green cabochon in

Figure 2. These rough samples of treated turquoise (5.75–10.11 g) show unusual colors and a polymer-like luster. Concentrations of colored polymer are visible as the yellow-brown area on the right corner of the upper yellow-green sample, and the red areas on the bottom purple to purple-pink samples. Photo by G. Choudhary.



methylene chloride for 48 hours and noted the reaction at occasional intervals. For comparison, a natural untreated turquoise was immersed in methylene chloride for the same duration.

We performed qualitative chemical analyses on all 15 cabochons with energy-dispersive X-ray fluorescence (EDXRF) spectroscopy, using a PANalytical Minipal 2 instrument operated with a voltage of 15 kV and current of 0.016 mA.

Infrared spectra were recorded on all cabochons in the 6000–400 cm^{-1} range with a Shimadzu IR Prestige 21 Fourier-transform infrared (FTIR) spectrometer operating at room temperature in diffuse reflectance mode, using a standard resolution of 4 cm^{-1} and 50 scans per sample. The results were then converted to absorbance using the spectrometer software.

RESULTS AND DISCUSSION

Visual Characteristics. As mentioned earlier, the turquoise samples were purple to purple-pink, yellow-green, and blue (again, see figures 1 and 2). The purple to purple-pink range is not associated with turquoise and indicates artificial coloration. The veins present contained metallic gold-colored “matrix” that generally appeared much brighter than that seen in natural turquoise. Except for the yellow-green unveined variety, the specimens displayed an uneven body color. The purple to purple-pink and veined yellow-green specimens displayed some distinct blue patches representing the original turquoise before treatment. These features were indicative of dyeing. The blue samples did not exhibit any obvious signs of dyeing and had a more natural appearance, though the thick-

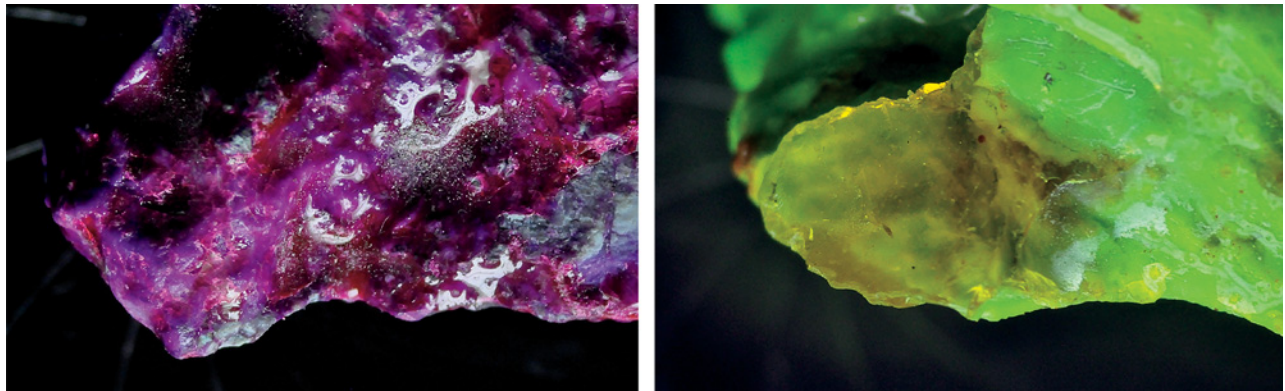


Figure 3. Concentrations of color appear on the surface of these rough samples of purple to purple-pink and yellow-green turquoise. The IR spectrum of the transparent yellow-brown area in the image on the right matched that of a polymer and some of the peaks recorded in the polished specimens. Photographs by G. Choudhary; magnified 30 \times .

ness of the veins raised suspicions about their origin.

The rough purple to purple-pink specimens displayed obvious reddish concentrations on their surface (figure 3, left) and were easily identified as artificially colored; they also displayed a dull to waxy and oily luster, which is associated with polymers and resins. The color of the yellow-green rough was more even, with only one specimen

displaying an obvious concentration of a transparent yellow-brown substance (figure 3, right). Similar concentrations of a transparent colored material were visible on the purple to purple-pink samples, too. The other two yellow-green pieces were fairly evenly colored, though they also displayed the luster associated with polymers and resins.

TABLE 1. Properties of natural turquoise and dyed composite turquoise.

Property	Natural turquoise (Webster [1994] unless noted otherwise)	Dyed composite turquoise (this study)		
Color	“Sky” blue to greenish blue (veined and unveined)	Purple to purple-pink (veined and unveined)	Yellow-green (veined and unveined)	Blue (veined)
Luster	Waxy	Dull to waxy		
RI	1.62 (mean)	1.61 (spot)	1.61 (spot) 1.54 for two samples, probably due to polymers	1.61 (spot)
SG	2.60–2.90	2.23–2.60	2.03–2.55	2.44–2.49
UV fluorescence				
Long-wave	Greenish yellow to bright blue	Strong patchy orange-red	Weak patchy blue; mostly inert	Strong patchy blue
Short-wave	Inert	Moderate patchy orange-red	Inert	Moderate patchy blue
Spectroscope spectrum	Vague band at 460 nm, fine lines at 420 and 432 nm	Bands in the green and yellow region at ~510, 540, and 580 nm	Diffused absorption in the blue region at 450–490 nm	No absorption features
Microscopic features	White clouds, crystals of various mineral inclusions (Fritz et al., 2007; Koivula and McClure, 2009)	Concentrations of red and yellow, patches of polymer, veins of “golden” material with or without brassy yellow fragments.		
EDXRF analysis	$\text{CuAl}_6(\text{PO}_4)_4(\text{OH})_8 \cdot 4\text{H}_2\text{O} + \text{Fe}$	Al, P, Fe, and Cu (and Zn in veined samples)		
FTIR analysis	Peaks at 1125, 1050, and 1000 cm^{-1} ; band at 1746 cm^{-1} (e.g., Moe et al., 2005)	Peaks related to polymers in the 3200–2800 and 2000–1000 cm^{-1} regions		
Reaction to metal probe	None	Indentations due to lower hardness of polymer		
Reaction to solvents	Blue color turns green after contact with body oils and the like	Loss of the impregnated color when soaked in acetone; veined sample completely disintegrated into fragments when soaked in methylene chloride		

Gemological Properties. The gemological properties of the studied turquoise are described below and summarized in table 1.

Refractive Index. Except for two yellow-green specimens, all samples (whether veined or unveined) yielded a spot RI of approximately 1.61 with a moderate birefringence blink. This value is consistent with those reported for natural turquoise. Two anomalous yellow-green samples—one veined and one unveined—displayed spot RIs of ~1.54, and no birefringence was visible. This lower RI value could have been due to a thicker layer of polymer on the surface or to a larger percentage of polymer in the structure of the turquoise.

NEED TO KNOW

- Purple-pink, yellow-green, and blue composite turquoise has been marketed since late 2008.
- The pieces of turquoise are bonded together using a polymer (colored to produce the purple-pink and yellow-green varieties).
- Some of the turquoise has veins or “matrix” material composed of a gold-colored polymer with fragments resembling pyrite/marcasite.
- The composite turquoise can be identified by its microscopic appearance, UV fluorescence, spectroscopy spectrum, and FTIR features.

Specific Gravity. The samples displayed a wide range of SG values, from 2.03 to 2.60. Webster (1994) and O'Donoghue (2006) reported SGs of 2.60–2.91 for untreated turquoise, depending on its porosity. Although porosity can cause fluctuations in SG readings, we did not observe such fluctuations in our samples, as expected for polymer-treated material. Only one of the 15 cut samples had an SG of 2.60, while the rest were below that. These lower values are consistent with the presence of a polymer. No consistent variations in SG were seen across colors or between veined and unveined samples.

UV Fluorescence. The samples showed distinct fluorescence reactions to long-wave UV radiation—which varied according to their bodycolor (figure 4)—and had weaker reactions or were inert to short-wave UV. The purple to purple-pink turquoise fluoresced a bright patchy orange-red to long-wave UV. The blue turquoise displayed a strong patchy blue fluorescence, while the yellow-green samples were mainly inert, with only the residual blue

areas fluorescing blue. In all the samples, the veined areas were inert. Webster (1994) also reported greenish yellow to bright blue fluorescence to long-wave UV, and the patchy blue in these specimens likely corresponded to residual areas of natural blue turquoise.

Spectroscopy Spectrum. The purple to purple-pink specimens displayed a series of three bands in the green and yellow regions at ~510, 540, and 580 nm; the intensity of the latter two bands was stronger than that of the 510 nm band. In the yellow-green samples, a broad diffused absorption was seen in the blue region between 450 and 490 nm. No absorption features were seen in the blue turquoise.

Magnification. Microscopic examination of the samples revealed the following features.

- **Luster:** Polymer-filled areas and cavities displayed a distinctly dull to waxy and oily luster compared to the turquoise areas (see figures 3 and 5). The areas of accumulated polymer in the cabochons also appeared to be indented.
- **Color Concentrations:** Most of the samples showed distinct color concentrations that varied according to bodycolor. The yellow-green turquoise displayed some yellow concentrations that formed swirly patches or followed veins (figure 6, left). The yellow appeared to be superimposed on the blue base of natural turquoise pieces, resulting in an overall green coloration. A few cavities in the cabochons were filled with the same yellow material. Similarly, the purple to purple-pink samples also displayed color concentrations (figure 6, right),

Figure 4. Here, the samples are shown in the same orientation as figure 1 during exposure to long-wave UV radiation. Their reactions varied with color. Note the striking orange-red fluorescence of the purple to purple-pink samples. The blue turquoise displayed a patchy blue fluorescence, while the yellow-green samples were inert with residual blue areas fluorescing blue. Photo by G. Choudhary.

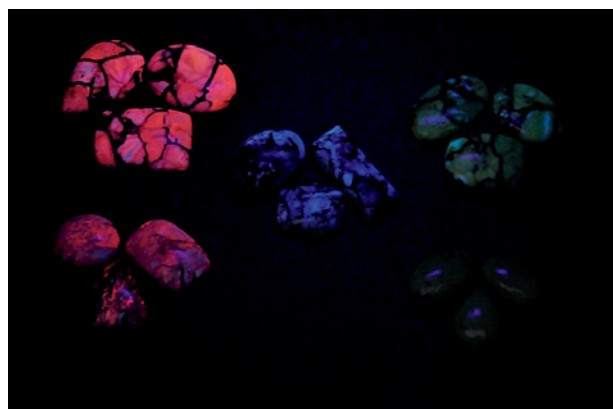




Figure 5. Polymer-filled areas and cavities in the turquoise appear to be indented and display a dull-to-waxy luster. Photomicrograph by G. Choudhary; magnified 45 \times .

with areas of red present as patches and in veins and cavities. The color concentrations indicated that the yellow-green and purple turquoise varieties had been dyed, and the presence of deep ridges suggested that these samples—veined and unveined—were composites, consisting of individual pieces of turquoise held together by a colored polymer matrix. Also, the yellow-green sample that was broken prior to soaking in acetone displayed uniform color in the broken areas, indicating that the dye penetrated completely through the stone. The blue samples did not display any color concentrations, which indicated that they were not dyed; the polymer seen on the surface and in the ridges of those samples was colorless.

- **Veins:** Natural turquoise usually contains matrix formed by brown-to-black veins of limonite (O'Donoghue, 2006). Grains of pyrite/marcasite may also be present, often along the veins or in the matrix (Fritz et al., 2007). In the study samples, the veins consisted predominantly of a brighter “golden” yellow substance that was colored by fine flakes (figure 7). Commonly present in this substance were fragments with a duller brassy appearance. It appeared that pieces of pyrite/marcasite were embedded in a gold-colored polymer during the production of the artificial veins.

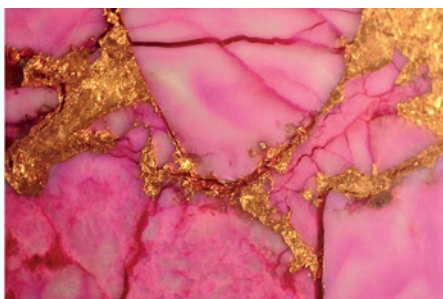
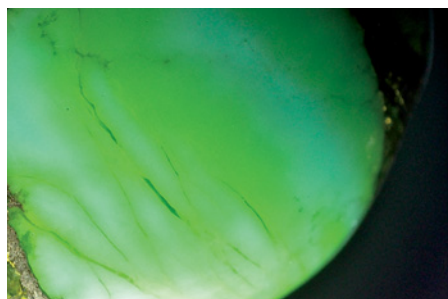


Figure 6. Concentrations of yellow (left, magnified 30 \times) and red (right, 45 \times) reveal the presence of an artificial dye. On the left, the yellow color superimposed on the blue base gives rise to a yellowish green bodycolor. Also note the deep ridges filled with color. Photomicrographs by G. Choudhary.

- **Reaction to a Metal Probe:** When probed with a needle to check for the presence of a polymer, both rough and cut samples readily indented. This test has been performed for many years to identify impregnated turquoise (see, e.g., Kammerling, 1994). The needle made indentations in the “golden” yellow veins or “matrix” as well (figure 7, right), revealing the softness expected for a polymer; the duller brassy fragments were not affected by the metal probe.

Reaction to Solvents. A cotton swab dipped in acetone and rubbed on the surface of one unveined yellow-green sample did not result in any loss of color. A piece of an unveined yellow-green sample that was soaked in acetone for 48 hours displayed an apparent loss of color and became patchy (figure 8, right sample), while the acetone became pale yellow-green. The soaked sample also had a significantly duller luster and showed a pimply surface and numerous cracks (figure 9).

A veined yellow-green sample that was soaked in methylene chloride showed significant changes after ~3 hours (figure 10). The metallic-appearing substance that formed the veins started to leave the specimen and showed a flaky appearance. After ~18 hours, individual pieces of the specimen were distinctly visible in the liquid, and the liquid turned slightly greenish yellow. After ~48 hours, the specimen had completely disintegrated into small grains and fragments, similar to the effect described by Rockwell (2008). The surface of the beaker in which the specimen was immersed also showed distinct color concentrations released from the sample after the methylene chloride evaporated. In contrast, a piece of natural untreated turquoise that was immersed in methylene chloride for comparison was unaffected.

The reaction in the methylene chloride bath and the similar structural features (e.g., the presence of deep ridges) seen in all samples confirmed they are composites and not merely dyed and/or impregnated. At this stage, we do not know what impact common household cleaning products and other solvents might have on the polymer(s) used in these composites.

EDXRF Analysis. Qualitative EDXRF analysis of all cabochons (veined and unveined) revealed the presence of Al, P,

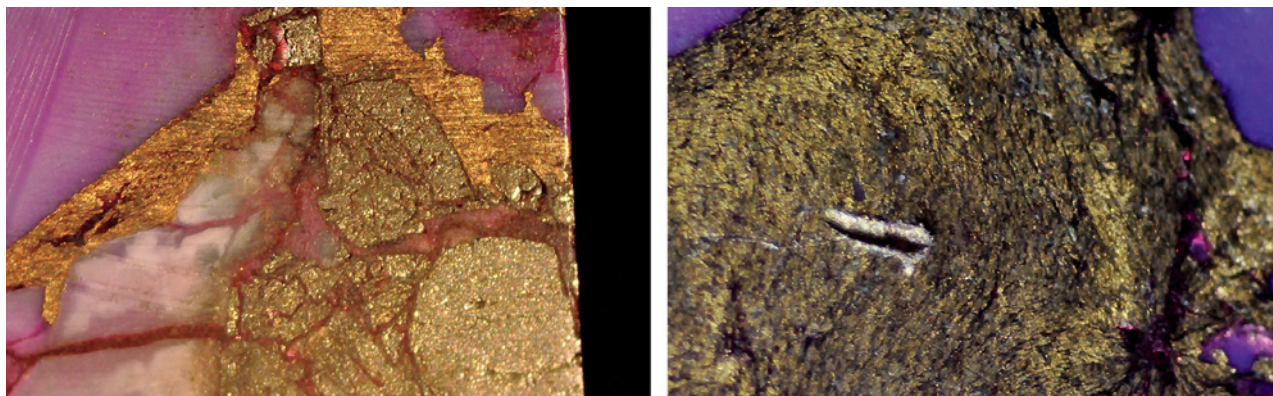


Figure 7. The veins or “matrix” in the turquoise appear to consist of a bright “golden” yellow material containing fragments with a brassy color resembling pyrite/marcasite (left). The photo on the right shows the tiny gold-colored flakes that color the matrix material; the gash made by the needle probe indicates its softness. Photomicrographs by G. Choudhary; magnified 30× (left) and 45× (right).



Figure 8. An 8.90 ct unveined yellow-green turquoise was broken and the portion on the right immersed in acetone for 48 hours, resulting in a duller luster and patchy loss of color. Photo by G. Choudhary.

Fe, and Cu, consistent with the chemical composition of turquoise. No potassium peak was present, which ruled out the possibility of Zachery treatment (Fritsch et al., 1999). Yet the veined samples displayed an additional Zn

peak. EDXRF analysis of the “golden” metallic-looking material that flaked off after soaking a veined sample in methylene chloride (discussed above) confirmed the presence of Zn as well as Cu.

FTIR Analysis. FTIR spectroscopy has long been the most powerful tool in the nondestructive identification of polymer-treated stones (e.g., Fritsch et al., 1992). In this study, FTIR analysis of all cabochons (veined as well as unveined) displayed fairly consistent absorption features in the 3200–2800 cm^{-1} and 2000–1000 cm^{-1} ranges.

In the 3200–2800 cm^{-1} region, distinct absorption bands were visible at ~3125 (consisting of twin humps), 2970, and 2875 cm^{-1} (figure 11, left); the latter two are associated with polymers (Fritsch et al., 1992; Moe et al., 2005). However, no peak was detected near 3035 cm^{-1} , which suggests the absence of Opticon or other resins (Johnson et al., 1999).

The 2000–1000 cm^{-1} region (figure 11, right) displayed major absorption bands at ~1750, 1595, 1487, 1270, and 1060 cm^{-1} , in addition to some fine absorption features at ~1896, 1857, 1825, 1380, and 1193 cm^{-1} . Moe et al. (2005) stated that peaks at ~1125, 1050, and 1000 cm^{-1} are associated with natural (not synthetic) turquoise. In the

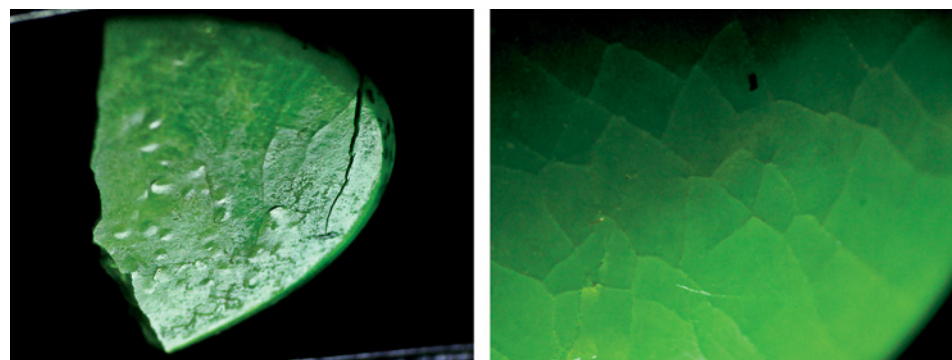


Figure 9. The immersed portion of the sample in figure 8 displayed a pimply surface (left, magnified 30×) and numerous cracks (right, 45×). Photomicrographs by G. Choudhary.

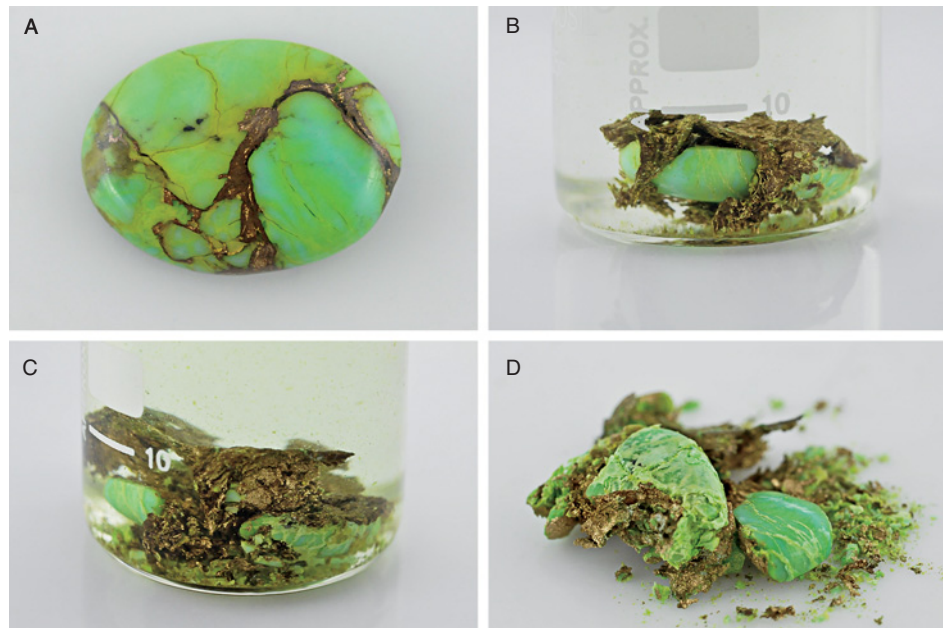


Figure 10. A veined 11.29 ct yellow-green sample (A) was soaked in methylene chloride. After ~3 hours, the metallic-appearing substance in the veins started to leave the specimen (B). After ~18 hours, separate pieces of the specimen were distinctly visible (C). After ~48 hours, the specimen completely disintegrated (D). Also note in C the color of the liquid, which turned slightly greenish yellow. Photos by G. Choudhary.

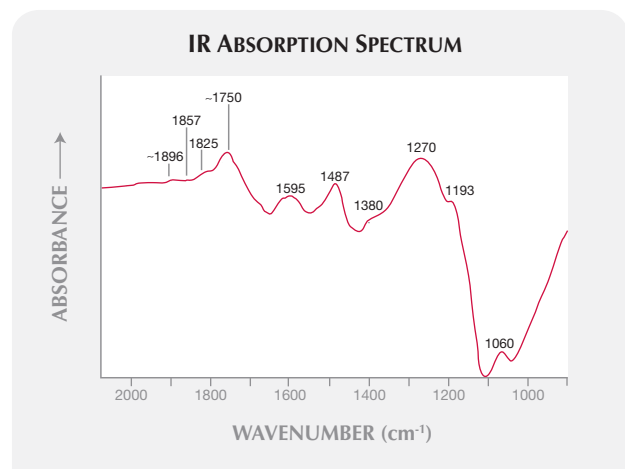
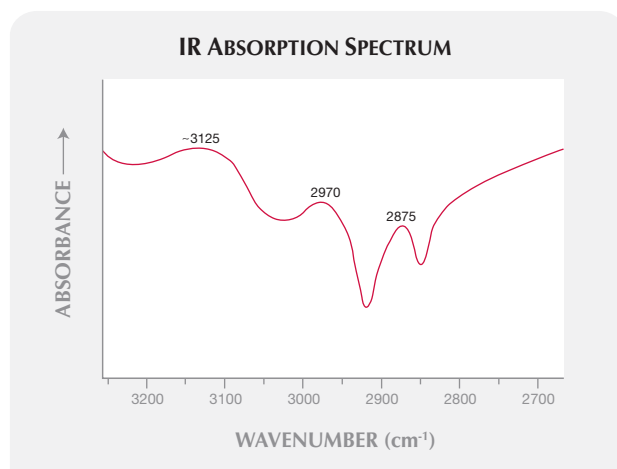
present samples, however, the peak at $\sim 1050\text{ cm}^{-1}$ varied from 1075 to 1045 cm^{-1} , there was no 1125 cm^{-1} peak, and the peak at 1000 cm^{-1} was present at around 1015 cm^{-1} (not shown in figure 11). The bands at ~ 1750 and 1595 cm^{-1} are related to polymers, in which the former is assigned to C=O stretching (~ 1744) and the latter to CH_3 bending ($\sim 1600\text{ cm}^{-1}$; Moe et al., 2007). The peak at $\sim 1000\text{ cm}^{-1}$ is associated with the styrene phenyl ring, but it does not play an important role in the identification of a polymer, because it is also present in natural turquoise (Moe et al., 2005). The cause of the ~ 1487 and $\sim 1270\text{ cm}^{-1}$ peaks is not known; the position of the latter varied from 1270 to 1240 cm^{-1} .

The FTIR spectrum of a yellow chip taken from the surface of a yellow-green sample in figure 3 displayed all the polymer-related peaks mentioned above. This confirms the presence of a polymer-like material within or on the surface of these turquoise. The spectrum of this chip displayed an additional peak at $\sim 1270\text{--}1240\text{ cm}^{-1}$, and the cause of this peak in the turquoise could have been the polymer.

CONCLUSION

These composites, typically marketed as “stabilized” turquoise, consist of small fragments of turquoise bond-

Figure 11. The infrared spectrum recorded for all cabochons in the $3200\text{--}2800\text{ cm}^{-1}$ region (left) displays distinct absorption bands at ~ 3125 , 2970 , and 2875 cm^{-1} ; the latter two are associated with polymers. The spectrum in the $2000\text{--}1000\text{ cm}^{-1}$ region (right) also displays some polymer-related peaks, at ~ 1750 , 1595 , and 1270 cm^{-1} , as well as the 1060 cm^{-1} peak associated with natural (not synthetic) turquoise.



ed together with a colored polymer (in the case of the purple to purple-pink and yellow-green samples) or a colorless polymer (blue samples). Furthermore, veined samples contain interstitial areas formed of a gold-colored polymer containing fragments that resemble pyrite/marcasite.

These materials provide a wider range of turquoise colors for the consumer. Identifying them should not pose any problem. Careful microscopic examination along with UV fluorescence, spectroscopy spectrum, and FTIR analysis should easily establish their dyed/composite nature.

REFERENCES

- Fritsch E., McClure S., Ostrooumov M., Andres Y., Moses T., Koivula J.I., Kammerling R.C. (1999) The identification of Zachery-treated turquoise. *G&G*, Vol. 35, No. 1, pp. 4–16.
- Fritz E.A., Koivula J.I., Laurs B.M. (2007) Gem News International: Turquoise from Nacozari, Sonora, Mexico. *G&G*, Vol. 43, No. 1, pp. 75–77.
- Johnson M.L., Elen S., Muhlmeister S. (1999) On the identification of various emerald filler substances. *G&G*, Vol. 35, No. 2, pp. 82–107.
- Kammerling R.C. (1994) Gem Trade Lab Notes: Turquoise, dyed and impregnated. *G&G*, Vol. 30, No. 2, pp. 120–121.
- Koivula J.I., McClure S. (2009) Lab Notes: Uranium mineral as inclusions in turquoise. *G&G*, Vol. 45, No. 4, pp. 294–295.
- Koivula J.I., Kammerling R.C., Fritsch E. (1992) Gem News: Modern-day turquoise oiling. *G&G*, Vol. 28, No. 2, p. 137.
- McClure S., Owens P. (2010) Lab Notes: Treated green turquoise. *G&G*, Vol. 46, No. 1, pp. 56–57.
- Moe K.S., Johnson P., Pearce C. (2005) Lab Notes: Identification of turquoise with diffuse reflectance spectroscopy. *G&G*, Vol. 41, No. 4, pp. 348–349.
- Moe K.S., Moses T.M., Johnson P. (2007) Polymer-impregnated turquoise. *G&G*, Vol. 43, No. 2, pp. 149–151.
- Nassau K. (1994) *Gemstone Enhancement: History, Science and State of the Art*, 2nd ed. Butterworth-Heinemann, Oxford, UK.
- O'Donoghue M. (2006) *Gems*, 6th ed. Butterworth-Heinemann, Oxford, UK.
- Owens P.A., Eaton-Magaña S. (2009) Lab Notes: Eljen treated turquoise. *G&G*, Vol. 45, No. 2, p. 140.
- Rockwell K.M. (2008) Lab Notes: Composite of coral and plastic. *G&G*, Vol. 44, No. 3, p. 253.
- Webster R. (1994) *Gems: Their Sources, Descriptions and Identification*, 5th ed. Revised by P. Read, Butterworth-Heinemann, Oxford, UK.

ABOUT THE AUTHOR

Mr. Choudhary (gtl@gjepcindia.com) is assistant director of the Gem Testing Laboratory, Jaipur, India.

ACKNOWLEDGMENTS

The author thanks Dolphin Gems of Jaipur for providing the study samples, and Tomas Burke for arranging to get the stones from this collection.



Your GIA diploma was just the beginning.

Introducing GIA's completely redesigned Continuing Education Program for Graduate Gemologists and Gemologists.

- Completing assignments in GIA's easy-to-use online learning environment is engaging and fun.
- Online discussions and live chats keep you connected with experts from all over the world.
- Access to all GIA eLearning gemology course materials keeps an entire gem and jewelry reference library right at your fingertips.
- Affordable \$189 annual fee, or bundle it with a G&G online subscription for just \$60 more.



GIA
GEMOLOGICAL INSTITUTE OF AMERICA®
Alumni Association

Visit www.gia.edu for more information or to get started today.

NEW OCCURRENCE OF FIRE OPAL FROM BEMIA, MADAGASCAR

Martina Simoni, Franca Caucia, Ilaria Adamo, and Pietro Galinetto

Twenty-two gem opals from a new volcanic deposit located near Bemia, in southeastern Madagascar, were investigated by classical gemological methods, SEM-EDS, powder X-ray diffraction analysis, LA-ICP-MS, and Raman and IR spectroscopy. Although none of the opals show play-of-color, they exhibit a wide variety of hues—including those typical of fire opal—that are related to iron content, mainly from Fe-rich inclusions. Consistent with their volcanic origin, these samples are microcrystalline and composed of opal-CT or opal-C. Among the inclusions are ilmenite needles, clay minerals, and iron oxides and hydroxides. The RI and, in particular, SG values are higher than those typical of natural fire opal (e.g., from Mexico) and some synthetic fire opal, allowing for a rapid separation.

Opals are water-bearing micro- and noncrystalline silica minerals, with the chemical formula $\text{SiO}_2 \cdot n\text{H}_2\text{O}$ (see, e.g., Graetsch et al., 1994; Downing, 2003; O'Donoghue, 2006). One attractive variety is fire opal, which is characterized by a red-orange-yellow bodycolor, with or without play-of-color (O'Donoghue, 2006). This opal variety does not have the typical structure of play-of-color opal; rather, it is composed of random aggregates of hydrated silica nanograins ~20 nm in diameter (Fritsch et al., 2006; Gaillou et al., 2008b).

The most famous locality for fire opal, one that has been producing fine material for more than 100 years, is the Querétaro area of Mexico (see, e.g., Koivula et al.,

1983; Gübelin, 1986). Other sources include the United States, Turkey, Australia, Indonesia, Ethiopia, Somalia, Kazakhstan, Canada, and Brazil (Ball and Daniel, 1976; Smith, 1988; Bittencourt Rosa, 1990; Holzhey, 1991; Bank et al., 1997; Enseli et al., 2001; O'Donoghue, 2006).

Opal, including the fire variety, is also known to come from various regions of Madagascar, particularly the Faratsiho deposit, located near the capital Antananarivo, in the center of the island (Lacroix, 1922). A new source of common opal, including fire opal (e.g., figure 1), was discovered a few years ago in the southeastern part of the island. According to A. and L. Pasqualini (pers. comm., 2010), who visited the deposit in May 2008, the opal is found near the city of Bemia, 70 km from the coast (figures 2 and 3). The opal occurs in Cretaceous rhyodacite volcanic rocks. Local people search for the opal by digging small pits, and ~200–400 kg of mixed-quality rough material has been produced. The opal generally occurs as nodules up to several centimeters in diameter or in veins up to 20–30 cm long, with large variations in quality and color. The rough opal is typically sent to the city of Antsirabe, 450 km north of Bemia, where it is fashioned into cabochons or faceted into fine gemstones that typically weigh up to 15 ct. Many of the various colors are typical of fire opal, but no play-of-color has been seen.

Building on the work of Simoni and Caucia (2009, in Italian), the present article describes the standard gemological properties of Bemia opal, as well as the inclusions, powder X-ray diffraction patterns, chemical composition, and spectroscopic features.

MATERIALS AND METHODS

We looked at 22 fashioned samples (0.32–21.05 ct, both faceted and cabochons) of opal from Bemia (e.g., figure 1), which were cut from material obtained by A. and L. Pasqualini at the mine. The specimens were examined by standard gemological methods to determine their optical properties, hydrostatic SG, UV fluorescence, and microscopic features.

Some inclusions in selected samples were characterized with a Zeiss Evo 40 scanning electron microscope

See end of article for About the Authors and Acknowledgments.

GEMS & GEMOLOGY, Vol. 46, No. 2, pp. 114–121.

© 2010 Gemological Institute of America

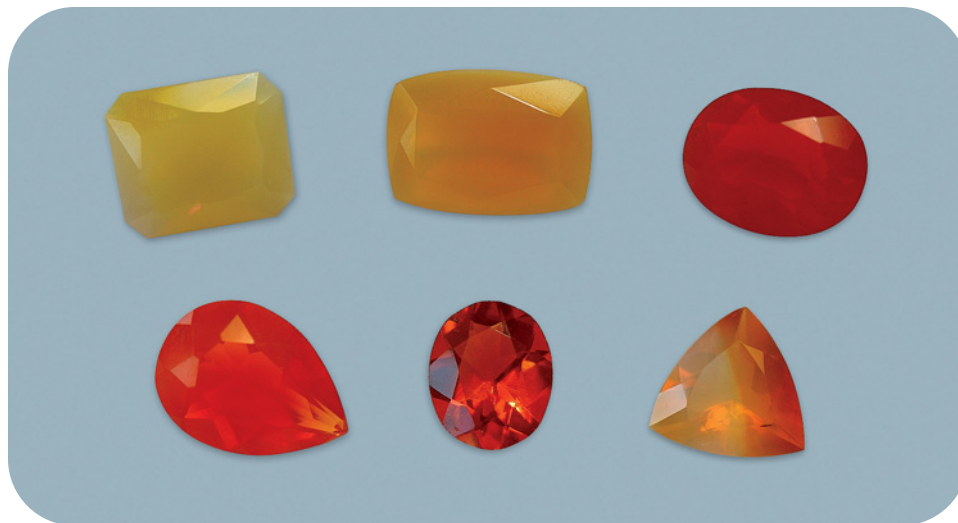


Figure 1. These fire opals (0.70–16.94 ct) are from a new deposit near Bemia, Madagascar. From left to right: top row—16.94 ct (sample no. 3), 3.96 ct (no. 5), 0.70 ct (no. 17); bottom row—1.40 ct (no. 21), 0.73 ct (no. 18), 2.88 ct (no. 14). Note the strong color zoning in sample 14. Composite photo by Andrea Pazzi.

(SEM) equipped with an Oxford Instruments energy-dispersive spectrometer (EDS), using an electron beam energy of 40 eV and a focal spot of 5 nm.

Laser ablation–inductively coupled plasma–mass spectrometry (LA-ICP-MS) was performed on four samples (nos. 3, 10, 18, and 22, selected to show a range of color). The instrument consisted of an Elan DRC-e mass spectrometer coupled with a Q-switched Nd:YAG laser source (Quantel Brilliant), with a fundamental emission (1064 nm) converted to 266 nm by two harmonic generators. The ablated material was transported to the mass spectrometer using helium as the carrier gas, mixed with Ar downstream of the ablation cell. The external and internal standards were NIST SRM 610 and Si, respectively. Four analyses per sample were collected, using a spot size of 50 μm . The results are reported in parts per million (ppm) by weight.

Powder X-ray diffraction (XRD) data were collected with a Philips PW 1800/10 diffractometer, using $\text{CuK}\alpha$ radiation in the range of 2° – 65° 2θ with a speed of 0.02° $2\theta/\text{sec}$. Since this is a destructive technique, we restricted these measurements to six samples (nos. 3, 10, 19, 20, 21, and 22) as designated by the Pasqualinis.

The Raman spectra of four samples (nos. 10, 20, 21, and 22) were recorded in the 3000 – 200 cm^{-1} range, using a Labram Dilor Raman H10 spectrometer equipped with an Olympus HS BX40 microscope and a cooled CCD camera as a photo-detector. The instrument employed an He-Ne laser (632.8 nm) as excitation radiation. A $100\times$ objective (numerical aperture = 0.99) was typically used, with a spatial resolution of ~ 1 μm and depth resolution of ~ 2 μm .

We collected the mid-infrared (4000 – 400 cm^{-1}) spectra of three samples (nos. 3, 19, and 22) in transmission mode with a Nicolet Nexus FTIR spectrometer, using KBr pellets and operating with a resolution of 4 cm^{-1} .

RESULTS AND DISCUSSION

Gemological Properties and Inclusions. The appearance and gemological properties of the Malagasy opal samples are reported in table 1. They showed a wide range of colors

and transparency, sometimes with strong zoning (with a characteristic banded structure), but all had a resinous luster and no play-of-color (again, see figure 1). UV fluorescence varied greatly, in both color and intensity, from one sample to another and even within the same sample in some cases. Moreover, the stones with the most intense bodycolors had no UV reaction. No phosphorescence was observed in any specimens.

The RI values of 1.415–1.462 overlapped and extended

Figure 2. The volcanic deposit near Bemia, in south-eastern Madagascar, is a relatively new source of gem-quality opal.





Figure 3. At Bemia, opal is recovered from small pits by local residents. Photo taken in May 2008 by A. and L. Pasqualini.

below the typical range for opal in general (1.44–1.46; O'Donoghue, 2006), whereas they were slightly higher than those typical of other volcanic opals, such as the famous stones from Querétaro, Mexico (1.42–1.43, rarely down to 1.37; Koivula et al., 1983; Gübelin, 1986). The SG values we measured for the Bemia opal samples (2.05–2.38) were higher than those typically measured both for opal in general and for Mexican fire opal, which generally range from 1.98 to 2.20 for the former (O'Donoghue, 2006) and from 1.97 to 2.06 for the latter (Webster, 1994). Gaillou et al. (2004) attributed an unusually high SG value (2.18) in a white Madagascar opal to inclusions of cristobalite (a polymorph of SiO₂), which probably caused the milky appearance of their sample. Although this could well explain the high SG values in our samples, we did not find an obvious correlation between SG and the presence of a silica polymorph. The Malagasy opals also exhibited higher RI and SG values than the original Mexifire synthetic opals described by Choudhary and Bhandari (2008), which have an RI <1.40 and SG <1.77. However, they are similar to the values of the Mexifire synthetic manufactured since late 2009, which has an RI of 1.470 and an SG of 2.19 (G. Choudhary, pers. comm., 2010).

Crystalline inclusions were noted in some samples. Analysis by SEM-EDS identified dark opaque blebs as iron oxides (probably hematite; see, e.g., figure 4) and hydroxides; also present were needles of ilmenite. We determined that other inclusions were probably clay minerals, on the basis of their fibrous morphology and chemistry. Only seven samples had fluid inclusions (within small feathers) that were visible with the optical microscope.

With respect to the stability of the opal to dehydration and crazing, we did not observe any significant changes in

these samples during our observations over a period of ~1.5 years. However, we did not conduct any specific stability tests.

Chemical Composition. Trace-element chemistry is important for understanding some physical properties of gem opals, such as color and luminescence, and is a useful tool for determining their geologic and geographic origin (Gaillou et al., 2006, 2008a). The LA-ICP-MS data of four samples from Bemia are reported in table 2.

The four main impurities (>500 ppm) were: Mg

Figure 4. Opaque blebs, identified by SEM-EDS as hematite, are easily seen in this 11.03 ct opal, from which sample 19 was faceted. Photo by Andrea Pazzi.



TABLE 1. Gemological properties of 22 opal samples from Bemia, Madagascar.

Sample no.	Weight (ct)	Color	Diaphaneity	RI ^a	SG	UV fluorescence	
						Long-wave (366 nm)	Short-wave (254 nm)
1	9.30	Yellowish white	Translucent	1.460	2.19	Inert	Weak yellow
2	13.75	Yellow	Opaque	1.458	2.17	Inert	Weak green
3	16.94	Yellow and yellowish white	Translucent	1.458	2.15	Inert	Inert
4	21.05	Yellow	Translucent	1.449	2.15	Inert	Weak green
5	3.96	Yellowish orange	Translucent	1.439	2.11	Inert	Inert
6	0.38	Colorless	Transparent	1.419	2.19	Moderate yellow-green	Moderate yellow-green
7	0.39	Yellow	Translucent	1.415	2.19	Inert	Moderate blue (core) and moderate yellow-green (rim)
8	0.49	White	Translucent	1.416	2.35	Moderate blue	Moderate blue (core) and moderate yellow-green (rim)
9	0.55	White	Translucent	1.428	2.16	Moderate blue (core) and moderate yellow-green (rim)	Moderate blue (core) and moderate yellow-green (rim)
10	0.32	Yellowish white and yellow	Transparent	1.440	2.38	Moderate blue	Moderate blue
11	0.46	Yellow	Transparent	1.449	2.21	Moderate blue (core) and moderate yellow-green (rim)	Moderate blue (core) and moderate yellow-green (rim)
12	0.35	White	Translucent	nd	2.26	Weak blue	Moderate-weak yellow-green
13	0.49	White	Translucent	1.429	2.12	Weak blue (core) and weak yellow-green (rim)	Weak blue (core) and weak yellow-green (rim)
14	2.88	Orange and yellowish white	Translucent	1.439	2.15	Moderate blue	Moderate blue
15	11.56	Yellow	Transparent	1.450	2.15	Moderate blue (core) and moderate yellow-green (rim)	Moderate blue (core) and moderate yellow-green (rim)
16	2.94	Colorless	Transparent	1.462	2.18	Moderate blue (core) and moderate yellow-green (rim)	Moderate blue (core) and moderate yellow-green (rim)
17	0.70	Red	Translucent	1.460	2.20	Inert	Inert
18	0.73	Orange	Transparent	1.453	2.24	Inert	Inert
19	1.11	Yellow	Translucent	1.460	2.05	Inert	Inert
20	0.36	Orange	Translucent	nd	2.19	Inert	Inert
21	1.40	Orange	Translucent	1.460	2.15	Inert	Inert
22	0.86	Yellow	Translucent	nd	2.06	Inert	Weak yellow

^a Abbreviation: nd = not determined because too many fractures were present.

(~890–17,730 ppm); Al (~3000–5000 ppm, except for sample 3, with only 23 ppm); Ca (369–1314 ppm); and Cl (average 543 ppm). Aluminum, which substitutes for silicon, is typically the most common impurity in opal (Bartoli et al., 1990; Gaillou et al., 2008a). This substitution results in a charge balance that must be compensated by the mono- and divalent cations such as Na, Mg, K, and Ca, or the substitution of a hydroxyl ion for an oxygen to form silanol (Webb and Finlayson, 1987; Gaillou et al., 2008a). Aluminum can also occur as occlusions of clay particles (Webb and Finlayson, 1987), which is consistent with our SEM-EDS observations (see above). With respect to Ca, our Bemia samples were more enriched than the fire opals from Mexico, which may contain up to 490 ppm Ca (Gaillou et al., 2008a).

Sodium (~60–1200 ppm) was present in all the Bemia opals, as was Fe, which varied greatly (~140–12,070 ppm) according to color (again, see table 2). This is consistent

with the presence of Fe-containing inclusions (particularly Fe oxyhydroxides) causing the yellow and orange bodycolor (Rossmann, 1994; Fritsch et al., 1999, 2002; Gaillou et al., 2008a); this, too, is in agreement with our SEM-EDS investigations. Other elements present in lesser amounts were, in order of decreasing average concentration: K, Zn, Ti, Ba, Zr, Sr, Be, Mn, Sc, Y, Cr, Ni, Rb, Pb, B, U, V, and Cu; Li and Co were always below 1 ppm. The Ba content of our samples (up to 42 ppm) is consistent with their volcanic origin (Gaillou et al., 2008a). With regard to chromophores other than Fe, all except Ti were less than ~10 ppm; Ti ranged from ~12 to 61 ppm (possibly due to the presence of ilmenite inclusions).

The green and blue luminescence of opal is known to be caused by uranium- or oxygen-related defects, respectively, though an excess of Fe³⁺ (>3000 ppm) may quench the effect (Fritsch et al., 1999; Gaillou et al., 2008a). Samples 3 and 18 were inert to both long- and short-wave

TABLE 2. Chemical composition (in ppm) of four opal samples from Bemia, Madagascar, as obtained by LA-ICP-MS.^a

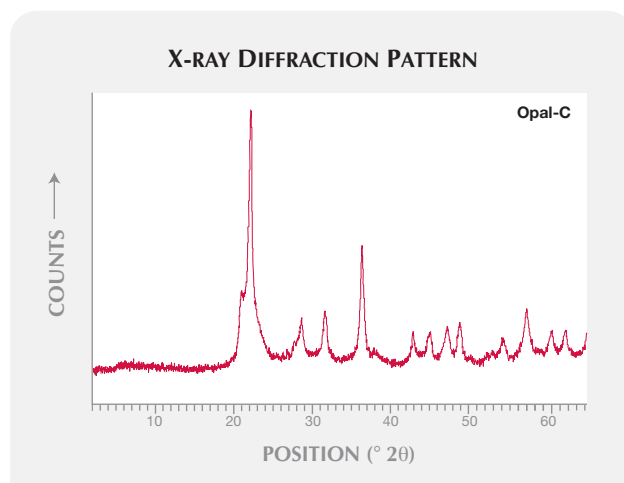
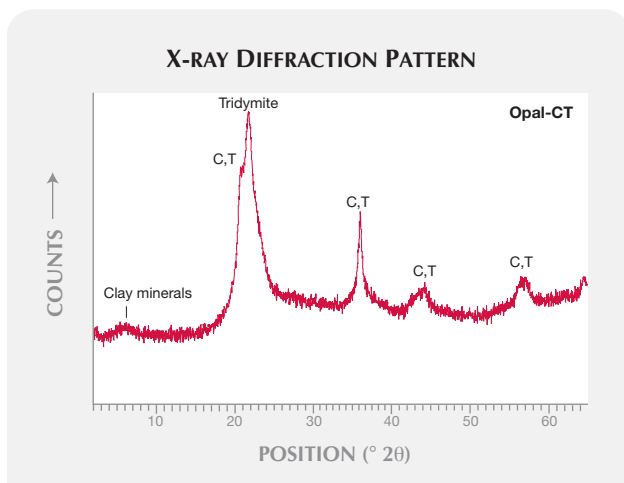
Element	No. 10 Yellowish white and yellow	No. 22 Yellow	No. 3 Yellow	No. 18 Orange
Li	0.15	0.21	0.30	0.44
Be	1.08	8.94	17.97	25.20
B	0.86	4.98	0.75	1.31
Na	1196	600.4	61.11	97.55
Mg	1122	891.0	5429	17730
Cl	412.3	453.1	443.7	870.4
Al	2890	3609	22.82	5040
K	336.2	197.2	51.73	398.9
Ca	1238	368.8	771.5	1314
Sc	3.09	4.60	3.09	2.70
Ti	53.76	61.29	15.15	12.10
V	0.30	3.30	0.29	1.66
Cr	1.02	3.77	1.40	5.90
Mn	1.09	12.44	10.97	9.73
Fe	137.1	1888	7251	12070
Co	0.41	0.73	0.18	0.39
Ni	0.78	4.44	2.24	2.98
Cu	0.20	1.70	0.53	1.61
Zn	1.09	6.98	71.09	86.56
Rb	3.89	1.38	0.36	3.44
Sr	43.40	10.69	1.68	2.28
Y	0.80	0.87	1.91	8.24
Zr	78.10	10.22	0.38	0.28
Ba	15.40	35.11	5.82	41.58
Pb	0.10	0.55	1.51	5.66
U	0.02	3.05	2.50	2.13

^a Average of four analyses per sample.

UV radiation (see table 1), which is consistent with their higher iron contents (>7000 ppm), despite the presence of U (>2 ppm). Sample 22, with 3 ppm U, was inert to long-wave UV but showed weak yellow fluorescence to short-wave UV, as would be expected from its Fe content (1888 ppm). Sample 10 exhibited blue (rather than green) luminescence, consistent with its low U and Fe contents; the oxygen-related defects causing this behavior cannot be measured by the techniques used on these samples.

X-ray Diffraction. Based on X-ray diffraction, according to Jones and Segnit's (1971) mineralogical classification, opal can be subdivided into three general groups: opal-C (relatively well ordered α -cristobalite), opal-CT (disordered α -cristobalite with α -tridymite-type stacking), and opal-A (amorphous). The powder X-ray diffraction measurements of four of the six samples analyzed by this method classified them as opal-CT, which is consistent with their volcanic origin (Jones and Segnit, 1971; Ostrooumov et al., 1999; Fritsch et al., 2004). Their patterns were characterized by main peaks in the 2θ range—attributed to cristobalite and tridymite phases—that showed various degrees of disorder (figure 5, left). The other two stones (nos. 20 and 21) can be considered opal-C on the basis of their X-ray patterns, which were similar to those of α -cristobalite (figure 5, right). Opal-C is also associated with volcanic deposits (Jones and Segnit, 1971), but in general it is rarer than opal-CT (Fritsch et al., 2004). Moreover, our results are consistent with the findings by Elzea and Rice (1996) that opal-C and opal-CT are part of a continuum of disor-

Figure 5. These powder X-ray diffraction patterns were collected from Malagasy samples consisting of opal-CT (left, no. 22) and opal-C (right, no. 21). The attribution of the main CT (cristobalite-tridymite) and tridymite peaks is shown for opal-CT, whereas all signals in the pattern on the right are related to cristobalite (the most important being the two peaks at 28.50 and 31.40° 2θ , which allow for a rapid identification). The broad band between 4.9 and 6.8° 2θ , especially visible in the pattern on the left, is due to clay minerals.



dered intergrowths between end-member cristobalite and tridymite stacking sequences.

The diffraction patterns of some samples also showed, in accordance with SEM-EDS observations, a broad band between 4.9 and $6.8^\circ 2\theta$, due to clay minerals. Identification of the specific clay mineral(s) requires further study.

Spectroscopy. Raman. This technique has been established as an effective, nondestructive method to characterize gem opal (Smallwood et al., 1997; Ostrooumov et al., 1999; Ilieva et al., 2007). The Raman spectra of our opal samples revealed several peaks between 3000 and 200 cm^{-1} , due to different stretching and bending vibration modes of the Si-O system (see, e.g., Smallwood et al., 1997). As expected, the most intense Raman peaks were located in the ~ 500 – 200 cm^{-1} range, which contains the typical features of tridymite and cristobalite (figure 6).

In the spectra of samples 10 and 22, we observed a broad band centered at $\sim 350\text{ cm}^{-1}$ and a weaker band at $\sim 300\text{ cm}^{-1}$, which are typical of opal-CT (e.g., Ostrooumov et al., 1999; Ilieva et al., 2007). These bands were not well resolved, as opal is a poor Raman scatterer, especially when a laser in the visible range (here, 632.8 nm) is used. Small features at 1086 , 955 , and 780 cm^{-1} were also present, together with a weak water signal at about 1620 cm^{-1} (not shown in figure 6).

Opal-C samples 20 and 21 exhibited Raman scattering at 412 and 226 cm^{-1} , revealing cristobalite as their dominant structural component (Ilieva et al., 2007), in agreement with the X-ray diffraction data. These peaks are broader than those of α -cristobalite, in accordance with the greater structural disorder of opal. However, they may contain contributions from inclusions of α -cristobalite, as suggested by Gaillou et al. (2004). The samples also contained minor peaks at 1620 , 1194 (in sample no. 21), 1090 , and 780 cm^{-1} .

Mid-Infrared. Although X-ray diffraction and Raman spectroscopy are the most informative techniques for determining an opal's structure and typology, IR spectroscopy can be usefully coupled with these other analytical methods. The IR spectra of the three opal-CT samples investigated (e.g., figure 7) were characterized by spectral features of molecular water and silanol (SiOH) groups, consisting of a broad absorption band at 3400 cm^{-1} and a feature at about 1650 – 1630 cm^{-1} (Farmer, 1974; Langer and Flörke, 1975; Bartoli et al., 1990). The three strong bands at ~ 1100 , 790 , and 470 cm^{-1} are related to the fundamental Si-O vibrations (see, e.g., Farmer, 1974; Plyusnina, 1979; Webb and Finlayson, 1987), whereas the two weak bands at ~ 2000 and 1880 cm^{-1} are probably due to overtones and combinations of Si-O fundamentals (Langer and Flörke, 1975). These IR spectra are consistent with the samples' microcrystalline nature, and in particular with their CT typology (see also Adamo et al., 2010).

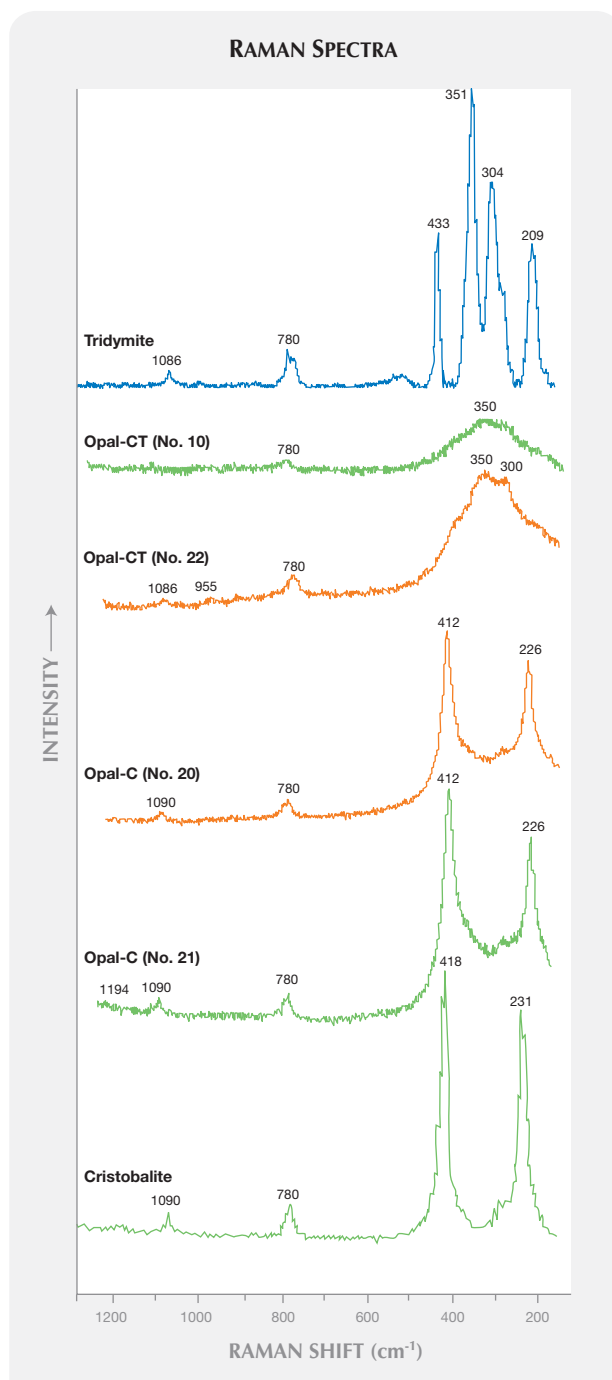


Figure 6. Raman spectra in the 1200 – 200 cm^{-1} range of the four Malagasy opals tested (nos. 10, 20, 21, and 22) are compared to those of standard α -cristobalite and α -tridymite minerals from the RRUFF database (rruff.info).

Clay-mineral impurities are responsible for the 3545 and 692 cm^{-1} absorption bands (Van Der Marel and Beitelspacher, 1976), which were observed in two of the three samples investigated.

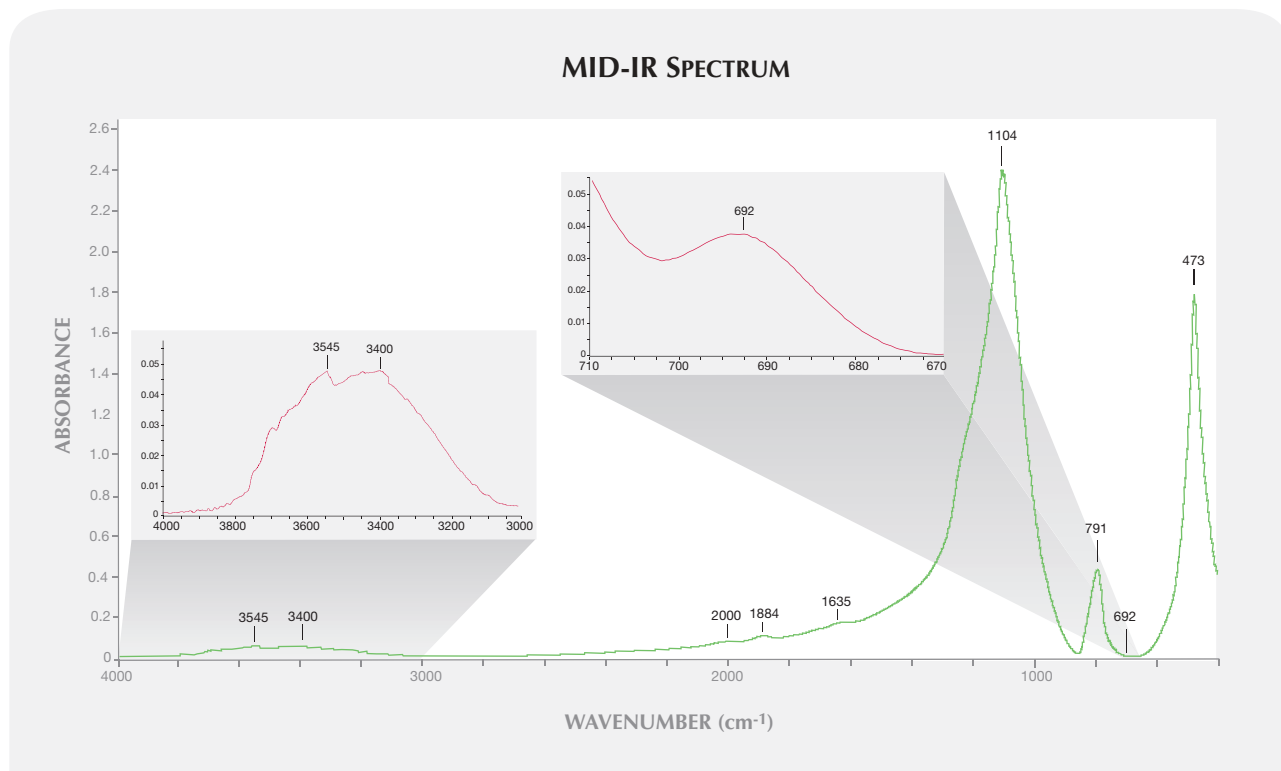


Figure 7. This mid-IR spectrum of an opal-CT sample (no. 22) shows features related to molecular water, SiOH groups, and Si-O bonds, as well as clay mineral impurities (insets).

IDENTIFICATION AND CONCLUSIONS

Opal samples from a new deposit near Bemia, Madagascar, show a wide variety of colors, including those typical of fire opal, but always without play-of-color and often with strong color zoning in a characteristic banded structure. Darker colors correspond to higher iron content (i.e., Fe-containing inclusions). The samples investigated here were all microcrystalline (opal-CT or opal-C) with varying degrees of order, as indicated by the X-ray diffraction data and Raman and IR spectra. The RI values (1.415–1.462) are higher than those typical of fire opals from other localities, such as Mexico, as are the SG values (up to 2.38), which

are also slightly higher than those reported for opal in general. The Malagasy opals are also distinguishable from the original Mexifire synthetics described by Choudhary and Bhandari (2008), on the basis of their higher RI and SG values. With respect to the Mexifire synthetic manufactured since late 2009, RI and SG are similar, though the slightly higher RI value of the new Mexifire material (1.470) should be diagnostic in most cases.

Opal from Bemia has been mined for a few years and is starting to enter the market. The material found so far, as well as ongoing work at the deposit, indicates the potential for economic production.

ABOUT THE AUTHORS

Dr. Simoni (arsimoni@tin.it) is a gemologist in Pavia, Italy. Dr. Caucia is professor of mineralogy in the Earth Sciences Department at the Università degli Studi di Pavia, Italy. Dr. Adamo is a postdoctoral fellow in the Earth Sciences Department at the Università degli Studi di Milano, and Dr. Galinetto is a researcher in the Theoretical Physics Department at the Università degli Studi di Pavia.

ACKNOWLEDGMENTS

The authors thank Armando and Luca Pasqualini of Pavia for providing samples and information about the opal investigated in this study. The authors are indebted to Giorgio Carbone and Marco Pelinzona (Università degli Studi di Pavia) for collaboration in X-ray diffraction data collection and SEM analyses, respectively, and to Dr. Alberto Zanetti (IGG-CNR, Pavia) for LA-ICP-MS measurements. Rajneesh Bhandari (Rhea Industries, Jaipur, India) and Gagan Choudhary (Gem Testing Laboratory, Jaipur) are acknowledged for information about the new Mexifire synthetic. The manuscript benefited considerably from thoughtful comments by Dr. Eloise Gaillou, Dr. Federico Pezzotta, and an anonymous reviewer.

REFERENCES

- Adamo I., Ghisoli C., Caucia F. (2010) A contribution to the study of FTIR spectra of opals. *Neues Jahrbuch für Mineralogie, Abhandlungen*, Vol. 187, No. 1, pp. 63–68.
- Ball R.A., Daniel A. (1976) Opal in south western Queensland: part one, a brief review; part two, some thoughts on Yowah Nuts. *Australian Gemmologist*, Vol. 12, No. 12, pp. 359–363.
- Bank H., Henn U., Milisenda C.C. (1997) Gems from Ethiopia. *Zeitschrift der Deutschen Gemmologischen Gesellschaft*, Vol. 46, No. 1, p. 4.
- Bartoli F., Bittencourt Rosa D., Doirisse M., Meyer R., Philipp R., Samama J.-C. (1990) Role of aluminium in the structure of Brazilian opals. *European Journal of Mineralogy*, Vol. 2, No. 5, pp. 611–619.
- Bittencourt Rosa D. (1990) Les opals nobles du district de Pedro II dans l'Etat de Piauí, région nord-est du Brésil. *Revue de Gemmologie A.F.G.*, Vol. 104, No. 1, pp. 3–7.
- Choudhary G., Bhandari R. (2008) A new type of synthetic fire opal: Mexifire. *G&G*, Vol. 44, No. 3, pp. 228–233.
- Downing P. (2003) *Opal Identification and Value*. Majestic Press, Estes Park, CO.
- Elzea J.M., Rice S.B. (1996) TEM and X-ray diffraction evidence for cristobalite and tridymite stacking sequences in opal. *Clay and Clay Minerals*, Vol. 44, No. 4, pp. 492–500.
- Enseli F., Kumbasar I., Eren R.E., Uz B. (2001) Characteristics of opals from Simav, Turkey. *Neues Jahrbuch für Mineralogie, Monatshefte*, Vol. 3, No. 5, pp. 97–113.
- Farmer V.C. (1974) *The Infrared Spectra of Minerals*. Mineralogical Society, London.
- Fritsch E., Rondeau B., Ostroumov M., Lasnier B., Marie A.-M., Barrault A., Wery J., Connoué J., Lefrant S. (1999) Découvertes récentes sur l'opale. *Revue de Gemmologie*, No. 138/139, pp. 34–40.
- Fritsch E., Ostroumov M., Rondeau B., Barreau A., Albertini D., Marie A.-M., Lasnier B., Wery J. (2002) Mexican gem opal: Nano and micro-structures, origin of color and comparison with other common opals of gemmological significance. *Australian Gemmologist*, Vol. 21, No. 6, pp. 230–233.
- Fritsch E., Gaillou E., Ostroumov M., Rondeau B., Devouard B., Barreau A. (2004) Relationship between nanostructure and optical absorption in fibrous pink opals from Mexico and Peru. *European Journal of Mineralogy*, Vol. 16, No. 5, pp. 743–752.
- Fritsch E., Gaillou E., Rondeau B., Barreau A., Albertini D., Ostroumov M. (2006) The nanostructure of fire opal. *Journal of Non-Crystalline Solids*, Vol. 352, pp. 3957–3960.
- Gaillou E., Mocquet B., Fritsch E. (2004) Gem News International—A new gem material from Madagascar: A mixture of cristobalite and opal. *G&G*, Vol. 40, No. 4, pp. 339–340.
- Gaillou E., Delaunay A., Fritsch E., Bouhnik-le-Coz M. (2006) Geologic origin of opals deduced from geochemistry. *G&G*, Vol. 42, No. 3, p. 107.
- Gaillou E., Delaunay A., Rondeau B., Bouhnik-le-Coz M., Fritsch E., Corner G., Monnier C. (2008) The geochemistry of gem opals as evidence of their origin. *Ore Geology Reviews*, Vol. 34, pp. 113–126.
- Gaillou E., Fritsch E., Aguilar-Reyes B., Rondeau B., Post J., Barreau A., Ostroumov M. (2008) Common gem opal: An investigation of micro- to nano-structure. *American Mineralogist*, Vol. 93, pp. 1865–1873.
- Graetsch H., Gies H., Topalovi I. (1994) NMR, XRD and IR study on microcrystalline opals. *Physics and Chemistry of Minerals*, Vol. 21, No. 3, pp. 166–175.
- Gübelin E.J. (1986) Opal from Mexico. *Australian Gemmologist*, Vol. 16, No. 2, pp. 45–51.
- Holzhey G. (1991) Feueropal aus Aleksejewskoje, Kasachische, UdSSR – ein Beitrag zu vergleichenden gemmologisch-mineralogische Untersuchungen mikrokristalline SiO₂-Minerale. *Zeitschrift der Deutschen Gemmologischen Gesellschaft*, Vol. 40, No. 1, pp. 11–13.
- Ilieva A., Mihailova B., Tsintov Z., Petrov O. (2007) Structural state of microcrystalline opals: A Raman spectroscopic study. *American Mineralogist*, Vol. 92, pp. 1325–1333.
- Jones J.B., Segnit E.R. (1971) The nature of opal. I. Nomenclature and constituent phases. *Journal of the Geological Society of Australia*, Vol. 18, No. 1, pp. 57–68.
- Koivula J.L., Fryer C., Keller P.C. (1983) Opal from Querétaro, Mexico: Occurrence and inclusions. *G&G*, Vol. 19, No. 2, pp. 87–96.
- Lacroix A. (1922) *Minéralogie de Madagascar*, Vol. 1. Augustin Challamel éditeur, Paris, pp. 269–273.
- Langer K., Flörke O.W. (1975) Near infrared absorption spectra (4000–9000 cm⁻¹) of opals and the role of “water” in these SiO₂ · nH₂O minerals. *Fortschritte der Mineralogie*, Vol. 52, No. 1, pp. 17–51.
- O'Donoghue M., Ed. (2006) *Gems*, 6th ed. Butterworth-Heinemann, Oxford, UK.
- Ostroumov M., Fritsch E., Lasnier B., Lefrant S. (1999) Spectres Raman des opales: Aspect diagnostique et aide à la classification. *European Journal of Mineralogy*, Vol. 11, No. 5, pp. 899–908.
- Plusynina I.I. (1979) Infrared spectra of opals. *Soviet Physics Doklady*, Vol. 24, No. 5, pp. 332–333.
- Rossmann G.R. (1994) Colored varieties of the silica minerals. In P.J. Heaney, C.T. Prewitt, G.V. Gibbs, Eds., *Silica—Physical Behavior, Geochemistry and Materials Applications*, Reviews in Mineralogy and Geochemistry, Vol. 29, Mineralogical Society of America, Washington, DC, pp. 433–467.
- Simoni M., Caucia F. (2009) Opali di fuoco dal Madagascar. *Rivista Gemmologica Italiana*, Vol. 4, No. 2, pp. 91–104.
- Smallwood A.G., Thomas P.S., Ray A.S. (1997) Characterisation of sedimentary opals by Fourier transform Raman spectroscopy. *Spectrochimica Acta*, Part A, Vol. 53, pp. 2341–2345.
- Smith K.L. (1988) Opals from Opal Butte, Oregon. *G&G*, Vol. 24, No. 4, pp. 229–236.
- Van Der Marel H.W., Beutelspacher H. (1976) *Atlas of Infrared Spectroscopy of Clay Minerals and Their Admixture*. Elsevier, Amsterdam.
- Webb J.A., Finlayson B.L. (1987) Incorporation of Al, Mg, and water in opal-A: Evidence for speleothems. *American Mineralogist*, Vol. 72, pp. 1204–1210.
- Webster R. (1994) *Gems: Their Sources, Descriptions and Identification*, 5th ed. Rev. by P.G. Read, Butterworth-Heinemann, Oxford, UK.

For online access to all articles in **GEMS & GEMOLOGY** from 1981 to the present, visit:

gia.metapress.com

X-RAY COMPUTED MICROTOMOGRAPHY APPLIED TO PEARLS: METHODOLOGY, ADVANTAGES, AND LIMITATIONS

Stefanos Karampelas, Jürgen Michel, Mingling Zheng-Cui, Jens-Oliver Schwarz, Frieder Enzmann, Emmanuel Fritsch, Leon Leu, and Michael S. Krzemnicki

X-ray computed microtomography reveals the internal features of pearls with great detail. This method is useful for identifying some of the natural or cultured pearls that are difficult to separate using traditional X-radiography. The long measurement time, the cost of the instrumentation, and the fact only one pearl at a time can be imaged are some of this method's disadvantages.

The value of a pearl is strongly dependent on its natural or cultured origin (for the exact definitions of natural and cultured pearls, see CIBJO, 2010). There are two major categories of cultured pearls: beaded (bead with a mantle-tissue graft; BCPs) and non-beaded (solely a mantle-tissue graft; NBCPs). (For more information regarding grafting and beading, see Sturman [2009] and references therein.)

Traditional X-radiographs are by far the most useful tool to separate cultured from natural pearls (Webster, 1994). Radiographs provide a projection on a plane of the X-ray transparency of the investigated object; typically, the bead or structures related to the tissue used to stimulate growth of the cultured pearl will have a different appearance from that of the pearl itself. In the last decade, however, the market has received large quantities of freshwater as

well as some saltwater NBCPs that are sometimes difficult to identify using radiography (Scarratt et al., 2000; Akamatsu et al., 2001; Hänni, 2006; Sturman and Al-Attawi, 2006; Sturman, 2009; figure 1). Moreover, drilling of pearls may remove the evidence laboratories need to determine their origin (Crowningshield, 1986a,b). Thus, there is a need to improve the acquisition of X-ray images of pearls—for example, through the use of multiple images taken in different directions. Even so, determination of the natural or cultured origin of a small number of pearls remains difficult with radiography alone (see questionable cases in Sturman, 2009). Recently, X-ray computed microtomography has shown promise for pearl identification (Strack, 2006; Wehrmeister et al., 2008; Kawano, 2009; Krzemnicki et al., 2009).

Developed in the 1960s, computed tomography (CT or μ -CT for computed microtomography) allows the user to investigate nondestructively the internal structure of an object with high spatial resolution, providing applications for biology/medicine, materials science, and geology (see Ketcham and Carlson, 2001; Van Geet et al., 2001; Jacobs and Cnudde, 2009). It works by iteratively taking radiographic projections of a rotating sample (usually through 360°; figure 2). X-rays are attenuated by the sample as a function of its thickness and the linear attenuation coefficient (also known as the absorption coefficient—in this case, how easily the material can be penetrated by the X-rays) of the material. Projections of the sample are typically recorded by a CMOS (complementary metal-oxide semiconductor) flat-panel detector with an integrated scintillator. These projections are used to reconstruct three-dimensional (3D) models of the investigated object. Then, two-dimensional (2D) slices can be cut through the 3D models in different directions. Depending on the size of the studied area, it is possible to attain resolutions down to the micrometer scale. Resolution is generally given as

See end of article for About the Authors and Acknowledgments.

GEMS & GEMOLOGY, Vol. 46, No. 2, pp. 122–127.

© 2010 Gemological Institute of America

the length of one pixel, or expressed as a volume element (voxel, a 3D pixel). To be resolved, features must be several voxels in dimension in at least one direction.

In this study, all the results are grayscale—the radiographs as well as the 2D and 3D slices/models. In the radiographic images, lighter colors indicate materials with higher density (e.g., calcium carbonate) and darker colors represent lower-density materials (e.g., organic matter or voids). With longer measurements, the calcium carbonate polymorphs can be separated (e.g., aragonite from calcite and vaterite: see Wehrmeister et al., 2008; Soldati et al., 2009).

MATERIALS AND METHODS

More than 50 samples known to be natural pearls and beaded or non-beaded cultured pearls from various reputable sources were imaged and compared using X-radiography and X-ray μ -CT. This study includes the results for 16 of these samples, representing different pearl categories: 6 natural pearls, as well as 4 beaded and 6 non-beaded cultured pearls (both freshwater and saltwater) from various mollusks. Five were drilled or half-drilled; two were mounted in jewelry (see table 1).

Film X-radiography was performed at the Gübelin Gem Lab, following the standard techniques used in most gemological laboratories (see, e.g., Akamatsu et al., 2001). X-rays were generated by a Comet X-ray unit, and the samples were immersed in a lead nitrate solution (used as scatter-reducing fluid). Two or more radiographs were taken in different directions for all samples. Each image required about 20 minutes.

Microtomography measurements were performed at the Institute of Geosciences of Mainz University, using a ProCon X-Ray CT-Alpha instrument equipped with a YXLON FXE 160.51 X-ray tube and a Hamamatsu flat-panel sensor detector (figure 3). Although this instrument is capable of taking images that are 2048×2048 pixels (50 μ m per pixel), all of the images we used were taken with a setting of 1024×1024 pixels (100 μ m per pixel); that is, four pixels were merged as one during image recording. This procedure allowed for a shorter measurement time and smaller volumes of data, but it halved the given reso-



Figure 1. Some white to yellowish brown (“golden”) pearls are difficult to identify by classical X-radiography, as they present questionable structures. A mixture of natural and cultured pearls (up to ~9.5 mm) are shown here. Photo by Evelyne Murer.

lution. The instrumentation could measure objects as small as 1 mm or as large as ~100 mm wide and 90 mm tall. The highest resolution could be obtained by placing small objects close to the X-ray source; this was done in some cases to more closely examine interesting or questionable structures. So-called region-of-interest (ROI) scans allow imaging of larger objects or magnifications of a specific part of an object. The drawbacks of such scans are typically an increase in artifacts and poorer image quality. The sample chamber is $30 \times 30 \times 30$ cm. Unlike radiography, microtomography can only image one pearl (loose or, in some cases, mounted) at a time, not a strand of pearls.

A series of tests were run to define the ideal parameters for the highest contrast between the different phases in pearls. X-rays were generated with 100 kV accelerating

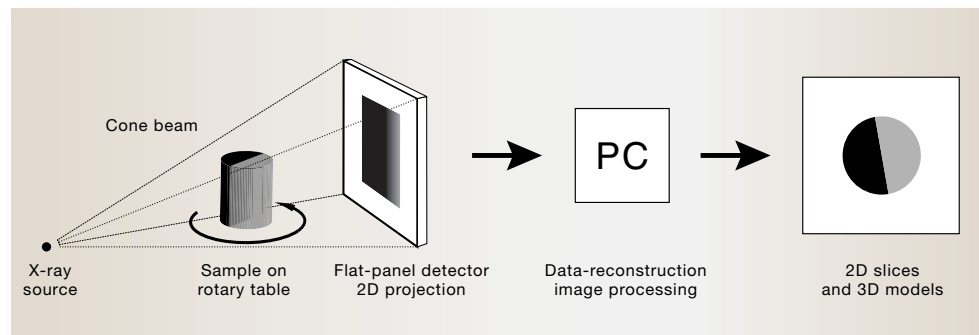


Figure 2. Components of the μ -CT analytical process are shown in this schematic drawing.

TABLE 1. Characteristics and μ -CT resolution of the studied pearl samples.^a

Sample no.	Type	Mollusk	Size (mm)	Shape	Color	Condition	μ -CT resolution (μ m)
SK-61	Natural SW	<i>Pteria spp.</i>	8.7 • 8.1	Drop	Gray-black	Drilled ^b	11.0
SK-46	Natural SW	<i>Pinctada spp.</i>	6.4	Round	Light "cream"	Drilled	7.0
Pp07	Natural SW	<i>Pteria spp.</i>	10.1 • 6.5 • 3.9	Baroque	Light "cream"	Sawn	11.0
GGL03	Natural FW	Unionida order	9.5–10.2 • 7.0	Button	Light gray	Whole	10.8
GGL33	Natural FW	Unionida order	6.9–7.4 • 6.3	Button	White	Whole	8.0
GGL27	Natural FW	Unionida order	6.0	Round	White	Whole	6.4
GGL17	Beaded SWCP	<i>P. margaritifera</i>	9.7	Round	Gray-black	Whole	10.6
GGL18	Beaded SWCP	<i>P. margaritifera</i>	10.4 • 9.9	Drop	Gray-black	Whole	11.3
GGL19	Beaded SWCP	<i>P. maxima</i>	12.7 • 11.3	Button	White	Whole	13.8
GGL32	Beaded FWCP	<i>Hyriopsis spp.</i>	6.9	Round	Light gray	Drilled	7.7
GGL22	Non-beaded SWCP	<i>P. margaritifera</i>	10.6 • 4.9 • 2.8	Baroque	Light gray	Whole	11.0
SK-50	Non-beaded SWCP	<i>P. sterna</i>	7.2 • 5.4 • 4.2	Baroque	Gray-purple	Whole	8.0
SK-51	Non-beaded SWCP	<i>P. sterna</i>	7.2 • 3.9 • 3.5	Baroque	Gray-purple	Whole	8.0
SK-54	Non-beaded FWCP	<i>Hyriopsis spp.</i>	10.0 • 8.8	Drop	Light gray-purple	Half-drilled	11.0
SK-62	Non-beaded FWCP	<i>Hyriopsis spp.</i>	11.0 • 8.9	Drop	Gray-purple	Half-drilled ^b	10.0
GGL26	Non-beaded FWCP	<i>Hyriopsis spp.</i>	6.3 • 6.0	Near round	Yellowish brown	Whole	6.9

^a Abbreviations: FW = freshwater, SW = saltwater, FWCP = freshwater cultured pearl, SWCP = saltwater cultured pearl.

^b Mounted

Figure 3. For microtomography, we used the ProCon X-Ray CT-Alpha instrument based at the Institute of Geosciences of Mainz University. The outer dimensions are 190 • 150 • 100 cm, and the sample chamber is 30 • 30 • 30 cm. The total weight of the instrument is 2.5 tons. Photo by J. Michel.



NEED TO KNOW

- X-ray computed microtomography can reveal the internal structure of a pearl with micrometer-scale resolution.
- The technique is particularly effective for identifying non-beaded cultured pearls.
- Drawbacks include artifacts produced by sample rotation and metal mountings, long measurement time, large data files, costly instrumentation, and the fact that only one pearl at a time can be imaged.

voltage and 110 μ A target current. The beam was prefiltered by 1-mm-thick aluminum foil to reduce beam-hardening effects. Projections were taken with an exposure time of 500 milliseconds. Each measurement consisted of 800 projections (over a 360° rotation), averaging 10 images for each position. Resolution was strongly dependent on the size of the studied area, and ranged from 6.4 to 13.8 μ m per voxel (see table 1).

Reconstruction of the raw data was done using Volex software developed by the Fraunhofer Institute, Germany, and image processing employed Amira software. Data were output as 3D models and 2D slices in the x-, y-, and z-directions. Each sample required about five hours for analysis (including sample mounting, machine set-up, measuring time, and data/image processing). All the calculations were carried out on PCs with >8 GB RAM. The data generated for each pearl consumed >10 GB of disk space.

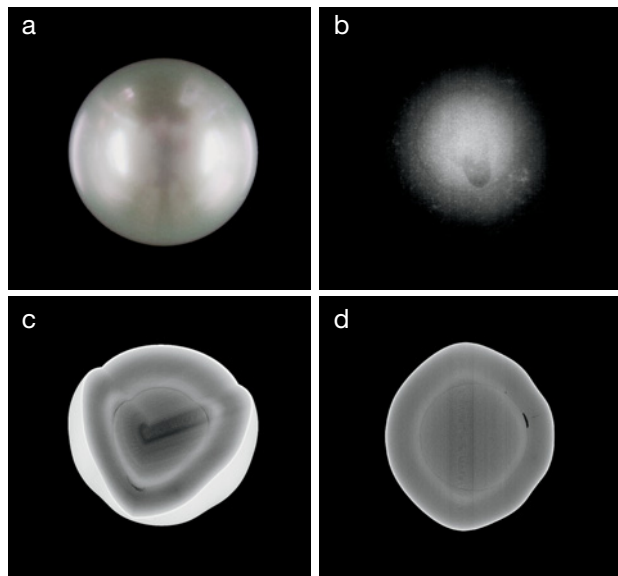


Figure 4. In this (a) white button-shaped beaded saltwater cultured pearl from *P. maxima* (sample GGL19), the bead is visible in the radiograph (b) as well as in the 3D (c) and 2D (d) μ -CT images; however, the boundary between the nacre and the bead is sharper in the μ -CT images, which also show organic matter surrounding the bead. (See also Depository item 1.)

RESULTS AND DISCUSSION

Selected results are shown in figures 4–8 (as well as in the *G@G* Data Depository at gia.edu/gandg), which provide photos of the samples, scans of the X-radiographic films, 3D μ -CT models, and 2D μ -CT slices in the most informative directions. (Note that the scanned films are of lower quality compared to the original films.) For the purpose of visualization, a portion of each 3D model has been removed to show the internal structures. The best structural visualization of the samples is revealed by the 3D μ -CT images. In addition to producing superior image quality, microtomography allows the user to scroll through a pearl virtually by combining the single CT sections into a “movie,” enabling the dynamic recognition of internal structures that are difficult to interpret when observing single CT sections or radiographs (see *G@G* Data Depository for this article and for Krzemnicki et al., 2010).

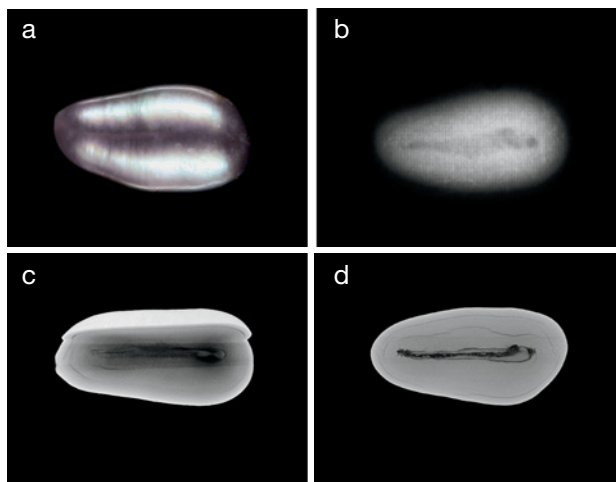
All the beaded cultured pearls as well as all but two of the non-beaded cultured pearls and natural pearls in this study could be identified by radiography. The beads in the BCPs (figure 4), the structures associated with the grafted tissue in the NBCPs (figure 5), and the onion-like layers with a black point in the center of the natural pearls (figure 6) typically were clearly seen in the radiographs. In some cases, however, the μ -CT scans revealed additional characteristics useful for pearl identification. In figure 7, for exam-

ple, it can be seen that a drill hole removed part of the pearl’s central structures, and identification with traditional radiography was uncertain. Although some growth structures appear on the radiograph, the μ -CT images reveal a more detailed and three-dimensional view of the central growth structures that enabled the identification of this pearl as natural. Additional features such as cracks and growth lines were also revealed in some of the μ -CT images. These characteristics were only $\sim 10\ \mu\text{m}$ thick (or less), and were not observed with radiography.

The μ -CT technique does have some limitations. Pearls that are mounted or that have a metal lining within the drill hole may show artifacts, which can mask the internal structures and thus make their identification difficult (figure 8 and Data Depository item 7). In radiographs, the metal mounting is less of an obstacle. Also, μ -CT sections show reconstruction artifacts due to rotation. Although these artifacts can be reduced with appropriate analytical parameters, generally they are not completely removed. The artifacts are manifested as perfectly centered fine circles in horizontal sections (i.e., transaxial sections), and as a blurry rotation axis in the center of the reconstructed image in vertical sections (i.e., sagittal and coronal sections, which are oriented 90° to one another), as illustrated in Data Depository items 1–6. Care must be taken so the fine circles in the transaxial sections are not misinterpreted by an inexperienced observer as (natural) onion-like growth structures.

More structures in natural and cultured pearls observed with μ -CT are well illustrated by Krzemnicki et al. (2010), in the *G@G* Data Depository, and at www.gubelingemlab.ch.

Figure 5. In this (a) gray-purple baroque-shaped non-beaded saltwater cultured pearl from *Pteria sterna* (“keshi”; sample SK-51), tissue-related structures are visible in the radiograph (b) and μ -CT images (c, d). Characteristically, these structures follow the shape of the pearl. Some finer-scale structures are seen in the μ -CT images. (See also Depository item 2.)



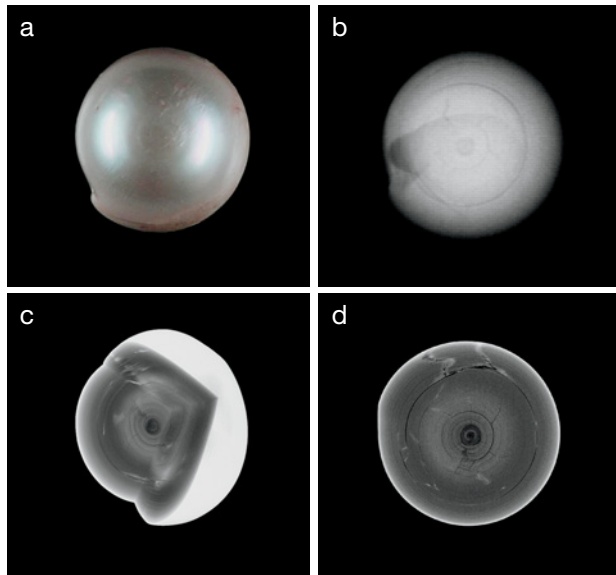


Figure 6. In this (a) light gray button-shaped freshwater natural pearl from the Unionida order (sample GGL03), typical onion-like structures with a black point in the center are visible in the radiograph (b) as well as in the μ -CT images (c, d), but are sharper in the latter. The μ -CT images also reveal fissures surrounded by a denser (white-appearing) material, which are barely visible in the radiograph. (See also Depository item 3.)

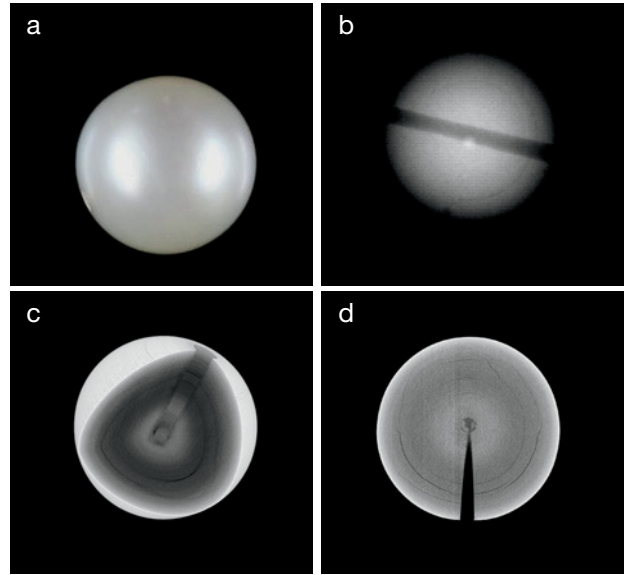
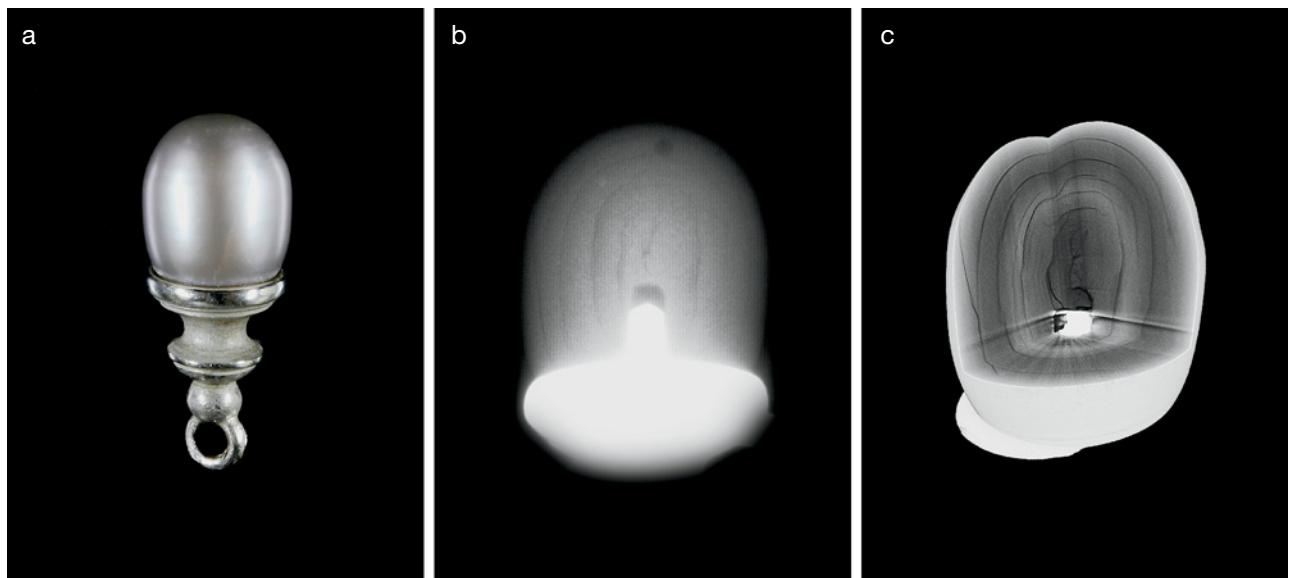


Figure 7. In this (a) drilled, light "cream," round salt-water natural pearl from Pinctada spp. (sample SK-46), concentric growth structures are observed in the radiograph (b), but the drilling has partially removed the structures in the center of the pearl and identification with the radiograph alone is inconclusive. In the μ -CT images (c, d), however, some remnants of the central growth structures are visible, revealing the pearl's natural origin. (See also Depository item 4.)

Figure 8. In this (a) mounted, half-drilled, gray-purple, drop-shaped non-beaded freshwater cultured pearl from Hyriopsis spp. (sample SK-62), characteristic structures of a cultured pearl are observed in the radiograph (b) as well as in the 3D μ -CT image (c). However, in the μ -CT image the metal partially masks the internal structure of the pearl. (See also Depository item 7.)



CONCLUSIONS

Although most cultured and natural pearls can be reliably separated with radiographs alone, their biomineralization is better visualized with X-ray μ -CT (unless they are mounted in metal). In fact, some non-beaded cultured pearls require high-resolution 3D imaging for a correct identification; in such cases, μ -CT can be quite helpful.

The main advantage of tomography is that it gives high-resolution information in three dimensions, whereas radiography condenses the 3D structures onto a flat film as a two-dimensional image. This becomes evident when observing fissures in pearls. Their position within the 3D volume of a pearl is sometimes difficult to interpret in radiographs, even when they are taken in different directions. With μ -CT, the tissue-related structures and the fissures are better revealed, so it is easier to make a correct identification. However, the technique is mainly useful for pearls that do not have metal mountings, it requires a long measurement time, and it consumes a huge amount of data storage space. In addition, μ -CT instrumentation is still costly—about US\$550,000 for the instrument and accessories—and the technique requires scientifically trained staff for analysis and interpretation. Note, though, that a new generation of instruments using X-rays are entering the market, which could be used for digital radiography as well as μ -CT, at the same or even lower prices.

Additional μ -CT studies of problematic pearls (e.g., the non-beaded types described by Sturman, 2009) are expect-

ed to reveal more of the strengths and limitations of this emerging method. Studies at higher resolution, magnifying a specific region of the sample (such as with synchrotron μ -CT), may reveal some very small details of pearl structure that are useful for their identification. Micro-CT analysis may also prove helpful for identifying organic gem materials protected by CITES, such as corals and ivory.

ABOUT THE AUTHORS

Dr. Karampelas (s.karampelas@gubelingemlab.ch) is a research scientist, and Mrs. Zheng-Cui is an analyst, at the Gübelin Gem Lab, Lucerne, Switzerland. Mr. Michel, Dr. Schwarz, and Dr. Enzmann are researchers, and Mr. Leu is an undergraduate student, in the Institute of Geosciences at Johannes Gutenberg University of Mainz, Germany. Dr. Fritsch is professor of physics at the University of Nantes, Institut des Matériaux Jean Rouxel (IMN)-CNRS, Team 6205, France. Dr. Krzemnicki is director of the SSEF Swiss Gemmological Institute, Basel.

ACKNOWLEDGMENTS

The authors thank Thomas Hainschwang (Gemlab, Balzers, Principality of Liechtenstein), Edigem Ltd. (Lucerne, Switzerland), Centre de Recherche Gemmologique (University of Nantes, France), and Perlas del Mar de Cortez (Guaymas, Mexico) for providing some of the study samples, as well as Alessandra Spingardi (Gübelin Gem Lab) for the photos of the samples.

REFERENCES

- Akamatsu S., Zansheng T.L., Moses T.M., Scarratt K. (2001) The current status of Chinese freshwater cultured pearls. *G&G*, Vol. 37, No. 2, pp. 96–113.
- CIBJO (2010) *The Pearl Book: Natural, Cultured & Imitation Pearls—Terminology & Classification*. The World Jewelry Confederation, Milan, Italy, 53 pp., http://download.cibjo.org/10_04_21_CIBJO_Pearl_Blue_Book.pdf.
- Crowningshield R. (1986a) Gem Trade Lab Notes: Pearls with unusual drilling features. *G&G*, Vol. 22, No. 1, pp. 50–52.
- Crowningshield R. (1986b) Gem Trade Lab Notes: Cultured pearls, miscellaneous oddities. *G&G*, Vol. 22, No. 2, pp. 110–111.
- Hänni H.A. (2006) A short review of the use of 'keshi' as a term to describe pearls. *Journal of Gemmology*, Vol. 30, No. 1–2, pp. 51–58.
- Jacobs P., Cnudde V. (2009) Applications of X-ray computed tomography in engineering geology or "looking inside rocks. . ." *Engineering Geology*, Vol. 103, No. 3–4, pp. 67–68.
- Kawano J. (2009) Observation of the internal structures of pearls by X-ray CT technique. *Gemmology*, Vol. 40, No. 478, Issue 7, pp. 2–4 [in Japanese].
- Ketcham R.A., Carlson W.D. (2001) Acquisition, optimization and interpretation of X-ray computed tomographic imagery: Applications to the geosciences. *Computers & Geosciences*, Vol. 27, No. 4, pp. 381–400.
- Krzemnicki M.S., Friess S., Chalup P., Hajdas I., Hänni H.A. (2009) New developments in pearl analysis: X-ray micro tomography and radiocarbon age dating. *Journal of the Gemmological Association of Hong Kong*, Vol. 30, pp. 43–45.
- Krzemnicki M., Friess D., Chalup P., Hänni H.A., Karampelas S. (2010) X-ray computed microtomography: Distinguishing natural pearls from beaded and non-beaded cultured pearls. *G&G*, Vol. 46, No. 2, pp. 128–134.
- Scarratt K., Moses T., Akamatsu S. (2000) Characteristics of nuclei in Chinese freshwater cultured pearls. *G&G*, Vol. 36, No. 2, pp. 98–109.
- Soldati A.L., Jacobi D.E., Wehrmeister U., Hofmeister W. (2008) Structural characterization and chemical composition of aragonite and vaterite in freshwater cultured pearls. *Mineralogical Magazine*, Vol. 72, No. 2, pp. 577–590.
- Strack E. (2006) *Pearls*. Rühle-Diebener Verlag, Stuttgart, Germany, 707 pp.
- Sturman N. (2009) The microradiographic structures on non-bead cultured pearls. GIA Thailand, Bangkok, November 21, www.giathai.net/pdf/The_Microradiographic_structures_in_NBCP.pdf [date accessed: Dec. 2, 2009].
- Sturman N., Al-Attawi A. (2006) The "Keshi" pearl issue. *G&G*, Vol. 42, No. 3, p. 142.
- Van Geet M., Swennen R., Wevers M. (2001) Towards a 3D petrography: Application of microfocus computer tomography. *Computers & Geosciences*, Vol. 27, No. 9, pp. 1091–1099.
- Webster R. (1994) *Gems: Their Sources, Description and Identification*, 5th ed. Rev. by P. G. Read, Butterworth-Heinemann, Oxford, UK, 1026 pp.
- Wehrmeister U., Goetz H., Jacob D.E., Soldati A.L., Xu W., Duschner H., Hofmeister W. (2008) Visualization of the internal structure of freshwater cultured pearls by computerized X-ray microtomography. *Journal of Gemmology*, Vol. 31, No. 1–2, pp. 15–21.

X-RAY COMPUTED MICROTOMOGRAPHY: DISTINGUISHING NATURAL PEARLS FROM BEADED AND NON-BEADED CULTURED PEARLS

Michael S. Krzemnicki, Sebastian D. Friess, Pascal Chalus, Henry A. Hänni, and Stefanos Karampelas

The distinction of natural from cultured pearls traditionally has been based on X-radiography. X-ray computed microtomography (μ -CT) has recently been applied to gain more insight into pearl structures. Using this technique, this article presents features observed in a selection of natural pearls and beaded and non-beaded cultured pearls. Based on these observations, μ -CT is shown to be a powerful tool for pearl identification.

In recent years, we have seen more interest in natural pearls, especially in the high-end jewelry trade (figure 1). A number of important historic natural pearls have been sold at auction in New York, Geneva, Hong Kong, and Dubai. However, the supply of newly harvested natural pearls is very small, and is restricted to only a few local sources, mainly in the Middle East and Southeast Asia. Therefore, most natural pearls in the market today are from old stocks and historical collections, accumulated over many years. They may be found in estate jewelry or restrung into contemporary necklaces.

Cultured pearls are far more abundant than natural pearls in today's market. They mainly consist of Chinese freshwater cultured pearls from *Hyriopsis* spp. (Akamatsu et al., 2001) and saltwater cultured pearls from several mollusks, including *Pinctada maxima* oysters in Australia and along the coast of Southeast Asia, *P. margaritifera* in the Pacific and the Red Sea, *P. martensii* in Japan, *P.*

chemnitzii in China, and *Pteria sterna* in Mexico. As cultivation techniques have improved (Hänni, 2007), the distinction between natural and cultured pearls has become more difficult (see, e.g., Scarratt et al., 2000; Akamatsu et al., 2001; Hänni, 2006; Sturman and Al-Attawi, 2006; Sturman, 2009), and we predict it will be even more challenging in the future.

For decades now, gemologists have relied primarily on X-radiographs for the separation of natural from cultured pearls (Webster, 1994; Sturman, 2009; and references therein). Only recently has X-ray computed microtomography (μ -CT) been applied to pearls (Strack, 2006; Soldati et al., 2008; Wehrmeister et al., 2008; Krzemnicki et al., 2009; Kawano, 2009) and gemstone analysis (Hänni, 2009). This article focuses on the features observed with μ -CT in natural and cultured pearls (non-beaded and beaded). For background on the technique, the reader is referred to Karampelas et al. (2010).

MATERIALS AND METHODS

From over 50 pearls analyzed with μ -CT, we selected 11 natural and 19 cultured pearls for this study, from both freshwater and saltwater mollusks (see table 1). The samples are from the SSEF reference collection, and from reputable sources consisting of pearl farms and collectors of natural pearls (see Acknowledgments).

Imaging was performed on a SkyScan 1172 high-resolution μ -CT scanner (SkyScan NV, Kontich, Belgium), equipped with a 100 kV / 100 μ A X-ray source and a 10 megapixel (4000 \times 2000) X-ray sensitive CCD camera. The system allows for a flexible geometry along the sample path (i.e., objects can be magnified until the boundaries of the field-of-view of the camera are reached). The sample chamber is roughly 30 \times 40 \times 15 cm, but the largest sample that can be imaged is 50 mm in diameter. The scanner allows for image formats up to 8000 \times 8000 pixels. The best achievable pixel size is 600 nm (isotropic), thus allowing a detail detectability below 1 μ m. Reconstruction by means

See end of article for About the Authors and Acknowledgments.

GEMS & GEMOLOGY, Vol. 46, No. 2, pp. 128–134.

© 2010 Gemological Institute of America



Figure 1. X-ray computed microtomography may be an important tool in the analysis of single pearls. This exceptional five-strand natural pearl necklace (4.45–12.20 mm) from the collection of Gourdji des Perles Fines, France, was certified recently at the SSEF Swiss Gemmological Institute. Photo by Luc Phan, © SSEF.

of a modified Feldkamp algorithm was performed on a four-PC 64-bit reconstruction cluster using SkyScan's NRecon platform.

Samples were scanned using an 88 kV accelerating voltage and a target current of 100 μ A, with a full 360° sample rotation (0.30 increment) and an exposure time of 2356 milliseconds per frame. For a voxel size of 2–8 μ m (a voxel is a three-dimensional [3D] pixel), the scan time was less than two hours. A full dataset typically was 30 GB per pearl, and reconstructions took about six hours each. The resulting cross sections were resolved at 2.97 μ m pixel size (4000 \times 4000), and were converted into black-and-white binary bitmap images to model the pearls' internal structures. Additionally, the files were transformed into 3D models using the CTVol platform (SkyScan NV). In the present article, the μ -CT images show a bit more noise than those reported in Karampelas et al. (2010) because we used double frame averaging, while Karampelas et al. used a 10-fold frame averaging with shorter exposure times.

RESULTS AND DISCUSSION

Natural Pearls. Natural pearls are mainly characterized by an onion-like structure of nacre layers, consisting of small aragonite tablets (Gutmansbauer and Hänni 1994; Sturman, 2009; and references therein). Additionally, pearls contain an organic substance (conchiolin) and some have cores composed of radial calcite columns, which appear darker (in cross-sections and radiographs) due to the enrichment of organic matter. When natural pearls are sawn in half (figure 2), this structure can be observed in detail with a microscope. The μ -CT images of natural pearls show these structures in three dimensions (see item 1 in the *G&G* Data Depository at www.gia.edu/gandg, and figures 6 and 7 of Karampelas et al., 2010). Scrolling through reconstructed virtual slices of a natural pearl is particularly effective for revealing the growth structures, which often are highly uniform in spherical layers. Also typically observed are: (1) fissures due to ageing/drying of

the pearl, which usually partially follow the growth rings of the nacre (see figure 3a and 3b); and (2) curved intersection lines in pearls grown together from two or more individuals (figure 3c). In radiographs, these features might be misinterpreted as cavity structures in a non-beaded cultured pearl.

Beaded Cultured Pearls. Although beaded cultured pearls are generally easy to separate from natural ones using radiography (see, e.g., figure 4 of Karampelas et al., 2010), μ -CT provides a much more detailed view of their structure. For example, the images of sample mxt 14b—an oval *P. maxima* saltwater cultured pearl from Australia—reveal that the bead broke during drilling (figure 4a). Furthermore, the large cavity at the top of this cultured pearl shows a complex structure of layers of organic matter (conchiolin) with small specks of calcium carbonate (seen as bright spots).

More challenging are cultured pearls with bead materials such as non-beaded freshwater and saltwater cultured pearls or even natural pearls of low quality (Hainschwang, 2010a,b; Hänni et al., 2010; Krzemnicki, 2010b). These are deliberately produced to resemble natural pearls as closely as possible. Although they can usually be detected by radiography, μ -CT further strengthens the identification of these cultured pearls (figure 4b).

Non-Beaded Cultured Pearls. The non-beaded cultured pearls analyzed for this study originate from both freshwater (*Hyriopsis* spp.) and saltwater (*P. maxima*, *P. margaritifera*, *P. sterna*) mollusks. The latter ones, sometimes also called “keshi” cultured pearls, have caused considerable concern in the trade (Hänni, 2006; Sturman and Al-Attawi, 2006; Krzemnicki et al., 2009; Sturman, 2009; Krzemnicki, 2010a), as increasing quantities are entering the market, often with excellent shape and color. They are thus rivaling the historic natural pearls and may, when misidentified as such, compromise the allure and rarity of the natural products. Gemological labs are striving to establish cri-

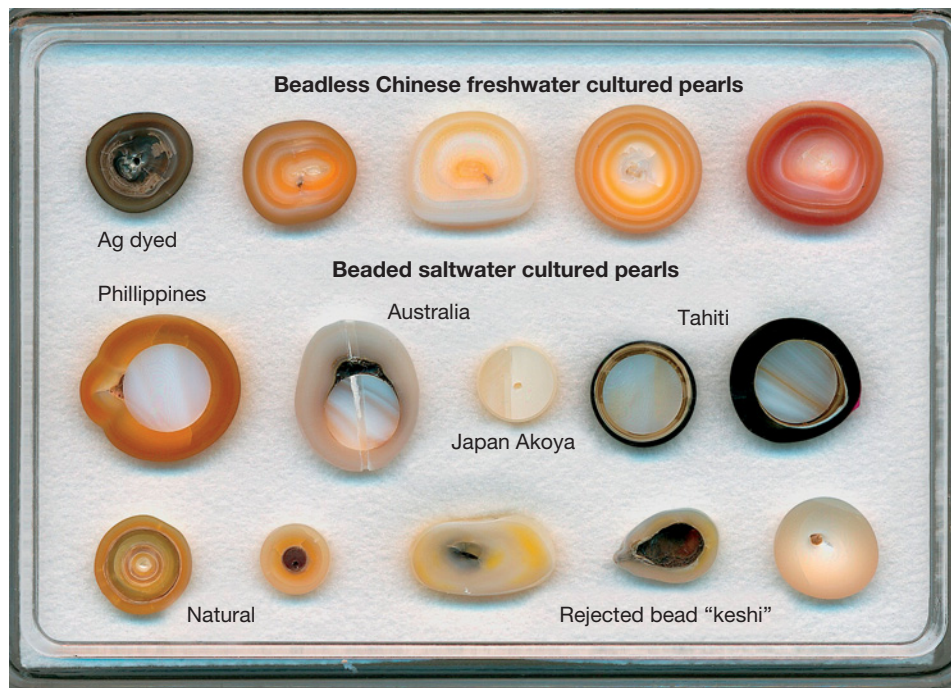


Figure 2. Shown here are sawn non-beaded freshwater cultured pearls (top), beaded saltwater cultured pearls (middle), and natural pearls and non-beaded “keshi” cultured pearls (bottom). Photo by H. A. Hänni, © SSEF.

TABLE 1. Characteristics and μ -CT resolution of the studied pearl samples.^a

Sample no.	Type	Mollusk	Size (mm)	Shape	Color	Condition	μ -CT resolution (μ m)
mxt 9	Natural SW	<i>P. radiata</i>	6.02–6.97	Oval	Light “cream”	Undrilled	6.0
mxt 57_2	Natural SW	<i>P. radiata</i>	8.32–8.55	Button	Light “cream”	Undrilled	3.6
mxt 29	Natural SW	<i>P. radiata</i>	9.84–11.20	Drop	White	Undrilled	3.0
mxt 44	Natural SW	<i>P. maxima</i>	9.55–19.95	Sl. baroque	White	Undrilled	3.1
mxt 45	Natural SW	<i>P. maxima</i>	7.60–13.50	Baroque	White	Undrilled	3.5
mxt 63_2	Natural SW	<i>P. radiata</i>	8.20–8.31	Round	“Cream”	Drilled	2.5
mxt 63_10	Natural SW	<i>P. radiata</i>	8.46–8.55	Round	“Cream”	Drilled	2.5
mxt 63_15	Natural SW	<i>P. radiata</i>	8.96–9.57	Oval	Light “cream”	Drilled	2.5
mxt 63_18	Natural SW	<i>P. radiata</i>	9.39–10.10	Oval	Light “cream”	Drilled	2.5
mxt 70	Natural SW	<i>P. radiata</i>	9.42–11.20	Button	Light “cream”	Undrilled	3.0
mxt 3	Natural FW	Unionida	6.87–7.18	Round	Slightly “rosé”	Undrilled	3.0
mxt 14b	Beaded SWCP	<i>P. maxima</i>	8.80–11.96	Oval	White	Drilled	4.9
mxt 31	Beaded SWCP	<i>P. maxima</i>	10.49–10.92	Round	Yellow	Half drilled	3.5
HAH_1	Beaded SWCP	<i>P. maxima</i>	9.12–9.25	Round	White	Undrilled	3.6
HAH_2	Beaded SWCP	<i>P. margaritifera</i>	9.26–9.47	Round	Dark gray	Undrilled	3.6
mxt 21_1	Beaded SWCP	<i>P. maxima</i>	6.55–18.54	Baroque	White	Undrilled	4.0
mxt 37_1	Non-beaded SWCP	<i>P. maxima</i>	9.19–12.98	Baroque	White	Undrilled	2.6
mxt 37_17	Non-beaded SWCP	<i>P. maxima</i>	8.05–11.10	Oval	White	Half-drilled	2.3
mxt 61_14	Non-beaded SWCP	<i>P. maxima</i>	6.59–8.56	Button	Yellow	Undrilled	3.5
mxt 61_20	Non-beaded SWCP	<i>P. maxima</i>	6.91–7.62	Oval	White	Undrilled	3.6
mxt 68	Non-beaded SWCP	<i>P. maxima</i>	12.68–12.92	Round	Light “cream”	Drilled	3.6
mxt 197	Non-beaded SWCP	<i>P. maxima</i>	10.66–14.95	Drop	White	Half drilled	3.6
mxt 198	Non-beaded SWCP	<i>P. maxima</i>	10.00–13.28	Drop	White	Half drilled	3.9
mxt 21_2	Non-beaded SWCP	<i>P. maxima</i>	14.30–20.52	Baroque	White	Undrilled	4.0
mxt 1	Non-beaded FWCP	<i>Hyriopsis spp.</i>	10.58–11.41	Oval	Light orange	Undrilled	4.9
mxt 2	Non-beaded FWCP	<i>Hyriopsis spp.</i>	8.51–10.82	Sl. baroque	White	Undrilled	4.0
mxt 13a	Non-beaded FWCP	<i>Hyriopsis spp.</i>	9.80–13.70	Drop	White	Undrilled	5.4
mxt 97	Non-beaded FWCP	Unionida	14.38–16.30	Button	Light “cream”	Undrilled	4.2
mxt 98	Non-beaded FWCP	Unionida	15.70–17.56	Oval	White	Undrilled	3.7
mxt 99	Non-beaded FWCP	Unionida	17.54–20.84	Oval	Orange	Undrilled	4.6

^a Abbreviations: FW = freshwater, SW = saltwater, FWCP = freshwater cultured pearl, SWCP = saltwater cultured pearl, Sl. = slightly.

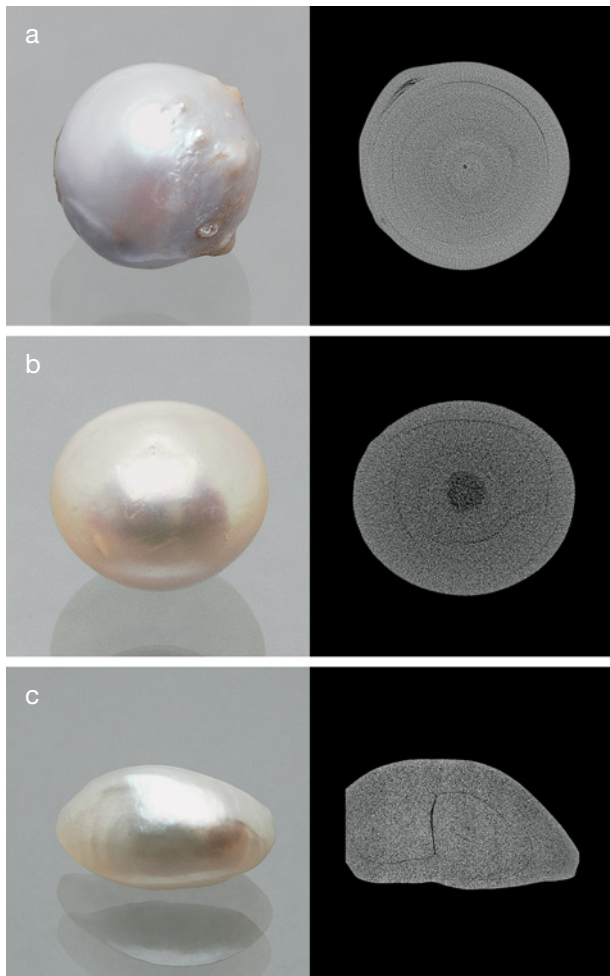


Figure 3. These photos and tomographic sections of natural pearls include (a) a *Unionida* natural freshwater pearl (sample mxt 3) from Mississippi showing a small dark dot in the center due to organic matter; (b) a *P. radiata* natural saltwater pearl (mxt 9) from the Persian Gulf showing a larger dark central zone consisting of columnar calcite interlayered with some organic matter as well as partially concentric fissures; and (c) a *P. maxima* natural saltwater pearl from Vietnam (mxt 44) showing structures due to the merging of two pearls during the growth history. The fine highly concentric circular structure seen in the tomographic section of (a) is an artifact, and is not the same as the growth structure of the pearl (see Karampelas et al., 2010). Photos by M. S. Krzemnicki, © SSEF. See also Data Depository item 1.

teria for separating these non-beaded saltwater cultured pearls from their natural counterparts. To better understand the structures in these cultured pearls, we have differentiated them into two categories: (1) cultivation from a piece of mantle tissue only, and (2) cultivation from mantle tissue after the bead inserted at the same time has been rejected.

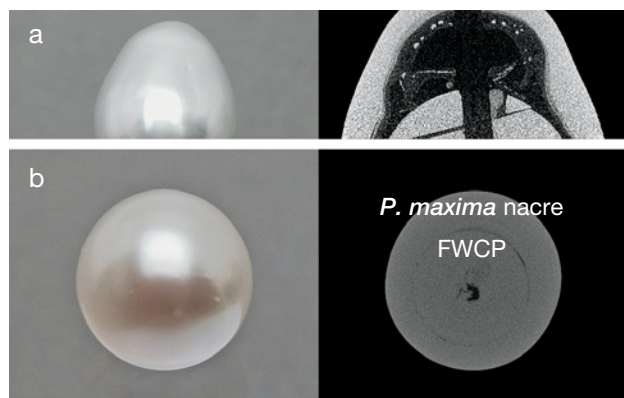
If a non-beaded cultured pearl is grown directly from a

NEED TO KNOW

- X-ray computed microtomography is effective for separating natural from cultured pearls, even those that contain pearls as bead materials.
- Natural pearls are mainly characterized by a uniform onion-like structure of nacre layers and conchiolin.
- Freshwater non-beaded cultured pearls contain small curved cavity structures in their centers.
- Saltwater non-beaded cultured pearls (“keshi”) may show these curved structures, as well as larger cavities or calcareous spots in their center.

piece of inserted mantle tissue—such as Chinese freshwater products, but possibly other varieties (Hänni, 2008)—then a small curved cavity structure (“moustache”) will be present in its center (Scarratt et al., 2000). This cavity structure represents the outline of initial nacre formation within the wrinkled mantle tissue after it has formed the pearl sac in the mollusk. The “moustache” may be difficult to see on radiographs, often requiring magnification. When we scroll through tomographic sections, however, this irregu-

Figure 4. Photos and tomographic images of beaded saltwater cultured pearls are shown for (a) a *P. maxima* specimen from Australia (mxt 14b) with a bead that broke during drilling, as well as a large cavity containing many small white calcium carbonate spots; and (b) a *P. maxima* sample (HAH_1) containing a non-beaded Chinese freshwater cultured pearl as the nucleus. The irregular cavity structure of the non-beaded cultured pearl nucleus is evident in the center. Photos by M. S. Krzemnicki, © SSEF. See also Data Depository item 2.



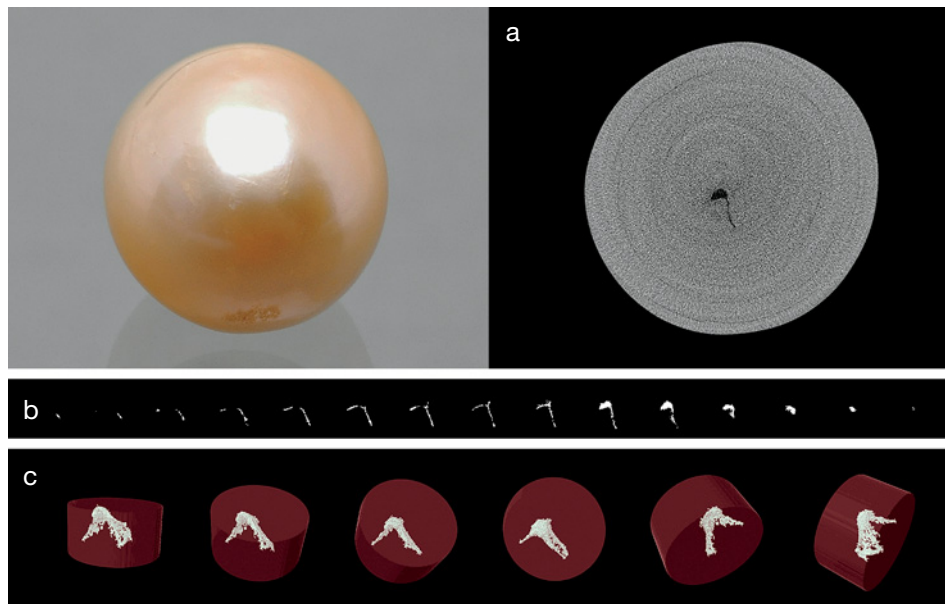
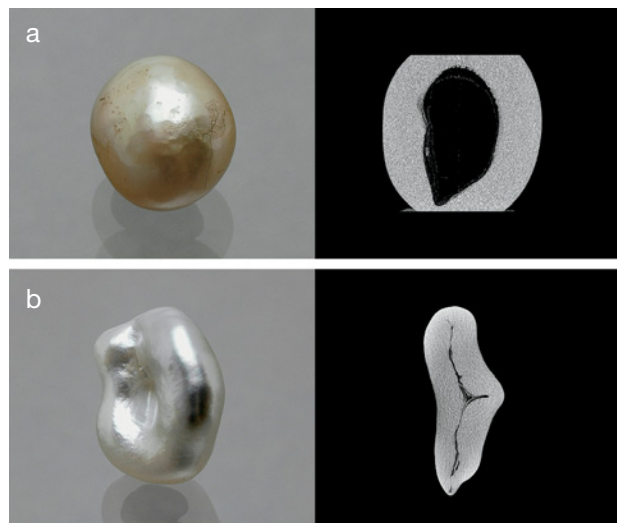


Figure 5. This non-beaded freshwater cultured pearl (mxt 1) from China has a characteristic curved “moustache” that was barely visible with radiography. With μ -CT, this structure is clearly seen in: (a) a transaxial (horizontal) section, (b) a series of overlying transaxial sections transformed into black/white bitmap files, and (c) movie stills that show it from different angles. Photo by M. S. Krzemnicki, © SSEF. See also Data Depository item 3.

larly curved structure is much more obvious (figure 5a) and can even be visualized in three dimensions (figure 5b,c). In the μ -CT images of some samples, we also observed portions with a slightly darker gray appearance (not necessarily located in the center), which were similar to those described by Soldati et al. (2008) and Wehrmeister et al. (2008) as vaterite-rich zones within freshwater cultured pearls. However, more research is needed to verify this.

Figure 6. Vertical (coronal) tomographic sections of these non-beaded saltwater cultured pearls show: (a) a large smoothly curved cavity structure (mxt 61_14; *P. maxima*, Australia), and (b) an irregular cavity structure due to a collapsed pearl sac (mxt 37_1). Photos by M. S. Krzemnicki, © SSEF. See also Data Depository item 3.



For the cultured pearls grown after bead rejection, we have observed two types of features, possibly dependent on the stage at which the bead was rejected. For beads rejected during the first generation of cultivation, the mantle tissue inserted (commonly into the gonad) behaves as described above, forming a pearl sac and subsequently precipitating calcium carbonate (Hänni, 2006). Thus, we expect to see a rather small and thin curved “moustache” structure in the cultured pearl (similar to figure 5c) or a small rounded hollow cavity. These cultured pearls are often button- to oval- and drop-shaped. Alternatively, for those formed after bead rejection during a second (or later) cultivation period (i.e., when a preexisting pearl sac, usually in the gonad, was filled again with a bead that was rejected shortly thereafter), we observe larger cavities within the cultured pearl (figure 6a), often slightly curved (Farn, 1984; Hänni, 2006; Sturman, 2009). In cases where the pearl sac collapsed, we will see large and flat irregular cavity structures (figure 6b) in pearls, which often show a baroque shape.

In some cases, especially in *Pinctada spp.* mollusks, small “additional” cultured pearls may form within the pearl sac, probably due to injuries during bead insertion (Hänni, 2006). Their internal structures are quite characteristic, often showing one or two small nacreous spots in the center (similar to the calcium carbonate spots seen in figure 4a), surrounded by an organic-rich core and a nacreous outer layer. Figure 7 shows a sliced specimen consisting of a pair of such “additional” cultured pearls attached to a beaded cultured pearl that formed within the gonad of a *P. maxima* oyster. The white calcareous spots in the centers are clearly visible. This feature is also evident in the μ -CT scans of a similar beaded cultured pearl (*P. maxima*) with an “additional” cultured pearl attached (figure 8a). However, the “additional” cultured pearls need not be attached to a beaded cultured pearl, and may be found loose in the pearl sac. Figure 8b shows a complex case that



Figure 7. This sliced specimen (12 mm in diameter) shows a beaded cultured pearl with two attached cultured pearls that formed additionally in the pearl sac (in the gonad of *P. maxima*). Note the white calcareous spots in the centers of these “additional” non-beaded cultured pearls. Photo by H. A. Hänni, © SSEF.

appears to consist of an “additional” non-beaded cultured pearl (again with a light-appearing spot in the center) that was apparently overlooked when harvesting a first-generation beaded cultured pearl from the pearl sac in the gonad of a *P. maxima* oyster. Soon after, a second bead was introduced into the existing pearl sac, but was rejected. As a result the pearl sac collapsed, producing the complex internal pattern of this baroque-shaped cultured pearl.

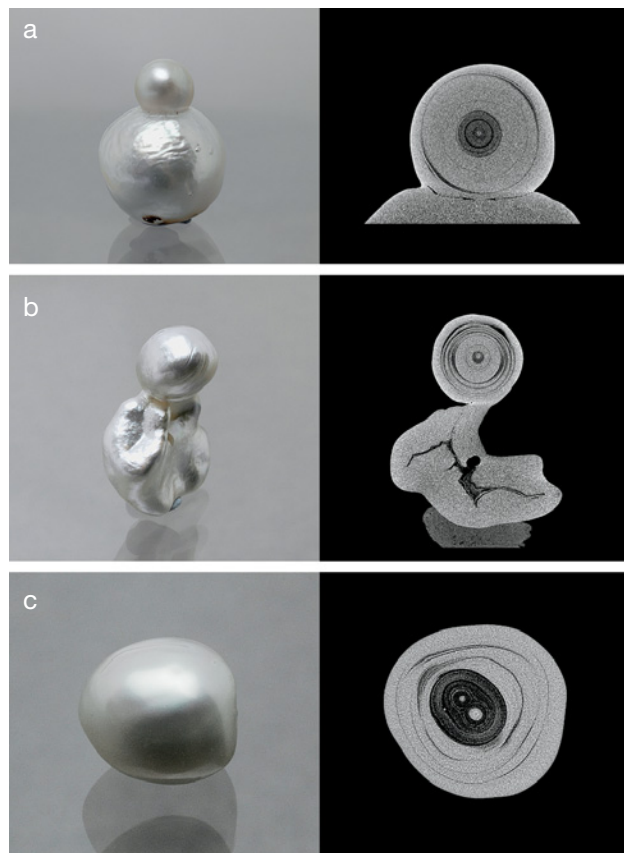
Furthermore, the loose “additional” cultured pearls may be harvested and used as “keshi” cultured pearls (Krzemnicki, 2010a). Figure 8c shows such a loose “additional” cultured pearl, again with a calcareous spot in the center. These cultured pearls show a disturbing resemblance to natural pearls, and can be identified only by careful observations of radiographs or μ -CT scans (Krzemnicki, 2010a). We have also found indications that attached “additional” cultured pearls (such as in figure 8a) have been sawn from beaded cultured pearls and then used as beads for new cultured pearls, deliberately imitating the internal structures of natural pearls as much as possible.

CONCLUSIONS

The separation of natural from cultured pearls can be quite challenging, especially in light of new developments in pearl cultivation. X-ray computed microtomography is a powerful technique for visualizing internal structures that provide diagnostic evidence of natural vs. cultured pearl

origin. The advantage of this method lies in its high-resolution 3D modeling capability (see also *GeG* Data Depository and www.ssef.ch). In contrast, traditional radiography only provides a condensed 2D image of pearl structures. Small curved or folded cavity structures indicative of tissue culturing may only be discernible by carefully examining multiple radiographs taken at various orien-

Figure 8. These non-beaded saltwater cultured pearls show some particularly interesting features; all have a small calcareous spot in the center. (a) An “additional” cultured pearl is attached to a beaded cultured pearl (mxt 21_2; *P. maxima*) from Australia. (b) A baroque-shaped specimen (mxt 21_1; *P. maxima*) shows complex structures formed by a non-beaded cultured pearl attached to a non-beaded cultured pearl with a large irregular cavity structure due to a collapsed pearl sac (see also Data Depository item 4). (c) This “additional” cultured pearl (mxt 61_20) probably formed due to injuries during grafting of a silver-lipped pearl oyster (*P. maxima*). Although the structures are similar to those seen in natural pearls, the presence of calcium carbonate spots surrounded by organic-rich layers and subsequent nacre deposition is characteristic of these cultured pearls. Photos by M. S. Krzemnicki, © SSEF.



tations. Furthermore, fissures may be misinterpreted as cavity structures, as their 3D position within the pearl is not readily visible in radiographs. (For more details on advantages and limitations of the μ -CT method, see Karampelas et al., 2010.)

Although all the described internal features may be

discernible with careful radiography, μ -CT provides additional useful structural information. Based on our experience, we conclude that μ -CT shows great potential for pearl testing. However, additional problematic samples need to be studied to fully assess the advantages of this method as compared to X-ray radiography.

ABOUT THE AUTHORS

Dr. Krzemnicki (gemlab@ssef.ch) is director, and Dr. Hänni is research associate, at the SSEF Swiss Gemmological Institute, Basel, Switzerland. Dr. Friess is a scientific consultant at Gloor Instruments AG, Uster, Switzerland. Dr. Chalus is a near-infrared spectroscopy specialist in the Global Technical Development division at F. Hoffmann La Roche AG, Basel. Dr. Karampelas is a research scientist at the Gübelin Gem Lab, Lucerne, Switzerland.

ACKNOWLEDGMENTS

The authors thank Dr. Laurent Adamy of the Global

Technical Development division at F. Hoffmann La Roche AG, Basel, for enabling access to the company's facility. They are also grateful to the following people for supplying pearl samples for testing: Andy Cohen, Geneva; Ronny Totah, Geneva; Patrick Flückiger, Geneva; Wolf Bialonczyk, Vienna; Andy Müller, Kobe, Japan; and Abdulkrazaq Al-Mahmood, Bahrain. Ali Mohammed Safar and Mrs. Abeer Tawfeeq from the Directorate of Precious Metals & Gemstone Testing, Ministry of Commerce, Bahrain, graciously provided fruitful discussions on pearls, as did colleagues at SSEF. The Mineralogical Institute of the University of Basel kindly provided analytical support

REFERENCES

- Akamatsu S., Zansheng I.T., Moses T.M., Scarratt K. (2001) The current status of Chinese freshwater cultured pearls. *G&G*, Vol. 37, No. 2, pp. 96–113.
- Farn A.E. (1980) Notes from the laboratory (on non-nucleated cultured pearls). *Journal of Gemmology*, Vol. 17, No. 4, pp. 223–229.
- Gutmansbauer W., Hänni H.A. (1994) Structural and chemical investigations on shells and pearls of nacre forming salt- and freshwater bivalve molluscs. *Journal of Gemmology*, Vol. 24, No. 4, pp. 241–252.
- Hainschwang T. (2010a) A difficult new type of cultured pearl entering the market. *Gemnotes*, Vol. 1, No. 2, pp. 6–11, www.gemlab.net/website/gemlab/fileadmin/user_upload/GEMNOTES/Gemnotes-16-05-10.pdf [date accessed: May 18, 2010].
- Hainschwang T. (2010b) The pearl story continues — A *Pinctada maxima* pearl beaded by a natural *Pinctada maxima* pearl. *Gemnotes*, Vol. 1, No. 3, pp. 5–7, www.gemlab.net/website/gemlab/fileadmin/user_upload/GEMNOTES/Gemnotes-24-06-10.pdf [date accessed: June 28, 2010].
- Hänni H.A. (2006) A short review of the use of 'keshi' as a term to describe pearls. *Journal of Gemmology*, Vol. 30, No. 1–2, pp. 52–58.
- Hänni H.A. (2007) A description of pearl farming with *Pinctada maxima* in South East Asia. *Journal of Gemmology*, Vol. 30, No. 7–8, pp. 357–365.
- Hänni H.A. (2008) Gem News International: *Pinctada maxima* cultured pearls grown beadless in the mantle. *G&G*, Vol. 44, No. 2, pp. 175–176.
- Hänni H.A. (2009) How much glass is in the ruby? *SSEF Facette*, No. 16, pp. 8–9.
- Hänni H.A., Krzemnicki M.S., Cartier L. (2010) Appearance of new bead material in cultured pearls. *Journal of Gemmology*, Vol. 32, No. 1–4 (in press).
- Karampelas S., Michel J., Zheng-Cui M., Schwarz J.-O., Enzmann F., Fritsch E., Leu L., Krzemnicki M.S. (2010) X-ray computed microtomography applied to pearls: Methodology, advantages, and limitations. *G&G*, Vol. 46, No. 2, pp. 122–127.
- Kawano J. (2009) Observation of the internal structures of pearls by X-ray CT technique. *Gemmology*, Vol. 40, No. 478, Issue 7, pp. 2–4 [in Japanese].
- Krzemnicki M.S. (2010a) Trade Alert: "Keshi" cultured pearls are entering the natural pearl trade. *SSEF Newsletter*, May, www.ssef.ch/en/news/news_pdf/newsletter_pearl_2010May.pdf [date accessed: May 12, 2010].
- Krzemnicki M.S. (2010b) Addendum: . . . And what happens with the beaded cultured pearls? *SSEF Newsletter*, May, www.ssef.ch/en/news/news_pdf/newsletter_pearl_2010May_add.pdf [date accessed: May 20, 2010].
- Krzemnicki M.S., Friess S., Chalus P., Hajdas I., Hänni H.A. (2009) New developments in pearl analysis: X-ray microtomography and radiocarbon age dating. *Journal of the Gemmological Association of Hong Kong*, Vol. 30, pp. 43–45.
- Scarratt K., Moses T.M., Akamatsu S. (2000) Characteristics of nuclei in Chinese freshwater cultured pearls. *G&G*, Vol. 36, No. 2, pp. 98–109.
- Soldati A.L., Jacob D.E., Wehrmeister U., Hofmeister W. (2008) Structural characterization and chemical composition of aragonite and vaterite in freshwater cultured pearls. *Mineralogical Magazine*, Vol. 72, No. 2, pp. 577–590.
- Strack E. (2006) *Pearls*. Rühle-Diebener Verlag, Stuttgart, Germany, 707 pp.
- Sturman N. (2009) The microradiographic structures of non-bead cultured pearls. GIA Thailand, Bangkok, August 20, www.giathai.net/pdf/The_Microradiographic_structures_in_NBCP.pdf [date accessed: Oct. 1, 2009].
- Sturman N., Al-Attawi A. (2006) The "keshi" pearl issue. *G&G*, Vol. 42, No. 3, p. 142.
- Webster R. (1994) *Gems: Their Sources, Description, and Identification*, 5th ed. Rev. by P. G. Read, Butterworth-Heinemann, Oxford, UK, 1026 pp.
- Wehrmeister U., Goetz H., Jacob D.E., Soldati A.L., Xu W., Duschner H., Hofmeister W. (2008) Visualization of the internal structure of freshwater cultured pearls by computerized X-ray microtomography. *Journal of Gemmology*, Vol. 32, No. 1–2, pp. 15–21.

HIBONITE: A NEW GEM MINERAL

Thomas Hainschwang, Franck Notari, Laurent Massi, Thomas Armbruster,
Benjamin Rondeau, Emmanuel Fritsch, and Mariko Nagashima

A 0.23 g orangy brown crystal, a 0.39 ct step-cut gem later faceted from it, and a 0.71 g crystal—all reportedly from Myanmar—were characterized for this report. Infrared spectroscopy, X-ray diffraction, and chemical analysis identified the material as hibonite. These samples represent the first gem-quality hibonite ever recorded.

In late 2009, two transparent orangy brown crystals weighing 0.23 and 0.71 g (figures 1 and 2) were submitted to the AIGS Gemological Laboratory in Bangkok for identification. The crystals were said to originate from

ther analysis and was identified as hibonite; it was subsequently cut into a 0.39 ct gemstone (figure 2, right). We believe these are the first gem-quality specimens of hibonite ever documented.

Hibonite is a hexagonal mineral with the chemical formula $(\text{Ca,Ce})(\text{Al,Ti,Mg})_{12}\text{O}_{19}$. It has a Mohs hardness of 7.5–8 and an SG of 3.84, and it is uniaxial negative with refractive indices of $\omega = 1.807$ and $\varepsilon = 1.790$ (Roberts et al., 1974). Hibonite was discovered in 1955 as opaque to partially translucent black grains in the Esiva alluvial thorianite and phlogopite deposit, located in Toliara (Tuléar) Province, Madagascar (Curien et al., 1956). This rather rare mineral was named after Paul Hibon, the French prospector who discovered it (Fleischer, 1957). Hibonite is known to occur in meteorites, but it is most often associated with moderate- to high-grade metamorphic calcareous rocks,

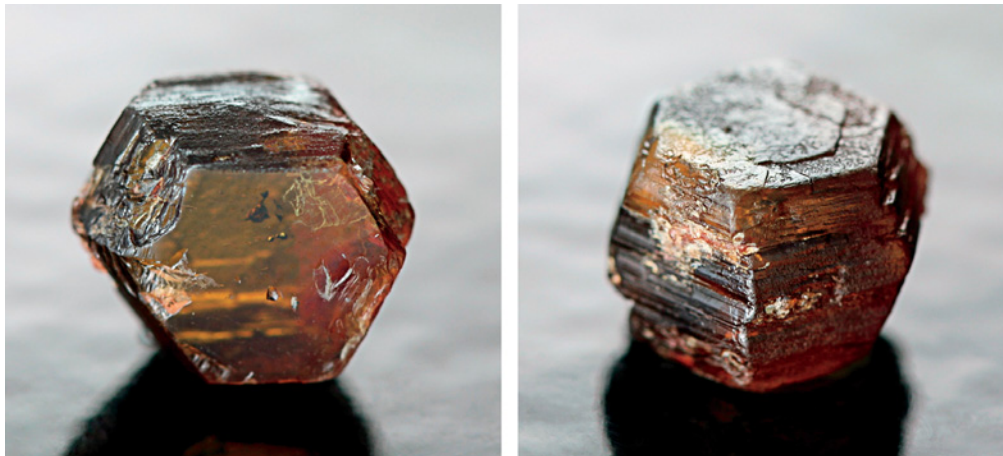


Figure 1. The 0.71 g ($7.02 \times 7.32 \times 5.44$ mm) gem-quality hibonite crystal, reportedly from Myanmar, is shown from two different angles. Photos by L. Massi.

Myanmar, with no additional specifics given. Standard gemological testing and semiquantitative chemical analysis were inconclusive. The smaller crystal underwent fur-

sometimes with corundum, spinel and/or sapphire, as documented at Andranondambo in Madagascar (Schwarz et al., 1996), in southern Tanzania (Maaskant et al., 1980), at Chyulu Hills in Kenya (Ulianov et al., 2005), and in the Achankovil shear zone in southern India (Rajesh, 2010). Macroscopic samples of hibonite are generally opaque and at best translucent, though very small transparent pale yellow to brown crystals were reported from the Tanzanian occurrence.

See end of article for About the Authors and Acknowledgments.

GEMS & GEMOLOGY, Vol. 46, No. 2, pp. 135–138.

© 2010 Gemological Institute of America



Figure 2. The 0.23 g hibonite crystal (left) was fashioned into a 0.39 ct step-cut gem (right). The smooth surface on the rough is a polished facet, which corresponds to the table of the faceted gem. The *c*-axis is nearly vertical. Photos by T. Hainschwang (left) and F. Notari (right).

Materials and Methods. Standard gemological properties of the two crystals and the faceted gem that was subsequently cut were determined at the AIGS and GemTechLab laboratories using a refractometer (RI), hydrostatic balance (SG), and 6W long- and short-wave UV lamp (fluorescence). Internal features were observed with standard gemological microscopes at up to 120 \times magnification.

Advanced testing was performed on the smaller crystal. Reflectance infrared spectra were recorded in the 7500–400 cm^{-1} range at 4 cm^{-1} resolution with Nicolet Nexus and Perkin Elmer BXII Fourier-transform infrared (FTIR) spectrometers at GemTechLab and Gemlab, respectively. Raman spectra were recorded at the IMN–University of Nantes with a Horiba T64000 dispersive Raman spectrometer employing a 514 nm argon laser. Single-crystal X-ray diffraction analysis was performed at the University of Bern using a Bruker Apex diffractometer with $\text{MoK}\alpha$ radiation and an X-ray power of 50 kV/30 mA. Semiquantitative chemical analysis was performed by energy-dispersive X-ray fluorescence (EDXRF) spectroscopy with an Eagle III system at AIGS, a Thermo QuanX system at GemTechLab, and a custom-built EDXRF spectrometer with a thermoelectrically cooled detector at Gemlab. Quantitative chemical analysis was achieved at the IMN–University of Nantes with two scanning electron microscopes (Zeiss Evo 40XVP and JEOL

5800LV), each equipped with a Princeton Gamma Tech energy-dispersive IMIX-PTS detector. Polarized ultraviolet-visible–near infrared (UV-Vis-NIR) absorption spectra were recorded with a xenon-based prototype spectrometer at 0.6 nm resolution in the 240–1050 nm range at Gemlab, and with a Hitachi spectrometer at 1 nm resolution in the 190–900 nm range at GemTechLab.

Results and Discussion. Standard gemological testing of the crystals and the faceted gem gave an SG of 3.84 and RIs of ~ 1.79 – 1.81 , consistent with the reference values for hibonite cited above. Since the upper RI values were at the limit of the refractometer, the optic character and birefringence could not be measured with certainty. The samples were inert to UV radiation.

With magnification, a variety of inclusions were visible in all the samples, most of them hexagonal and some triangular (figure 3). SEM-EDX analysis of several surface-reaching grains gave a chemical composition indicative of very pure corundum. A tiny (~ 50 nm) inclusion within one of these inclusions was found to be fluorite by the same method. Some of the other inclusions may be micas, similar to those found in association with blue sapphire and hibonite in the Andranondambo deposit (Schwarz et al., 1996), but they could not be identified by Raman analysis due to the interfering luminescence from the host (see below).

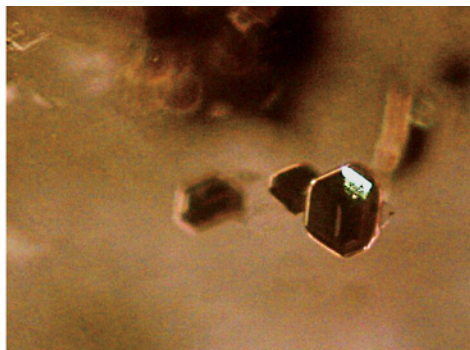
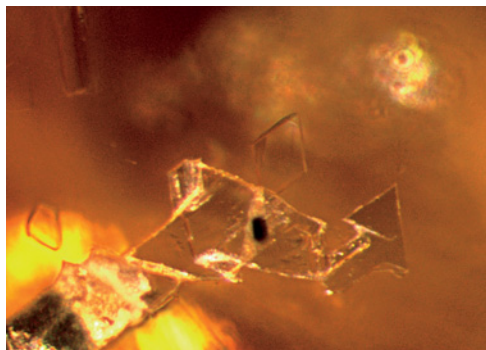


Figure 3. Small triangular and hexagonal inclusions (possibly corundum and mica) were present in the hibonite. Photomicrographs by T. Hainschwang (left, field of view 0.5 mm) and L. Massi (right, magnified 50 \times).

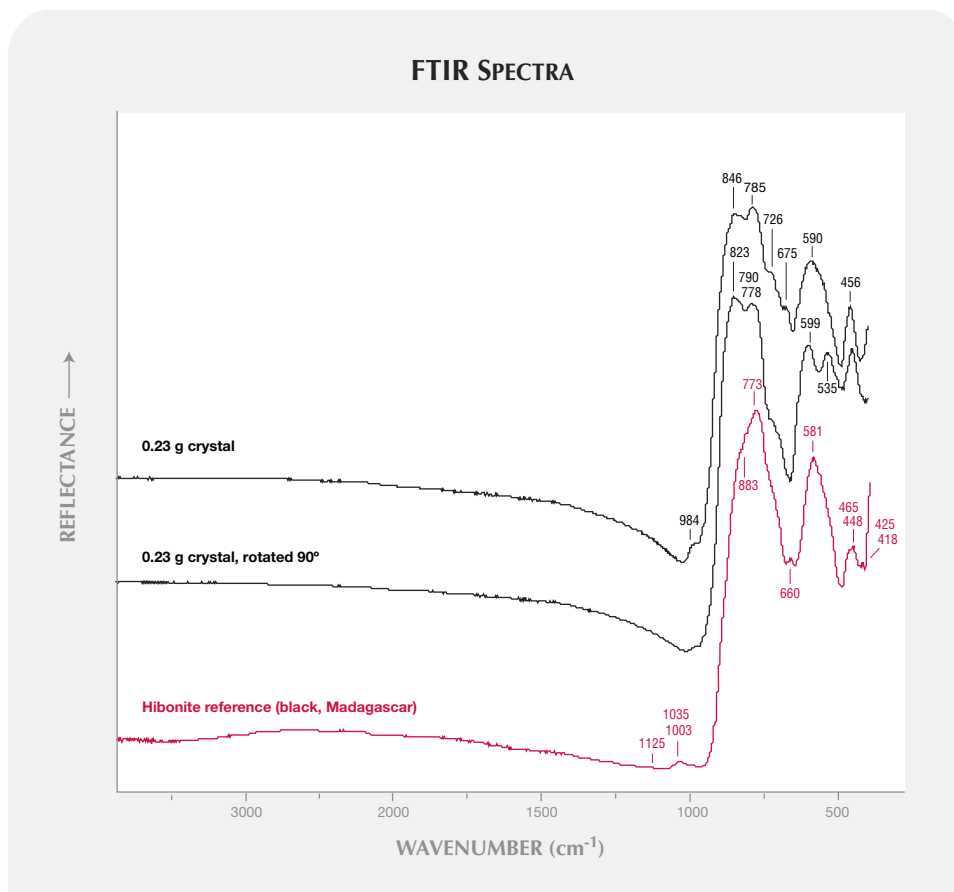


Figure 4. Reflectance FTIR spectra of the smaller crystal, taken in two orientations, show some similarities to the reference spectrum of black hibonite from Madagascar.

TABLE 1. Gemological properties and SEM-EDX quantitative chemical analysis of the 0.23 g hibonite.

Gemological Properties	
Color	Orangy brown
Refractive indices	1.79–1.81
Specific gravity	3.84
Mohs hardness	7 ½–8
Fluorescence	Inert to long- and short-wave UV
Internal features	Triangular and hexagonal crystal inclusions, among others
Quantitative Chemical Analysis ^a	
Element	Atomic %
Al	32.93
Ca	3.37
Mg	1.98
Ti	1.97
Zn	0.46
Fe	0.08
O	59.21

^aResults are normalized to 100%.

Reflectance IR spectroscopy of the smaller crystal yielded patterns relatively close to that of a reference spectrum of hibonite from Madagascar (internal reference, GemTechLab and Gemlab). Nevertheless, the spectra recorded from the sample were sufficiently different that the crystal's identity remained in doubt (figure 4).

It proved very difficult to obtain useful Raman data, and the spectrum recorded on the smaller crystal was inconclusive. The main features were two weak bands at 903 and 880 cm^{-1} , a more distinct broad band at 740 cm^{-1} , and a weak broad band at 330 cm^{-1} . Hibonite appears to have a weak Raman signal, as many of the published spectra are of poor quality. The hibonite reference spectra in the RRUFF database (<http://rruff.info>), for example, are not pure Raman scattering signals, but appear to consist of luminescence signals.

The identification as hibonite was further supported by X-ray diffraction analysis, which established the material as hexagonal with unit-cell dimensions of $a = 5.592(2) \text{ \AA}$, $c = 21.989(3) \text{ \AA}$, and volume = 595.5(3) \AA^3 . This limited the possible mineral groups to taaffeite, hōgbomite, or hibonite. A crystal-structure refinement achieved from the X-ray diffraction data indicated near-end member hibonite.

This result was confirmed by chemical analysis. EDXRF spectroscopy of several areas of the smaller crystal indicated mainly Al, plus Ca, Ti, Mg, Zn, and traces of Fe

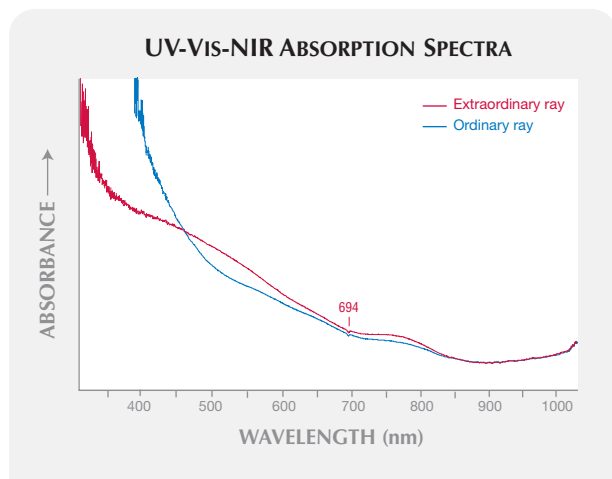


Figure 5. The polarized UV-Vis-NIR spectra of the smaller hibonite crystal are characterized by an absorption continuum with superimposed broad bands, which is responsible for the orangy brown color. The small negative peak at 694 nm is due to Cr^{3+} luminescence.

and Sr; Cr was barely detectable (detection limit ~20 ppm). Quantitative SEM-EDX chemical analysis of this crystal gave a similar result, with slight differences due to the lower sensitivity of this method (detection limit ~100 ppm; see table 1). The significant traces of Zn are surprising for hibonite, as Zn is regarded as an uncommon impu-

rity in this mineral (e.g., Maaskant et al., 1980; Hofmeister et al., 2004). Also, we did not detect Ce (or any other rare-earth element), which is usually present in hibonite.

The polarized UV-Vis-NIR spectra (figure 5) were characterized by broad bands overlaying an absorption continuum with increasing absorbance from lower to higher energies (higher to lower wavelengths). This continuum is responsible for the orangy brown color. Its origin is unclear, but it could be due to an Fe-Ti intervalence charge transfer, as both elements were detected by chemical analysis. Because this color mechanism absorbs light efficiently, it does not require high concentrations of these elements. This mechanism gives similar colors to a number of minerals and gems such as dravite, andalusite, and micas (Fritsch and Rossman, 1988). The origin of the superimposed broad bands is uncertain; they contribute only very slightly to the color. The absence or very low concentrations of Ce and Fe, both potential light absorbers, may explain why this sample is lightly colored when hibonite is usually black and opaque.

Conclusions. Hibonite can be identified by its gemological properties (RI = 1.79–1.81, SG = 3.84, no UV fluorescence) and composition as determined by semiquantitative or quantitative chemical analysis. Gem-quality hibonite can now be added to the list of known gem minerals. Its rarity classifies it as an exotic collector's stone. If more of this material is discovered, its qualities (hardness, attractive color, etc.) make it suitable for general use in jewelry.

ABOUT THE AUTHORS

Mr. Hainschwang (thomas.hainschwang@gemlab.net) is a director and research gemologist at Gemlab in Balzers, Liechtenstein. Mr. Notari is director of GemTechLab in Geneva, Switzerland. Dr. Massi is director of the AIGS Gemological Laboratory in Bangkok. Dr. Armbruster is head of the mineralogical crystallography group of the Institute of Geological Sciences at the University of Bern, Switzerland. Dr. Fritsch is professor of physics at the Institut des Matériaux Jean Rouxel (IMN)-CNRS, Team 6205, University of Nantes, France. Dr. Rondeau is assistant professor at the Laboratory of Planetology and Geodynamics, University of Nantes, and belongs to CNRS Team 6112. Dr. Nagashima is a postdoctoral researcher in mineralogy at the University of Bern.

ACKNOWLEDGMENTS

The authors thank Mr. N. Emmenegger, a lapidary in Geneva, for sample preparation and final cutting.

REFERENCES

- Curien H., Guillemin C., Orcel J., Sternberg M. (1956) La hibonite, nouvelle espèce minérale. *Comptes Rendus de l'Académie des Sciences*, Paris, Vol. 242, pp. 2845–2847.
- Fleischer M. (1957) New mineral names. *American Mineralogist*, Vol. 42, pp. 117–124.
- Fritsch E., Rossman G.R. (1988) An update on color in gems. Part 2: Colors involving multiple atoms and color centers. *G&G*, Vol. 24, No. 1, pp. 3–15.
- Hofmeister A.M., Wokenpa B., Lockok A.J. (2004) Spectroscopy and structure of hibonite, grossite, and CaAl_2O_4 : Implications for astronomical environments. *Geochimica et Cosmochimica Acta*, Vol. 68, pp. 4485–4503.
- Maaskant P., Coolen J.J.M.M., Burke E.A.J. (1980) Hibonite and coexisting zoisite and clinozoisite in a calc-silicate granulite from southern Tanzania. *Mineralogical Magazine*, Vol. 43, pp. 995–1003.
- Rajesh V.J., Arai S., Santosh M., Tamura A. (2010) LREE-rich hibonite in ultrapotassic rocks in southern India. *Lithos*, Vol. 115, pp. 40–50.
- Roberts W.L., Rapp G.R. Jr., Weber J. (1974) *Encyclopedia of Minerals*. Van Nostrand Reinhold, New York, 693 pp.
- Schwarz D., Petsch E.J., Kanis J. (1996) Sapphires from the Androndambo region, Madagascar. *G&G*, Vol. 32, No. 2, pp. 80–99.
- Ulianov A., Kalt A., Pettke T. (2005) Hibonite, $\text{Ca}(\text{Al,Cr,Ti,Si,Mg,Fe}^{2+})_{12}\text{O}_{19}$, in granulite xenoliths from the Chyulu Hills volcanic field, Kenya. *European Journal of Mineralogy*, Vol. 17, pp. 357–366.

CIRCLE OF HONOR*

\$100,000 and higher, cumulative

The Aaron Group	Dallas R. Hales	Marshall and Janella Martin
Dr. Suman Agrawal	Dr. H. Tracy Hall	Roz & Gene Meieran
Almaza Jewelers (Ziad H. Noshie)	Dr. Gary R. and Barbara E. Hansen	Nancy B & Company
American Pearl Company	James Y. Hung, M.D.	Kurt Nassau, Ph.D.
Amsterdam Sauer	Inta Gems Inc.	John & Laura Ramsey
Robert and Marlene Anderson	J.O. Crystal Company, Inc. (Judith Osmer)	R. Ed Romack
Aurafin Oro America	JewelAmerica, Inc. (Zvi & Rachel Wertheimer)	Art Sexauer
Banks International Gemology, Inc. (Daniel & Bo Banks)	Kazanjan Bros, Inc.	Shades of the Earth (Laura & Wayne Thompson)
The Bell Group/Rio Grande	KCB Natural Pearls (K.C. Bell)	Ambaji Shinde
Allan Caplan	William F. & Jeanne H. Larson	S.H. Silver Company (Stephen & Eileen Silver)
Chatham Created Gems, Inc. (Thomas H. Chatham)	Honoring Betty H. Llewellyn	Dr. Geoffrey A. Smith
PierLuigi Dalla Rovere	Stephen Lentz	D. Swarovski & Co
The De Beers Group	Sophie Leu	Touraine Family Trust
Debbie and Mark Ebert		United States Pearl Co. (James & Venetia Peach)
Fabricjewelry		Robert H. Vanderkay
		Vicenza Fair

2009 DONORS*

\$50,000 to \$99,999

Steve and Betty Neely

\$10,000 to \$49,999

Adeler Jewelers
(Jorge Adeler)
Cos Altobelli
Dudley Blauwet
Christopher L. Johnston
Timothy Zielinski.
Zultanite Gems LLC

\$5,000 to \$9,999

Barker & Co.
Ferjenni
(Van Tuyen Tran and
Randall Otten)
Pamela and Richmond Grant
House of Onyx, Inc.
J. Blue Sheppard
Kempf's Jewelers
SK Originals

\$2,500 to \$4,999

Boingoc
(Cuc Nguyen)
Jim Coote
Syed Iftikhar Hussain
Honoring Richard T.
Liddicoat
Hussain Rezayee
G. Richard Settles

\$1,000 to \$2,499

Aurora Gem Inc.
(Alan Bronstein)
Thomas Hunn Co., Inc.
Al Gilbertson
Mary Johnson Consulting
Mobu Gems, Inc.
(Amarjit Saini, G.G.)
Terri Ottaway

\$500 to \$999

John Anthony, Jr., G.G.
Crest Gems, Inc.
Kaufman Enterprises
(Mark Kaufman)
Michele Macri
Gabriela Natera
Frank L. Webber, G.G.

Under \$500

Zohreh Amini
Philip C. Azzolina
Paul Binder
William A. Bray
Honoring Burton Burnstein
California Loan & Jewelry
Fred Chaldy
Fabrice Danet
Elegant Gems, Ltd.

The Gem Trader
(Bradley J. Payne)
The Goldsmiths' Company
HardasDiamond.com
Huffords Jewelry
Jaroslav HyrsI
Jewelry Television
Vivian Komu
John Lindell
New Prosperity Gems
Renée Newman
Karen O'Neill
Kerem Ozutemiz
Patagonia Minerals
PearlParadise.com
Rachminov Diamonds 1891
Werner Radl
Nathan Renfro
William Shuster
Carlyn Soriano
Stowe Gems
Union Associations of
Goldsmiths of Serbia
Mike W.
Orpha Wagner
Paul W. Wickstrom
Richard D. Wilson

• All are cumulative donations



THANK YOU DONORS

GIA appreciates gifts to its permanent collection, as well as gemstones, library materials, and other non-cash assets to be used in GIA's education and research activities. These contributions help GIA further its public service mission while offering donors philanthropic benefits. We extend sincere thanks to all 2009 contributors.



If you are interested in making a donation and receiving tax benefits information, please contact Terri Ottaway at (800) 421-7250, ext. 4157. From outside the U.S., call (760) 603-4157, fax (760) 603-4056, or e-mail terri.ottaway@gia.edu.

Unusual Polyphase Inclusions In CORUNDUM

The New York laboratory recently identified some inclusions in corundum that have not previously been reported in the gemological literature. While examining a 3.79 ct unheated blue sapphire of metamorphic origin, we noted a small, transparent, surface-reaching crystal, which Raman analysis identified as zircon. Much to our surprise, the high-powered microscope built into the Raman instrument showed numerous (>10) inclusions within the zircon crystal (figure 1). We noted several transparent rounded inclusions, a few euhedral crystals, and a reddish material. Raman analysis of the rounded features showed peaks associated with CO₂, while the spectrum from the reddish regions indicated the presence of hematite. We had never before observed such “inclusions within inclusions” of zircon in sapphire.

As part of GIA's continuing effort to provide country-of-origin determinations for corundum, the New York laboratory has been characterizing more than 500 unheated corundum samples known to be from the Winza region of

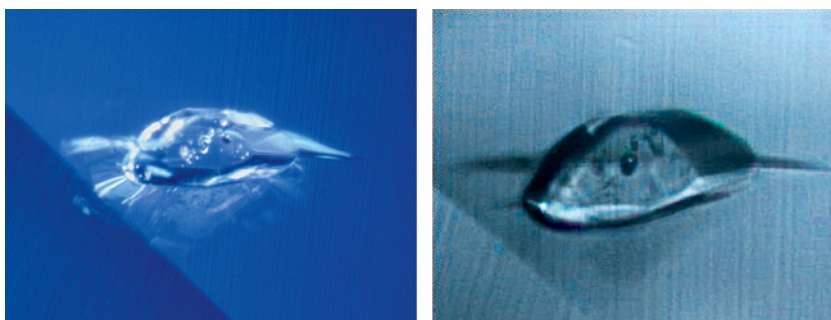
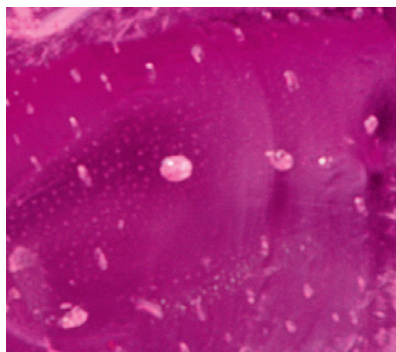


Figure 1. The zircon crystal (~210 μm long, left) in an unheated blue sapphire has inclusions of its own that are visible at higher magnification (right).

Tanzania. During this project, we found what we believe to be diaspore on the basis of Raman analysis (figure 2); we also detected hematite in two samples (figure 3). Although polyphase

Figure 2. The large white inclusion in this pink sapphire from Winza, Tanzania, had a Raman spectrum consistent with diaspore. Field of view ~0.5 mm.



inclusions in corundum from Winza have been characterized previously (D. Schwarz et al., “Rubies and sapphires from Winza, central Tanzania,” Winter 2008 *G&G*, pp. 322–347; A. Peretti, “Winza rubies identified,” *Contributions to Gemology*, No. 7, 2008, www.gemresearch.ch/journal/No7/No7.htm), we believe this is the first time diaspore and hematite have been identified as components of inclusions from this locality.

David Kondo

DIAMOND Black Diamond with Solid CO₂ Micro-Inclusions and Phosphorescent Zones

Also recently examined at the New York lab was the 0.45 ct natural-color black heart-shaped diamond shown in figure 4 (left). Microscopic observa-

Editors' note: All items were written by staff members of the GIA Laboratory.

GEMS & GEMOLOGY, Vol. 46, No. 2, pp. 140–146.

© 2010 Gemological Institute of America

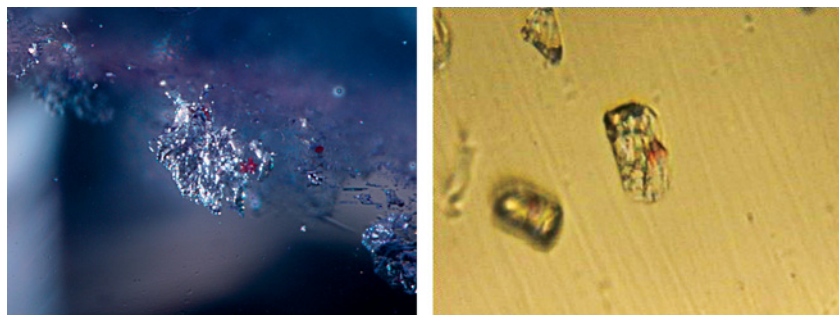


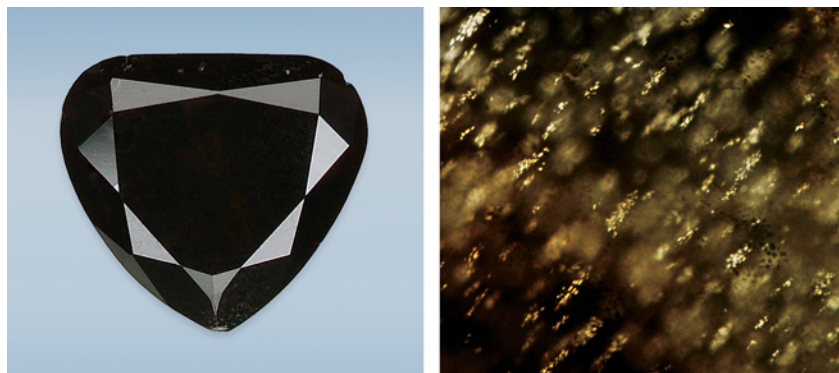
Figure 3. For these inclusions in a violetish blue sapphire (left) and a pink sapphire (right, taken with a Raman microscope)—both from Winza—Raman spectra for the red regions matched hematite. Fields of view 1.2 and 0.15 mm, respectively.

tion revealed an abundance of clouds, and higher magnification showed clusters of round, disc-like inclusions ~32 μm across (figure 4, right). This is the first time we had observed such features in a black diamond, which derives its color from its inclusions.

Due to time constraints, we did not have the opportunity to identify these inclusions using Raman microspectroscopy. However, the mid-infrared (IR) spectrum demonstrated that the diamond's major impurity was solid CO_2 , with dominant absorption peaks at ~2370 and ~658 cm^{-1} (figure 5). Features associated with micro-inclusions such as silicates and apatite also were observed, at 1055 and 575 cm^{-1} , respectively (though not visible in figure 5). Sharp absorption bands at 871 and 721 cm^{-1} , together with a broad

band at 1430 cm^{-1} , suggested the presence of carbonates. Quartz absorption bands detected at 798 and 779 cm^{-1} were shifted from their normal positions. This diamond also contained hydrous components, as revealed by a broad band at ~3220 cm^{-1} that indicated asymmetric OH^- stretching (see D. A. Zedgenizov et al., "Carbonatitic melts in cuboid diamonds from Udachnaya kimberlite pipe [Yakutia]: Evidence from vibrational spectroscopy," *Mineralogical Magazine*, Vol. 68, No. 1, 2004, pp. 61–73). Another broad band at ~1713 cm^{-1} may be related to the H_2O -bending mode. Small hydrogen bands were observed at 4703 and 3107 cm^{-1} . These features are not common in gem-quality diamonds. Absorption bands in the 1300–1000 cm^{-1} region suggested this was a type Ia stone.

Figure 4. This 0.45 ct black diamond (left) contains abundant microscopic clouds. With high magnification (112.5 \times), clusters of round, disc-like inclusions are also seen (right).



When examined with the strong ultra-short-wave (~225 nm) ultraviolet radiation of the DiamondView, most of the stone fluoresced strong yellowish green, but there were three rectangular nonfluorescent zones (figure 6, left). Unlike the rest of the diamond, these zones exhibited strong phosphorescence (figure 6, right). Photoluminescence (PL) spectroscopy using 488 and 633 nm lasers showed similar features for both these zones and the fluorescent areas, but a few PL bands—such as at 511, 572, 696.2, and 739 nm—were observed only in the nonfluorescent zones. The assignment for these bands is not clear, but they may be related to the unusual phosphorescence. The clouds in the diamond were confined to the {100} crystal plane in the dominant yellowish green fluorescent area, while the phosphorescent zones were formed in {111} directions.

This black diamond offered a valuable opportunity to study the geologic conditions of diamond growth. The micro-inclusions of solid CO_2 and water—which we have seen only rarely in gem-quality diamonds—suggested that this diamond formed from carbonate-rich melts. Internal pressure from these volatiles caused the quartz absorption bands to shift, which further suggests that these micro-inclusions were trapped during the diamond's growth.

Paul Johnson and Kyaw Soe Moe

Fancy Vivid Blue HPHT-Treated Diamond

As we have noted previously, many natural type IIb blue diamonds have gray or brown overtones that can be removed by high-pressure, high-temperature (HPHT) annealing, thus enhancing the blue color (see, e.g., Spring 2010 Lab Notes, pp. 51–52). Recently, the New York laboratory examined one such diamond with a hue more saturated than most other HPHT-treated blue diamonds we have tested.

The 3.81 ct pear-shaped diamond

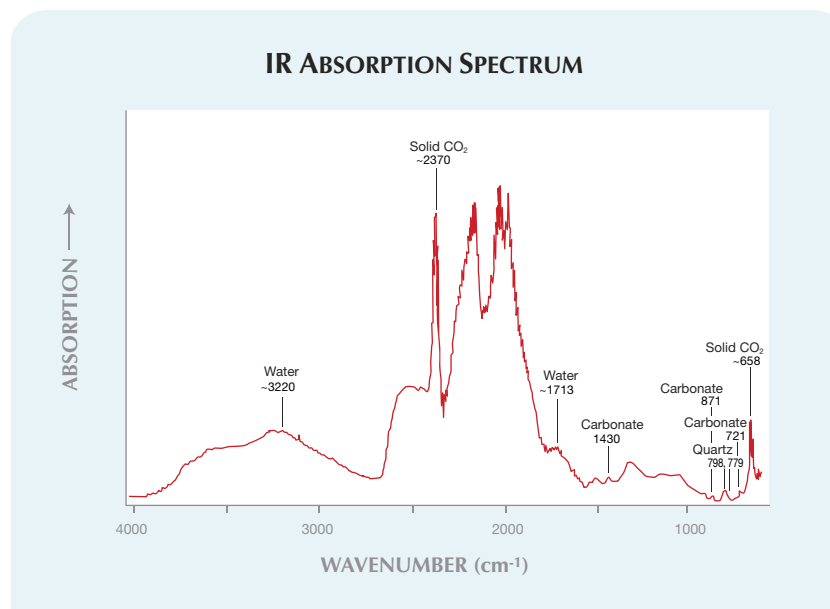


Figure 5. The IR spectrum of this natural-color black diamond demonstrates the presence of various micro-inclusions, such as solid CO₂, carbonates, quartz, and water.

(13.24 × 9.22 × 5.42 mm) was graded Fancy Vivid blue and displayed even color distribution (figure 7). The highly saturated hue in combination with well-balanced transparency was reminiscent of a fine blue sapphire.

Two tiny graphite flakes were seen when the stone (clarity graded VS₂) was examined through the pavilion. No graining was detected. The diamond was inert to conventional long- and short-wave UV radiation. Only a

weak blue fluorescence and very weak blue phosphorescence were visible with the strong ultra-short-wave UV radiation of the DiamondView; these less intense reactions are clearly different from those of most natural-color or HPHT-treated type IIb diamonds.

The mid-IR spectrum showed strong boron-related absorptions (such as a peak at ~2800 cm⁻¹), which are typical of type IIb diamond. We established that the diamond was HPHT



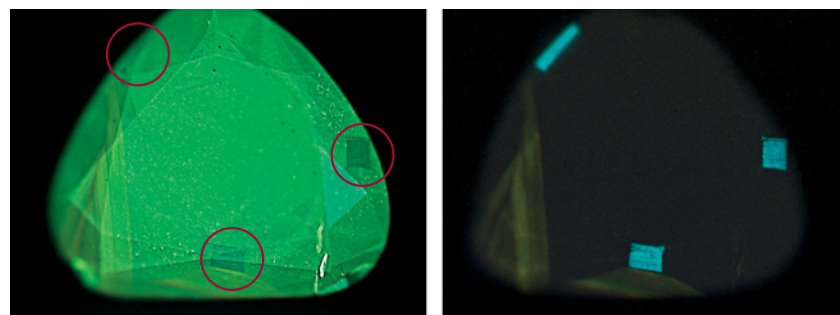
Figure 7. This 3.81 ct Fancy Vivid blue type IIb diamond was identified as HPHT treated.

annealed on the basis of its gemological properties and PL spectra collected at liquid-nitrogen temperature with laser excitations from UV to IR.

The color of an HPHT-treated diamond can be affected by many factors, such as the chemical purity of the starting material, the treatment conditions, and even the cut. In our experience, extremely attractive colors such as that seen in this diamond are rare. This is the fourth-largest Fancy Vivid blue HPHT-treated diamond GIA has graded to date. The largest weighed more than 7.5 ct.

Wuyi Wang

Figure 6. In the DiamondView, the black diamond displays strong yellowish green fluorescence except for three nonfluorescent rectangular zones (left). However, these rectangular zones show strong phosphorescence, while the rest of the diamond does not (right).



Interesting Display of the H3 Defect in a Colorless Diamond

Type IIa diamonds contain few impurities and usually show little variation in their gemological and spectroscopic characteristics. However, fluorescence imaging with the strong ultra-short-wave UV radiation of the DiamondView occasionally reveals interesting internal features. Recently, a 2.24 ct pear-shaped diamond (11.63 × 7.43 × 4.34 mm) was submitted to the New York laboratory for grading. IR absorption spectroscopy confirmed that the

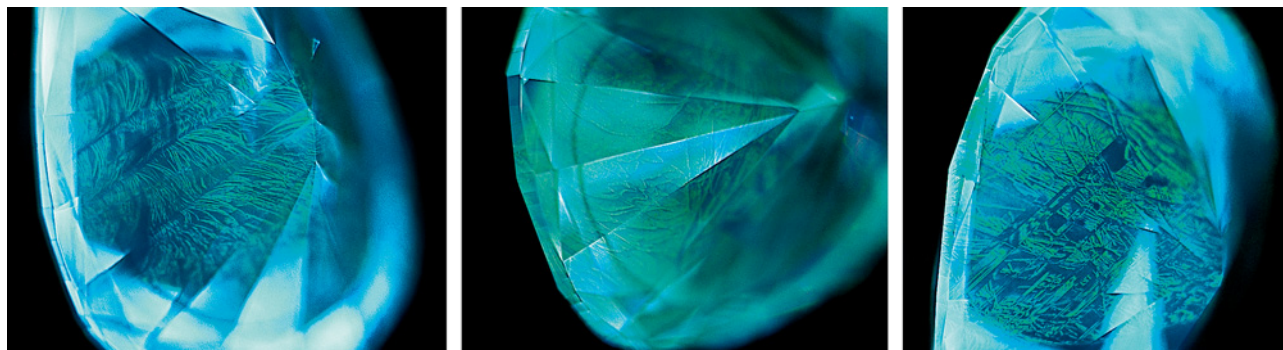


Figure 8. These DiamondView images of a 2.24 ct colorless type IIa diamond display the H3 defect in fern-like (left), flame-like (center), and distorted vein (right) structures.

E-color, internally flawless stone was a typical type IIa diamond, with no impurity-related defects.

A striking feature displayed in the DiamondView was the stone's dominant blue fluorescence with unusual green patterns. Depending on the direction of observation, these green regions showed fern-like, flame-like, or distorted vein structures over the entire pavilion (e.g., figure 8). We also observed strong blue phosphorescence in the DiamondView.

PL spectroscopy at liquid-nitrogen temperature with 488 nm laser excitation showed relatively strong emission from the H3 optical center with a zero-phonon line (ZPL) at 503.2 nm, weak emission from NV⁰ at 575.0 nm, and a sharp peak at 648.2 nm (figure 9). The 648.2 nm emission is very likely a boron-related defect, and type IIa diamonds with this emission often display strong blue phosphorescence. The unusually strong H3 emission, together with the distinctive patterns observed in the DiamondView, demonstrated that the green fluorescence is caused by the H3 optical center (see, e.g., Spring 2010 Lab Notes, pp. 49–50).

Such an interesting pattern of H3 distribution in a type IIa diamond is rare. The formation mechanism is not fully understood, but it could be related to the presence of lattice impurities (such as A-form nitrogen and vacancies) in a specific crystal orientation.

Erica Emerson and Wuyi Wang

CVD SYNTHETIC DIAMOND Over One Carat

Single-crystal synthetic diamonds grown by chemical vapor deposition (CVD) are occasionally submitted to the GIA Laboratory for identification and grading reports. For the first time, the New York laboratory has identified a near-colorless CVD synthetic diamond larger than one carat that was submitted for grading.

The 1.05 ct pear shape (9.81 × 5.95

× 3.06 mm) was color-graded as equivalent to G (figure 10). In addition to pinpoint inclusions, it contained some feathers and fractures along the girdle, and its clarity grade was equivalent to I₁. No fluorescence was observed when it was exposed to conventional long- and short-wave UV radiation. The mid-IR absorption spectrum showed no absorption in the one-phonon region and no hydrogen-related absorption, which classified it as type IIa. (It is unusual to

Figure 9. The 2.24 ct colorless diamond's PL spectrum shows a relatively strong emission from the H3 center.

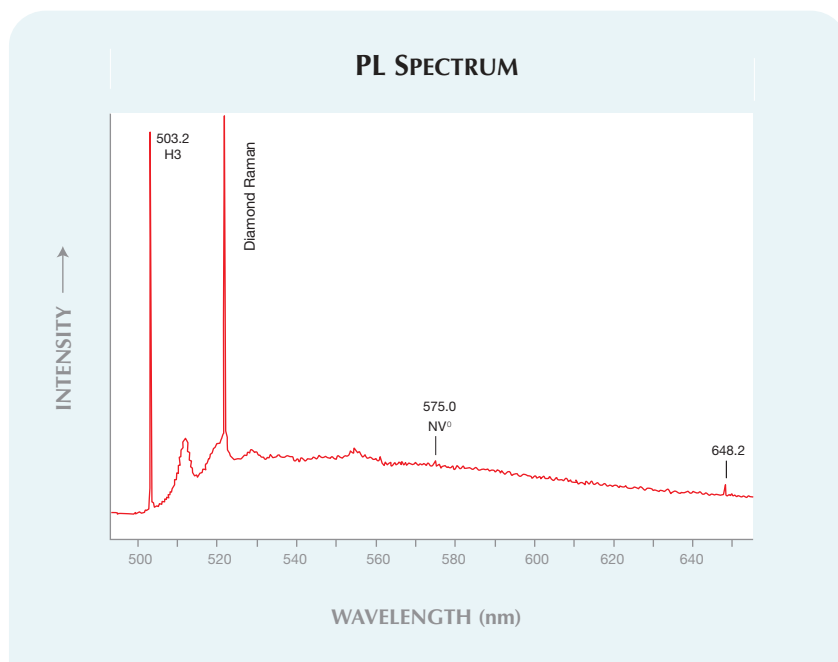




Figure 10. This G-color CVD synthetic diamond weighs 1.05 ct.

encounter a “white” CVD-grown diamond without H-related absorption at 3123 cm^{-1} .) Images taken with the DiamondView showed strong pink fluorescence with some irregularly shaped areas of blue fluorescence (figure 11). PL spectra collected at liquid-nitrogen temperature with laser excitations from the UV to IR regions revealed features typical of CVD synthetic diamond: strong emissions from NV centers, a doublet at 596.5 and 597.1 nm, and $[\text{Si-V}]^-$ doublet

Figure 11. When exposed to the strong short-wave UV radiation of the DiamondView, the 1.05 ct CVD synthetic diamond displays strong pink fluorescence with irregular areas of blue.



emissions at 736.6 and 736.9 nm. The gemological and spectroscopic features confirmed that this sample was a CVD synthetic diamond.

It is clear that larger, better-quality CVD synthetic diamonds are being produced as there is continued improvement in the growth techniques.

Wuyi Wang and Kyaw Soe Moe

Synthetic Diopside in Manufactured GLASS

Manufactured glasses are familiar gem simulants, and are usually identifiable by included gas bubbles. If the glass has begun to devitrify, however, it may contain natural-appearing crystalline inclusions, so identification may be confusing for all but the most experienced gemologists. Devitrification usually occurs in colored glasses, which contain additional elements that increase the likelihood of developing crystals. These crystals typically nucleate on gas bubbles or foreign particles in the glass (J. I. Koivula, “A photolexicon of inclusion-related terms for today’s gemmologist: Part 27,” *Canadian Gemmologist*, Vol. 17, No. 2, 1996, p. 40).

The Carlsbad laboratory recently

Figure 12. Synthetic diopside crystals decorate an elongated colorless rod of synthetic wollastonite in a piece of manufactured glass. Magnified 70 \times .



examined an unusual example of this phenomenon. The standard gemological properties (RI of 1.52 and hydrostatic SG of 2.55) were consistent with manufactured glass. The piece displayed three distinct color zones: greenish blue, green, and essentially colorless. The colorless zone ran through the green area and contained numerous well-formed blocky green crystals, several of which had strongly saturated green cores (e.g., figure 12). Raman analysis identified the crystals as diopside. Because these green synthetic diopside crystals only occurred in the colorless area, they appeared to have caused a “chromophore cannibalization” effect on the originally green glass, rendering those portions of the sample colorless. Energy-dispersive X-ray fluorescence analysis of the host confirmed the presence of chromium, the likely chromophore of both the green portion of the glass and the synthetic diopside crystals.

Also present were elongated colorless crystals, which Raman analysis identified as wollastonite. These appeared to be the initial devitrification product, followed by the synthetic diopside crystals, which were commonly distributed along the length of the synthetic wollastonites (again, see figure 12). Irregularities along the synthetic wollastonite crystals likely served as nucleation sites for the synthetic diopside.

While synthetic wollastonite has been reported previously in manufactured glass (H. A. Hänni et al., “A glass imitation of blue chalcedony,” *Journal of Gemmology*, Vol. 27, No. 5, 2001, pp. 275–285), this is the first time we have seen synthetic diopside as a devitrification product.

Nathan Renfro and John Koivula

Green Be-Diffused SAPPHIRE

Beryllium diffusion can produce a wide range of colors in corundum. The Carlsbad laboratory routinely encounters blue, yellow, orange, pink, and red examples. Green is one of the more

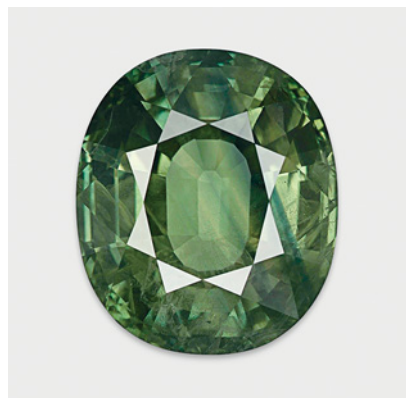


Figure 13. Chemical analysis revealed that this 14.20 ct green sapphire had been treated by beryllium diffusion.

unusual colors for this material, especially in larger sizes, but we recently examined a 14.20 ct sample that was beryllium diffused (figure 13).

The standard gemological properties for this stone were consistent with corundum. Microscopic examination revealed particulate clouds, flux-healed “fingerprints,” discoid-like fractures, and planar growth features. The desk-model spectroscope showed strong iron-related absorption centered at 450 nm. As expected, immersion displayed alternating blue and yellow color zones, a common feature in green sapphires.

Beryllium diffusion was first detected in the early 2000s because of surface-conformal color zoning in orangy pink to pinkish orange sapphires. However, the vast majority of Be-diffused corundum currently being processed does not show this type of zoning because the stones are diffused all the way through. Nevertheless, microscopic examination can offer clues to the likelihood of Be diffusion, such as synthetic overgrowth, significantly altered crystal inclusions, and localized blue zones of internal diffusion (caused by the release of Ti from inclusions such as rutile into the Fe-containing corundum host). While these clues alone are not proof of Be diffusion, their presence does suggest high-temperature heat treatment (see J. L. Emmett et al., “Beryllium diffu-

sion of ruby and sapphire,” Summer 2003 *G&G*, pp. 84–135).

The GIA Laboratory uses laser ablation–inductively coupled plasma–mass spectrometry (LA-ICP-MS) to test all heat-treated corundum for the presence of beryllium. This stone, which had features consistent with heat treatment, was no exception. LA-ICP-MS indicated an average Be concentration of just over 13 ppmw (27 ppma), enough to dramatically alter the color.

The appearance in the marketplace of this large green Be-diffused sapphire reinforces the need to send all suspect stones to a qualified laboratory for chemical analysis. Microscopic evidence of high-temperature treatment can raise suspicion of Be diffusion, but chemical analysis by a technique capable of detecting traces of Be is necessary to confirm the treatment.

Nathan Renfro

Heat-Treated SPINEL

This spring, the New York laboratory examined a 17.02 ct reddish orange oval modified brilliant (figure 14) that was singly refractive, had an RI of 1.719 and SG of 3.59, and displayed a series of chrome lines with the desk-model spectroscope—all properties consistent with spinel. Magnification revealed

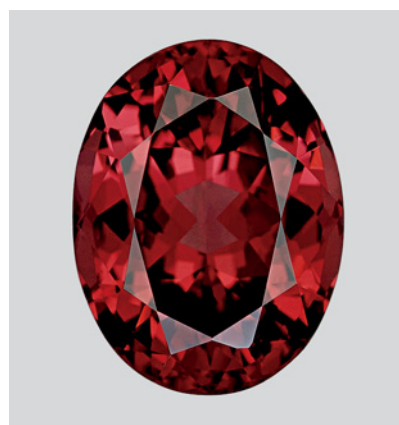
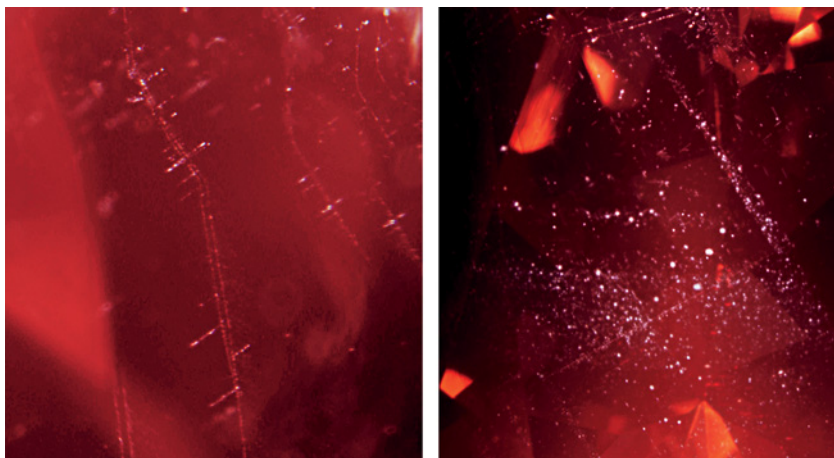


Figure 14. Based on standard gemological observations and advanced testing, this 17.02 ct reddish orange oval modified brilliant was identified as a heated natural spinel.

particulates and strings of minute inclusions (figure 15). These were reminiscent of boehmite in spinel (see E. J. Gübelin and J. I. Koivula, *Photoatlas of Inclusions in Gemstones*, Opinio Verlag, Basel, Switzerland, 1986, p. 375), which suggested a natural origin. A few small expansion halos or “blebs” emanating from the strings of inclusions indicated that the stone might have been subjected to heat.

Since first experimenting on heat-treated Tanzanian spinels in 2005, the GIA Laboratory has tested several hun-

Figure 15. The internal features observed in the reddish orange spinel were limited to particulates and strings of minute inclusions.



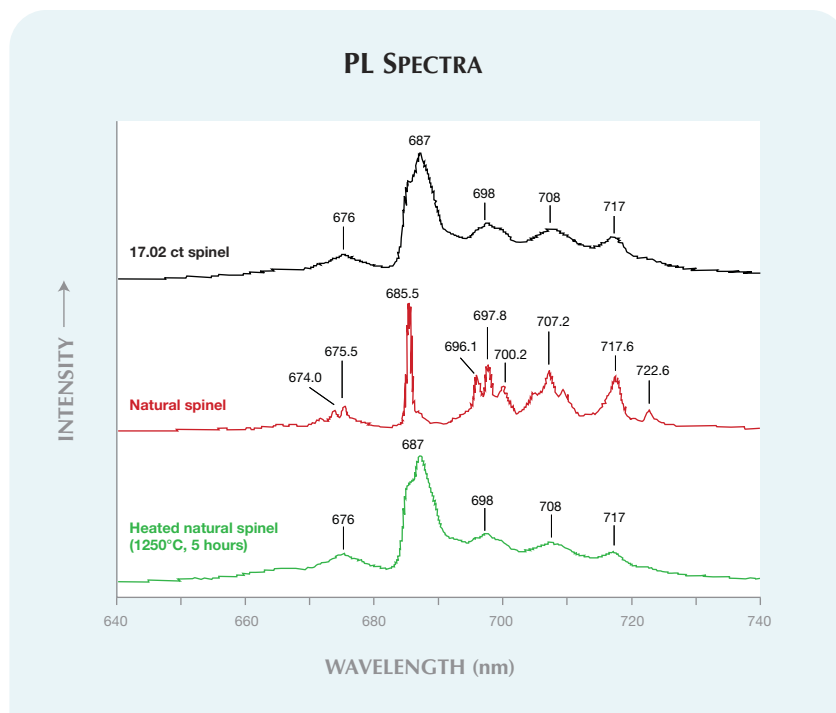


Figure 16. PL spectra display a clear difference between unheated and heated natural Cr-bearing spinels. The spectra were collected using 514.5 laser excitation, except for the heated natural spinel (which employed a 488 nm laser, with no effect on the peak width).

dred other samples (see S. Saeseaw et al., "Distinguishing heated from unheated natural spinels: A short review of ongoing research," March 22, 2009, www.gia.edu/research-resources/news-from-research). Our research has shown that unheated natural Cr-bearing (pink-to-red) spinel can be distinguished from synthetic or heated spinel through room-temperature photoluminescence spectroscopy. Cr-related emission peaks in unheated stones are usually very sharp. With heat treatment, these become broad bands due to conversion of the crystal structure from "ordered" to "disor-

dered." We performed PL spectroscopy on the 17.02 ct stone using 514.5 nm laser excitation. The broad chromium emission bands observed at 676, 687, 698, 708, and 717 nm indicated either a natural spinel that had been heat treated (figure 16) or a synthetic spinel. In contrast, a well-defined "organ-pipe" structure of the emission bands is typical of unheated natural Cr-bearing spinel (S. Muhlmeister et al., "Flux-grown synthetic red and blue spinels from Russia," Summer 1993 *G&G*, pp. 81–98).

To make the further separation of heated natural spinel from synthetic

spinel in the absence of diagnostic inclusions, chemical analysis by LA-ICP-MS can be used. In general, synthetic materials have a purer chemical composition than their natural counterparts. We detected significant amounts of impurities—including Li (77 ppm by weight), Be (32.6 ppm), Mn (243 ppm), and Ga (67 ppm)—in this sample. Concentrations of these elements in synthetic pink-to-red spinels are extremely low or not detectable.

Based on the gemological, spectroscopic, and chemical testing, we identified this stone as natural spinel with "indications of heating." It is our understanding (from the gem trade and our own research) that heat treatment may improve the clarity of some spinels, though not their color. The relative lack of inclusions suggests that this stone was heated to improve its clarity.

David Kondo, Riccardo Befi, and
Donna Beaton

Erratum

The Winter 2009 Lab Note "Diamond with flower-shaped cloud" (p. 290) erroneously stated that the hydrogen cloud followed the "{111} crystallographic direction." It should have read "{100} crystallographic direction." *Gems & Gemology* regrets the error.

PHOTO CREDITS

David Kondo—1–3; Jian Xin (Jae) Liao—4 (left), 7, 10, and 14; Kyaw Soe Moe—4 (right); Paul Johnson—6; Erica Emerson—8; Wuyi Wang—11; Nathan Renfro—12; Robison McMurtry—13; Riccardo Befi—15.

For online access to all issues of **GEMS & GEMOLOGY** from 1981 to the present, visit:

store.gia.edu

DIAMONDS

Unusual facet arrangement produces scalloped appearance in diamond. Facet arrangement can have an important impact on a diamond's appearance. We recently had the opportunity to examine a stone cut by independent diamond cutter Zev Weitman (New York) that creates an interesting optical effect.

Figure 1. In this unusual diamond cut, the stone has a scalloped appearance due to light leakage from the small crown facets adjacent to the upper edge of the girdle (1.19 ct, photo by Robert Weldon). The drawings of the stone's crown and profile show the placement of the triangular crown facets. Note in the profile view that the girdle facets are uneven in size.

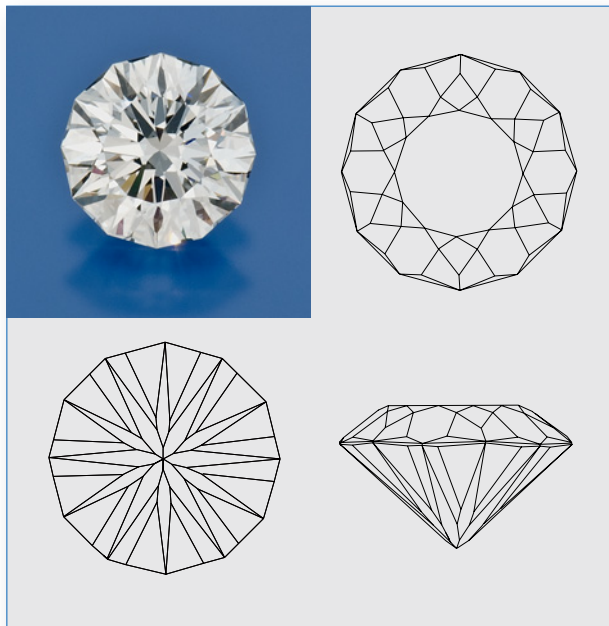


Figure 2. Setting the diamond in figure 1 in a ring with the six prongs placed at alternate facet junctions emphasizes the scalloped-edge pattern. Photo by Robert Weldon.

Mr. Weitman's bright and lively 12-sided modified round brilliant design appears to have a scalloped outline (figure 1). This visual effect is due to the presence of small, steep triangular crown facets near the girdle edge (figure 2). These facets are tilted to provide a direct light path through the stone. Since they "leak" light, they appear dark, which creates the scalloped appearance seen face-up.

This cut variation provides a challenge for jewelry designers: Four prongs upset the apparent six- or 12-fold symmetry, and bezels or heavy prongs hide the girdle and

Editor's note: Interested contributors should send information and illustrations to Brendan Laurs at blaurs@gia.edu or GIA, The Robert Mouawad Campus, 5345 Armada Drive, Carlsbad, CA 92008. Original photos will be returned after consideration or publication.

GEMS & GEMOLOGY, Vol. 46, No. 2, pp. 147–162.
© 2010 Gemological Institute of America



Figure 3. These chrysocolla chalcedony samples (13.68–31.25 ct) were recently produced from the Acari mine in southern Peru. Photo by Robert Weldon.

this optical effect. Prongs set along the flat face of a facet can also hide the effect, but they can enhance it if carefully placed at specific facet junctions (see, e.g., figure 2). The optical effect is easiest to see when lighter prongs can be employed (as with pendants or earrings).

Al Gilbertson (agilbert@gia.edu)
GIA Laboratory, Carlsbad

COLORED STONES AND ORGANIC MATERIALS

Chrysocolla chalcedony from Acari, Peru. The Acari copper mine in the Arequipa region, southern Peru, has become an

important source of gem materials such as “Andean” pink and blue opal and chrysocolla chalcedony (Summer 2006 Gem News International [GNI], pp. 176–177). During the past two years especially, the mine produced a significant amount of high-quality chrysocolla, ranging from green to blue, according to Hussain Rezayee (Rare Gems & Minerals, Beverly Hills, California). In April 2008, he received an initial rough parcel of 5 kg, from which he cut ~500 carats of cabochons weighing up to 5 ct; ~20% were translucent. Five months later, he obtained an additional 300 kg of “mine run” material in Peru, from which he cut an additional 4,000 carats of good-quality cabochons that ranged up to 30+ ct. The stones reportedly were mined by hand methods and have not undergone any treatments.

Mr. Rezayee loaned five cabochons (13.68–31.25 ct; figure 3) to GIA for examination, and the following properties were collected: color—green-blue and blue-green; diaphaneity—translucent; spot RI—1.54–1.55; birefringence—0.01; hydrostatic SG—2.63; and inert to both long- and short-wave ultraviolet (UV) radiation. The desk-model spectroscope showed a 650 nm cutoff, and no absorption lines indicative of dyeing. Microscopic examination revealed subtle spotty green inclusions, along with small fractures in some of the samples. These properties are consistent with those given for chrysocolla in the literature, except for the relatively high SG (compare to 1.93–2.40; R. Webster, *Gems*, 5th ed., revised by P. G. Read, Butterworth-Heinemann, Oxford, UK, 1994, pp. 399–400) and their homogeneous overall color appearance.

Chemical analysis by energy-dispersive X-ray fluorescence (EDXRF) indicated major amounts of Cu and Si, as well as traces of Pb and Fe in two of the samples. Infrared and Raman spectroscopy were performed to further characterize the samples. The IR spectra showed absorption

Figure 4. A kunzite crystal (the dark-appearing object) is carefully extracted from a gem pocket at the Oceanview mine in Pala, California (left). Illuminated by a miner’s lamp, this just-extracted kunzite crystal shows fine color (right). Photos by M. Mauthner.



peaks at ~ 7077 , 5234 , 4440 , and 2502 cm^{-1} , plus broad saturation at $\sim 3708\text{--}2546$ and $2405\text{--}800\text{ cm}^{-1}$, as are typical of chrysocolla. The Raman spectra matched those of quartz in our database.

Ultraviolet-visible-near infrared (UV-Vis-NIR) spectroscopy can be used to detect dyed chrysocolla chalcedony (see A. Shen et al., "Identification of dyed chrysocolla chalcedony," Fall 2006 *G&G*, p. 140) by calculating the ratio of the integrated intensity of the Cu^{2+} band to that of the structurally bonded OH band. Natural chalcedony colored by chrysocolla has a ratio between 7 and 44, while samples dyed with a copper solution have ratios from 0.5 to 3.0. The samples we examined had ratios from 33.5 to 54.7, confirming that they were not dyed.

Erica Emerson (*eemerson@gia.edu*) and Jason Darley
GIA Laboratory, New York

Recent finds of kunzite in Pala, California. California's Pala pegmatite district, the type locality for kunzite ("lilac"-colored gem spodumene), still occasionally produces fine gem material. In December 2009, workers at the Oceanview mine (owned by Jeff Swanger, Escondido, California) broke into a significant spodumene-bearing pocket. Other mines in the district have produced gem spodumene since its discovery there in 1903, but this was the first such find at the Oceanview mine after nearly 10 years of regular part-time operation. The Elizabeth R mine, located nearby on the same pegmatite dike, produced small quantities of kunzite on several occasions during the 1980s and as recently as two years ago (Winter 2008 *GNI*, p. 373).

Shortly after the discovery of the aquamarine- and morganite-bearing 49er Pocket in September 2007 (see Spring 2008, *GNI*, pp. 82–83), workers found traces of pale kunzite in the footwall below the 49er stope. In November 2009, they recovered a few gem-quality kunzite crystals up to several centimeters long. Further mining entered a roughly $2 \times 1.5 \times 1\text{ m}$ zone in December that produced 7+ kg of kunzite, more than a quarter of which was clean, deep-colored gem material (e.g., figure 4)—including a very limpid and well-developed crystal weighing over 300 g (figure 5). Some of the production has been sent to cutters, and a few dozen gems have been faceted so far (e.g., figure 6). More cutting material is in the possession of local dealers, and additional gems will undoubtedly find their way to the market in the future.

Just before this issue went to press, on June 28 the miners opened another kunzite pocket. However, this one was larger and contained spodumene ranging from "lilac" to pale blue-green to green, as well as some gem-quality green, pink, and bicolored tourmaline. The largest spodumene crystal uncovered so far measured $\sim 20 \times 10 \times 1.5\text{ cm}$. More information and photos from this pocket are available in the *G&G* Data Depository (gandg.edu/gandg).

Mark Mauthner (*mmauthner@gmail.com*)
Carlsbad, California



Figure 5. These kunzite crystals (the largest is 11.2 cm tall) were recovered from the Oceanview mine in December 2009. Photo by M. Mauthner.

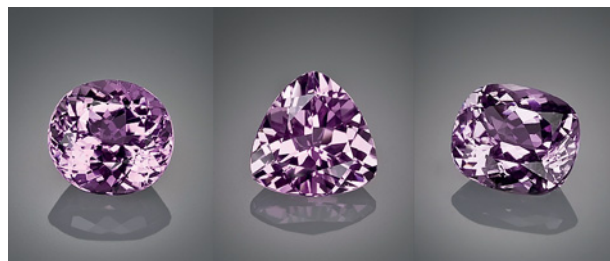


Figure 6. These kunzites (6.0, 7.5, and 6.5 ct) were faceted from material found recently at the Oceanview mine. Photos by M. Mauthner.

Natural pearls of the Pectinidae family: Review and origin of color. Interest in non-nacreous natural pearls has been growing recently, mainly because of the attractive structures they can exhibit (e.g., "flame" structures found in the *Strombus gigas* "queen conch" pearls). The Pectinidae (classified by Rafinesque, 1815) bivalves have been used for food and adornment since ancient times, and they are still harvested for their meat. Natural Pectinidae pearls can be found in *Placopecten magellanicus* (Gmelin, 1791), *Argopecten spp.* (Monterosato, 1889), and *Nodipecten spp.* (Dall, 1898); they are also known as "scallop" pearls (*The Pearl Book: Natural, Cultured & Imitation Pearls—Terminology & Classification*, CIBJO, Milan, Italy, 2010, 53 pp.). However, the best-known "scallop" pearls are those from *Nodipecten spp.* These bivalves are found mainly in Baja California and in the eastern Pacific. To our knowledge, no cultured pearls from mollusks of the Pectinidae family have been reported.

Scallop pearls range from white to "cream" white to light gray to yellow to brown, as well as pink to brownish purple (figures 7 and 8); the interior of the Pectinidae

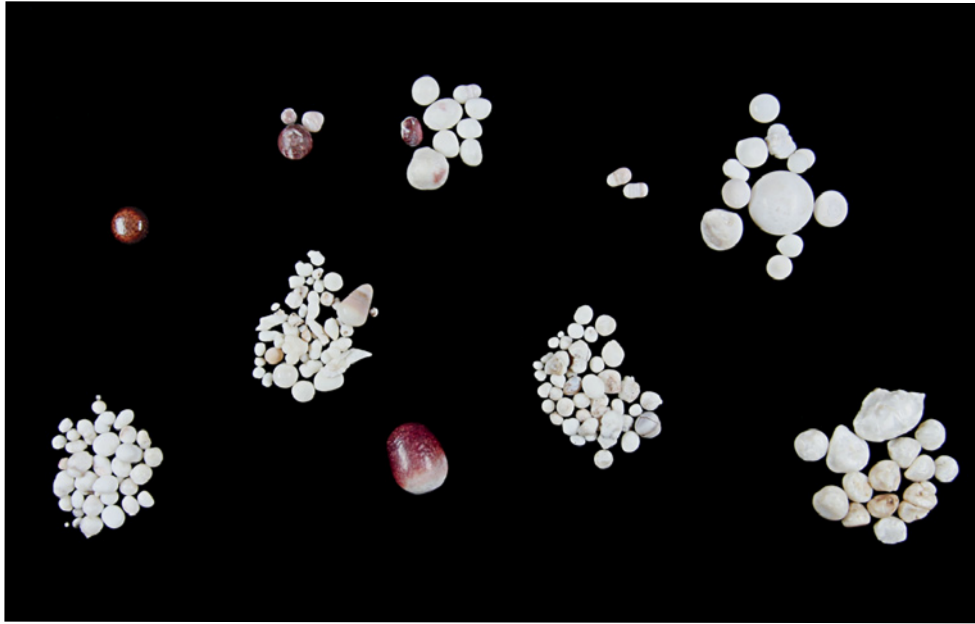


Figure 7. These natural “scallop” pearls display a variety of colors, shapes, and qualities. The largest sample is 12.4 × 9.7 mm (8.45 ct). Courtesy of K. C. Bell; photo by Evelyne Murer.

shell can show similar colors. The pearls commonly measure up to 6 mm, and those larger than 12 mm are rare. They exhibit a variety of shapes; buttons, ovals, and drops are most common, sometimes circled. These shapes appear to be due to the pearls’ rotation during formation. Sometimes they vary in color along their rotational axis (e.g., figure 8, left).

Some scallop pearls present interesting macroscopic and microscopic structures (e.g., figures 8 and 9). These structures have been described as a segmented patchwork of cells, with each cell comprising three differently oriented subsegments (K. Scarratt and H. A. Hänni, “Pearls from the lion’s paw scallop,” *Journal of Gemmology*, Vol. 29, No. 4, 2004, pp. 193–203). This is probably because of their prismatic calcite microstructure, similar to that observed in some pearls from the Pinnidae family (“pen shell” pearls; see Fall 2009 GNI, pp. 221–223).

Raman spectroscopy of the scallop pearls in figure 8 (left) and several shells showed that their colored regions

contain a mixture of unsubstituted polyenic (polyacetylenic) compounds. UV-Vis-NIR reflectance spectra of samples of various colors showed a gradual absorption from the UV to the NIR region, with the polyenic pigments absorbing in the blue and green portions of the spectrum. The specific color of each pearl seems to be due to the relative intensities of these absorptions. To the best of our knowledge, colored Pectinidae are the only gem-quality natural pearls that consist of calcite and contain polyenic pigments. Similar pigments with calcitic structures are observed in *Corallium spp.* corals.

Acknowledgments: The authors are grateful to Thomas Hochstrasser (Hochstrasser Natural Pearls, Dörflingen, Switzerland) and K. C. Bell (KCB Natural Pearls, San Francisco) for supplying pearls for this study.

Stefanos Karampelas
(s.karampelas@gubelingemlab.ch)
Gübelin Gem Lab, Lucerne, Switzerland

Thomas Hainschwang
Gemlab Laboratory, Balzers, Liechtenstein

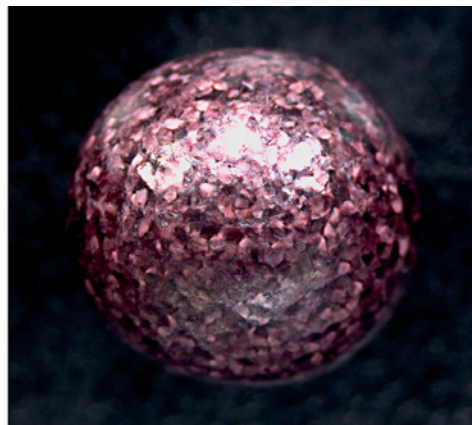


Figure 8. Scallop pearls are non-nacreous and exhibit a range of colors. The yellowish brown sample in the left photo is 6.8 × 4.1 mm, and the brownish purple pearl in the right image is 7.5 × 7.2 mm. Courtesy of Gübelin Gem Lab, K. C. Bell, and Gemlab; photos by Evelyne Murer (left) and T. Hainschwang (right).

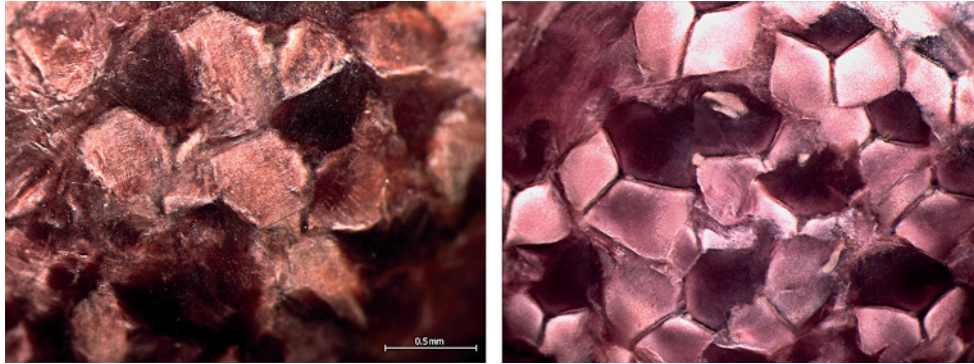


Figure 9. The structures observed in these scallop pearls are due to the arrangement of the calcitic prisms. Photomicrographs by T. Hainschwang; width of right image is ~2 mm.

More on ruby from Cabo Delgado, Mozambique. In April 2010, these authors visited the ruby mining site in Cabo Delgado Province, east of Montepuez, in northern Mozambique (see Winter 2009 GNI, pp. 302–303). Our associates in the evaluation of the deposit were Trevor Robson (Lusaka, Zambia) and Jeremy Rex (Transglobe, London). Located on a private game farm, the concession has been granted to Mwiriti Mining, based in Pemba. We were hosted and guided by Mwiriti's Carlos Asghar. Mwiriti employs 15–20 people and has an active exploration and mining program under way, but the deposit has been overrun by illegal miners. In fact, we saw several shafts (up to 20 m deep) they had sunk. As many as 4,000 illegal miners have been evicted in recent months, with several arrested while we were at the deposit. A number of foreigners have also been arrested while attempting to smuggle the rubies out of Mozambique.

Our exploration activities revealed that the rubies are hosted by eluvial material as well as the underlying weathered bedrock. The bedrock consists of the Montepuez Complex, a Neoproterozoic suite of metamorphosed sedimentary rocks (amphibolite-grade schists and gneisses) that were intruded by granite, granodiorite, and tonalite. In the deeply weathered area we examined, the eluvium appeared to lie directly on Montepuez gneisses, which were crosscut by light-colored veins (now mostly weathered to clay; figure 10). These veins ranged up to 20 cm thick, and probably originally consisted of syenitic (silica-deficient) pegmatites and aplites. Ruby was seen in these veins and also in the overlying boulder-rich eluvium. The miners dig pits in the lateritic soil to search for light-colored, sand-rich layers that are indicative of underlying boulder beds (figure 11). We recovered the crystals in figure 12 from the eluvial deposits. Their tabular euhedral form is characteristic of the ruby crystals from this area.

The Montepuez deposits appear to extend over a large region. Mwiriti's concession includes licenses for six contiguous properties that cover an area of 11,060 hectares. Additional ruby finds have been reported nearby, but outside of the concession. Reliable local sources told us that rubies of similar color and character were being recovered 10–20 km from the site we visited.

Lawrence W. Snee (lawrencew.snee@gmail.com)
Global Gems and Geology, Denver, Colorado

Tommy Wu
Shire Trading Ltd., Hong Kong

Ruby, sapphire, and spinel mining in Vietnam: An update. After intense activity during the 1990s (see, e.g., R. E. Kane et al., "Rubies and fancy sapphires from Vietnam," Fall 1991 *G&G*, pp. 136–155; R. C. Kammerling et al., "Update on mining rubies and fancy sapphires in northern Vietnam," Summer 1994 *G&G*, pp. 109–114), gem mining in Vietnam slowed considerably in the 2000s. During three expeditions, in January and May of 2009 and April 2010, these authors were accompanied by Philippe Ressigeac (France), Jean Baptiste Senoble (Switzerland), Lou Pierre Bryl (Canada), Kham Vannaxay (Thailand), Tracy Lindwall (USA), Jazmin Amira Weissgärber Crespo (Germany), and David Bright (USA), to visit most of Vietnam's ruby, sapphire, and spinel mines (figure 13) and collect specimens on-site for the GIA reference collection.

Today, most gem mining is performed by independent miners and local farmers who dig for gems when agricultural activity is low (generally March–June and October–January in the north, and December–March in

Figure 10. At the Montepuez ruby deposit, tabular crystals of corundum are hosted by deeply weathered light-colored veins that crosscut metasedimentary rocks. A clay-covered ruby crystal is being pointed out here, still in situ within a vein. Photo by L. W. Snee.





Figure 11. In the eluvial areas at Montepuez, the miners dig pits through dark gray/red overburden to reach the boulder-rich layers containing the ruby. These beds are usually found beneath light-colored sandy layers. Photos by L. W. Snee.

the south) using simple hand tools. In northern Vietnam's Yen Bai Province, ruby (mainly cabochon quality), star ruby, and dark red spinel are recovered sporadically around Tan Huong and Truc Lau, and on some islands in Thac Ba Lake. In addition, as of April 2010, an estimated 500 miners were working near the town of Yen The (e.g., figure 14), as well as the villages of An Phu and Minh Tien, in the Luc Yen district. Besides ruby, the main production consists of spinel of various colors, blue sapphire, and green tourmaline; blue spinel (figure 15) has become increasingly popular with buyers since 2007. Luc Yen's production of fine gems is limited, however. Its output consists predominantly of small gems and specimens destined for use in decorative items, such as marble carvings

Figure 12. These ruby samples were washed from a 1 kg concentration of corundum and mica that was excavated from eluvial material at Montepuez. Photo by L. W. Snee.



and gem paintings, which are popular in Asian markets. These goods provide a steady income for most miners, enabling them to keep working the area and hopefully find fine gems from time to time.

Beginning in 2010, some new operations were initiated in the Luc Yen district. Near An Phu, an Indian-Vietnamese joint venture (Vietnam Alliance Minerals Ltd.) secured an exploration license for the Cung Truoi and Mai Thuong areas, known for their ruby and spinel matrix specimens. At Truc Lau, an area known for large rubies and spinels, a private Vietnamese company (Doji Cie) is preparing for a mechanized operation.

Further south, around Quy Hop in Nghe An Province, some rubies and sapphires are being recovered from the Chau Hong area as a byproduct of tin mining. Gem mining around Quy Chau is limited to nighttime digging by a few illegal miners. Nevertheless, the Doi Thy ruby mine could reopen at the end of 2010.

In southern Vietnam, we witnessed small-scale mining of basalt-related blue, yellow, and green sapphires at Hong Liem near Phan Thiet (Binh Thuan Province), and also at Dak Nong (Dak Lak Province). In other areas around Di Linh (Lam Dong Province), former jungle-covered sapphire mining areas have been replaced by coffee plantations.

Vincent Pardieu (vincent.par@giathai.net)
GIA Laboratory, Bangkok

Pham Van Long
Center for Gem and Gold Research and Identification
Hanoi, Vietnam

Sphene from northern Pakistan. Attractive gem-quality sphene has been known from Pakistan's North West Frontier Province since mid-2004 (see Spring 2006 GNI, pp. 67–68). At this year's Arizona Mineral & Fossil Show (Hotel Tucson), Syed Iftikhar Hussain (Syed Trading Co., Peshawar, Pakistan) had some faceted sphene from a new locality in Pakistan: the Shigar Valley area, which is



Figure 13. Vietnam's main ruby, sapphire, and spinel localities are shown on this map. Adapted from Kane et al. (1991).

already famous for its production of aquamarine, topaz, black tourmaline, and other minerals. The sphene deposit is reportedly located near Niesolo in the Basha Valley, which is situated within Pakistan's Gilgit-Baltistan territory (formerly known as the Northern Areas). Sphene was initially found there in 2008, and Mr. Hussain knew of ~7 kg of crystal fragments containing gem-quality areas. Although stones weighing 25–30 ct could be cut, they appeared too dark above 6–7 ct. The ~160 faceted stones



Figure 14. This small ruby mining operation is located in Khoan Thong Valley, west of Yen The town, in the Luc Yen district. This area was worked by Thai companies during the 1990s. Photo by V. Pardieu, April 2010.

that Mr. Hussain had in Tucson showed fairly consistent color (figure 16), appearing yellowish green in daylight and brownish green in incandescent light.

Brendan M. Laurs

Figure 15. These blue spinels were mined in Vietnam's Luc Yen district. The largest faceted stone weighs ~2 ct. Photo by V. Pardieu, January 2009.





Figure 16. These spinels (up to ~1.7 ct) are reportedly from a new locality in northern Pakistan's Shigar Valley area. Photo by Jeff Scovil.

Spinel from Bawma, Myanmar. Fine-quality spinel has been known from Myanmar for many years, especially in bright red hues. Recently Hussain Rezayee informed us about a new find of orangy red to purplish red spinel near the village of Bawma in the Mogok area of Myanmar. He

Figure 17. These spinels (0.35–3.52 ct) were cut from a piece of rough that was recently found at a new deposit in the Mogok area of Myanmar. The 0.59 ct stone is GIA Collection no. 38203; photo by Robert Weldon.



was told that a total of 1–2 kg of facetable rough were produced in October–November 2009 before the mine was closed by the government. Although transparent pieces up to 20 g were found, most of the material was too dark for cutting attractive stones in large sizes.

From a 6.8 g piece of rough, Mr. Rezayee cut five spinels weighing 0.35–3.52 ct (figure 17), which he supplied to GIA. The following properties were recorded: color—red; RI—1.718; hydrostatic SG—3.60; fluorescence—weak-to-moderate red to long- and short-wave UV radiation; and a broad absorption observed in the green region along with a sharp absorption line at 684 nm visible with a desk-model spectroscope. Microscopic examination revealed “fingerprints” composed of minute octahedral negative crystals. All properties and observations were consistent with natural red spinel. Raman photoluminescence spectra showed no indications of heating (see background on this technique in the Lab Note on pp. 145–146 of this issue).

During a recent trip to Myanmar, Mr. Rezayee was told that the Burmese government may be planning to mine the deposit in a joint venture with private companies, so additional production seems likely.

Editor's note: Consistent with its mission, GIA has a vital role in conducting research, characterizing gemstones, and gaining knowledge that leads to the determination of gemstone origins. The gemstones studied in this report are not subject to the Tom Lantos Block Burmese JADE Act of 2008, and their import was in accordance with U.S. law.

Nathan Renfro (nrenfro@gia.edu)
GIA Laboratory, Carlsbad

Brendan M. Laurs

Tsavorite and other green garnets reportedly from Afghanistan. In December 2008, Farooq Hashmi (Intimate Gems, Jamaica, New York) loaned GIA some green gem material that was sold to him as garnet in Peshawar, Pakistan. He purchased it several years ago, and was told it came from Kala, Kunar Province, Afghanistan. He reported seeing several parcels over the years in Peshawar, although the pieces tended to be small, mostly suitable for cutting melee stones.

Examination of the 18 rough samples (0.08–0.21 g) and three faceted stones (0.09–0.20 ct; figure 18) revealed the following properties: color—medium-light to medium-dark yellowish green to green; RI—1.74 to 1.77 (spot readings of the rough samples fell within this range); hydrostatic SG—3.43–3.64; fluorescence—inert to long-wave UV radiation, and inert to very weak orange to short-wave UV; and absorption bands or cutoffs at 440 nm visible with the desk-model spectroscope. These properties are consistent with those reported for grossular to grossular-andradite garnet, although some of the SG values are somewhat low (as compared to the 3.57–3.66 range reported by C. M. Stockton and D. V. Manson, “A proposed new classifica-



Figure 18. These samples of grossular to grossular-andradite are reportedly from Afghanistan. The faceted stones weigh 0.09–0.20 ct, and were cut by Matt Dunkle; the two darker green ones are tsavorite. Photo by Jian Xin (Jae) Liao.

tion of gem-quality garnets,” Winter 1985 *G&G*, pp. 205–218). EDXRF spectroscopy of all the samples revealed major amounts of Ca, Al, and Si, with minor Mn, Fe, Ti, Cr, Cu, and Zn. Microscopic examination revealed needles, liquid inclusions, partially healed “fingerprints,” dark crystal inclusions, and iron staining.

Some of these samples of grossular to grossular-andradite were green enough to be considered tsavorite. We are unaware of tsavorite from Afghanistan being previously produced.

Erica Emerson and Jason Darley

SYNTHETICS AND SIMULANTS

An unusual lab-grown garnet: Calcium niobium gallium garnet. There are two species of green laboratory-grown garnets that gemologists sometimes encounter: yttrium aluminum garnet (YAG) and gadolinium gallium garnet (GGG). Occasionally, though, a less familiar manufactured garnet will come through the laboratory.

A 5.43 ct green stone resembling tsavorite (figure 19) was submitted to AGL for an origin report. The following gemological properties were recorded: singly refractive with weak anomalous double refraction; RI—over the limits of the standard refractometer; hydrostatic SG—4.73; and no reaction to long- or short-wave UV radiation. When examined with a desk-model spectroscope, it showed general absorption to 470 nm, with bands centered at 585, 625, and 670 nm. Microscopic examination showed no inclusions or growth structures. Although the client believed it was demantoid, this was not supported by the SG value or spectrum.

EDXRF spectroscopy revealed major amounts of gallium and niobium, with minor Ca. (Oxygen, a light element, is not detectable with this instrument.) The FTIR spectrum



Figure 19. This 5.43 ct green sample proved to be calcium niobium gallium garnet, a lab-grown product with no natural counterpart. Photo by Bilal Mahmood.

showed one distinct peak at 3532 cm^{-1} and a smaller, broader peak at 3448 cm^{-1} ; it had some similarities to other lab-grown garnets in our database, but did not match any of them precisely. Based on these properties, we identified the sample as calcium niobium gallium garnet.

Like YAG and GGG, calcium niobium gallium garnet has industrial use as a lasing material. Since this lab-grown garnet has no known natural counterpart, it would not be considered a “true” synthetic, which is also the case with YAG and GGG.

Elizabeth Quinn Darenius
(eqdarenius@aglgemlab.com)

American Gemological Laboratories, New York

Glass imitations of emerald with straight zones. For centuries, glass has been the most widely used gem simulant. This versatile substance is capable of imitating almost any gem material—organic or inorganic, transparent or opaque, in any color—and possessing phenomena such as chatoyancy, sheen, adularescence, opalescence, orient, and color change. Gas bubbles, swirl marks, or devitrification effects are useful for identifying glass.

Recently, the Gem Testing Laboratory of Jaipur, India, received for identification the two green specimens in figure 20 (17.05 and 1.79 ct), which were submitted as emeralds. Although the stones’ appearance initially suggested emerald, their exceptional color and clarity raised doubts regarding their origin.

Both specimens displayed anomalous double refraction in the polariscope, ruling out emerald. The 17.05 ct specimen had an RI of 1.730 and a hydrostatic SG of 4.36, while the 1.79 ct gem had an RI of 1.630 and an SG of 3.03. Both were inert to long- and short-wave UV radiation and displayed no absorption features in the desk-model spectroscope. These properties indicated glass.



Figure 20. These 17.05 and 1.79 ct specimens, represented as emerald, were identified as glass imitations. Photo by G. Choudhary.

Striking features were observed with magnification. Both specimens displayed a series of sharp, straight lines along their lengths (figure 21, left), which were visible with darkfield illumination but were much clearer when the stones were observed under immersion. Such straight lines are often associated with growth lines or zoning in natural gemstones. Viewed from different angles, some of these lines were revealed to be planes with sharp edges (figure 21, right). In addition, a few scattered gas bubbles were present in the 1.79 ct specimen.

These glass imitations were readily identified with classical gem testing instruments, but they may pose a problem for jewelers or field gemologists who attempt to identify them with only a 10× lens.

Gagan Choudhary (gtl@gjepcindia.com)
Gem Testing Laboratory, Jaipur, India

“Nanogems”—A new glass-ceramic material.* Glass-ceramic is a class of manufactured materials that consists of glass matrix and nanometer-size crystalline particles (oxides and silicates) that are grown within the matrix. It

has unusual physical properties—such as negative thermal expansion—that make it useful for specialized industrial applications. Glass-ceramic became known to the general public during the 1970s, when it was first used as a surface for cooking ranges. Until now, though, we have not seen glass-ceramic materials produced as gem simulants. One Russian manufacturer, Formica LLC (Moscow, with a factory in Bangkok), has developed a new glass-ceramic material that it calls “Nanogems.” According to the company, the material is available in a variety of colors, has a Mohs hardness of 7–7½, and its high thermal shock resistance makes it suitable for a variety of jewelry manufacturing processes.

At the 2010 Tucson show, Formica LLC donated four samples to GIA, consisting of two blue and two green brilliants ranging from 2.59 to 3.15 ct (figure 22). Standard gemological testing yielded the following properties: RI—1.621 (blue) and 1.629 (green); no dispersion evident; hydrostatic SG—3.02–3.07; aggregate reaction in the polariscope; fluorescence—inert to long-wave UV and inert (green samples) or weak white (blue samples) to short-wave UV, with no phosphorescence; spectroscopy spectrum—three distinct bands in the green, yellow, and red regions (blue samples) and two distinct bands in the orange and red regions (green samples). Microscopic observation revealed only a few pinpoint inclusions and conchoidal fractures in the green samples. However, all four showed prominent graininess, in most cases throughout the entire specimen (figure 23). When illuminated with a fiber-optic light source, all also had a somewhat milky appearance, as would be expected for light scattering from nano-crystals.

Laser ablation–inductively coupled plasma–mass spectrometry (LA-ICP-MS) of all samples indicated a mainly Mg-Ti-Zn-Zr alumino-silicate composition. The blue samples contained ~80 ppm Co and the green samples ~7000 ppm Ni. We believe these two elements are the

*The original title read “Nanogems’—A new lab-grown gem material.” This was an improper use of the terms lab-grown and gem material. —Eds,

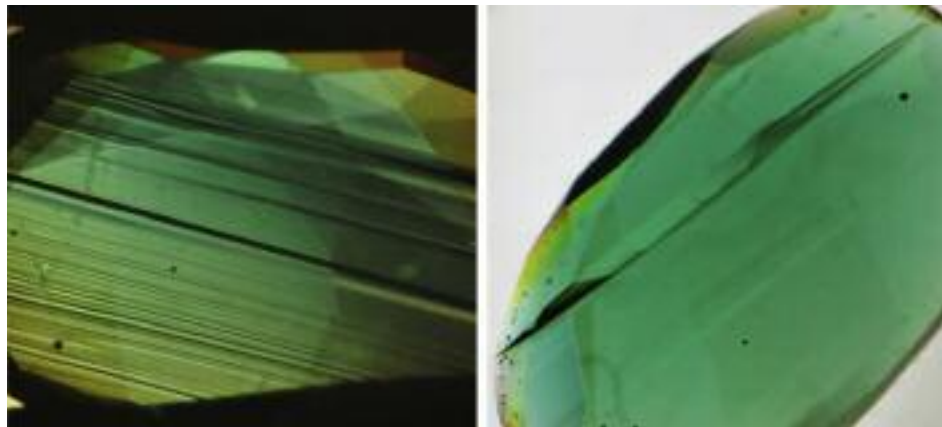


Figure 21. Both specimens in figure 20 displayed sharp, straight lines along the length of the gem, reminiscent of growth lines and zones in natural gemstones (left). Viewed from various angles, some of the lines were actually planes with sharp edges (right). Photomicrographs by G. Choudhary; magnified 45×.

main coloring agents. UV-Vis spectroscopy showed results equivalent to those seen with the desk-model spectroscope: three obvious bands in the blue samples (545, 583, and 624 nm) and two in the green samples (593 and 633 nm). The infrared spectra of all samples displayed a general absorption edge at 2150 cm^{-1} and two distinct bands at 3641 and 3394 cm^{-1} , probably related to the hydroxyl group. Four additional minor absorption bands were observed, at 4521 , 4252 , 2677 , and 2244 cm^{-1} . Raman spectroscopy indicated a broad hump typical of an amorphous material (i.e., glass), with some sharper bands (most prominently at 656 and 415 cm^{-1}) that matched those of gahnospinel. Therefore, the properties of this material are consistent with a glass-ceramic.

The aggregate polariscope reaction and strong graining should allow separation of this material from glasses typically used as gem simulants. However, it is possible that not all faceted glass-ceramics will exhibit these features, making them more difficult to distinguish from glass—despite their unusual chemical composition. The most definitive separation criteria would be provided by X-ray diffraction, but this technique is not available in most gemological laboratories.

Andy Shen (andy.shen@gia.edu)
GIA Laboratory, Carlsbad

Serpentine doublets, sold as pietersite, from Arizona. At the 2010 Tucson gem shows, one of these contributors (PH) purchased a few samples represented as pietersite that reportedly came from Globe, Arizona. The sample group contained rough pieces as well as cabochons (doublets) consisting of “pietersite” attached to black resin bases. Pietersite is composed of chatoyant silicified crocidolite (a fibrous asbestos mineral)—in the form of brecciated dark blue hawk’s-eye and/or brownish yellow tiger’s-eye. It was discovered in 1962 in northern Namibia (see *Gem News*, Summer 1988, pp. 117–118, and Spring 1992, p. 61), and a similar rock was found in 1993 in Xichuan, Henan Province, China. Considering the rarity of pietersite deposits, a U.S. locality for this material would be noteworthy.

The following properties were obtained from five of the Arizona cabochons (9.40–87.85 ct; e.g., figure 24): color—very light yellow to brownish yellow; spot RI—1.54–1.55; and fluorescence—inert to long- and short-wave UV radiation. Specific gravity measurements would not be meaningful because of the resin backing. Microscopic examination revealed that the gem material consisted of parallel fibers oriented perpendicular to the chatoyant bands, and those fibers were thus responsible for the tiger’s-eye effect. The fibers varied from white to light yellow, and some were brownish red as expected for staining by iron oxides/hydroxides.

Three pieces of rough (45.16–420.12 g) also were examined. They were composed of white to light yellow fibers with crosscutting deep green and brown crystalline



Figure 22. These four glass-ceramic samples (2.59–3.15 ct) were manufactured by Formica LLC. Photo by Robert Weldon.

aggregates. Their structure consisted of asbestiform parallel fibers oriented normal to the surfaces of fracture veins that were hosted within a massive brown-black matrix. Hydrostatic SG measurements of the three samples yielded values of 2.43–2.46. Powder X-ray diffraction data identified the major mineral as serpentine, formed by an admixture of chrysotile and lizardite. The samples also contained minor amounts of quartz and calcite.

This Arizona material is quite different from pietersite. Although its refractive index overlaps that expected for pietersite, its SG values are lower (cf., 2.50–2.58 from Namibia and 2.67–2.74 from China), which is consistent with serpentine. In addition, the Namibian and Chinese pietersite consists of fibers that are oriented in an irregular fashion, unlike this serpentine from Arizona.

Figure 23. This green glass-ceramic specimen contains a few pinpoints, as well as prominent graining when viewed in certain orientations. Photomicrograph by A. Shen; field of view 1.8 mm wide.

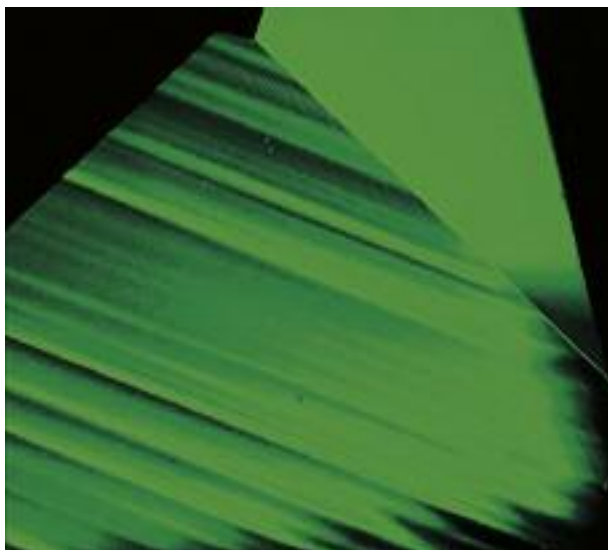




Figure 24. This stabilized Arizona serpentine doublet (here, 87.85 ct) bears a resemblance to *pietersite*, and has been marketed as such.
Photo by K. Hu

According to Bruce Barlow (Barlow's Gems, Cave Creek, Arizona), from whom the Arizona material was purchased, it is impregnated with resin to stabilize the fibers and create a polishable mass. Although this gem exhibits an attractive chatoyancy that is the hallmark of material from Namibia and China, its mineralogy is very different.

Kaifan Hu (hukaifan@gmail.com)
China University of Geosciences, Wuhan, China

Peter Heaney
Pennsylvania State University, University Park

TREATMENTS

A composite coral bangle. With China's economic growth, more enhanced gem materials are being seen in that country's jewelry markets. One of them is red coral, which has a long history as an ornamental gem. Because most corals are dendritic (branch-like), they are usually fashioned as carvings or sculptures that suit this form, or as smaller cabochons and beads. Recently, the National Gemstone Testing Centre in Beijing received for identification a bangle that was represented as red coral (figure 25). While the piece showed a uniform appearance in general, our suspicions were immediately raised because coral could not have been carved into such a shape due to the limitations nature imposes on its size and form.

The outer surface of the bangle appeared uniform (figure 26, left), but close examination of the inner surface revealed discontinuities in the pattern, as well as a layered structure (figure 26, right). Such features indicate an assembled piece. Closer examination showed that the bangle consisted of more than 250 sections. Each individual piece was elongated and approximately the same size. Detailed microscopic examination revealed distinct junc-

tions between the sections, as well as impregnation in some areas by a filling material that resembled wax (figure 27). Unfortunately, we were unable to study the filler with IR spectroscopy because the client did not give us permission to take the powdered sample necessary for the analysis.

Further examination revealed properties typical for natural coral: the distinctive red color; a refractive index of 1.58–1.60; and ribbed, pitted growth structures. Raman analysis of five spots on the outside of the bangle gave peaks at 1520, 1123, 1087, and 714 cm^{-1} , a typical combination of bands associated with both the coral matrix and the natural compounds responsible for its color (see C. P. Smith et al., "Pink to red coral: A guide to determining origin of color," Spring 2007 *G&G*, pp. 4–15).

This is the first coral assemblage we have encountered in our laboratory. According to the client, such bangles have been on the Chinese market since 2009. Often referred to as "salmon coral," they are manufactured primarily by a Taiwanese-Italian joint venture. Based on conversations with the client, we believe that the pieces were assembled with an adhesive and cut into a bangle shape, which was then polished and carved with decorative patterns.

Although this coral bangle is a manufactured composite, its fine craftsmanship is remarkable.

Jun Su (suj@ngtc.gov.cn), Taijin Lu,
and Zhonghua Song
National Gemstone Testing Centre, Beijing

Figure 25. This bangle (74 mm diameter) proved to be an assemblage of more than 250 pieces of coral.
Photo by Jun Su.





Figure 26. The outer surface of the bangle (left, 15 mm wide) appears smooth and uniform, belying its composite nature. However, the layered structure is clearly visible on the inner surface (right). Photos by Jun Su.

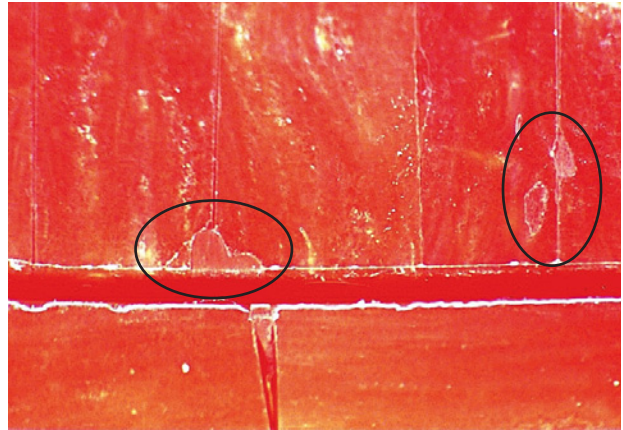


Figure 27. Magnification reveals distinct junctions between some of the individual coral pieces, discontinuities in the pattern, and areas containing a filling material (circled). Photomicrograph by Jun Su; magnified 15 \times .

Lead glass-filled ruby in antique jewelry. Treated rubies have recently been a hot topic for both the trade and mainstream news organizations, particularly the heavily lead glass-filled rubies that are widely available in the gem trade and can even be found in retail stores, jewelry websites, and TV shopping channels. AGL has adopted the term *composite ruby* to better distinguish this material from traditional heated rubies, while recognizing that it is neither an imitation ruby nor a synthetic. This treatment significantly impacts the original corundum's appearance (perceived transparency and color), and it also requires special care to avoid damage to the stone. We know that the lead-glass filler can be etched by common household cleaning products and a jeweler's pickling solution, and the application of a jeweler's torch can cause it to degrade.

Despite the prevalence of this material in the marketplace, we were still surprised by the piece in figure 28, which was submitted for identification. This antique pendant was set with old-mine-cut diamonds and seed pearls, but the center stone was identified as a composite ruby (using microscopy and EDXRF spectroscopy) that was estimated to weigh 7.5 ct. The pendant did not appear to be a replica, and the workmanship was indicative of an older piece. The composite ruby had been carefully reset, as the milgrain around the bezel was in good condition, and we saw no degradation of the glass in the stone that could be caused by the jeweler's torch.

The fact that this material has started showing up in antique jewelry is representative of how far it has penetrated the market and reinforces the importance of proper disclosure.

Elizabeth Quinn Darenius

Tanzanite and other gems set with colored adhesive. In March 2010, GIA was informed by goldsmith Ed Barker (Artistry in Gold, Yountville, California) about various gemstones he had encountered in bezel-set rings that were mounted with colored glue. The rings were pur-

Figure 28. This antique pendant contains an approximately 7.5 ct lead glass-filled ruby. Photo by Bilal Mahmood.





Figure 29. This 1.87 ct tanzanite was mounted in a ring with a colored adhesive. Residual adhesive is still present on some of the crown facets, particularly at the corners. Photo by Robert Weldon.

chased during 2009 from a customer who had obtained them from a TV shopping network. When he removed the stones from their mountings, Mr. Barker noted that an adhesive—colored to enhance the appearance of the ruby, amethyst, or tanzanite gems—was present along the bezel area.

Mr. Barker sent one of the stones, a 1.87 ct tanzanite, to GIA for examination (figure 29). A purple-colored flexible adhesive was visible on some of the crown facets, particularly at the corners (e.g., figure 30). The material was slightly tacky, making it attractive to dust particles. After the adhesive was removed, the color of the tanzanite appeared very slightly lighter. Mr. Barker indicated that the other stones he removed from the rings became noticeably lighter (particularly the amethyst). The colored adhesive was obviously intended to enhance the appearance of the stones, as well as help hold them in their mountings . . . buyer beware!

Brendan M. Laurs

CONFERENCE REPORTS

1st Italian Conference on Scientific Gemology. Organized by Dr. Eugenio Scandale (University of Bari Aldo Moro), Drs. Adriana Maras and Michele Macri (Sapienza University of Rome), and Dr. Giancarlo Della Ventura (Roma Tre University), this conference took place June 15–16, 2010, in Rome. There were ~120 registrants.

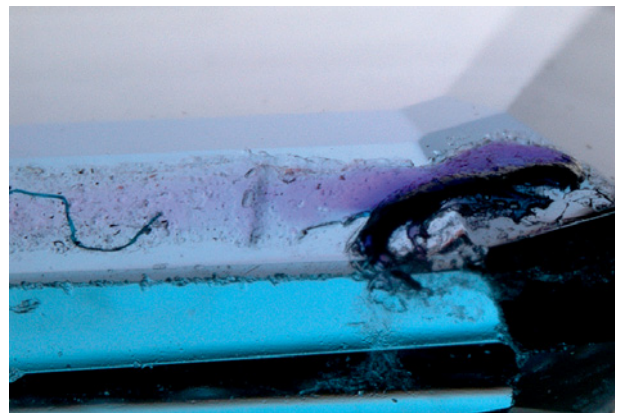
In the plenary lecture, **this author** explored scientific gemology through several case studies: country-of-origin determination for ruby and sapphire, characterization of the Wittelsbach-Graff and Hope diamonds, and identifying new coated gems and CVD synthetic diamonds. **Dr. Ilaria Adamo** (University of Milan) reviewed the growth of synthetic gem materials, with an emphasis on beryl; Tairus and Malossi are currently the main producers. **Dr. David Ajò** (CNR - Institute of Inorganic Chemistry and

Surfaces, Padova, Italy) discussed the chemistry and physics of gem treatment, focusing on tanzanite. In a presentation delivered by **Dr. Cristiano Ferraris** (National Museum of Natural History, Paris), **Dr. François Farges** (National Museum of Natural History, Paris, and Stanford University, California) hypothesized that the original piece of rough that yielded the Tavernier Blue/French Blue/Hope diamonds was naturally or manually cleaved from a rhombicuboctahedral crystal that could have weighed ~300 ct.

Dr. Gioacchino Tempesta (University of Bari) reviewed the application of X-ray diffraction topography to imaging growth striations, dislocations, and subgrains in crystalline materials. These features may be optically invisible but are useful for fingerprinting individual gemstones. **Dr. Giancarlo Della Ventura** (Roma Tre University) examined applications of micro-FTIR spectrometry to gemology, including analysis of H₂O and CO₂ in opal to differentiate various localities. **Dr. Alessandro De Giacomo** (University of Bari) reviewed the use of laser-induced breakdown spectroscopy in gemology, and noted that the technique allows for 10–15% accuracy in a range from ~2 to 800 ppm. **Dr. Davide Bleiner** (University of Berne, Switzerland) discussed LA-ICP-MS, and briefly mentioned a case study that documented higher Cu contents and heavy Cu isotope depletion with increasing temperature in Cu-diffused labradorite from Oregon.

Dr. Caterina Rinaudo (University of Eastern Piedmont, Alessandria, Italy) differentiated sapphires from various localities (metamorphic and magmatic) using micro-Raman spectroscopy of inclusion suites. **Ron Ringsrud** (Ronald Ringsrud Co., Saratoga, California) conveyed the romance and science of emeralds, noting that highly saturated stones from Colombia's La Pita mine can be effectively cut as shallow cushions since abundant light return is not necessary to best display their color. **Dr. Stella**

Figure 30. With magnification, the colored adhesive is plainly visible on these crown facets of the tanzanite. Photomicrograph by Nathan Renfro; magnified 20×.



Nunziante Cesaro (Sapienza University of Rome) studied archeological emeralds from Oplontis, Italy, and determined that their origin could be Egypt, Austria (Habachtal), or Russia (Ural Mountains). **Dr. Alberto Paleari** (University of Milan - Bicocca) used UV-Vis, EPR, and PL spectroscopy to determine that Mn^{3+} is the cause of iolite's strong pleochroism. **Dr. Cristiano Ferraris** used high-resolution transmission electron microscopy to investigate the origin of color in blue apatite from Bahia, Brazil. He found strained microdomains of fluorine- and hydroxyl-rich apatite with dimensions in the violet-to-blue range of visible light (400–470 nm).

Extended abstracts of the presentations will be published in a future issue of *Rivista Gemmologica Italiana*. The conveners hope to hold a similar event next year in Italy.

Brendan M. Laurs

Sinkankas Symposium 2010—Gem Feldspars. The eighth annual symposium in honor of John Sinkankas took place April 17 at GIA in Carlsbad. Co-hosted by GIA and the San Diego Mineral and Gem Society, the sold-out event was attended by 144 people.

After opening remarks by convener **Roger Merk** (Merk's Jade, San Diego, California), GIA's **Robert Weldon** provided a photographic exploration of gem feldspar varieties, noting that feldspars show more types of phenomena—including chatoyancy, schiller, labradorescence, and adularescence—than any other gem species. **Dr. William "Skip" Simmons** (University of New Orleans) reviewed the mineralogy of feldspars and described an important gem orthoclase deposit in southern Madagascar. He obtained typical pale yellow as well as colorless and pale green samples from local Malagasy dealers; X-ray diffraction analysis showed they consisted of sanidine as well as orthoclase.

Si Frazier (El Cerrito, California) recounted the discovery of spectrolite (gem-quality labradorite) at Ylämaa, Finland, which was found during the Winter War (1939–1940) when Lieutenant Peter Laitakari had a rocky outcrop blasted for boulders to be used as tank traps. **Lisbet Thoresen** (Beverly Hills, California) described the archaeogemology of amazonite and the ancient Egyptian mining sites surveyed by geologist Dr. James A. Harrell (University of Toledo). One of the oldest known gem materials, amazonite was used for beads by prehistoric tribes in northern Africa and the civilizations of Mesopotamia and the Indus Valley (ca. 5200–3000 BC); however, it was most popular in Dynastic Egypt (3000–332 BC), especially for amulets and jewelry inlays.

Meg Berry (Mega Gem, Fallbrook, California) described the challenges and rewards of cutting gem feldspar. With Oregon sunstone, considerations include fractures/cleavages, the distribution of the schiller-causing particles, and the best direction to view the schiller phenomenon.

Rock Currier (Jewel Tunnel Imports, Baldwin Park, California) conveyed his experiences with amazonite—mining at Pikes Peak, Colorado, and buying in Ethiopia. In both cases, the crystals had considerable iron staining, which was removed by soaking for several days in oxalic acid or Waller solution (sodium dithionite dissolved in water). **Bill Larson** (Pala International, Fallbrook, California) showed beautiful examples of gem feldspars from deposits around the world. He indicated that Sri Lanka has produced the best moonstones with strong blue adularescence, while Myanmar's moonstones include a rare variety with orangy yellow adularescence and a four-rayed star.

John Koivula (GIA Laboratory, Carlsbad) illustrated the "microworld" of gem feldspar, featuring inclusions in feldspar, feldspar as inclusions in other gem minerals, and structures and zoning in feldspar. **Dr. George Rossman** (California Institute of Technology, Pasadena) indicated that the wide variety of colors in feldspar are created by impurities or structural variations.

Shane McClure (GIA Laboratory, Carlsbad) addressed the controversy about whether the red and green andesine reportedly from Tibet is naturally colored. The composition (i.e., anorthite content) of Tibetan andesine overlaps that of Mongolian material, but not Mexican or Oregon labradorite. There are no obvious differences in the internal features of Mongolian, Mexican, and Oregon material, except for larger copper platelets and potential differences in color zoning seen in some untreated Oregon stones. Material from all three locations has overlapping UV fluorescence. Currently GIA knows of no way to reliably separate Tibetan from treated Mongolian stones. In a second presentation, **Dr. George Rossman** provided convincing evidence that all the samples of red/green feldspar he has analyzed so far that were represented as being from Asia and the Congo were treated.

The theme of next year's Sinkankas symposium (date to be determined) will be diamond.

Brendan M. Laurs

MISCELLANEOUS

Gem news from Myanmar. On January 29, 2010, the *Myanmar Times* reported that Max Myanmar Co. recovered a jadeite boulder weighing 115 tonnes from the Phakant (Hpakan) mining area. It reportedly measured 21 m long × 4.8 m wide × 10.5 m high, and was found 12 m below the surface near Sai Ja Bum village (plot no. Mupin 1).

In March 2010, the 47th Gem Emporium realized sales of ~US\$500 million from nearly 7,000 lots of jadeite and other gem materials. The 29th Pearl Emporium was held in Naypyidaw on May 13–15, 2010, offering 350 lots by tender and 31 lots by auction. Merchants from 27 companies attended, and the 174 lots sold comprised a total of 39,835 cultured pearls weighing 16,905 mommes. Some previous Burmese gem sales data are compiled in

TABLE 1. Yearly Burmese gem sales.

Year	Sales (kyats)
2000–2001	363,000,000
2001–2002	127,000,000
2002–2003	249,000,000
2003–2004	357,000,000
2004–2005	616,000,000
2005–2006	1,359,000,000
2006–2007	2,236,000,000
2007–2008	3,559,000,000

table 1, and additional information can be found at www.palagems.com/gem_news_burma_stats.php.

At Mong Hsu, miners are working an extension of the old deposit on the east side of the Thanlwin River, to the northeast of Mong Hsu. The quality of the rubies is reportedly the same as the material from the old deposit.

On three occasions—in 2005, 2008, and 2010—this author has encountered African rubies (with no glass filling) being sold in Myanmar.

*U Tin Hlaing
Dept. of Geology (retired)
Panglong University, Myanmar*

ANNOUNCEMENTS

Updated CIBJO Blue Books released. The World Jewellery Confederation (CIBJO) has released updated versions of its guides for gemstones, pearls, and precious metals, and will soon release a Gemmology Laboratory Book. These publications can be downloaded from www.cibjo.org.

The Gemstone Book includes a new coding system for gem treatments developed in cooperation with the American Gem Trade Association and the International Colored Gemstone Association. The codes are listed as part of the nomenclature guide in Annex A. The Precious Metals Book was revised to prohibit the use of rhodium coating on yellow gold and require disclosure of any metal coating that changes the color of the base material. Also new is an annex listing national standards for precious metal marking. The updated version of The Pearl Book contains only minor revisions.

The Gemmology Laboratory Book will be released later in 2010, as a guide for the management and technical operations of gemological laboratories. It will outline best practices and general requirements for testing and grading colored stones, diamonds, and pearls.

In Memoriam Roy E. “Chip” Clark: 1947–2010

Scientific and studio photographer Chip Clark of the Smithsonian Institution’s National Museum of Natural History passed away June 13. In photographing the museum’s exhibits, Mr. Clark captured some of the world’s most famous gems. Several of his photos have appeared in *G&G*—including the shots of the Wittelsbach-Graff and Hope diamonds in this issue—as well as in numerous other publications and on Tucson Gem and Mineral Show posters.

A native of Newport News, Virginia, where he was a member of the Junior Gem and Mineral Society, Mr. Clark earned a bachelor’s degree in biology from Virginia Tech University. He worked for NASA and taught high school biology and physical sciences before joining the Smithsonian in 1973. In addition to gems, he photographed rainforests, caves, and deep-sea environments around the world. He also shot freelance assignments for the National Geographic Society, the National Wildlife Federation, and *Scientific American*. Mr. Clark is survived by his wife and his daughter by a previous marriage. He and his talent will be sorely missed.



LAMINATED REFERENCE CHARTS

The information you need... at a glance!
Perfect for home or office use.

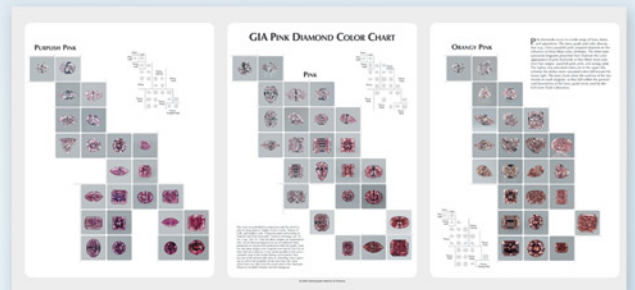
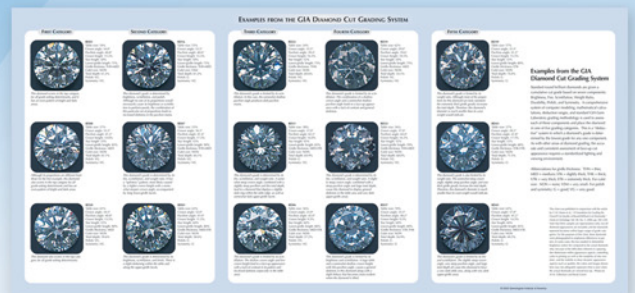


- HPHT-Grown Synthetic Diamonds
- World Gem Localities
- Gem Treatments
- GIA Diamond Cut Grading System
- Pink Diamond Color Chart
- Recognizing Be-Diffused Rubies & Sapphires

Also available:

- Separation of Natural & Synthetic Diamonds
- Identification of Filled Diamonds

Only \$16.95 (plus shipping)



GEMS & GEMOLOGY®

Order Yours Today!

Visit store.gia.edu

Or call 800-421-7250, ext. 7142
(outside the U.S., 760-603-4000, ext. 7142).

Buy two or more and **SAVE!**

EDITORS

Susan B. Johnson
Jana E. Miyahira-Smith
Thomas W. Overton

2010 BOOK REVIEWS

American Luxury: Jewels from the House of Tiffany

Edited by Jeannine Falino and Yvonne J. Markowitz, 207 pp., illus., publ. by Antique Collectors Club [www.antique-acc.com], Woodbridge, Suffolk, UK, 2009. US\$65.00

This book pays tribute to Tiffany & Co.'s enduring ingenuity since 1842. What sets it apart from others written about Tiffany is the series of original essays by well-known authorities. Editors Falino and Markowitz contribute sections and are joined by Elise Misiorowski, Elizabeth Ann Coleman, and Gerald W. R. Ward, who each lend a wealth of information.

The reader will enjoy learning how Tiffany & Co. earned its reputation. The United States, a country of unbridled progress through the late 19th and 20th centuries, offered the ideal environment for the firm to evolve and grow, lavishly meeting the luxury needs of the affluent while developing a quintessentially American style using native materials and motifs. Tiffany displays at the International Expositions were met with great success, further enhancing the company's reputation and earning it a place beside great European jewelers such as Cartier and Boucheron. The firm was quick to adopt technological advances, including the raised diamond mount (the "Tiffany setting"), new diamond-cutting techniques, and a system of hallmarking.

One section covers Tiffany's renowned gemologist, George Frederick Kunz. Having Kunz on staff during the latter 19th and early 20th cen-

turies kept Tiffany at the forefront of new and unusual gemstone discoveries. Kunz was allowed to collect both personally and for Tiffany, and this trust enabled him to fulfill his passion while leading the company in a creative direction.

Other sections review the work of artistic greats such as Paulding Farnham and Louis Comfort Tiffany. One learns of the turbulent relationship between Farnham and LCT, and why pieces designed by both artists are rare. Founder Charles Lewis Tiffany's successors in the 20th century continued to create extraordinary adornments designed by artists such as Jean Schlumberger, Angela Cummings, Elsa Peretti, and Paloma Picasso.

Of particular interest is an entire section devoted to men's jewelry. It covers the fascinating evolution from military, civic, and fraternal objects such as rings, badges, and swords to more recent items such as NFL Super Bowl rings.

There is some repetition from one chapter to the next. Although the reader benefits from the individual perspective of each author, perhaps the editors could have planned the subjects a little tighter to avoid such overlap.

Through the years, Tiffany & Co. has understood jewelry's ability to evoke memories and people. This book is a must for the bookshelves of appraisers, designers, jewelers, and antique and estate dealers.

MELINDA ADDUCCI
*Joseph DuMouchelle Appraisers
Grosse Point Farms, Michigan*

Gemstones

By Karen Hurrell and Mary L. Johnson, 319 pp., illus., publ. by Metro Books [www.barnesandnoble.com], New York, 2008. US\$12.98

Billed as a "complete color reference for precious and semiprecious stones of the world," that covers "every aspect" of gems, this reference guide doesn't quite meet such lofty claims. Yet it does provide a useful elementary overview and may be handy as a quick resource for basic physical properties of common gems.

The book's attempt to address a wide range of topics may also be to its detriment; each section is simple and brief, and the work may be spread too broadly for such a concise volume. The clearly written text is excellent for anyone interested in learning about gem materials, though the more complex terminology and descriptions of advanced testing equipment may be lost on the layperson.

The guide begins with a simple, easy-to-understand introduction. The first section explains the basics of minerals, gems, and precious metals, and contains simple definitions of some gemological characteristics. The bulk of the book showcases 130 gems, gem minerals, natural glasses, and organic gems that are attractively laid out in a fashion similar to a field guide. The gem minerals are divided into sections based on the crystal systems (an arrangement not obvious to the lay reader), but the question remains as to how the gem entries are organized within each section, as there does not seem to be an intuitive order.

Unfortunately, the entry headings and subheadings do not have a consistent format. Some primary headings identify the mineral species, with the subheading citing the mineral group; other main headings denote the gem variety, followed by the species as the subheading. Also, some common mineral groups (such as tourmaline and garnet) are identified within the headings, while others (e.g., feldspar) are not noted. At least one of the large bold entry headings (that of iolite) was misspelled (as "Lolite").

Each gem entry has four sections containing basic information on properties and characteristics, as well as cutting, setting, and valuing. The top of each page contains a quick reference list of physical properties along with notable geographic sources. Most common gemstones are included in this guide, although hematite is conspicuously missing. The book does not include listings of synthetic gemstones, and treatments and enhancements are not addressed.

This reviewer did not take on the arduous task of checking the accuracy of all technical data; however, a quick spot check unveiled some confusion or errors in the stated refractive indexes for three of four random gemstones. This seemed largely related to the approach of listing the maximum extent of the value's ranges. (Instead, the reviewer believes that citing *standard* R.I. values with their tolerances listed separately would have corrected much of the confusion and been more useful.)

Following the gemstone directory is an attractive thumbnail photo gallery of each cut gem that is described. This can be used as a quick and basic reference guide to the gems' colors. The color representations are okay, although the illustrated color for the padparadscha sapphire looks distinctly red. The next section, "Identifying and Collecting Minerals and Gemstones," contains five informative subsections, each comprising two pages. The first, "Identifying minerals," cannot aid in the identification of individual speci-

mens, but it provides a general and very simplified approach for the curious hobbyist. "Identifying Gems" attempts to consolidate a very complex "course" into little more than a page of instruction. "Further Testing" contains information that is beyond the elementary nature of the rest of this book, but is interesting for a more knowledgeable reader or tech-savvy hobbyist. "Gemstone Evaluation" provides a very good overview of the traits and methods by which gemstone values are judged, and "Mineral Evaluation and Storing" is very informative as well as interesting. The last subsection, "Gemstones by color," is a valuable aid that lists gemstones under corresponding color headings.

Incidentally, the bangle in the photo in the "Identifying Gems" section is misidentified in the caption, which describes gas bubbles in "jadeite"; since jadeite does not contain gas bubbles, this reviewer guesses that the caption contained a typographical error and meant to indicate that the bangle is a jadeite *imitation*—probably glass.

The book also contains a "Resources" section that is conveniently divided into two parts for gemology and mineralogy. Books, peer-reviewed journals, trade publications, selected gem testing laboratories, associations and societies, clubs, appraisal references, and useful websites are included. Note, too, that the book's style and design are very attractive, it is nicely colored with abundant photographs, and has a high-quality paper and stiff paperboard cover.

Although this book is not suited for use by a practicing gemologist or serious field collector, it is an enjoyable and useful reference for anyone interested in learning about the basics of gem materials, or for a beginning collector-hobbyist. It may also have an appeal in jewelry stores as a counter reference for employees and as a colorful and attractive marketing aid for their colored-stone clients.

CHERYL WENTZELL
GIA Laboratory, Carlsbad

Diamonds: The Quest from Solid Rock to the Magic of Diamonds

By Christine Gordon, 430 pp., illus., publ. by Tectum Publishers, Antwerp, 2008. US\$135

This beautifully produced coffee table book presents the story of diamonds from mine to wearer through magnificent photographs and clearly written text. It is aimed at the general reader rather than professional geologists or gemologists, and for its audience it succeeds brilliantly. The photographs are reproduced in full-page splendor, and the last 200 pages are nearly all photos with short captions. My only quibble is that many captions are either absent or do not identify the mine, person, or collection of diamonds being portrayed.

The first chapter briefly discusses the formation of diamonds deep in the earth's crust, some up to 3.5 billion years ago, and includes a useful timeline of diamond history. There is an interesting aside on carbonado, the grayish black diamonds found in Brazil and the Central African Republic. They are very old, hard, and tough, and may have formed in the heart of giant red stars that exploded and scattered debris throughout the galaxies. Chapter 2 examines the countries in which diamonds are produced. There are beautiful images of the ice road and the Ekati mine in Canada, the Mir mine in Siberia, and many large mines in Botswana, South Africa, Namibia, Lesotho, and Australia. There are also snapshots of small-scale artisanal miners in Angola, the Democratic Republic of Congo, and Sierra Leone.

Some errors have crept into the section on Botswana, where diamonds were first discovered in 1960 (not 1974 as stated), and the first mine opened in 1970. The latest diamond mine to come onstream, and the first one not connected with De Beers, was the Lerala mine, located in northeast Botswana, which started in 2008 and closed six months later because of the global financial crisis. However, it had no connection (as the book states)

with the AK6 project, which is located near Orapa and is being developed by Dublin-based African Diamonds.

The discussion of trading in rough diamonds mentions the shift from the near monopoly of De Beers in London to centers in Antwerp, Tel Aviv, Mumbai, and Dubai, and the requirement of a Certificate of Origin by the Kimberley Process. Before being traded, diamonds must be sorted by size, category (industrial or gem), shape (cuttable or noncuttable), and color, and this sorting may be repeated many times in more detail.

The chapter on cutting describes the shift from the traditional centers in Amsterdam and Antwerp to the producing countries of Botswana, Namibia, and South Africa, and from Antwerp to Tel Aviv, Surat (India), and Guangzhou (China). The next chapter covers the four Cs (cut, clarity, color, and carat weight) and grading reports issued by GIA, HRD, EGL, and IGI. The text is rudimentary but is accompanied by beautiful photographs in which the true color of the diamonds is revealed.

The subsequent chapter, on creating a jewel, is very short on description but shows some magnificent images of crown jewels from Portugal, France, and especially England. A chapter on celebrities shows them wearing beautiful diamond jewelry, and a final chapter on industrial diamonds contains a magnificent photograph (over 1½ pages) of a collection of industrial rough.

The book is not inexpensive, but discounts may be found. Regardless, it is a worthwhile addition to one's library.

A.J.A. (BRAM) JANSE
Perth, Western Australia

Schiffer Earth Science Monographs

Publ. by Schiffer Publishing
[www.schifferbooks.com], Atglen,
PA, 2008–2009. US\$19.95 each

The Schiffer Earth Science Mono-

graphs are (currently) a seven-volume series of collectors' guides to (1) the mica group, (2) the epidote group, (3) fluorite, (4) the axinite group, (5) the vesuvianite group, (6) the three phases of titania (rutile, anatase, and brookite), and (7) the pyroxene group. (Volumes 2 and 3 were reviewed in the Spring 2009 and Winter 2009 issues of *G&G*.) Robert J. Lauf is the author of all the monographs except the third, Arvid Eric Pasto's *Collector's Guide to Fluorite*. This series was created for mineral collectors and addresses topics of general concern to them, without requiring a doctorate in mineralogy to comprehend the material. Each monograph follows a similar format, with sections on "Taxonomy," "Formation and Geochemistry," and "The Minerals."

In "Taxonomy," special attention is given to how the minerals of each group or subgroup vary from the basic formula. The compositional diagrams, listings of accepted species with their formulas, tables of obsolete and correct names of minerals, and diagrams of crystal structure on the molecular level are tremendously useful. The crystal-habit diagrams are particularly helpful to any collector who is attempting to identify a specimen. Information on substitutions of atoms and on solid solutions and their extent is also provided.

The "Formation and Geochemistry" section explores the conditions and geologic settings essential to the formation of the minerals. This information is vital to collectors, as it explains differences in crystal habits and associated species that are seen in various formations. It can also be of great assistance to field collectors who know which kinds of geologic environments are likely to contain minerals of interest. Because of the unique relationship the titania minerals have with each other, their phase relationships are explained in volume 6.

For the true mineral collector, though, the heart of each volume is the "Minerals" section. An abundance of color photographs of speci-

mens, often from the best-known localities, grace this section. Most are fine examples of their species, often crystals rather than the massive ore-type specimens that typically appear in geology manuals. Many photos show the species in question with associated minerals or on matrix, providing a valuable visual aid. Each soft-cover 8½ × 11 inch volume contains about 90–120 color photographs of the minerals, as well as tables and diagrams.

Though not specifically written for a gemological audience, this series offers information of value to the gemologist. Where applicable, cut examples of the gem varieties of mineral species are shown in color with brief descriptions. The first volume is perhaps of least interest to gemologists, since few mica species appear as cut gems. Axinite and vesuvianite minerals and the three phases of titania are sometimes cut as gems for the collector but are not often seen in your local jeweler's showcase. The pyroxene volume, however, describes many different kinds of gem species, including jadeite, spodumene, and diopside, and is worthwhile reading for the gemologist.

MICHAEL T. EVANS, G.G.
Gemological Institute of America
Carlsbad, California

OTHER BOOKS RECEIVED

Minéraux Remarquables. By Jean-Claude Boulliar with photography by Orso Martinelli, 252 pp., illus., publ. by Plage [plage2@wanaadoo.fr], Paris, 2009, €69 [in French and English]. This dual-language coffee table book depicts the finest specimens from the Mineral Collection of the University of Paris–Sorbonne. The specimens are arranged by mineral group and displayed in full-color life-size photos. Also included is a series of short essays on photographing minerals, the history of the collection, and mineral collecting in general.

TWO



2010 GEMOLOGICAL ABSTRACTS

EDITORS

Brendan M. Laurs
Thomas W. Overton
GIA, Carlsbad

REVIEW BOARD

Edward R. Blomgren
Owl's Head, New York

Annette Buckley
Austin, Texas

Jo Ellen Cole
Vista, California

Emily V. Dubinsky
GIA Laboratory, New York

R. A. Howie
Royal Holloway, University of London

Edward Johnson
GIA, London

Michele Kelley
Monmouth Beach, New Jersey

Guy Laloue
Academy for Mineralogy, Antwerp, Belgium

Kyaw Soe Moe
GIA Laboratory, New York

Keith A. Mychaluk
Calgary, Alberta, Canada

Joshua Sheby
New York, New York

James E. Shigley
GIA Research, Carlsbad

Russell Shor
GIA, Carlsbad

Elise Skalwold
Ithaca, New York

Jennifer Stone-Sundberg
Portland, Oregon

Rolf Tatje
Duisburg, Germany

Dennis A. Zwigart
State College, Pennsylvania

COLORED STONES AND ORGANIC MATERIALS

Application of mineralogical methods to the investigation of some gem-quality corals. L. Natkaniec-Nowak [natkan@agh.edu.pl], M. Dumańska-Slowik, J. Fijał, and A. Krawczyk, *Journal of Gemmology*, Vol. 31, No. 5–8, 2009, pp. 226–234.

Coral samples were studied using scanning electron microscopy–energy-dispersive spectroscopy (SEM-EDS), X-ray diffraction (XRD) analysis, Fourier-transform infrared (FTIR) spectroscopy, and cathodoluminescence (CL). Observations with a loupe and polarizing microscope are also reported. The calcareous corals (white, red, pink, and blue) consisted mainly of poorly structured Mg-bearing calcite, and SEM-EDS analyses revealed a homogeneous composition. The FTIR spectra for all colors were similar, and also indicated only trace amounts of silicate minerals and organic matter. None showed cathodoluminescence, which is consistent with their recent formation. FTIR spectroscopy demonstrated that the organic corals (black and gold) were composed mainly of collagen-type biopolymers, with subordinate carbonate. They had a concentric-radial structure, and XRD analysis confirmed that the coral skeleton was largely amorphous or poorly crystalline. Overall, spectroscopic methods appear to be the most effective way to distinguish between natural and treated coral. *ERB*

La turchese e i suoi giacimenti [Turquoise and its deposits].

M. C. Venuti, *Rivista Gemmologica Italiana*, Vol. 4, No. 1, 2009, pp. 13–33 [in Italian with English abstract].

Important aspects of turquoise (gemological properties, treatments, imitations, main producers, and consumers, etc.) are

This section is designed to provide as complete a record as practical of the recent literature on gems and gemology. Articles are selected for abstracting solely at the discretion of the section editors and their abstractors, and space limitations may require that we include only those articles that we feel will be of greatest interest to our readership.

Requests for reprints of articles abstracted must be addressed to the author or publisher of the original material.

The abstractor of each article is identified by his or her initials at the end of each abstract. Guest abstractors are identified by their full names. Opinions expressed in an abstract belong to the abstractor and in no way reflect the position of Gems & Gemology or GIA.

© 2010 Gemological Institute of America

reviewed, and the history and characteristics of turquoise from North American and Mexican deposits are discussed in detail, as are their uses in jewelry. The classic deposits in Egypt, Iran, and China are described only briefly. Numerous color photographs illustrate the mines, typical samples of rough, and cut stones and jewelry. *RT*

DIAMONDS

Argyle type Ia brown diamonds: Gemmological properties, FTIR, UV-Vis, CL and ESR features. A. Brajkovic [anna.brajkovic@unimib.it], V. Rolandi, and R. Scotti, *Australian Gemmologist*, Vol. 23, No. 12, 2009, pp. 539–550.

The authors examined 35 light brown rough diamonds from Australia's Argyle mine. Hexagonal depressions and etching were the most common surface features; internal characteristics were irregular cracks, dislocation planes, and inclusions of graphite and eclogitic minerals. The nitrogen content was low (~700 ppm), and all samples contained hydrogen. The diamonds were found to be type IaAB. Raman and electron spin resonance spectra are presented; cathodoluminescence imaging showed a general bright green emission with two broad components centered at 450 and 512–520 nm. From these observations, the authors suggest that the diamonds developed in a moderately nitrogen-poor eclogitic environment, where they experienced dissolution and resorption processes, as well as platelet degradation and post-growth plastic deformation.

RAH

Diamonds: Exploration, mines and marketing. G. H. Read [gread@shoregold.com] and A. J. A. (Bram) Janse, *Lithos*, Vol. 112S, 2009, pp. 1–9.

The most significant diamond discovered in recent years is the 603 ct Lesotho Promise, recovered in 2006 from the Letšeng-la-Terae mine in the northeastern highlands of Lesotho. The rough stone sold for \$12.4 million, and diamonds cut from it are expected to bring \$100 million. This type of find helps drive a multi-billion-dollar diamond exploration, mining, and marketing industry that operates in 45 countries worldwide. Five countries—Botswana, Russia, Canada, South Africa, and Angola—account for 83% of annual production by value and 65% by weight. This production is attributed to four principal companies: De Beers, Alrosa, Rio Tinto, and BHP Billiton. Sixteen diamond mines have been opened and four have reopened in the past 12 years, and 11 advanced projects are being developed into mines. One recent trend has seen mid-tier and junior diamond exploration companies involved in takeovers, mergers, and option agreements that consolidate exploration areas and projects into fewer hands. In another trend, De Beers, BHP Billiton, and Rio Tinto have been farming out many of their large exploration holdings to juniors.

Diamond exploration worldwide amounted to \$600 million in 2007, followed by a similar total in 2008. The main activity was in Canada, followed by Botswana, Angola, and the Democratic Republic of the Congo. There has been minor but intriguing activity in Brazil and India. During the past five years, exploration has benefited from higher-resolution geophysical techniques operating from a variety of platforms, including fixed- and rotary-wing aircraft. Dense-media separators are seeing more frequent application in the processing of kimberlite bulk samples. In addition, exploration companies have a much better understanding of the relationship of major- and trace-element ratios in diamond indicator minerals.

The market for rough diamonds has been strong and prices have risen dramatically over the past five years. The outlook for the diamond market suggests that demand will evolve to become considerably larger than supply. *DAZ*

Formation of various types of graphite inclusions in diamond: Experimental data. A. F. Khokhryakov [khokhr@mail.ru], D. V. Nechaev, A. G. Sokol, and Y. N. Palyanov, *Lithos*, Vol. 112S, 2009, pp. 683–689.

Graphite is a common inclusion in natural diamond, and there are several kinds of graphite that may be present. In this experimental study, synthetic diamonds were crystallized from various chemical systems at high pressures and temperatures using split-sphere equipment. In some cases, the crystals were then annealed under HPHT conditions. Depending on the growth environment, the authors produced three types of graphite inclusions in the synthetic diamonds, which they suggest correspond to protogenetic, syngenetic, and epigenetic origins in natural diamonds. The inclusions appear to form at different times relative to diamond crystallization, under pressure-temperature regimes that are within the graphite stability field, but also under diamond-stable conditions. The morphology of the graphite inclusions, the appearance of strain patterns around them, and Raman spectroscopy of the graphite indicate particular geologic environments and mechanisms for the formation of graphite inclusions in diamond.

JES

Laser inscriptions on diamonds. R. Bauer [klepners@vicnet.net.au], *Australian Gemmologist*, Vol. 23, No. 12, 2009, pp. 575–578.

In recent years, laser inscriptions (usually of diamond report numbers) have become common practice for identifying individual stones. First, a diamond is inspected to find the best place on the girdle for the inscription; surface-reaching inclusions and feathers must be avoided. The girdle is then painted with an opaque solution, and a 1064-nm infrared laser is used to inscribe the stone. It is important to make sure that the certificate and the corresponding diamond actually belong together; examples have been

seen of mismatched reports and inscription numbers and, in one case, a diamond inscribed with a false GIA logo.

RT

Metasomatic origin of diamonds in the world's largest diamondiferous eclogite. Y. Liu [yangl@utk.edu], L. A. Taylor, A. B. Sarbadhikari, J. W. Valley, T. Ushikubo, M. J. Spicuzza, N. Kita, R. A. Ketcham, W. Carlson, V. Shatsky, and N. V. Sobolev, *Lithos*, Vol. 112S, 2009, pp. 1014–1024.

During their volcanic eruption, kimberlite magmas can transport not only diamonds but also rock fragments from the earth's mantle to the surface. In most instances, these mantle xenoliths are peridotites or eclogites. In this study, a large 8.8 kg eclogite xenolith from the Udachnaya kimberlite in Yakutia was carefully documented. High-resolution X-ray computed tomography of the xenolith revealed more than 100 diamonds 1–5 mm across, as well as two clusters of intergrown diamond crystals ~10 mm across. The xenolith was sectioned into pieces for removal and study of the diamonds and adjacent minerals (sulfides, garnets, clinopyroxenes, and secondary minerals).

The diamond crystals had a linear distribution along alteration zones in the xenolith. They exhibited various internal growth zoning patterns, as seen by cathodoluminescence, and different carbon-isotope values from the cores to the rims. There were also differences in the chemical composition of inclusions and the same minerals in eclogite adjacent to the diamonds. The two diamond clusters exhibited dodecahedral crystal morphologies that were the result of partial resorption. All of these features supported the conclusion that the diamonds formed by a multistage process involving several metasomatic-fluid events. Similar observations have been published on diamonds from other eclogite xenoliths. The authors concluded that the formation of diamonds in most mantle eclogites involves repeated resorption and growth accompanied by plastic deformation after the formation of the other minerals in the eclogite. JES

Mid-tier diamond producer emerges from Africa. A. Ruffini, *Engineering and Mining Journal*, Vol. 210, No. 9, 2009, pp. 32–34.

A few years ago, Petra Diamonds was a junior diamond exploration company focused on the promising Alto Cuilo project in Angola. With the economic downturn, Petra withdrew from Alto Cuilo and also pulled back from the Kono project in Sierra Leone. Petra then went on a diamond resource buying spree that has seen it become one of the world's largest players outside the established majors. After purchasing Crown Diamonds, it bought the shutdown Koffiefontein mine from De Beers in July 2007 for about \$11 million. This was the start of several purchases from De Beers, followed a year later by the famous Cullinan mine for \$140 million. Next came Kimberly Underground Mines, and a 75% interest in Tanzania's

Williamson mine for \$10 million. The company now has a resource base of 265 million carats worth \$27.3 billion, compared to a mere 11 million carats three years ago. Petra has emerged as a mid-tier diamond producer, not via exploration, but through acquisitions, primarily of operations De Beers saw as peripheral to its own interests.

DAZ

On the unusual characteristics of the diamonds from Letšeng-la-Terae kimberlites, Lesotho. D. C. Bowen [recovery@letseng.co.ls], R. D. Ferraris, C. E. Palmer, and J. D. Ward, *Lithos*, Vol. 112S, 2009, pp. 767–774.

The Letšeng-la-Terae kimberlites are located in Lesotho's Maloti Mountains. The two pipes, along with their associated eluvial and alluvial deposits, are renowned for their large colorless gem diamonds. Early artisanal (1959–1977) and large-scale (1977–1982) mining yielded a total of 335,000 carats of diamonds, including the 601 ct Lesotho Brown in 1968. Recent operations (2003 through July 2008) recovered 265,000 carats, including 24 crystals weighing 100+ ct (the largest being the colorless 603 ct Lesotho Promise). The authors studied ~200,000 carats of diamonds recovered from the two pipes during the recent mining period, and documented a number of interesting features.

The Letšeng diamond population averages 75% gem quality, well above the global average for kimberlites (and more typical of alluvial deposits). The average size of ~1 ct per stone is also more typical of alluvial occurrences. The dominant crystal form is the dodecahedron, with a lesser percentage (about 30%) of irregular or elongated shapes; octahedrons and cubes are rare. The crystals typically appear rounded and resorbed. Brown diamonds are more prevalent in the larger Main pipe, while light yellow diamonds are more common in the Satellite pipe; in both, ~33% are colorless. Eighteen of the 24 100+ ct crystals were colorless type IIa diamonds. This combination of characteristics, most notably the abundance of large, high-quality colorless diamonds, makes the Letšeng-la-Terae kimberlites economically viable despite the low ore grade and the remoteness and harsh climate of the locality. JES

Tectonic setting of kimberlites. H. Jelsma [hjelke.jelsma@debeersgroup.com], W. Barnett, S. Richards, and G. Lister, *Lithos*, Vol. 112S, 2009, pp. 155–165.

Kimberlites are the products of ancient volcanism that brought rocks (xenoliths) as well as diamonds and other minerals up from great depths (~150 km or more) in the subcontinental lithosphere. As such, they can be considered time capsules of global tectonic events and the evolution of continents. In this article, the authors present an overall model for the geologic setting of kimberlites in southern Africa and other parts of the world. Kimberlites are distributed in clusters in geologic time and space, and their ages span the assembly and breakup of a number of supercontinents such as Rodinia and Gondwana. These

supercontinents' geologic timelines consist of long periods devoid of kimberlite magmatism that correspond to periods of continental stability, and intervening brief periods of kimberlite emplacement related to continent reorganization. The onset of kimberlite magmatism appears to be linked to thermal disturbances in the asthenosphere beneath continents, which may have contributed to their breakup. This magmatism seems to have taken place along distinct corridors where fracturing and rifting occurred in the lithosphere. Such zones apparently provided favorable conditions for kimberlite formation and eruption.

JES

GEM LOCALITIES

Ambanja, premier gisement d'andradite démantôïde gemme à Madagascar [Ambanja, first gem-producing area in Madagascar to produce andradite demantoid of gem quality]. B. Mocquet [blanca.mocquet@free.fr], Y. Lulzac, B. Rondeau, E. Fritsch, J. Le Quere, B. Mohamady, G. Crenn, C. Lamiraud, and S. Scalie, *Revue de Gemmologie*, No. 169, 2009, pp. 6–10 [in French].

This article describes gem-quality andradite found in northern Madagascar, northeast of Ambanja. The majority of the stones are green or yellow-green, while ~10% are brown and a few are bicolored. Refractive indices measured with a Gemeter 90 microreflectometer ranged from 1.85 to 1.87. Specific gravity was 3.72–3.89. These values are consistent with those reported for andradite. Raman spectra were also consistent with andradite. The major coloring agent of this demantoid is Fe³⁺; the yellow component is due to an Fe²⁺-Ti⁴⁺ charge transfer. No chromium or vanadium was detected in these stones, which were almost pure andradite, Ca₃Fe₂(SiO₄)₃. The authors suggest that such andradite colored by Fe³⁺ may be sold as demantoid; many yellow-green Russian demantoids also do not contain chromium as a coloring agent. The geologic context of the deposit is still under investigation.

GL

Ancient deposit of blue chalcedony in Turkey. M. Hatipoglu [murat.hatipoglu@deu.edu.tr] and S. C. Chamberlain, *Australian Gemmologist*, Vol. 23, No. 12, 2009, pp. 567–574.

The Saricakaya deposit, ~56 km north of Eskişehir in northwestern Turkey, contains massive deep blue chalcedony with a thick brownish yellow crust, as well as massive light blue chalcedony showing slight adularescence. Mining has taken place since Roman times, and ample reserves are available at the current rate of mining. The distribution and quality of the chalcedony varies throughout the deposit. Cabochons of this material are set in gold or silver and used as earrings, brooches, rings, and pendants.

RAH

Famous mineral localities: Volodarsk-Volynski, Zhitomir Oblast, Ukraine. P. Lyckberg [lyckberg@pt.lu], V. Chornousenko, and W. E. Wilson, *Mineralogical Record*, Vol. 40, No. 6, 2009, pp. 473–506.

Mined for decades by the Soviets for piezoelectric quartz, the pegmatites of the Volodarsk-Volynski area west of Kiev have also been an important source of large, etched crystals of yellow-green beryl as well as topaz for the collector market. This article provides a thorough history of the geology and discoveries of the district's key gem-producing areas, generously illustrated with color photographs of gem crystals, associated minerals, and the mines themselves. The emphasis is on key discoveries made in 1953, 1973, 1982, 1992, and since 1995, which account for most of the specimens seen in the market. Faceted and heat-treated material is briefly discussed. Due to the strategic importance of the deposits to the Soviets, these pegmatites are among the most studied in the world, greatly adding to our knowledge of these complex formations. The enormous size of some of the pegmatite pockets (up to 8,000 m³) and the gem crystals that formed within them (including beryl >20 kg, topaz >100 kg, and quartz >10 tonnes) are particularly impressive. Gem mining in the district ceased in August 2009, and the authors conclude that the deposits are likely exhausted.

KAM

Gem-corundum megacrysts from east Australian basalt fields: Trace elements, oxygen isotopes, and origins.

F. L. Sutherland [lin.sutherland@austmus.gov.au], K. Zaw, S. Meffre, G. Giuliani, A. E. Fallick, I. T. Graham, and G. B. Webb, *Australian Journal of Earth Sciences*, Vol. 56, 2009, pp. 1003–1022.

Though usually mined from placer deposits weathered from Cenozoic basalts in the eastern part of the continent, Australian ruby and sapphire did not form within these rocks. Rather, these corundum xenocrysts were entrained into the basaltic magma from some other source. Trace-element content (using laser ablation-inductively coupled plasma-mass spectrometry) and oxygen-isotope values of the corundum were obtained from a broad sampling of Australia's sapphire and ruby fields and compared to data from other basaltic deposits worldwide. These results showed how chromophores (Fe, Cr, Ti, and V) along with Ga and Mg contents, as well as δ¹⁸O values, could be combined to "fingerprint" corundum to its locality and original genetic source (e.g., magmatic, metamorphic, or metasomatic). A triangular plot of Ga-Mg-δ¹⁸O values clearly segregated the various deposits. These geochemically distinct groups give researchers a better understanding of gem corundum genesis and emplacement, and ultimately may aid in prospecting and in determining the provenance of faceted material.

KAM

Gemstone deposits in Turkey. M. Hatipoglu [murat.hatipoglu@deu.edu.tr], H. Babalik, and S. C. Chamberlain, *Rocks & Minerals*, Vol. 85, No. 2, 2010, pp. 124–132.

Turkey has viable reserves of six gem materials: diaspore, fire opal, blue chalcedony, amethyst, smoky quartz, and agate. Commercial sources of these gems are known elsewhere in the world, with the exception of facetable diaspore. The deposits are found in various rock types, in areas of volcanic and tectonic activity along major fault zones. The gem rough is typically exported, demonstrating that there is international demand for Turkish gems. The country is believed to have a large economic potential for gem production. *MK*

Jadeite jade from Myanmar: Its texture and gemmological implications. G. Shi [shiguanghai@263.net.cn], X. Wang, B. Chu, and W. Cui, *Journal of Gemmology*, 2009, Vol. 31, No. 5–8, pp. 185–195.

The authors investigated gemmologically useful correlations between textural features and jade quality by studying the microstructural, chemical, and crystal dynamics of white jadeite from Myanmar. Two textural types are discerned: *primary texture* is coarse-grained, porous, and characteristic of nontransparent jadeite, but can be used as B-jade (acid-bleached and resin-impregnated); *deformed and recrystallized texture* is intermediate- to fine-grained and has the most potential as fine gems. B-jade can be quickly identified with a loupe or unaided eye by the damage to its texture from the bleaching process.

The study also presents a model for how Myanmar's rare "icy" or "glassy" jadeites formed, and maps their geologic setting. At least two coupled processes took place in this material: grain size reduction (via rotation recrystallization, grain boundary migration and diffusion, mechanical twinning, and shearing) and crystallographic orientation, produced by ductile deformation under high-pressure, low-temperature metamorphism.

Toughness is another important factor in grading jadeite—the tougher the jade, the better its quality. Jadeites with serrated high-angle-sutured and interlocking grain boundaries are tougher than other specimens of similar grain size. Observing the crystal orientations and textures in "windowed" rough can provide an indication of overall quality.

Because green jadeite appears to have similar deformation textures as the white type studied, the conclusions can be provisionally extended to green material. *ERB*

Les gisements de saphirs et rubis associés aux basaltes alcalins de Madagascar: Caractéristiques géologiques et minéralogiques. 1ère partie: Caractéristiques géologiques des gisements [Sapphire and ruby deposits associated with alkali basalts in Madagascar: Geological and mineralogical characteristics. First part: Geological characteristics of the deposits]. S. Rakotosamizany, G. Giuliani, D. Ohnenstetter, A. F. M. Rakotondrazafy, and A. E. Fallick, *Revue de Gemmologie*, No. 169, 2009, pp. 13–21 [in French with English abstract].

Madagascar is one of the principal producers of gem corundum from basaltic fields. The main deposits are located at Ambondromifehy in the northern Antsiranana Province, Soamiakatra-Mandrosohasina in the central Antananarivo Province, and Vatomandry in the eastern Toamasina Province. Soamiakatra is the only primary deposit, where ruby is found in metagabbro and pyroxenite xenoliths. Petrographic studies have demonstrated two different conditions of ruby formation, at the boundary of the eclogite domain and in the granulite facies. In contrast, Madagascar's basalt-related sapphires originated from alkaline mafic magmatic activity at the boundary between the lower continental crust and the mantle. They occur within syenite and anorthoclase xenoliths in the basalts that transported them to the surface. *GL*

New geological origin: Ruby from Mozambique. J. Kawano [laboratory@gaaj-zenhokyo.co.jp], H. Kitawaki, A. Abduriyim, and M. Okano, *Gemmology*, Vol. 40, No. 483, 2009, pp. 13–15 [in Japanese with English translation].

Rubies were recently discovered in northern Mozambique's Niassa Province (M'sawize village in the Lichinga district) and Cabo Delgado Province (Montepuez area). The rubies' internal features consist of twin planes, fluid-film inclusions, negative crystals, and crystalline inclusions. Many of the crystalline inclusions were colorless-to-green amphibole (possibly pargasite), while others were confirmed as apatite. Also observed were needle-like inclusions that produce "silk." Material resembling hematite was seen in some fractures. The IR spectrum of unheated Mozambique ruby shows a broad band composed of absorptions at 3309 and 3081 cm^{-1} , which disappears when the ruby is heated. In some cases, weak absorptions at 2074 and 1980 cm^{-1} may be present, presumably from diaspore. Energy-dispersive X-ray fluorescence chemical analysis detected about 0.3–0.8 wt.% Cr and about 0.2–0.5 wt.% Fe. The iron content is higher than in most non-basalt-related ruby, and lower than in stones with a basaltic origin. Most rubies from Mozambique have been heat-treated, leaving flux residues in the fissures. *GL*

Scavengers from jade mines. N. Moe, *Weekly Eleven News*, No. 25, Vol. 5, March 31, 2010, p. 21.

At Myanmar's jade mines, scavengers commonly search the tailings for overlooked gem material. Groups of 10–15 people work day and night, using improvised flashlights in the darkness. The scavengers keep track of which companies are dumping material and when; discards from successful companies can bring crowds of 700–800 people.

Potential jadeite boulders are captured as they roll down the dump pile. According to the scavengers, the jadeite rolls down slowly, twisting and turning, while other boulders roll quickly. Hammers are used to strike the boulders and test their hardness; jadeite produces a solid sound and the rock remains undamaged. The scav-

engers also know the various textures of the boulders and how to differentiate the jadeite.

The jadeite scavenging has been practiced since 1997–1998. At first most of the people were unemployed heroin addicts, but youths hoping to strike it rich soon joined them. The reward for finding a good-quality piece of jadeite is about 500,000 kyats (US\$5,000), and profits are shared equally among the group. *U Tin Hlaing*

A study of zircon from Tanzania—Malaya zircon.

U. Henn [ulihenn@dgemg.com], *Australian Gemmologist*, Vol. 23, No. 10, 2009, pp. 453–456.

So-called Malaya zircon originates from the region between Mkujani and Umba in the Tanga Province of northern Tanzania. The material shows an attractive range of colors, from yellow to brown and red. Both rough (as waterworn pebbles) and faceted stones were examined for this study. They showed relatively high SG (4.67–4.70) and RI (1.957–1.967) values. Microprobe analyses are reported for three zircons (yellow, light brown, and dark brown), revealing up to 0.24 wt.% UO₂. The absorption spectra show the narrow bands and fine lines of U⁴⁺ in the 510–690 nm region. *RAH*

Zultanite, or colour-change diaspore from the Milas (Mugla) region, Turkey. M. Hatipoglu [murat.hatipoglu@deu.edu.tr] and M. Akgun, *Australian Gemmologist*, Vol. 23, No. 12, 2009, pp. 559–563.

A color-change variety of diaspore occurs in the same area of Turkey as the well-known transparent, nonphenomenal diaspore. It exhibits an alexandrite-like color change, dependent on the nature of the incident illumination. Material with fine chatoyancy also has been found. An editor's addendum (pp. 564–566) provides typical gemological data; the UV-Vis spectrum shows Fe- and Mn-related absorptions. *RAH*

JEWELRY HISTORY

82,000-year-old shell beads from North Africa and implications for the origins of modern human behavior. A. Bouzouggar, N. Barton [nick.barton@arch.ox.ac.uk], M. Vanhaeren, F. d'Errico, S. Collcutt, T. Higham, E. Hodge, S. Parfitt, E. Rhodes, J.-L. Schwenninger, C. Stringer, E. Turner, S. Ward, A. Moutmir, and A. Stambouli, *Proceedings of the National Academy of Sciences*, Vol. 104, No. 24, 2007, pp. 9964–9969.

Thirteen small, perforated marine shells (*Nassarius gibbosulus*) were recovered from an archeological site in eastern Morocco. The find supports related evidence that marine shells were collected in the North African regions ~82,000 years ago (40 millennia before similar events in Europe). The shells were either perforated deliberately or carefully collected for their large perforations; wear patterns suggest suspended strung beads. Residues of red pigment found on 10 of the shell beads indicate an added visual value. An

early distribution of beaded jewelry, used as symbolic, nonutilitarian objects for personal adornment, marks a fundamental stage in the emergence of modern social behavior. *ERB*

What did the well-dressed Neanderthal wear? Jewelry. M.

Lemonick, *Time*, January 12, 2010, www.time.com/time/health/article/0,8599,1952933,00.html.

In two caves in southern Spain, a team of paleoanthropologists discovered ornaments dating back 50,000 years. The objects were primarily seashells, most of them pierced and bearing remnants of pigment, suggesting they were worn as jewelry. The scientists noted that these items predated the arrival of modern humans in Europe by an estimated 10,000 years and were thus fashioned by Neanderthals. *RS*

JEWELRY RETAILING

Consumer insights into luxury goods: Why they shop where they do in a jewelry shopping setting. T.

Sanguanpiyapan [sanguanpiyan@wisc.edu] and C. Jasper, *Journal of Retailing and Consumer Services*, No. 17, 2010, pp. 152–160.

The authors surveyed jewelry buyers on why they chose to purchase at a particular retail outlet. The respondents were 60% women and 40% men; 56% were buying for themselves. The survey found a clear preference (60%) for freestanding jewelers, with respondents citing trust, the ability to interact with sales associates, a larger selection of merchandise and price ranges, and a more pleasurable shopping experience overall. While the survey indicated a growing acceptance of online shopping, retail jewelers can compete by understanding their clientele and presenting the products, prices, and shopping experience that appeal to them. *RS*

Pricing anomalies in the market for diamonds: Evidence of conformist behavior. F. Scott [fscott@uky.edu]

and A. Yelowitz, *Economic Inquiry*, Vol. 48, No. 2, 2010, pp. 353–368.

This article looks at the relationship between diamond pricing and consumer preferences. The authors examined the inventories of a number of popular online diamond sites and discovered substantial price differences centered around "focal-point" sizes—0.50, 1.00, and 1.50 ct. The study found that comparable-quality diamonds weighing just over 0.50 ct were priced from 17.5% to 28% higher than diamonds just under 0.50 ct. The difference between diamonds just over and just under 1.00 ct was 5.2–10%. Between those key sizes, the price gap was about 3% for each 0.01 ct increase. The authors note that such pricing reflects an established concept whereby shoppers conform to focal points such as round-number carat weights as a standard for behavior. *RS*

SYNTHETICS AND SIMULANTS

Spatial distribution of the nitrogen defects in synthetic diamond monocrystals: Data of IR mapping. Yu. V. Babich [babich@uiggm@nsc.ru] and B. N. Feigelson, *Geochemistry International*, Vol. 47, No. 1, 2009, pp. 94–98.

The authors used FTIR mapping to obtain nitrogen-defect data from a synthetic diamond grown under high-pressure, high-temperature (HPHT) conditions. The 0.8 ct yellow-brown crystal was grown in the Fe-N-C metal-carbon system for 128 hours under 6.0 GPa pressure and at temperatures ranging from 1390 to 1475°C. A Fourier IT Bruker Vertex-70 spectrometer equipped with a Hyperion 2000 microscope was used to study the composition, distribution, and concentration of nitrogen defects, based on known specific absorptions (1130 cm⁻¹ for C defects, 1282 cm⁻¹ for A defects, and 1332 cm⁻¹ for N⁺ defects). The defects were mapped from seed-to-edge along the cubic and octahedral growth sectors on a {110}-oriented polished plate.

The synthetic diamond was found to contain up to 300 ppm nitrogen. Only C defects were present along the cubic sector, and only in the inner zones, with gradually decreasing concentration. C, A, and N⁺ defects were all present along the octahedral growth sectors, with C defects only near the outer surface and A defects only within the inner portion. N⁺ concentration gradually decreased from seed to edge, with better-developed octahedral sectors showing higher concentrations. The FTIR data matched previous reports of nitrogen-defect distributions, and they provide a useful basis for studying and visually representing nitrogen defects related to crystal growth parameters in synthetic and natural diamonds. JS-S

TREATMENTS

Differentiation of naturally-coloured and artificially irradiated blue topaz specimens by their cathodoluminescence properties. Y. Song [psuyw@gm.com] and X. Yuan, *Australian Gemmologist*, Vol. 23, No. 12, 2009, pp 551–558.

Natural blue topaz is rare; most of the commercially available material has been treated with gamma radiation, neutrons, electrons, or a combination of these to induce the blue color. This detailed investigation showed that natural blue and artificially irradiated topaz can be distinguished by their cathodoluminescence responses. Natural blue topaz exhibited a strong (40–50 counts) CL fluorescence peak at around 492–500 nm, while irradiated material had a much weaker peak (15 counts). RAH

Identification of dyed jadeite using visible reflection spectra. Y. Liu, T. Lu, M. Wang, H. Chen, M. Shen, J. Ke, and B. Zhang, *Journal of Gemmology*, Vol. 31, No. 5–8, 2009, pp. 181–184.

Dyed, or C-type, jadeite is often identified by observing the dye in the pores and the spaces between interlocking crys-

tals. This article describes a method to identify dyed jadeite using a new type of visible reflection spectrometer (TrueColor) with dual integrating spheres. By combining reflection spectra in the visible range with IR absorption spectra, dyed-only and impregnated-and-dyed jadeites can be accurately identified. The reflection spectra of natural-color green jadeites typically show absorption lines at 433, 437, 630, 655, and 691 nm; most dyed green jadeites do not show these absorption lines. The 437 nm absorption is the strongest of the five lines, and its presence in vivid green dyed jadeite suggests that the starting material was a low-grade pale green jadeite. GL

Prevention of cracking in Ethiopian opal. S. V. Filin and A. I. Puzynin, *Australian Gemmologist*, Vol. 23, No. 12, 2009, pp. 579–582.

Many opals from Ethiopia's Shewa Province are prone to cracking over time or after minor heating. This is due to the presence of water in open pores and shrinkage cracks. A new treatment technique uses supercritical drying in an autoclave with anhydrous ethanol, for which the critical temperature is 245°C at 6.4 MPa. Hydrated low-molecular-weight silica sols are then introduced into the open pores of the opal at a pressure of 500–600 bars. When this treated material is carefully polished, no significant cracks appear. RAH

MISCELLANEOUS

The commodification of fetishes: Telling the difference between natural and synthetic sapphires. A. Walsh [awalsh33@uwo.ca], *American Ethnologist*, Vol. 37, No. 1, 2010, pp. 98–114.

Synthetic sapphires are often superior to natural stones in color and clarity. Why, then, do people place such value on natural goods? Using Ambondromifehy, Madagascar, as a backdrop, the author reviews how natural sapphire is brought to market and some of the controversies and procedures surrounding sapphire mining and processing. The article also discusses at length several spectacular, highly publicized specimens and concludes that a combination of locale, mystique, and storytelling sets natural sapphire apart from synthetic, adding value in the eyes of the public. RS

Comprare gemme alla fonte: e se la sorgente fosse inquinata? [Buying gemstones at the source: And if the source is contaminated?] S. P. de Almeida, L. S. Souto, and M. Macrì, *Rivista Gemmologica Italiana*, Vol. 4, No. 1, 2009, pp. 39–51 [in Italian with English abstract].

Tourists and even professionals often think that buying gems from cutters and dealers in mining areas, or directly from the mine, is a good way to avoid fraud. Unfortunately, this is not true. The article describes the situation in Brazil, where synthetics and simulants are frequently offered as genuine. The most common deceptive practices are substituting green glass for tourmaline, citrine for imperial topaz, irradiated blue topaz for aquamarine, and synthetic amethyst for natural amethyst. RT

BECAUSE PUBLIC EDUCATION HAPPENS AT THE COUNTER.

GIA LAUNCHES RETAILER SUPPORT KIT AND WEBSITE



A \$97.00 value, shipping and handling extra.



GIA's Retailer Support Kit has been developed to help sales associates educate the public about diamonds, the 4Cs, and thoroughly explain a GIA grading report. Take full advantage of all that GIA has to offer by visiting www.retailer.gia.edu

To order your FREE kit, log on to www.retailer.gia.edu



GIA
GEMOLOGICAL INSTITUTE OF AMERICA®



GIA

GEMOLOGICAL INSTITUTE OF AMERICA